Iranian Association of Electrical and Electronics Engineers

Shahid Chamran University of Ahvaz

Journal of Applied Research in Electrical Engineering

Vol. 4, No. 1, Winter and Spring 2025



Publisher: Shahid Chamran University of Ahvaz

E-ISSN: 2783-2864
P-ISSN: 2717-414X

Iranian Association of Electrical and Electronics Engineers

Journal of Applied Research in Electrical Engineering

E-ISSN: 2783-2864
P-ISSN: 2717-414X

Shahid Chamran University of Ahvaz

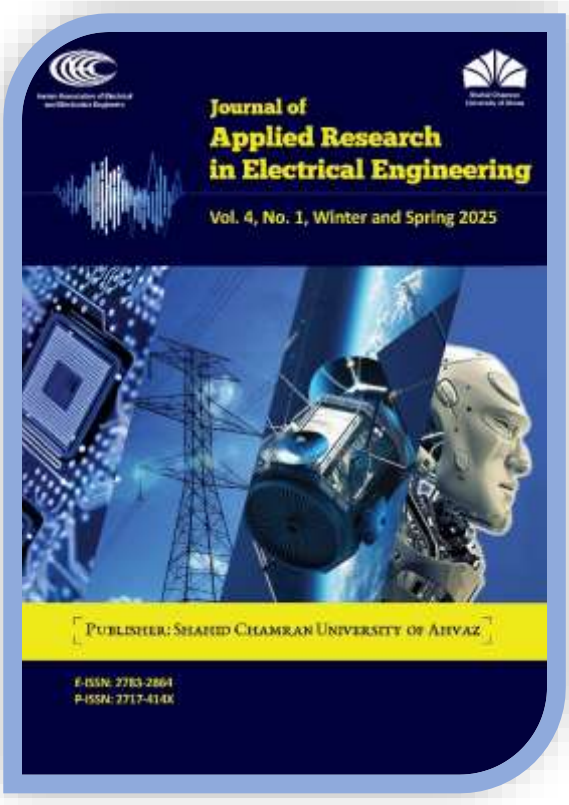
Journal of Applied Research in Electrical Engineering (JAREE), Volume 4, Number 1, Winter and Spring 2025

Publisher: Shahid Chamran University of Ahvaz, Iran

This magazine is the result of a formal partnership of **Shahid Chamran University of Ahvaz** and **Iranian Association of Electrical and Electronics Engineers**

Website: https://jaree.scu.ac.ir

E-mails: jaree@scu.ac.ir; jaree.scu@gmail.com



Address: **Department of Electrical Engineering, Faculty of Engineering, Shahid Chamran University of Ahvaz, Golestan Street, Ahvaz, Iran**
P.O. Box: **61357-85311**
Tel: **+986133226782, +989122876375**
Fax: **+986133226597**

Managing Committee and Staff



Editor-in-Chief

Prof. Mahmood Joorabian
Shahid Chamran University of Ahvaz, Ahvaz, Iran

Power System Planning, Renewable Energy and Smart Grid, FACTS Devises
mjoorabian@scu.ac.ir



Director-in-Charge

Prof. Seyed Ghodratolah Seifossadat
Shahid Chamran University of Ahvaz, Ahvaz, Iran

Power System Protection, Power Electronics, Power Quality
seifossadat@yahoo.com



Managing Editor

Dr. Alireza Saffarian)Associate Professor(
Shahid Chamran University of Ahvaz, Ahvaz, Iran

Power System Protection, Power System Stability, Power Quality, Distribution Systems
a.saffarian@scu.ac.ir



Executive Assistant

Dr. Hossein Farzin)Associate Professor(
Shahid Chamran University of Ahvaz, Ahvaz, Iran

Reliability of Power Systems, Microgrids and Distributed Energy Sources, Smart Grids
farzin@scu.ac.ir



Associate Editor
(Electronics and Telecommunications)

Prof. Yousef Seifi Kavian
Shahid Chamran University of Ahvaz, Ahvaz, Iran

Digital Circuits and Systems, Communication Networks and Distributed Systems
y.s.kavian@scu.ac.ir



Associate Editor
(Power and Control)

Prof. Mohsen Saniei
Shahid Chamran University of Ahvaz, Ahvaz, Iran

Power System Dynamics, High Voltage Engineering, Electricity Market, Microgrid
m.saniei@scu.ac.ir



Language Editor

Majid Sadeghzadeh Hemayati
English Language Editing

m_s_hemayati@yahoo.com



Page Designer

Mehdi Mohammadian Mehr
Shahid Chamran University of Ahvaz, Ahvaz, Iran

eng.mohammadianmehr@gmail.com



Executive Director

Masoomeh Shaygan
Shahid Chamran University of Ahvaz, Ahvaz, Iran

masoomeh.shaygan@gmail.com

Editorial Board



Prof. Mahmood Joorabian
Shahid Chamran University of Ahvaz, Ahvaz, Iran

Power System Planning, Renewable Energy and Smart Grid, FACTS Devises
mjoorabian@scu.ac.ir



Prof. Seyed Ghodratolah Seifossadat
Shahid Chamran University of Ahvaz, Ahvaz, Iran

Power System Protection, Power Electronics, Power Quality
seifossadat@yahoo.com



Prof. Saeedallah Mortazavi
Shahid Chamran University of Ahvaz, Ahvaz, Iran

Intelligent Control Systems, Power System Control, Automation, Fuzzy Logic, Neural Networks
mortazavi_s@scu.ac.ir



Prof. Abdolnabi Kosarian
Shahid Chamran University of Ahvaz, Ahvaz, Iran

Solid State Electronic Devices, Solar Cell Fabrication Technology
a.kosarian@scu.ac.ir



Prof. Ebrahim Farshidi
Shahid Chamran University of Ahvaz, Ahvaz, Iran

Analog and Digital Integrated Circuits, Data Converters, Microelectronics
farshidi@scu.ac.ir



Prof. Naser Pariz
Ferdowsi University of Mashhad, Mashhad, Iran

Nonlinear Control, Hybrid Systems, Aeronautics, Industrial Control, Applied Mathematics
n-pariz@um.ac.ir



Prof. Yousef Seifi Kavian
Shahid Chamran University of Ahvaz, Ahvaz, Iran

Digital Circuits and Systems, Communication Networks and Distributed Systems
y.s.kavian@scu.ac.ir



Prof. Mohsen Saniei
Shahid Chamran University of Ahvaz, Ahvaz, Iran

Power System Dynamics, High Voltage Engineering, Electricity Market, Microgrid
m.saniei@scu.ac.ir



Prof. Reza Ghaderi
Shahid Baheshti University, Tehran, Iran

Control Theory, System Identification, Control Systems, Fuzzy Engineering
r_ghaderi@sbu.ac.ir



Dr. Edris Pouresmaeil)Associate Professor(
Aalto University, Espoo, Finland

Integration of Renewable Energies into the Power Grid
edris.pouresmaeil@aalto.fi



Prof. Abbas Zarifkar
Shiraz University, Shiraz, Iran

Optical Electronics
zarifkar@shirazu.ac.ir



Prof. Fushuan Wen
Tallinn University of Technology, Tallinn, Estonia

Power Systems and Power Economics
fushuan.wen@taltech.ee



Prof. Majid Sanaye-pasand
University of Tehran, Tehran, Iran

Power Systems Protection, Digital Protective Relays, Power Systems Automation, Power System Transients
msanaye@ut.ac.ir



Prof. Zabih (Fary) Ghassemlooy
North Umbria University, Newcastle upon Tyne, United Kingdom

Optical Communications, Visible Light, Communication Systems
z.ghassemlooy@northumbria.ac.uk



Prof. Mahdi Tavakoli
University of Alberta, Alberta, Canada

Robotics and Telerobotics, Haptics and Teleoperation Control, Surgical and Therapeutic Robotics, Image-Guided Surgery
mahdi.tavakoli@ualberta.ca



Prof. Mohamad Hassan Modir Shanechi
Illinois Institute of Technology, Chicago, USA

Nonlinear and intelligent systems, Power system dynamics and security, Power system planning and maintenance scheduling
shanechi@iit.edu



Prof. Mohammad Shahidehpour
Illinois Institute of Technology, Chicago, USA

Power Systems, Microgrids, Power System Operation, Power System Planning
ms@iit.edu



Prof. Gholamreza Akbarizadeh
Shahid Chamran University of Ahvaz, Ahvaz, Iran

Image Processing, Machine Vision, SAR Satellite Imaging Systems and Remote Sensing, Machine Learning and Deep Learning
g.akbari@scu.ac.ir



Prof. Mohammad Soroosh
Shahid Chamran University of Ahvaz, Ahvaz, Iran

Photonic Crystals, Optoelectronics, Plasmonic Devices, Graphene, Photodetectors
m.soroosh@scu.ac.ir



Dr. Alireza Saffarian)Associate Professor(
Shahid Chamran University of Ahvaz, Ahvaz, Iran

Power System Protection, Power System Stability, Power Quality, Distribution Systems
a.saffarian@scu.ac.ir

About Journal

Journal of Applied Research in Electrical Engineering (J. Appl. Res. Electr. Eng.) is a single-blind peer-reviewed, open access and free of charge international journal published by Shahid Chamran University of Ahvaz in cooperation with Iranian Association of Electrical and Electronics Engineers (IAEEE). The JAREE is a medium for global academics to exchange and spread the latest discoveries and advances in their applied research in electrical engineering. The JAREE aims at presenting important results of analytical, computational and experimental works within all specialized fields of electrical engineering (electronics, power, control and telecommunications). It welcomes high quality original research papers from contributors throughout the world. All papers are subject to a peer reviewing procedure. Submission, processing and publication of the papers in JAREE is free of charge.

Types of accepted papers include:

- **Research articles**
- **Review articles**
- **Applied articles**

Research papers are expected to present innovative solutions, novel concepts, or creative ideas that can help to address existing or emerging technical challenges in electrical engineering.

Application papers are expected to share valuable industry experiences on dealing with challenging technical issues, developing/adopting new standards, applying new technologies or solving complex problems. JAREE welcomes application papers that can have a significant impact on industry practices in the coming years.

Review papers are expected to provide insightful and expert reviews, tutorials, or study cases on an important, timely and widely-interested topic in electrical engineering.

All researchers in the fields of electrical science are invited to publish their scientific and research achievements in this journal. Interested authors can submit their manuscripts in the journal's website. More information is available in the website on how to prepare and submit the manuscripts.

Amis and Scope

The *Journal of Applied Research in Electrical Engineering* aims to provide a medium for dissemination of innovative and consequential papers that present analytical, computational and experimental works within all specialized fields of electrical engineering (electronics, power, control and telecommunications). The scope of the journal includes, but is not limited to, the following topic areas:

Electronics:

- **Optical electronics, photonics and solar cells**
- **Integrated analog circuits and mixed signals**
- **Integrated radio frequency circuits**
- **Digital electronics (VLSI)**
- **Semiconductor devices**
- **Sensor technology**

Power:

- **Dynamics and stability of the power systems**
- **Power system protection**
- **Electric power quality**
- **Operation and planning of the power systems**
- **High voltage insulation technology**
- **Flexible AC Transmission Systems (FACTS)**
- **Electric power distribution systems**
- **Smart grids, micro-grids, renewable energies and distributed generation**
- **Reliability of electrical energy systems**
- **Energy management and electricity market**
- **Electric machines and transformers**
- **Power electronic and electric drives**

Control:

- **Linear and non-linear control systems**
- **Adaptive, optimal and stochastic control**
- **Fuzzy systems, neural networks and intelligent control**
- **Robotic and mechatronic**
- **Modeling, Identification and optimization of systems**
- **Guidance and navigation systems**
- **Automation, industrial control and instrumentation**

Telecommunications:

- **Signal and image processing**
- **Wireless and cellular communication systems**
- **Telecommunication networks**
- **Radar and sonar**
- **Information theory and coding**
- **Cognitive radio**
- **Antenna design**
- **Microwave devices**
- **Wave propagation and electromagnetic compatibility**

Indexing Databases and Social Networks

	Scopus: **JAREE articles are indexed in Scopus.** https://www.scopus.com/results/results.uri?st1=2783-2864&st2=&s=ISSN%282783-2864%29&limit=10&origin=searchbasic&sort=plf-f&src=s&sot=b&sdt=b&sessionSearchId=c250309f5b53a538326bd4219cbf8ffb
	Islamic World Science Citation Center (ISC): **JAREE articles are indexed in ISC.** https://mjl.isc.ac/Searchresult.aspx?Cond=2&SrchTxt=27832864
	Iran Ministry of Science, Research and Technology Scientific Journals: **(Journal Rank: International)** https://journals.msrt.ir/home/detail/16058/
	Directory of Open Access Journals (DOAJ): **JAREE articles are indexed in DOAJ.** https://doaj.org/toc/2783-2864
	Google Scholar: https://scholar.google.com/citations?user=F7KQPtYAAAAJ&hl=en&authuser=1
	Directory of Open Access Scholarly Resources (ROAD): https://portal.issn.org/resource/ISSN/2783-2864
	Elton B. Stephens Company (EBSCO): https://jaree.scu.ac.ir/news?newsCode=204
	CIVILICA: https://en.civilica.com/l/140583/
	National Publications Information Bank (magiran): https://www.magiran.com/magazine/8471
	Digital Object Identifier (DOI): https://www.doi.org/
	Zeitschriften Datenbank (ZDB) https://zdb-katalog.de/title.xhtml?idn=125396940X&direct=true&view=full
	Electronic Journals Library (EZB) https://ezb.ur.de/?3114079-8
	Système Universitaire de Documentation (SUDOC) https://www.sudoc.abes.fr/cbs/DB=2.1/SET=1/TTL=1/LNG=EN/NXT
	OPENALEX https://openalex.org/sources/S7407060855
	LinkedIn: https://www.linkedin.com/in/journal-of-applied-research-in-electrical-engineering-jaree-7540871b2/
	Academia: https://shahidchamranahwaz.academia.edu/JournalAppledResearchinElectricalEngineering

Indexing Databases and Social Networks (Continued)

	**Mendeley:** https://www.mendeley.com/profiles/journal-of-applied-res-in-electrical-engineer/
	**Twitter:** https://twitter.com/jaree_scu
	**Facebook:** https://www.facebook.com/jaree.scu
	**Researchgate:** https://www.researchgate.net/profile/Jaree_Engineering
	**Telegram:** https://t.me/jareescu
	**Instagram:** https://www.instagram.com/jaree.scu/
	**Journal homepage:** https://jaree.scu.ac.ir

Guide for Authors

How to submit a manuscript

For the initial submission, the authors have to just send the main manuscript file and the signed Copyright Form of the journal. While preparing manuscripts for initial submission, authors are kindly requested to follow the guidelines, described below:

- **The manuscript should be written in a Microsoft Word file (.doc or .docx).**
- **The file should include text (preferably in 10 points, "Times New Roman" font) and all figures (figures can be placed within the text at the appropriate point or at the end of the text).**
- **The manuscript pages should be prepared either using a double-column single-line spacing layout or a single-column double-line spacing layout. A margin of at least 1.5 cm on each side is required.**
- **All papers should be composed of Title, Author Name, Affiliation, Corresponding author email, Abstract, Keywords, Body, and References.**
- **The manuscript should be written in good English. It should have been carefully checked for clarity, conciseness, the correctness of grammar, and typographical errors.**
- **The corresponding author should sign the journal copyright form on behalf of any and all co-authors and upload it to the Journal's Submission System when submitting the manuscript. The journal copyright form can be downloaded from here.**
- **The corresponding author can use the JAREE Template for Cover Letter as a default text for the cover letter when submitting the manuscript.**
- **It is recommended that the title of the paper does not contain abbreviations or formulae.**
- **The abbreviations used in the abstract should be introduced both in the abstract and again on first use in the body.**
- **References should be numbered in the order they are mentioned in the text.**

Manuscript Submission

Submission to this journal proceeds totally online and you will be guided stepwise through the creation and uploading of your files. All correspondence, including notification of the Editor's decision and requests for revision, takes place by e-mail. To submit your manuscript, click on the Submit Manuscript link on the journal's homepage. Then, click on Register to create an author account. A message is sent to your email address containing your username and password. Then, login to the Journal's Submission System at the User's login page using the username and password to submit your new manuscript. Once you have logged in, you can change your password by clicking on the My Home link at the top menu.

Copyright and Open Access License

An author submitting a paper should ensure that he or she has the right to submit the paper to JAREE and that it contains nothing defamatory. The JAREE will assume that all co-authors have agreed to the submission of any paper received. The corresponding author should sign the journal copyright form on behalf of any and all co-authors and upload it to the Journal's Submission System when submitting the manuscript.

Contents

Article Title and Authors	Page No.
A Hybrid Technique Combining Robust and DNN for Thyroid Disease Prediction on Imbalanced Dataset Elahe Moradi	**1**
An Algorithm for Determining the Desirability of the Amount of Transient Limiting Reactors in Shunt Capacitor Banks Sadegh Rekabeslami Zadeh, Gholamali Torabi, Sasan Najafi Birgani, Mehdi Enayat Zare, Mostafa Sarlak	**11**
Deep Learning based Underwater Object Detection and Recognition for Multi-Robot Systems Valimohammad Nazarzehi Had, Zobeir Raisi	**24**
A Review on Blockchain-based Gaming: Existing Insights, Deficits, and Emerging Avenues Patikiri Arachchige Don Shehan Nilmantha Wijesekara	**34**
Performance Evaluation of a PV-Based Multilevel Inverter with Improved THD and Efficiency Parimalasundar Ezhilvannan, Kumar Reddy Cheepati, Suresh Krishnan	**56**
Power Resource Allocation in Downlink NOMA Systems Using Joint Sum-Rate and Bit-Error-Rate Optimization Mohammad Hasheminejad, Mohsen Sheikh-Hosseini	**69**
Constrained MIMO Reference-Based Offline Steady–State (RBOSS) NMPC for PMSM using Voltage Source Inverter Stephen Ofori, Francis Boafo Effah, Daniel Opoku	**76**
Compact Two-Stage CMOS Operational Amplifier with Enhanced Gain and Bandwidth via Cascode and Negative Capacitance Techniques MohammadMehdi Derakhshannia, Mohsen Shakiba, Maryam Shakiba	**86**
Texture Classification Using Deep Learning and Enhanced Local Binary Pattern Behzad Abbasi, Majid Ghandchi, Sirous Tannaz, Javad Ostadieh, Saeed Barghandan	**94**
Enhancing Integration of Advanced Power Control Strategies for High-Penetration Photovoltaic System in Power Grid Naveen Kumar Bind, Anil Kumar	**106**
Comparative Analysis of Various Optimization Techniques for Battery Management Systems in Electrical Vehicles Mohammad Junaid Khan, Ram Murat Singh, Md Naqui Akhtar, Asyraf Afthanorhan	**122**
Optimal Energy Management in Solar-powered Battery-Ultracapacitor Hybrid Electric Vehicles: Leveraging ANN-HDKR for Tilt Angle Optimization Shraddha Kaushik, Kunamneni Rachnanjali	**137**

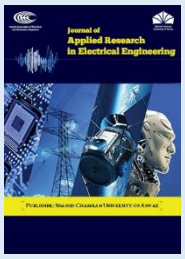
Copyrights
© 2025 Licensee Shahid Chamran University of Ahvaz, Ahvaz, Iran. This article is an open-access article distributed under the terms and conditions of the Creative Commons Attribution –Non-Commercial 4.0 International (CC BY-NC 4.0) License (http://creativecommons.org/licenses/by-nc/4.0/).

Shahid Chamran University of Ahvaz

Iranian Association of Electrical and Electronics Engineers

Journal of Applied Research in Electrical Engineering

E-ISSN: 2783-2864
P-ISSN: 2717-414X
Homepage: https://jaree.scu.ac.ir/



Research Article

A Hybrid Technique Combining Robust and DNN for Thyroid Disease Prediction on Imbalanced Dataset

Elahe Moradi [1,*]

[1] *Department of Electrical Engineering, YI.C., Islamic Azad University, Tehran, Iran*

* *Corresponding Author: Elahe.Moradi@iau.ac.ir*

Abstract: Thyroid disease poses an important public health risk, reducing the quality of life and increasing healthcare expenditures. In recent years, Artificial Intelligence (AI) algorithms have become essential tools for diagnosing and predicting thyroid disease. Although various AI-based algorithms have been applied to this task, their performance is often hindered by imbalanced data. This research proposes a hybrid approach that combines robust techniques and Deep Neural Networks (DNN) to address this challenge in thyroid disease prediction. The present paper employs the publicly available thyroid disease dataset, obtained from the University of California, Irvine machine learning repository. To manage the data imbalance, Random Under (RU) and Random Over (RO) sampling techniques are applied. A comparative analysis reveals that the hybrid approach, combining robust and DNN with RO sampling, significantly outperforms the RU sampling method on the imbalanced dataset. To assess the effectiveness of the proposed technique, the variant criteria are employed such as accuracy, F1-score, recall, precision, Area Under Curve (AUC), confusion matrix, and Receiver Operating Characteristic (ROC) curve. The hybrid approach achieves superior results, with a testing accuracy of 98.71%, recall of 100%, precision of 97.45%, and an F1-score of 98.71%. These findings demonstrate the robustness and effectiveness of the approach, underscoring its potential for real-time disease prediction.

Keywords: Deep Neural Network (DNN), Robust, Prediction, Imbalanced Dataset, Thyroid Disease, Accuracy.

Article history
Received 21 September 2024; Revised 06 June 2025; Accepted 01 September 2025; Published online November 8, 2025.
© 2025 Published by Shahid Chamran University of Ahvaz & Iranian Association of Electrical and Electronics Engineers (IAEEE)
How to cite this article
E. Moradi, "A hybrid technique combining robust and DNN for thyroid disease prediction on imbalanced dataset," *J. Appl. Res. Electr. Eng.*, vol. 4, no. 1, pp. 1-10, 2025. DOI: 10.22055/jaree.2025.48019.1138



1. INTRODUCTION

The thyroid gland is one of the main glands of the body, which indirectly affects all the organisms of the body, such as the heart and kidneys. Thyroid disorders can slow or speed up metabolism. When hormone levels are too low or too high, the signs of this disorder can be seen in hyperactivity and hypoactivity. The most common thyroid diseases include hypothyroidism, hyperthyroidism, thyroid gland enlargement (goiter), thyroid masses, thyroid cancer, and thyroid inflammation (thyroiditis) [1, 2]. Recently, techniques based on data mining and artificial intelligence algorithms such as machine learning, deep learning, and reinforcement learning have attracted the attention of many researchers in the diagnosis of diseases [3, 4]. These algorithms can discover patterns in medical data and thereby improve the decision-making process. Therefore, they can influence treatment costs and increase the quality of medical care [5-8].

Several data-driven algorithms for the prediction and diagnosis of thyroid disease have been discussed in the literature. In [9], the authors presented five machine learning algorithms including Support Vector Machine (SVM), K-Nearest Neighbor (KNN), Random Forest (RF), Logistic Regression (LR), and Multilayer Perceptron (MLP) for diagnosis thyroid disease. The results displayed SVM had the best effect of diagnosing this disease with an accuracy rate of 92%. The authors of [10] studied seven AI models including Decision Tree (DT), SVM, KNN, MLP, RF, Gaussian Process, and XGBoost. Among them, RF algorithm performed the best with the accuracy 81.30%. In [11], two different classifiers including Naïve Bayes (NB), and KNN were analyzed for thyroid disease detection and the results exhibited that KNN was the most accurate classifier with 93.44% accuracy. In [12], the authors employed eleven AI algorithms to normalize which one achieved the best accuracy for diagnosing thyroid disease and the artificial neural

network classifier obtained the highest accuracy with a value of 95.87%. In [13], the authors compared two machine learning methods, decision tree and random forest, to enhance the accuracy of thyroid disease detection. A thyroid dataset from the UCI machine learning repository was utilized in the study, with the random forest model achieving an accuracy of 85%.

In [14], the authors classified thyroid disease into four categories: hyperthyroid, hypothyroid, euthyroid patient and euthyroid. They did this by using a multi-class support vector machine. A high accuracy of 83.37% in a high-dimensional feature space was displayed in the results of training the proposed approach with a dataset from the UCI repository. To do a comparative analysis for improved thyroid disease prediction, several machines learning techniques, including decision trees, random forests, KNN, and artificial neural networks, were applied to the dataset in [15]. For a more comparison, classification was done on both the sample and non-sample datasets. Following the dataset's preprocessing, the random forest technique produced the best results, with an accuracy rate of 94.8%. The three machine learning methods for thyroid texture segmentation and classification that the authors compared in [16] were support vector machine, artificial neural network, and random forest classifier. Employing a feature extraction technique, they extracted features to train the classifiers. The technique achieved an accuracy of about 90% across all three approaches. The authors of [17] explored the potential predictive value of thyroid hormones in clinical outcomes using a retrospective analysis of 2,086 inpatients. They employed supervised learning techniques to create a prediction model that included sensitivity and specificity of 91%, 79%, and 0.86 on the ROC-AUC. In [18], the authors evaluated a proposed feature technique using ten machine learning classifiers. The dataset consisted of 2,211 instances from 247 patients treated at a Naples hospital. Due to class imbalance, the Synthetic Minority Oversampling Technique (SMOTE) was applied to oversample the minority class. Among the tested models, the EXTC model demonstrated the best performance with an F-score of 84%.

In [19], the authors developed diagnostic models for the thyroid disease via multilayer perceptron technique. The study found that the genetic algorithm with multilayer perceptron model achieved a classification accuracy of 95%, outperforming the particle swarm optimization with multilayer perceptron model, which reached 85.5%. In [20], the authors investigated a deep learning model using a modified ResNet-based Convolutional Neural Network (CNN) to detect five types of thyroid diseases. The training process was optimized using dual optimizers, Adam and Stochastic Gradient Descent (SGD), to enhance accuracy. The proposed model achieved 97% accuracy after retraining with SGD, compared to 94% with the standard ResNet. In [21], a sequential Convolutional Neural Network (CNN) method was assessed for detecting thyroid abnormalities, leveraging its ability to automate feature extraction and focus on regions-of-Interest. The proposed technique achieved an accuracy of 81.5%, with a precision of 97.4% and a sensitivity of 83.1%, demonstrating its effectiveness in classifying. Enhanced data segmentation employing K-means clustering improved scalability and efficiency with large medical datasets. The hybrid technique displayed an improvement in diagnostic accuracy and precision, with performance gains of approximately 15-20% over traditional methods.

In [22], a deep neural network (DNN) model was developed to predict thyroid disease using demographic data from an imbalanced dataset. The model incorporated various sampling techniques and activation functions, achieving a classification accuracy of 93.90% and outperforming the Random Forest (RF) baseline by 36.63% in lift performance. In [23], thyroid disease prediction was performed using both machine learning and deep learning methods. Among the evaluated models, Random Forest and Recurrent Neural Networks (RNN), combined with SMOTE for data balancing, achieved the highest classification performance with accuracies of 98.16% and 97%, respectively. In [24], the authors employed the synthetic minority oversampling technique (SMOTE-NC) technique to address data imbalance and applied a deep learning model based on Long Short-Term Memory (LSTM) for thyroid disease prediction, achieving an accuracy of 93%. Furthermore, the study reported that the Light Gradient Boosting Machine (LGBM) outperformed the LSTM model, demonstrating higher predictive accuracy in the same experimental setting. In [25], a novel hybrid model named TDIP, integrating Long Short-Term Memory (LSTM) and Support Vector Machine (SVM), was proposed for thyroid disease classification. To address class imbalance, the study applied SMOTE and employed Bidirectional Feature Elimination for optimal feature selection. The combined approach effectively enhanced model performance, achieving a classification accuracy of 97%.

Existing research shows that predictive accuracy requires further improvement when conventional techniques are applied, as prediction accuracy plays a critical role in the application of AI algorithms in medicine. Furthermore, the features of thyroid disease datasets exhibit wide ranges and the presence of outliers. Previous works have commonly utilized normalization and standardization techniques. Therefore, it is essential to explore algorithms that can ensure robustness in the presence of outliers. Additionally, considering the imbalanced nature of the dataset, appropriate balancing techniques are essential. In many previous studies, synthetic minority oversampling technique has been predominantly used.

The main objectives of this research can be summarized as follows:

- Tackling the challenges of imbalanced data: The focus is on addressing the limitations posed by imbalanced datasets, a frequent challenge in disease prediction. In this study, both random over (RO) sampling and random under (RU) sampling are used to generate synthetic samples, and balance the dataset, leading to a more robust predictive algorithm.
- Employing Robust technique in dataset preprocessing: The application of this technique on the thyroid disease dataset, in the presence of outliers, leads to improved performance and enhanced accuracy of the proposed algorithm.
- Developing an improved prediction method for thyroid disease: This research introduces a hybrid technique combining robust and deep neural networks with RO

sampling to improve thyroid disease prediction and diagnosis.

This study is structured as follows: Section 2 provides an overview of the dataset for thyroid disease and explores the application of hybrid deep neural network techniques combined with data balancing methods to enhance performance. Section 3 presents the results and discusses the efficacy of the proposed methods. Finally, Section 4 concludes the research.

2. THYROID DISEASE DATASET AND PROPOSED TECHNIQUES

In this section, the thyroid disease dataset and the techniques applied in the present paper are presented.

2.1. Thyroid Disease Dataset

This study utilizes the thyroid dataset from the University of California, Irvine (UCI) Machine Learning repository [26]. The dataset includes 3772 instances with 29 attributes as input features, supports binary classification. In the thyroid disease dataset, the target variable was categorical, where 'P' denoted the presence of hypothyroidism and 'N' indicated its absence. The attributes included factors such as age, sex, thyroxine medication, query on thyroxine, sick, thyroid surgery, antithyroid medications, query hyperthyroid, treatment, pregnant, query hypothyroid, TSH measured, TSH (actual TSH value), T3, referral source, TT4 measured, T4U, T3 measured, TBG, TT4, FTI measured, TBG measured, T4U measured, FTI, lithium, tumor, goiter, psych, and hypopituitary, all assessed based on their corresponding blood levels. Hypothyroidism served as the target variable [12, 26]. The thyroid dataset consists of 3772 instances, with 92.29% (3481 samples) are classified as 'P', and only 7.71% (291 samples) are classified as 'N', indicating a significant class imbalance in the dataset. Fig. 1 depicts the distribution of the imbalanced dataset for each class in this binary classification. Fig. 2 illustrates the flowchart of the hybrid DNN techniques proposed for thyroid disease prediction. This diagram presents the overall workflow, including data preprocessing, class balancing, model training, and performance evaluation steps designed to improve predictive accuracy on an imbalanced dataset.

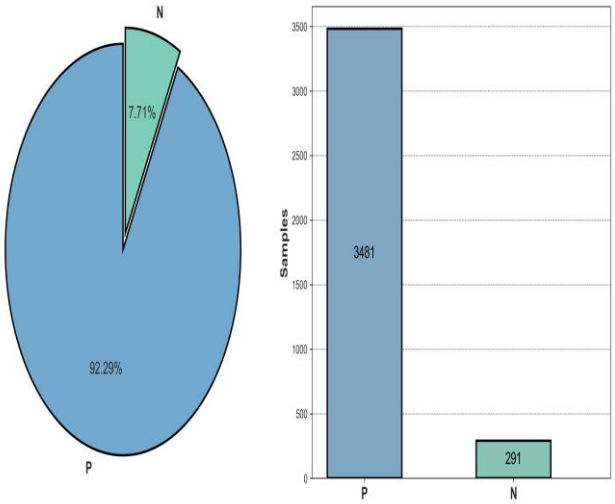


Fig. 1: Distribution of imbalanced thyroid dataset.

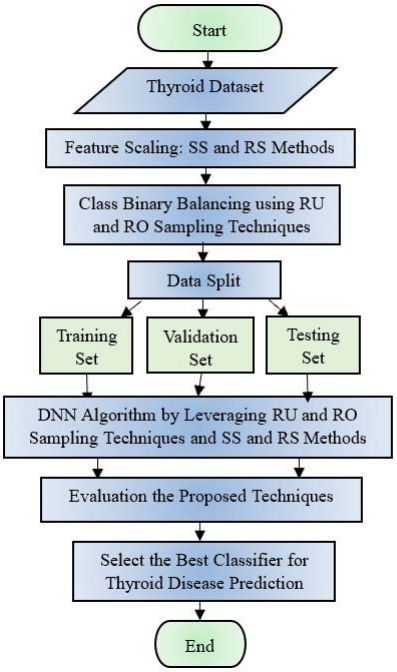


Fig. 2: Flowchart of the hybrid DNN techniques for Thyroid disease prediction.

2.2. Proposed Techniques

Outliers present in the thyroid dataset adversely influence the classifier's training, leading to longer training times and diminishing performance. Furthermore, some features have large values and a wide range, which further exacerbates the increase in training durations. As a result, the implementation of a robust feature scaling technique is required.

- **Feature Scaling**

In previous research, common feature scaling techniques such as normalization scaling and standard scaling (SS) were applied to the thyroid disease dataset. In this study, due to the presence of outliers in the public dataset, the robust scaling (RS) method is proposed, which demonstrates superior performance compared to the two conventional scaling techniques. Robust scaling approach addresses the problem of outliers by using the median and quartiles. This technique scales data based on the interquartile range (IQR), which is the difference between the third quartile (Q_3) and the first quartile (Q_1), rather than relying on the mean. The mathematical formulation of the robust scaling equation is as follows:

$$x_{rs} = \frac{x - Q_1}{Q_3 - Q_1} \quad (1)$$

Here, x denotes the main value, and x_{rs} is the scaled value [27, 28]. This paper will compare two scaling techniques, standardization and robust scaling, along with dataset balancing methods applied to the thyroid disease dataset in Section 3.

- **RU and RO Sampling Techniques**

The imbalance refers to the unequal distribution of data across classes, which can significantly impair the performance of the classifiers, often biasing them toward the

class with more data. Therefore, balancing the dataset is crucial for improving the predictive performance in thyroid disease diagnosis. In this paper, random over and random under sampling techniques have been applied to balance the dataset.

Under sampling is a popular method for addressing class imbalance issues. It selects a subset of the majority class, resulting in high efficiency. The major limitation is that many majority class samples are discarded. By decreasing the size of the dominant class, under sampling achieves dataset balance. Retaining all instances from the minority class while randomly selecting an equal number of instances from the majority class creates a balanced dataset, suitable for further analysis [29]. Over sampling approach seeks to balance the dataset by increasing the representation of minority class samples. Instead of eliminating the abundant instances, new unique data points are generated through techniques such as resampling, bootstrapping, or the synthetic minority over-sampling [30].

The algorithms below formalize the implementation details of both class - balancing strategies employed in this study. Algorithm 1 specifies the RU Sampling procedure, which systematically reduces majority - class instances to equalize class proportions. Algorithm 2 outlines the RO Sampling procedure, which incrementally replicates minority - class instances until parity with the majority class is achieved.

Algorithm 1: Random Under (RU) Sampling Technique for Balancing Thyroid Dataset

Input:
- Original dataset $\mathcal{D} = \{(x_i, y_i)\}$ where $x_i \in \mathbb{R}^m$ represents feature vector, and $y_i \in \{0, 1\}$ represents class label.

Output:
- Balanced dataset $\mathcal{D}_{RU}$ with equal representation of minority and majority classes.

1. Identify minority and majority classes:
   - Let $\mathcal{D}_{min} = \{(x_i, y_i) \in \mathcal{D} | y_i = minority\ class\}$.
   - Let $\mathcal{D}_{maj} = \{(x_i, y_i) \in \mathcal{D} | y_i = majority\ class\}$.
2. Determine target sample count:
   - $n_{min} = |\mathcal{D}_{min}|$ (number of minority samples).
   - $n_{maj} = |\mathcal{D}_{maj}|$ (number of majority samples).
   - Set target_count $= n_{min}$.
3. Randomly under sample the majority class:
   - Shuffle $\mathcal{D}_{maj}$.
   - Select the first target_count samples from shuffled $\mathcal{D}_{maj} \rightarrow \mathcal{D}_{majSub}$.
4. Construct the balanced dataset:
   - $\mathcal{D}_{RU} = \mathcal{D}_{min} \cup \mathcal{D}_{majSub}$.
5. Return $\mathcal{D}_{RU}$.

Algorithm 2: Random Over (RO) Sampling Technique for Balancing Thyroid Dataset

Input:
- Original dataset $\mathcal{D} = \{(x_i, y_i)\}$ where $x_i \in \mathbb{R}^m$ represents feature vector, and $y_i \in \{0, 1\}$ represents class label.

Output:
- Balanced dataset $\mathcal{D}_{RO}$ with equal representation of minority and majority classes.

1. Identify minority and majority classes:
   - Let $\mathcal{D}_{min} = \{(x_i, y_i) \in \mathcal{D} | y_i = minority\ class\}$.
   - Let $\mathcal{D}_{maj} = \{(x_i, y_i) \in \mathcal{D} | y_i = majority\ class\}$.
2. Determine target sample count:
   - $n_{min} = |\mathcal{D}_{min}|$ (number of minority samples).
   - $n_{maj} = |\mathcal{D}_{maj}|$ (number of majority samples).
   - Set $target_{count} = n_{maj}$.
3. Randomly oversample the minority class:
   - Initialize $\mathcal{D}_{minRep} = \mathcal{D}_{min}$.
   - While $|\mathcal{D}_{minRep}| < target_count$:
     - Shuffle $\mathcal{D}_{min}$.
     - For each sample (x, y) in shuffled $\mathcal{D}_{min}$:
       - Append a copy of (x, y) to $\mathcal{D}_{minRep}$.
       - If $|\mathcal{D}_{minRep}| = target_count$, break.
4. Construct the balanced dataset:
   - $\mathcal{D}_{RO} = \mathcal{D}_{maj} \cup \mathcal{D}_{minRep}$.
5. Return $\mathcal{D}_{RO}$.

Table 1 presents the number of samples in the original (imbalanced) and balanced datasets through the RU and RO sampling techniques. Figs. 3 and 4 demonstration the balanced distribution of the thyroid dataset achieved through the RU sampling method and the RO sampling method.

- **Dataset Splitting for Thyroid Disease Prediction**

After applying standard scaling and robust scaling methods, as well as random under (RU) and random over (RO) sampling techniques to the thyroid dataset, the data was split into testing and training sets with an 80:20 ratio.

Table 1: Imbalanced and balanced instances of thyroid disease.

	Total number of instances	Minority of instances	Majority of instances	Ratio of majority to minority instances
Imbalanced samples	3772	291	3481	11.96
RU sampling method	582	291	291	1.00
RO sampling method	6962	3481	3481	1.00

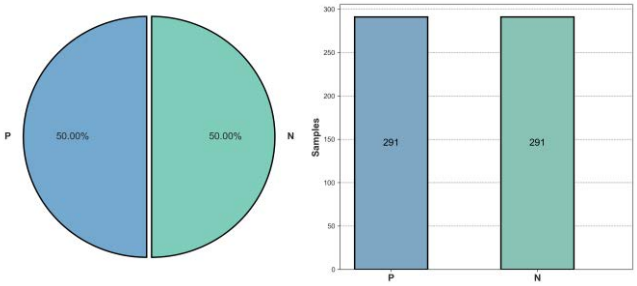


Fig. 3: Distribution of balanced thyroid dataset using RU sampling method.

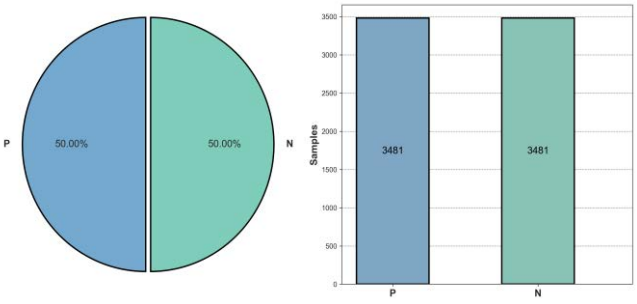


Fig. 4: Distribution of balanced thyroid dataset using RO sampling method.

The training set was further divided into training and validation subsets in an 85:15 ratio. All experiments, aimed at comparing deep neural network algorithms, were conducted using Jupyter Notebook and the Python programming language. Pre-processing was carried out using Python libraries, such as NumPy, Pandas, Matplotlib, and Seaborn. The Scikit-learn library, along with Keras and TensorFlow, was used for training of the DNN algorithm.

- **Deep Neural Network algorithm**

Most prior studies on thyroid disease prediction have predominantly utilized classical machine learning algorithms. This paper, leverages deep neural networks (DNN), a subset of deep learning, to classify the dataset and detect thyroid disease. Fig. 5 illustrates the overall architecture of the DNN used in this study, consists of one input layer, two hidden layers, and one output layer. A sequential approach was used to initialize the model and build the layers. In the proposed algorithm, the number of neurons in the input layer was aligned with the features of the dataset. The first hidden layer comprised 256 neurons, the second hidden layer contained 64 neurons, and the output layer, designed for the classification of the thyroid dataset, featured a single neuron. The activation of the input and hidden layers was facilitated by a Rectified Linear Unit (ReLU) function, which processes inputs by converting any negative values to zero. The ReLU function is mathematically defined as:

$$ReLu(x) = \max(0, x) \quad (2)$$

The output layer utilized a sigmoid activation function, defined as follows:

$$sigmoid(x) = \frac{1}{1 + e^{-x}} \quad (3)$$

Here, x is equal value of the sum of weighted, and e is equal Euler's number [16].

To prevent overfitting, a dropout layer was added after each layer. For optimization, the Adam optimizer was applied for training the deep learning algorithm. The loss was calculated using binary cross-entropy, while accuracy served as the metric for evaluating the algorithm. The model was trained for 300 epochs, with a batch size of 32, a learning rate of 0.001, and a validation split of 0.15. Deep neural network classification was performed by Python 3.9.12, leveraging libraries such as Scikit-learn, Keras, and TensorFlow for algorithm development and evaluation. To provide a concise overview of the experimental setup, all key parameters used in the proposed deep neural network algorithm are summarized in Table 2.

- **Performance Assessment Metrics**

This study utilizes various measures, including accuracy, precision, F1-score, recall, receiver operating characteristic (ROC) curve, and area under the curve (AUC) to assess the performance of robust artificial intelligence methods applied to the thyroid dataset. Also, the performance of the proposed algorithms is evaluated using the confusion matrix, as shown in Table 3. To define the metric formulas, it is essential to first outline the main components of the confusion matrix. TP, TN, FP, and FN indicate true positive, true negative, false positive, and false negative, respectively.

Table 2: Parameters for the proposed deep neural network algorithm.

No.	Parameter	Value / Description
1	Activation Function (Hidden)	ReLU
2	Activation Function (Output)	Sigmoid
3	Optimizer	Adam
4	Loss Function	Binary Cross-Entropy
5	Learning Rate	0.001
6	Batch Size	32
7	Epochs	300
8	Hidden Layer 1 Neurons	256
9	Hidden Layer 2 Neurons	64
10	Output Layer Neurons	1

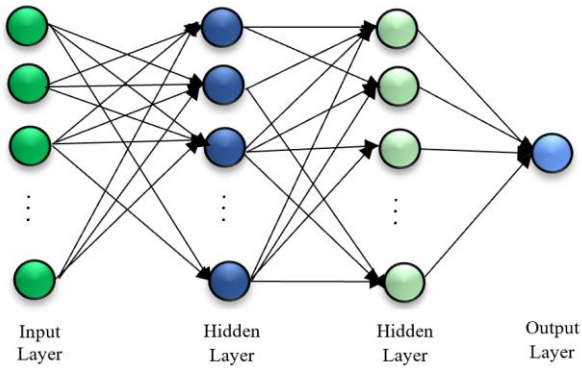


Fig. 5: Deep neural network for thyroid disease prediction.

- **Performance Assessment Metrics**

This study utilizes various measures, including accuracy, precision, F1-score, recall, receiver operating characteristic (ROC) curve, and area under the curve (AUC) to assess the performance of robust artificial intelligence methods applied to the thyroid dataset. Also, the performance of the proposed algorithms is evaluated using the confusion matrix, as shown in Table 3. To define the metric formulas, it is essential to first outline the main components of the confusion matrix. TP, TN, FP, and FN indicate true positive, true negative, false positive, and false negative, respectively.

Accuracy serves as a measure of the model's overall proficiency, signifying the percentage of the test dataset that the model accurately classifies. Correctly identified instances are termed TP and TN, whereas misclassified instances are FP and FN. Accuracy is determined as follows:

$$Accuracy\ (\%) = \frac{TP + TN}{TP + FP + TN + FN} \times 100 \quad (4)$$

Table 3: The confusion matrix.

		Actual Class	
		+	-
Predicted Class	+	**TP**	**FP**
	-	**FN**	**TN**

Conversely, precision and recall seek to capture the proportion of TP and TN. Precision, in particular, assesses the classifier's ability to refrain from incorrectly labeling negative instances as positive, and it is defined as follows:

$$Precision\ (\%) = \frac{TP}{TP + FP} \times 100 \quad (5)$$

Alternatively, recall quantifies the sensitivity of the model. It represents the proportion of correctly predicted instances for a given class relative to the total occurrences of that class, and is expressed as follows:

$$Recall\ (\%) = \frac{TP}{TP + FN} \times 100 \quad (6)$$

The F1-score, primarily used for comparing classifier models rather than global precision, reflects the weighted harmonic average of the Precision and Recall metrics. By giving more importance to lower values, the F1-score ensures that a classifier achieves a high score only when both precision and recall are strong. The formula is defined as follows [18, 20]:

$$F1 - measure\ (\%) = 2 \times \frac{1}{(1/Precision) + (1/Recall)} \times 100 \quad (7)$$

Furthermore, a thorough evaluation of the hybrid algorithms is conducted using the AUC and ROC curve, providing a comprehensive analysis of their performance.

3. Results and Discussion

After preprocessing the thyroid disease dataset, which includes examining missing values and outliers, feature scaling is performed using both standard scaling and robust scaling methods. Due to the imbalance in the binary classes, the dataset is balanced utilizing the RU and RO sampling techniques. Subsequently, the data is partitioned into three segments including training, validation, and testing, employing the train-test split function from the Scikit-learn framework in Python. Finally, the deep neural network algorithm is applied in four scenarios to evaluate the prediction of thyroid disease using various classifier metrics. The following are the four hybrid approaches used for the classification of thyroid disease in this study:

- Hybrid technique deep neural network and RU sampling, by leveraging standard scaling,
- Hybrid technique deep neural network and RU sampling, by leveraging robust scaling,
- Hybrid technique deep neural network and RO sampling, by leveraging standard scaling,
- Hybrid technique deep neural network and RO sampling, by leveraging robust scaling.

Table 4 presents a comparison and evaluation of the deep neural network algorithm across the four specified scenarios, utilizing metrics including accuracy, recall, F1-score, and precision. In Table 5, the performance of the hybrid deep neural network techniques is assessed using two criteria: AUC and computational time, providing a more comprehensive comparison. Figs. 6 and 7 illustrate the comparison and evaluation of the performance of four hybrid deep neural network techniques based on classifier metrics. It is evident that the hybrid deep neural network approach utilizing RO sampling and robust scaling achieves superior performance among the proposed hybrid techniques.

Table 4: Assessment of the proposed techniques.

Techniques	Assessment criteria (%)			
	Accuracy	Precision	Recall	F1-score
RU_SS	94.87	96.23	92.73	94.44
RU_RS	95.73	94.64	96.36	95.50
RO_SS	98.64	97.31	100.00	98.64
RO_RS	98.71	97.45	100.00	98.71

Table 5: Comparison of AUC and computational time for the proposed techniques.

Criteria	Techniques			
	RUS_SS	RUS_RS	ROS_SS	ROS_RS
AUC (%)	97.62	98.21	99.08	99.31
Computational Time (s)	21.11	22.42	143.18	141.72

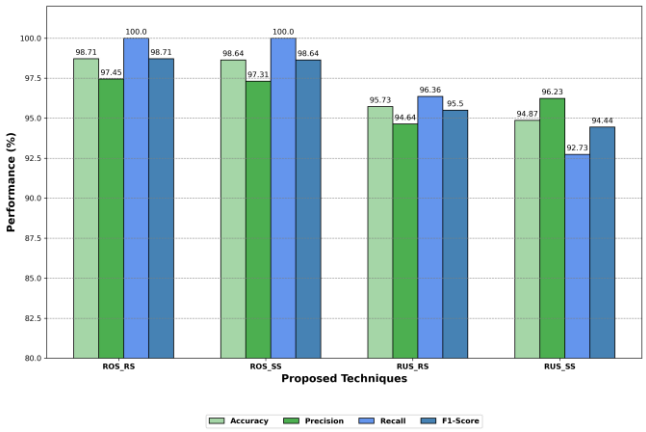


Fig. 6: Performance evaluation of the proposed techniques on thyroid dataset.

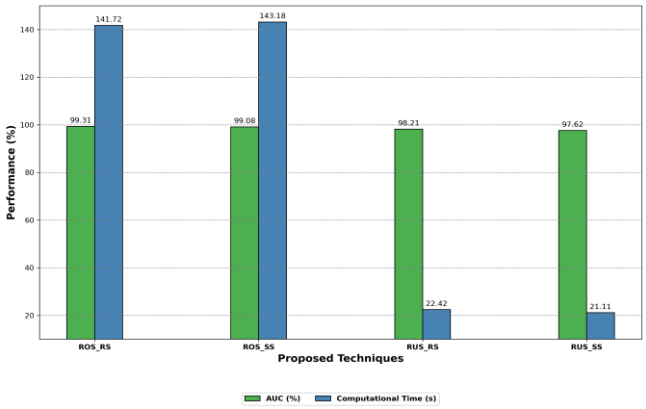


Fig. 7: Comparison AUC (%), and computational time of the proposed techniques on thyroid dataset.

It is also worth mentioning that the two hybrid deep neural network techniques employing RO sampling, in conjunction with both standard scaling and robust scaling methods, outperform the hybrid techniques using RU sampling in classifying the thyroid disease dataset. Nevertheless, the RU sampling hybrid models show computational times approximately one-seventh of their RO sampling counterparts. For a more comprehensive evaluation, Figs. 8, 9, 10, and 11 present the ROC curves and confusion matrices of the proposed techniques, demonstrating the advantage of the hybrid deep neural network technique utilizing RO sampling and robust scaling.

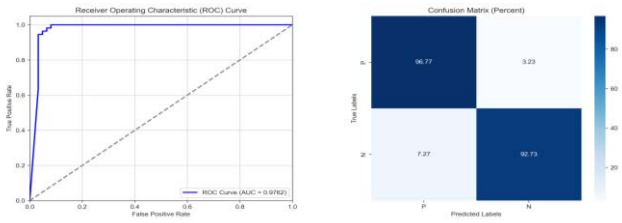


Fig. 8: ROC curve and confusion matrix of hybrid DNN technique utilizing RU sampling and SS.

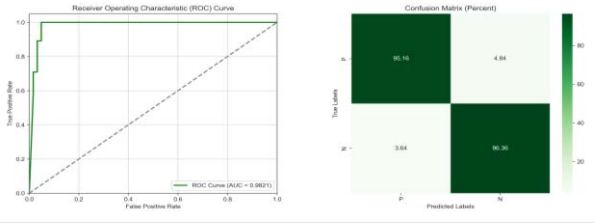


Fig. 9: ROC curve and confusion matrix of hybrid DNN technique utilizing RU sampling and RS.

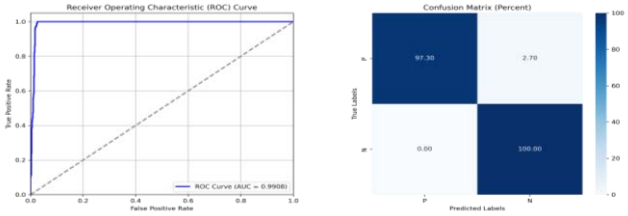


Fig. 10: ROC curve and confusion matrix of hybrid DNN technique utilizing RO sampling and SS.

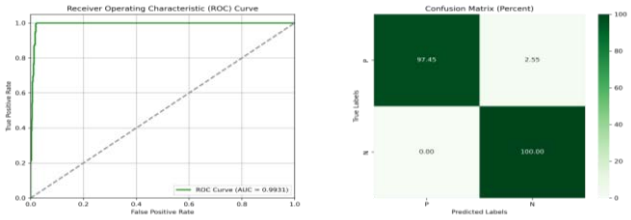


Fig. 11: ROC curve and confusion matrix of hybrid DNN technique utilizing RO sampling and RS.

Figs. 12, 13, 14, and 15 illustrate the accuracy curves for the training and testing techniques of deep neural networks utilizing RU sampling with standard scaling (SS), RU sampling with robust scaling (RS), RO sampling with standard scaling (SS), and RO sampling with robust scaling (RS), respectively. These findings indicate that the deep neural networks using RO sampling with RS achieve the best performance after 300 epochs.

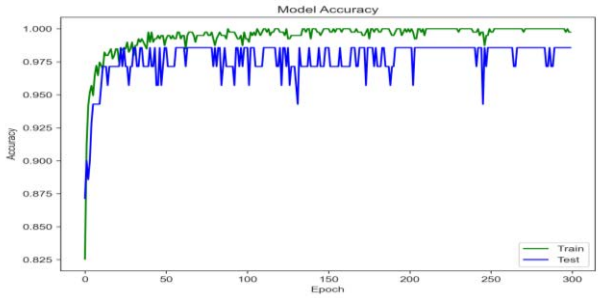


Fig. 12: The training and testing accuracy for the DNN employing RU sampling with SS.

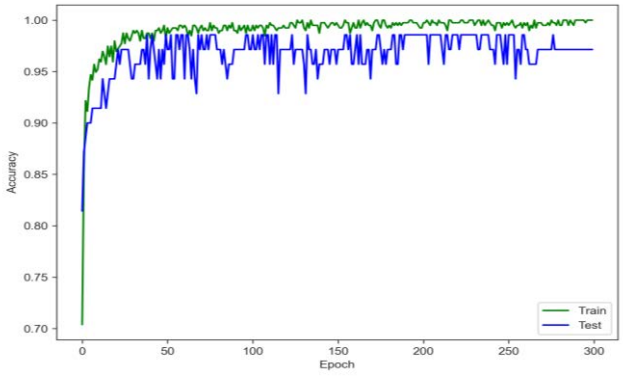


Fig. 13: The training and testing accuracy for the DNN employing RU sampling with RS.

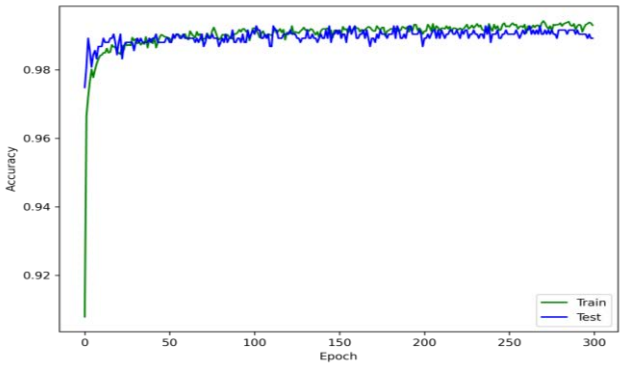


Fig. 14: The training and testing accuracy for the DNN employing RO sampling with SS.

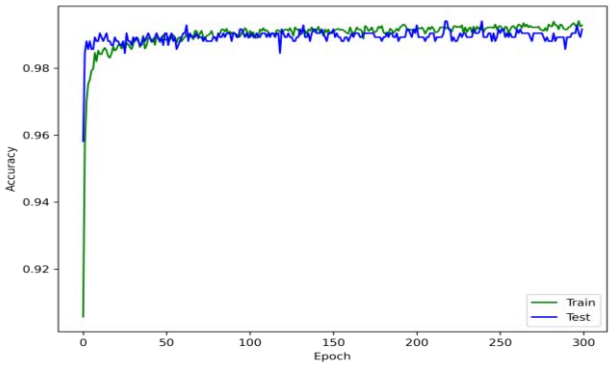


Fig. 15: The training and testing accuracy for the DNN employing RO sampling with RS.

In Table 6, the accuracy and loss values of the proposed techniques are compared. The hybrid deep neural network technique with RO sampling and robust scaling outperforms the other techniques. Figs. 16, 17, 18, and 19 depict the loss curves for the training and testing techniques of hybrid DNN employing RU sampling with SS, RU sampling with RS, RO sampling with SS, and RO sampling with RS, respectively. These results illustration that the hybrid DNN using RO sampling with RS achieve the best performance after 300 epochs.

Table 6: Accuracy and loss comparison of the proposed techniques.

Criteria	Techniques			
	RUS SS	RUS RS	ROS SS	ROS RS
Accuracy (%)	94.87	95.73	98.64	98.71
Loss	0.52	0.44	0.09	0.07

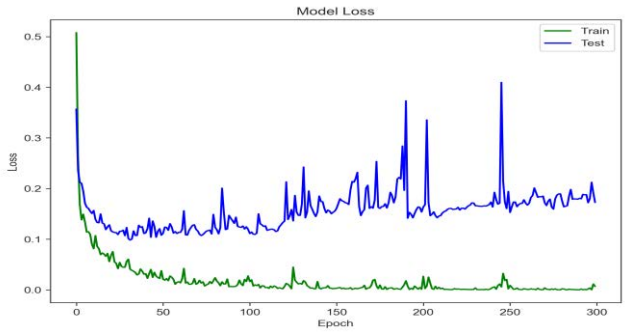


Fig. 16: The training and testing loss for the DNN employing RU sampling with SS.

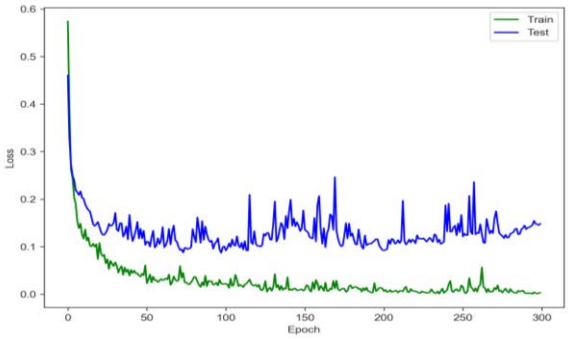


Fig. 17: The training and testing loss for the DNN employing RU sampling with RS.

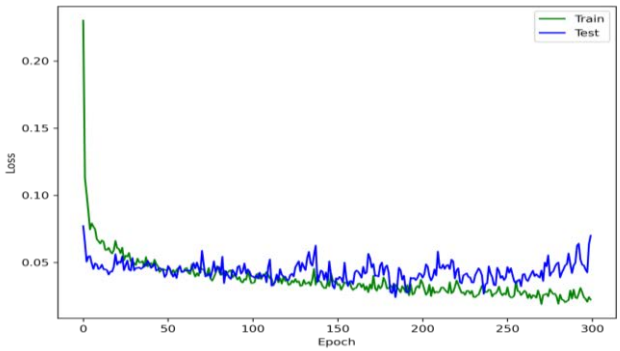


Fig. 18: The training and testing loss for the DNN employing RO sampling with SS.

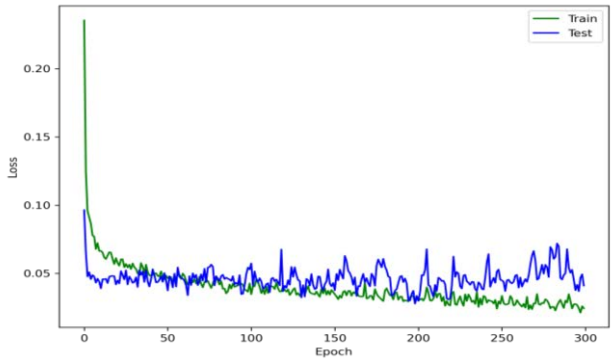


Fig. 19: The training and testing loss for the DNN employing RO sampling with RS.

The figures depicting the accuracy and loss curves for the training and testing sets of the hybrid deep neural network techniques with class balancing methods reveal that random over sampling exhibits higher accuracy and reduced loss compared to random under sampling, thereby delivering enhanced performance in the diagnosis and prediction of thyroid disorders.

To highlight the effectiveness of the proposed hybrid deep learning approach, a comparative analysis was conducted against recent deep learning methods applied to thyroid disease prediction on imbalanced datasets. Table 7 presents a side-by-side comparison of the proposed model with four relevant studies using key performance metrics: accuracy, precision, and recall. Additionally, Fig. 20 visually illustrates these comparisons to provide a clearer understanding of relative performance across models.

4. CONCLUSION

The identification of thyroid disorders has gained significant importance in the medical field, particularly due to the necessity of early diagnosis and appropriate treatment to prevent complications and reduce mortality rates. One of the significant techniques for disease prediction in recent years has been the application of artificial intelligence methods, such as machine learning and deep learning. These methods have attracted considerable attention from researchers due to their ability to enhance predictive accuracy. This study utilized a publicly available thyroid dataset comprising 3772 imbalanced samples from the UCI Machine Learning Repository. A hybrid robust neural network technique was employed to predict thyroid disease, incorporating class-balancing algorithms such as Random Over (RO) sampling and Random Under (RU) sampling. To address the presence of outliers in the thyroid dataset, the Robust Scaling method was applied to enhance the algorithm's performance. Four hybrid deep neural network techniques were evaluated on this dataset. Upon evaluating and comparing the performance of these hybrid techniques using standard classification metrics, it was observed that the deep neural network combined with RO sampling outperformed the model employing RU sampling in terms of classification accuracy, although at the expense of higher computational time. The findings highlight the superiority of the hybrid deep neural network technique by leveraging random over sampling combined with robust scaling, achieving an accuracy of 98.71%, recall of 100%, precision of 97.45%, F1-score of 98.71%, AUC of 99.31%, and a loss function value of 0.07.

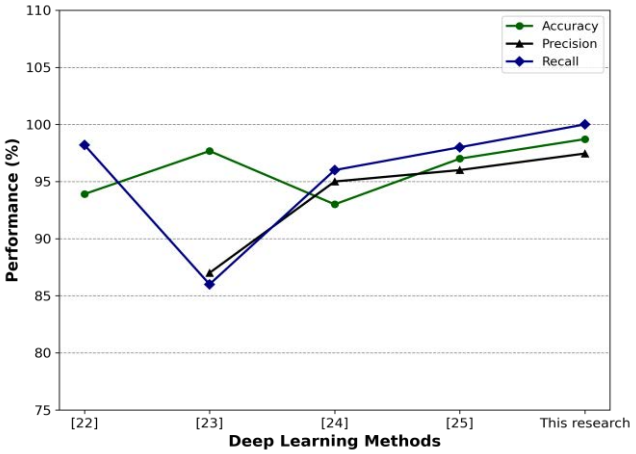


Fig. 20: Performance comparison of the proposed technique with recent deep learning methods on the imbalanced thyroid datasets

Table 7: Comparison of the proposed technique with recent deep learning methods for Thyroid disease prediction on the imbalanced dataset.

Ref.	Deep Learning Method	Balancing Technique	Accuracy (%)	Precision (%)	Recall (%)
[22]	RF, DNN	SMOTE	93.90	-	98.20
[23]	RNN	SMOTE	97.67	87.00	86.00
[24]	LSTM	SMOTE-NC	93.00	95.00	96.00
[25]	SVM, LSTM	SMOTE	97.00	96.00	98.00
This research	DNN	RO Sampling	98.71	97.45	100.00

CREDIT AUTHORSHIP CONTRIBUTION STATEMENT

Elahe Moradi: Conceptualization, Data curation, Formal analysis, Investigation, Methodology, Software, Supervision, Validation, Visualization, Writing - original draft, Writing - review & editing.

DECLARATION OF COMPETING INTEREST

The author declares that she has no known competing financial interests or personal relationships that could have appeared to influence the work reported in this paper. The ethical issues; including plagiarism, informed consent, misconduct, data fabrication and/or falsification, double publication and/or submission, redundancy has been completely observed by the authors.

REFERENCES

[1] M. L. Raymer, T. E. Doom, L. A. Kuhn, and W. F. Punch, "Knowledge discovery in medical and biological datasets using a hybrid bayes classifier/evolutionary algorithm," *IEEE Transactions on Systems Man and Cybernetics Part B (Cybernetics)*, vol. 33, no. 5, pp. 802–813, Oct. 2003.

[2] A. Mehrno, R. Oktaş, and M. S. Odabas, "Feature selection of thyroid disease using deep learning: A literature survey," *Black Sea Journal of Engineering and Science*, vol. 3, no. 3, pp. 109–114, Jun. 2020.

[3] A. Koliji, S. MihanDoost, N. Ezzati, and E. Mostafapour, "Improving the diagnosis of sudden cardiac death by using non-linear features of the ECG signal and hybrid RBF," *J. Appl. Res. Electr. Eng.*, vol. 2, no. 2, pp. 120-126, 2023.

[4] P. Vafadoost Sabzevar, A. Hajipour, and H. Tavakoli, "Investigating robust tracking of type 1 diabetes control using model-free controllers," *J. Appl. Res. Electr. Eng.*, vol. 3, no. 2, pp. 232-239, 2024.

[5] E. Moradi, "Diagnosis of coronary heart disease via robust artificial neural network classifier by adaptive synthetic sampling approach," *Iranian Journal of Electrical and Electronic Engineering (IJEEE)*, vol. 20, no. 4, pp. 55–67, 2024.

[6] N. M. Xi, L. Wang, and C. Yang, "Improving the diagnosis of thyroid cancer by machine learning and clinical data," *Scientific Reports*, vol. 12, no. 1, Jul. 2022.

[7] G. Mollica et al., "Classification of thyroid diseases using machine learning and bayesian graph algorithms," *IFAC-PapersOnLine*, vol. 55, no. 40, pp. 67–72, Jan. 2022.

[8] M. Parishani and M. Rasti-Barzoki, "CWBCM method to determine the importance of classification performance evaluation criteria in machine learning: Case studies of COVID-19, diabetes, and thyroid disease," *Omega*, vol. 127, p. 103096, Sep. 2024.

[9] X. Ren et al., "Machine learning reveals salivary glycopatterns as potential biomarkers for the diagnosis and prognosis of papillary thyroid cancer," *International Journal of Biological Macromolecules*, vol. 215, pp. 280–289, Aug. 2022.

[10] Z. Chen et al., "Machine learning-aided metallomic profiling in serum and urine of thyroid cancer patients and its environmental implications," *The Science of the Total Environment*, vol. 895, p. 165100, Oct. 2023.

[11] K. Chandel, V. Kunwar, S. Sabitha, T. Choudhury, and S. Mukherjee, "A comparative study on thyroid disease detection using K-nearest neighbor and Naive Bayes classification techniques," *CSI Transactions on ICT*, vol. 4, no. 2–4, pp. 313–319, Dec. 2016.

[12] S. S. Islam, Md. S. Haque, M. S. U. Miah, T. B. Sarwar, and R. Nugraha, "Application of machine learning algorithms to predict the thyroid disease risk: an experimental comparative study," *PeerJ Computer Science*, vol. 8, p. e898, Mar. 2022.

[13] V. Manimekalai, S.Gomathi alias Rohini, "Enhanced accuracy in thyroid disease cassification: A comparative analysis of random forest and decision tree methods," *Tuijin Jishu/Journal of Propulsion Technology*, vol. 44, no. 6, 2023.

[14] H. H. S. Kumar, "A novel approach of SVM based classification on thyroid disease stage detection," in *2020 Third International Conference on Smart Systems and Inventive Technology (ICSSIT)*, Aug. 2020.

[15] T. Alyas, M. Hamid, K. Alissa, T. Faiz, N. Tabassum, and A. Ahmad, "Empirical method for thyroid disease classification using a machine learning approach," *BioMed Research International*, vol. 2022, pp. 1–10, Jun. 2022.

[16] P. Poudel, A. Illanes, E. J. G. Ataide, N. Esmaeili, S. Balakrishnan, and M. Friebe, "Thyroid ultrasound texture classification using autoregressive features in conjunction with machine learning approaches," *IEEE Access*, vol. 7, pp. 79354–79365, Jan. 2019.

[17] D. Qiao et al., "Exploring the potential of thyroid hormones to predict clinical improvements in depressive patients: A machine learning analysis of the real-world based study," *Journal of Affective Disorders*, vol. 299, pp. 159–165, Feb. 2022.

[18] L. Aversano et al., "Thyroid disease treatment prediction with machine learning approaches," *Procedia Computer Science*, vol. 192, pp. 1031–1040, Jan. 2021.

[19] A. Sharifi and K. Alizadeh, "Comparison of the particle swarm optimization with the genetic algorithms as a training for multilayer perceptron technique to diagnose

thyroid functional disease," *Shiraz E-Medical Journal*, vol. 22, no. 1, Jun. 2020.

[20] S. Prathibha, D. Dahiya, C. R. R. Robin, C. V. Nishkala, and S. Swedha, "A novel technique for detecting various thyroid diseases using deep learning," *Intelligent Automation & Soft Computing*, vol. 35, no. 1, pp. 199–214, Jan. 2023.

[21] D. K. Gummalla, S. Ganesan, S. Pokhrel, and N. Somasiri, "Enhanced early detection of thyroid abnormalities using a hybrid deep learning model: A sequential CNN and K-means clustering approach," *Journal of Innovative Image Processing*, vol. 6, no. 3, pp. 244–261, Jun. 2024.

[22] Y. Attiga et al., "Applying deep learning to public health: using unbalanced demographic data to predict thyroid disorder," in *2018 IEEE 9th Annual Information Technology, Electronics and Mobile Communication Conference (IEMCON)*, IEEE, 2018, pp. 851–58.

[23] S. Tabassum, S. F. F. Rumky, and M. F. Shahariar, "Thyroid Disease Analysis and Prediction by Using Machine Learning and Deep Learning: A Comparative Approach," B.Sc. thesis, Dept. of Information and Communication Engineering, East West University, Dhaka, Bangladesh, Sep. 2022.

[24] A. Raza et al., "Enhanced interpretable thyroid disease diagnosis by leveraging synthetic oversampling and machine learning models" *BMC Medical Informatics and Decision Making*, vol. 24, no. 1, Nov. 2024, p. 364.

[25] K. Anitha et al., "Exploring the experimental effectiveness of a hybrid deep learning approach in detecting thyroid disease using intelligent predictions," in *2024 International Conference on Computing and Data Science (ICCDS)*, IEEE, 2024, pp. 1–5.

[26] Q. Ross, Thyroid Disease. *UCI Machine Learning Repository*. 1987 [Online]. Available: https://archive.ics.uci.edu/dataset/102/thyroid+disease.

[27] E. Moradi, "A data-driven based robust multilayer perceptron approach for fault diagnosis of power transformers," in *20th CSI International Symposium on Artificial Intelligence and Signal Processing (AISP)*, Feb. 2024.

[28] E. Moradi et al., "Robust deep neural network-based internet of things for power transformer fault diagnosis under imbalanced data and uncertainties," *International Journal of Electrical Power & Energy Systems*, vol. 168, July 2025.

[29] N. X.-Y. Liu, N. J. Wu, and N. Z.-H. Zhou, "Exploratory undersampling for class-imbalance learning," *IEEE Transactions on Systems Man and Cybernetics Part B (Cybernetics)*, vol. 39, no. 2, pp. 539–550, Apr. 2009.

[30] T. Zhu, Y. Lin, and Y. Liu, "Synthetic minority oversampling technique for multiclass imbalance problems," *Pattern Recognition*, vol. 72, pp. 327–340, Jul. 2017.

BIOGRAPHY



Elahe Moradi received her Bachelor's degree in Electrical-Electronic Engineering from K. N. Toosi University of Technology, her Master's degree in Electrical Control Engineering from the Islamic Azad University, South Tehran Branch, and her Ph.D. in Electrical Control Engineering from the Islamic Azad University, Science and Research Branch in Tehran. Her research activities and interests lie in robust control, delay systems, optimal control, fault detection and diagnosis, and artificial intelligence, including machine learning and deep learning. She is currently serving as an Assistant Professor in the Department of Electrical and Computer Engineering at the Yadegar-e-Imam Khomeini (RAH) Shahre Rey Branch of Islamic Azad University, Tehran, Iran.

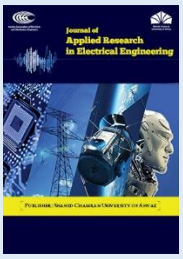
Copyrights
© 2025 Licensee Shahid Chamran University of Ahvaz, Ahvaz, Iran. This article is an open-access article distributed under the terms and conditions of the Creative Commons Attribution –NonCommercial 4.0 International (CC BY-NC 4.0) License (http://creativecommons.org/licenses/by-nc/4.0/).

Shahid Chamran University of Ahvaz

Iranian Association of Electrical and Electronics Engineers

Journal of Applied Research in Electrical Engineering

E-ISSN: 2783-2864
P-ISSN: 2717-414X
Homepage: https://jaree.scu.ac.ir/



Research Article

An Algorithm for Determining the Desirability of the Amount of Transient Limiting Reactors in Shunt Capacitor Banks

Sadegh Rekabeslami Zadeh[1], Gholamali Torabi[2], Sasan Najafi Birgani[2], Mehdi Enayat Zare[1], and Mostafa Sarlak[1,*]

[1] *Department of Electrical and Computer Engineering, Jundi-Shapur University of Technology, Dezful, Iran*

[2] *Khuzestan Regional Electric Company, Amanieh- Felestin, Ahwaz, Iran*

* *Corresponding Author: sarlak@jsu.ac.ir*

Abstract: Capacitor banks are commonly used in power grids for purposes such as power control and power factor correction. Capacitor banks are exposed to high-amplitude and high-frequency currents in circuit breaker switching. Also, if a fault occurs near the substation where the capacitor bank is installed, the energy stored in the capacitor bank at the fault location is discharged. The discharge of this energy causes currents to pass through at a high frequency and in large quantities. These high currents cause damage to the circuit breaker. To prevent these deleterious effects, the use of transient limiting reactor in capacitor banks is recommended. In this paper, an algorithm for determining the desirability of the amount of transient limiting reactors in shunt capacitor banks is designed based on the IEC Std 62271 standard. The algorithm was then developed for use in the electrical industry in the form of a software called Transient Analyzer. In the developed software, the C# programming language is used to develop and implement algorithms and data processing. The software has been tested and debugged using data from 20 regional electricity substations in Khuzestan. The proposed software is highly efficient compared to the conventional simulation method and can be used with simple data entry and fast processing and presentation of results and data analysis in a short time.

Keywords: Inrush currents, Shunt capacitor bank, Transient limiting reactor, Transient analysis software, IEC standard.

Article history
Received 10 July 2024; Revised 06 October 2024; Accepted 19 April 2025; Published online 08 November 2025.
© 2025 Published by Shahid Chamran University of Ahvaz & Iranian Association of Electrical and Electronics Engineers (IAEEE)

How to cite this article
S. Rekabeslami Zadeh, G. Torabi, S. Najafi Birgani, M. Enayat Zare, and M. Sarlak, "An algorithm for determining the desirability of the amount of transient limiting reactors in shunt capacitor banks," *J. Appl. Res. Electr. Eng.*, vol. 4, no. 1, pp. 11-23, 2025. DOI: 10.22055/jaree.2025.47408.1125

Check for updates

1. INTRODUCTION

1.1. Background

Shunt capacitor banks are used for correction of voltage profile, power factor and elimination of specific harmonics in the power network [1]. Among the essential considerations related to the use of these equipment in the power network are the presence of transient states caused by them. These transient states are 1) the inrush current caused by the transient state of a single capacitor bank connected, 2) the inrush current caused by the back-to-back connected capacitor bank transient state, and 3) the transient current caused by the energy discharge of the capacitor bank in the event of a near external fault. Modes (2) and (3) can be seen in Fig. 1.

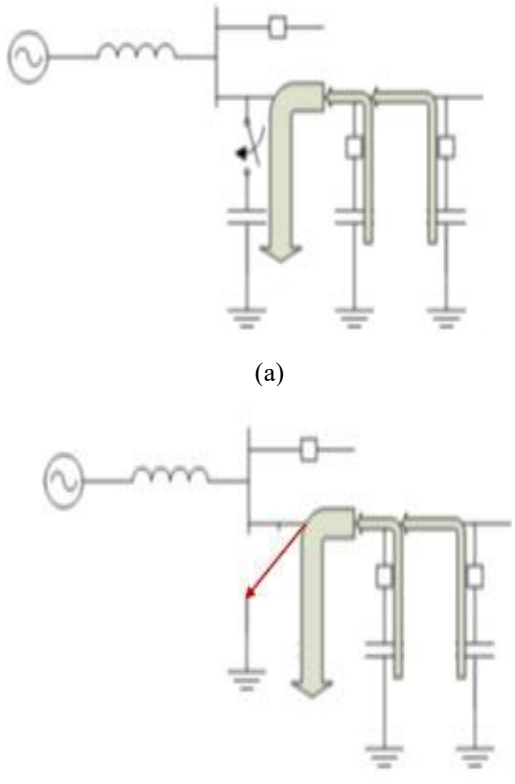
These transient states can have dangerous consequences, such as the failure of circuit breaker connections due to the passage of high-frequency current for single and back-to-back capacitor bank switching and the failure of the circuit breaker to operating properly for the near-fault. To prevent or reduce these transient states, there are various solutions, one of which is the use of transient limiting inductors [2]. This solution is reliable and economical, and the mentioned inductors do not need a short-term maintenance period. The mentioned inductors are installed in series with the capacitor bank to limit transient current. For example, in shunt capacitor banks with a star connection, these inductors are placed between the busbar and the circuit breaker, between the circuit breaker and the capacitor bank or between the capacitor bank and the neutral point in each phase.

1.2. Related Research

In [2], the issue of using transient limiting inductors, which are placed in series with shunt capacitor banks in each phase, is discussed in detail. The primary purpose of these inductors is to limit the transient currents caused by the energization of the capacitor bank and the discharge current of the capacitor bank in the event of nearby faults. In banks with star connection, said inductors are placed between bus and circuit breaker, circuit breaker and capacitor or neutral point and capacitor in each phase. Since the primary purpose of these fixed inductors is to limit the transient currents associated with the capacitor bank, they are called transient limiting inductors.

In general, these inductors are introduced as damping inductors in the IET literature, current-reducing inductors in common use in the US, and for inductors used to limit large fault currents, and transient limiting inductors, which is the choice of the IEEE capacitor subcommittee.

In [3], firstly, national and international standards and authoritative articles related to the removal of destructive effects caused by transient currents caused by shunt capacitor banks and considerations for the use of transient limiting inductors in shunt capacitor banks were reviewed and then based on the IEC standard [5], reference article [1] and IEEE standard [4, 6-11].



(a)

(b)

Fig. 1: (a) The inrush current caused by the transient state of the capacitor bank connected back-to-back, (b) The transient current caused by the discharge of the energy of the capacitor bank in the condition of the occurrence of an external fault

In the paper [12], first, the capacitor current is accurately calculated when the capacitor bank is placed in the circuit, and the constant component and the transient component of the capacitor current are obtained, respectively. Then, a pre-charge strategy is proposed to reduce the inrush current caused by the capacitor being placed in the circuit according to the calculation results. The proposed strategy can make the transient component of the current at the closing moment zero or minimal. Then a pre-charge strategy for single-phase, two-phase and three-phase pre-charge is proposed and the topology of the pre-charge device is presented based on the target value. Finally, a PSCAD simulation model is built to validate the proposed precharge strategy. The simulation results show that the inrush current can be limited below 1.7 p.u. Also, the duration of the temporary closure has been greatly shortened. Thus, the effectiveness of the proposed pre-charge strategy is confirmed.

In the article [13], simulation has been done to study the inrush current characteristics of capacitor bank switching in Indonesia. The simulation results show that the inrush current for switching meets the IEC standard. However, for back-to-back switching, the inrush current exceeds the standard limit. With measurement data, the value of contact resistance for CB with back-to-back switching condition for each phase has a very different value and tends to fail. To reduce the inrush current, the use of damping inductor has been studied and the results show that the damping inductor can minimize the amount of inrush current by setting the correct value of the inductance of the damping inductor related to the reactive power of the capacitor bank.

In reference [14], in order to reduce the inrush current of shunt capacitors, the mathematical model of the real system in the shunt capacitor placement circuit has been created. The strategy in the three-phase shunt capacitor placement circuit is calculated when the inrush current is minimum and the effectiveness of the strategy is verified. The mechanical closing of the breaker is analysed. The measurement error of the synchronous voltage, the error reduction method is presented, and the closing delay is calculated to ensure that the shunt capacitor can be closed accurately at a certain time, and the impact of the closing current of the shunt capacitor on the power system is reduced.

1.3. Motivation

In this article, according to the standard IEC 62271-100 and, of course taking into account the supplementary materials from standards [4,5,7], a comprehensive algorithm for calculating the transient currents caused by the single capacitor bank switching, back-to-back capacitor bank switching and the discharge of the capacitor bank [1,8] is extracted.

The advantage of this algorithm is calculating the mentioned currents without computer simulation. Of course, it is worth mentioning that the outputs of this algorithm have been discussed and investigated by conducting computer simulations of sample substations in the EMTP-RV environment, which will be discussed in this article. Finally, the mentioned algorithm is completed by adding the

necessary criteria for the transient limiting inductor based on the IEC standard, in such a way that by receiving information from the power network, it is possible to reach the output of the utility value of the inductor after the implementation of the proposed algorithm. Also, if the inductor is not installed, it is possible to obtain the required amount of inductor based on the proposed algorithm.

1.4. Contribution

The algorithm presented in this article is based on [15] which reviews the single-line diagram of Khuzestan province substations and concludes that we are able to develop a software called Transient Analyzer to determine the amount of the series reactor of shunt capacitor banks in the power grid. The information of 20 substations studied in Khuzestan province was simulated by EMTP-RV software and its results were used to verify the designed algorithm. The software is highly efficient compared to the conventional simulation method and can be used with simple data entry and fast processing and presentation of results and data analysis in a short time.

2. REQUIREMENTS FOR SHUNT CAPACITOR BANK SWITCHING BASED ON STANDARD IEC STD 62271-100

The IEC committee develops standards and guidelines which are constantly updated. For this reason, it is essential to have access to the latest relevant instructions. Additionally, due to the continuous technical advances in the field of circuit breakers, it is essential to obtain the recommendations of the equipment manufacturer regarding the transient current capabilities of the circuit breaker. In general, two circuit breaker parameters are mentioned in the IEC standard [4] for shunt capacitor bank circuit breakers, 1) peak value of transient current and 2) frequency of transient current. In this standard, the exact requirements have been considered for all circuit breakers at all voltage levels; 1) The inrush current peak is less than or equal to 20 kA (i_peak≤20 kA) and the inrush current frequency is less than or equal to 4.25 kHz (f≤4.25 kHz). It is worth noting that in IEEE standards [9-11], the requirements of capacitor bank switching are given, which are different for every voltage level than the IEC standard, which is the same for different voltage levels.

3. CIRCUIT DIAGRAM FOR CAPACITOR BANK SWITCHING CALCULATIONS BASED ON STANDARD IEEE STD C37.012

The circuit diagram that is conventionally considered to perform capacitor bank switching calculations, as an example for the capacitor bus with the presence of two capacitor banks, is shown in Fig. 2. The transient current limiting inductance consists of the bus inductance between the switches, L_{bus}, the inductances between the switches and the capacitor banks, L_1 and L_2, the inductances of the capacitor banks, L_{c1} and L_{c2}, and any additional inductance. The total sum of the inductance between the capacitor banks, $L_{c1} + L_1 + L_{bus} + L_2 + L_{c2}$, is very small compared to the source inductance, L_s. In most cases, the total inductance is less than 1% of the source inductance, and the contribution of the source inductance to the back-to-back switching inrush current is negligible [5]. However, regarding the switching of a separate capacitor bank, the said inductance has a dominant effect. In connection with the external network, to perform switching calculations, the said network is replaced with the Tonen equivalent circuit including voltage source and short circuit impedance (L_s) as source inductance. The capacitor bank itself is not simple. But, in general, its value is in the order of 10 μH and 5 μH for banks with a voltage higher than 52 kV and lower than 52 kV, respectively. In Table 1, for different voltage levels, the conventional values of inductance between capacitor banks are given [4].

Transients are the result of sudden changes in the power grid. Opening or closing a circuit breaker changes the topology of the network and the related flows. It always takes a period for the network conditions to stabilize after the changes as mentioned earlier. All transients occur due to electrical connection or disconnection in the power grid or energy injection through lightning strikes or static discharges. In the following, it will be introduced how to calculate the size and frequency of the inrush currents caused by electrifying the capacitor bank and discharging the current of the capacitor bank.

3.1 Inrush currents caused by energizing shunt capacitor banks

Energizing the capacitor bank by the circuit breaker creates a connected inrush current, which is a function of the applied voltage, the value of the capacitor's capacity, the value of the inductance of the connected path, and the remaining charge of the capacitor at the moment of the circuit connection. In general, there are two different scenarios for energizing capacitor banks in shunt.

- Energizing a single capacitor bank
- Back-to-back energization of the capacitor bank

The connected inrush current in a charged capacitor bank can be higher than in an uncharged (uncharged) capacitor bank, depending on the polarity of the main voltage and the remaining charge on the capacitor. Calculating the value of peak inrush current and the corresponding frequency can be done relatively simply by assuming that the capacitor bank is discharged and connected when the maximum inrush current is produced.

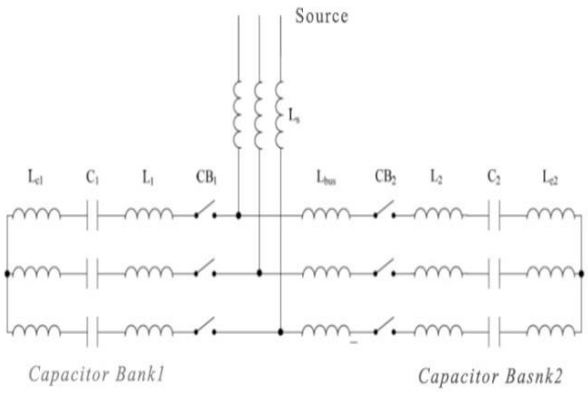


Fig. 2: Conventional circuit for switching calculations of two capacitor banks [4].

It is always assumed that the capacitor bank has been discharged before it is energized. This assumption is reasonable. The reason for this is the existence of discharge resistors in the capacitor bank building. Conventionally, the duration of the discharge of the capacitor bank is within 5 minutes [4].

4. The inrush current of a single capacitor bank switching transient

The switching phenomenon of a single capacitor bank can be well understood through Fig. 2. As it can be seen from the circuit theory, after connecting the switch in the circuit of Fig. 3, the current flows in the circuit, and this current has two components: constant and transient. The mentioned transient current will have the highest amplitude when the switch closing action occurs at the peak of the voltage wave. If the voltage wave is sinusoidal, the transient current component will be in (1) [6].

$$\mathrm{i}(t) = i_{i\,peak} \times e^{-\frac{R_s}{L_s}t} \times \sin \omega_i t \tag{1}$$

where R_s is the source series resistance, L_s is the inductance of the source series, and $i_{i\,peak}$ is the peak value of the passing current. Also, $f_i = 1/2\pi\sqrt{(L_s C_1)}$ is the frequency of the inrush current of the circuit, and because the ohmic resistance of the circuit is relatively small, the value of the transient current peak is determined by the wave impedance of the circuit, Z [6].

$$i_{i\,peak} = \frac{\sqrt{2}u}{Z} = \sqrt{2}u \times \sqrt{\frac{C_1}{L_s}} = U \times \sqrt{\frac{2}{3}\frac{C_1}{L_s}} \tag{2}$$

Where u is the single-phase RMS voltage, U is the nominal line-to-line voltage of the network, and C_1 is the capacitor bank value. Also, the value of the peak capacitance current of the constant component is obtained from (3) [6].

$$\sqrt{2} \times i_1 = \sqrt{2}u \times \omega C_1 = \sqrt{\frac{2}{3}} \times U \times \omega C_1 \tag{3}$$

where ω and i_1 are the effective value of the permanent capacitor current and the value of the grid frequency, respectively.

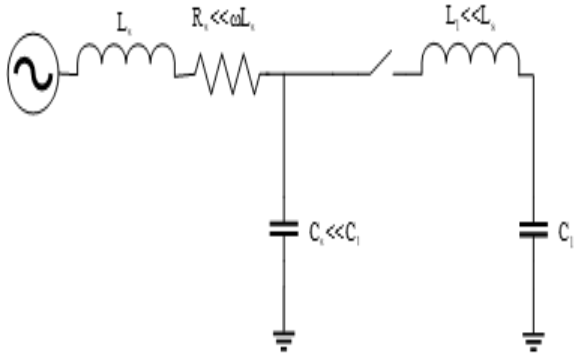


Fig. 3: Simplified circuit diagrams of the single capacitor bank: Cs (dissipation capacitor), Rs (source-series resistance), and Ls (source-series inductance) circuit parameters on the grid side, C1 and L1 are circuit parameters on the capacitor bank side [5].

From the ratio of peak currents of constant and transient components from (2) and (3), the following relation will be obtained [6]:

$$\frac{i_{i\,peak}}{\sqrt{2} \times i_1} = \frac{1}{\omega\sqrt{L_s C_1}} = \frac{\omega_i}{\omega} = \frac{f_i}{f} \tag{4}$$

Also, if I_{sc} is considered as the RMS value of the nominal short circuit current, equation (2) and the frequency of the inrush current can be written as (5) and (6) [6]:

$$i_{i\,peak} = \sqrt{2}\sqrt{I_{sc} i_1} \tag{5}$$

$$\omega_i = \omega \sqrt{\frac{I_{sc}}{i_1}} \tag{6}$$

Specifically based on Fig. 3, the power of a single-phase short circuit in the capacitor bank busbar is equal to [6]:

$$P_k = \frac{u^2}{\omega L_s} \tag{7}$$

Moreover, the power of single-phase capacitor bank is equal to [4]:

$$P_C = u^2 \omega C_1 \tag{8}$$

The ratio of the equations (7) and (8) is equal to [6]:

$$\frac{P_k}{P_C} = \frac{1}{\omega^2 L_s C_1} = \frac{\omega_i^2}{\omega^2} = \frac{f_i^2}{f^2} \tag{9}$$

which can be written using (4) and (9):

$$\frac{i_{i\,peak}}{\sqrt{2} \times i_1} = \sqrt{\frac{P_k}{P_C}} \tag{10}$$

Equations (9) and (10) show that the peak value of the transient component of the current is usually higher than the peak value of the steady component of the current. In the IEEE standard [4], it is pointed out that the peak value of the transient current component is usually about 20 times the peak value of the constant current component.

5. Back-to-back Capacitor Bank Switching Inrush Current

The energization of one capacitor bank while the other adjacent capacitor bank is in service is known as back-to-back switching. By increasing the number of shunt capacitor banks in service, the amplitude and frequency of inrush current flowing between the capacitor banks increases. To understand the back-to-back switching phenomenon, we can consider Fig. 4. In this figure, the capacitor bank C_2 is in the circuit before the capacitor bank C_1 is energized. By putting the equivalent capacitor and the equivalent series inductance in equation (2) and the equation $f_i = 1/2\pi\sqrt{(L_s C_1)}$, the equations (11) and (12) will be obtained [4]:

$$i_{i\,peak} = \sqrt{2} \times u \times \sqrt{\frac{C_{eq}}{L_{eq}}} = U \times \sqrt{\frac{2}{3} \times \frac{C_{eq}}{L_{eq}}} \quad (11)$$

$$f_i = \frac{1}{2\pi\sqrt{C_{eq} \times L_{eq}}} \quad (12)$$

$$C_{eq} = \frac{C_1 \times C_2}{C_1 + C_2} \quad (13)$$

$$L_{eq} = L_1 + L_2 \quad (14)$$

Considering the two equations $i_1 = u \times \omega C_1$ and $i_2 = u \times \omega C_2$ as permanent currents of two capacitor banks, equations (15) and (16) can also be considered for the peak inrush current and its frequency [4].

$$i_{i\,peak} = \sqrt{2} \times u \times \sqrt{\frac{i_1 i_2}{u\omega L_{eq}(i_1 + i_2)}} = \sqrt{2} \times \sqrt{\frac{u i_1 i_2}{\omega L_{eq}(i_1 + i_2)}} \quad (15)$$

$$f_i = \frac{1}{2\pi} \times \sqrt{\frac{\omega u(i_1 + i_2)}{L_{eq} i_1 i_2}} = \frac{1}{2\pi} \times \sqrt{\frac{2\pi f u(i_1 + i_2)}{L_{eq} i_1 i_2}} \quad (16)$$

Also, considering $C_2 = aC_1$ in which $a \geq 1$ means $C_2 \geq C_1$ and $L_2 = \frac{L_1}{a}$ from equations (11) and (12), equations (17) and (18) will be extracted [5]:

$$i_{i\,peak} = \sqrt{2} \times u \times \frac{a}{a+1} \times \sqrt{\frac{C_1}{L_1}} = \sqrt{\frac{2}{3}} \times U \times \frac{a}{a+1} \times \sqrt{\frac{C_1}{L_1}} \quad (17)$$

$$f_i = \frac{1}{2\pi\sqrt{L_1 C_1}} \quad (18)$$

Comparing (4) and (17), it can be seen that the inrush current of capacitor bank C_1, i.e., (17), can be expressed as a function of the constant component of the first bank current [5].

$$i_{i\,peak} = \frac{a}{a+1} \times \frac{f_i}{f} \times \sqrt{2} i_1 \quad (19)$$

Equation (19) is used in practice to calculate the transient component of the inrush current of back-to-back capacitor banks with two or more banks.

Capacitance banks with n+1 branches, according to Fig. 5, can first be combined as equivalent to two capacitor banks and then using equations (11) and (12), provided that L_2 and C_2 from Fig. 3 with the following parameters should be replaced [5].

$$L' = \frac{1}{\sum_{j=(n+1)}^{j=1} \frac{1}{L_j}} = \quad (20)$$

$$C' = \sum_{j=(n+1)}^{j=2} C_j \quad (21)$$

6. Outrush Current of Capacitor Banks

In the condition that there is a fault near the shunt capacitor bank(s) at the substation and one of circuit breakers at the beginning of the adjacent feeder is closed in the presence of the fault (for example, during the single-pole reclosing, in addition to the main current component, another current component with the frequency and a significant amount will pass through the mentioned switch, which is the outrush current of the capacitor bank in the fault location. Fig. 6 shows an example single-line diagram that calculate the value and frequency of outrush current in the presence of a single capacitor bank [1]. The peak value of the capacitor bank outrush current, and its frequency can be calculated based on the diagram shown in Fig. 6 through the following equations [1, 7, 8]:

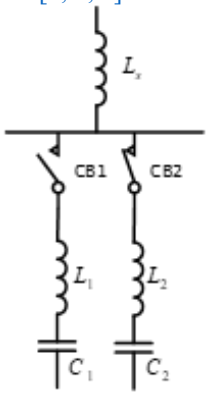


Fig. 4: Circuit diagram of two back-to-back capacitor banks [5].

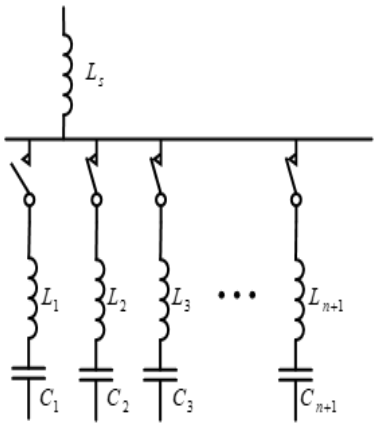


Fig. 5: Back-to-back n+1 capacitor banks diagram [5].

$$L_{eq} = \frac{1}{\sum_{j=(n+1)}^{j=1} \frac{1}{L_j}} \quad (22)$$

$$C_{eq} = \sum_{j=(n+1)}^{j=1} C_j \quad (23)$$

$$f_i = \frac{1}{2\pi\sqrt{(L_{adj} + L_{eq})(C_{eq})}} \quad (24)$$

$$i_{\mathrm{pk_i}} = V_o \times \sqrt{\frac{2}{3} \times (C_{eq}) \times \frac{1}{(L_{adj} + L_{eq})}} \quad (25)$$

In these relationships, i_{pk} is the maximum outrush current (kA), f_i is the transient current frequency of discharge of the capacitor bank, V_o is equal to the line voltage, L_{adj} is the inductor at the beginning of the adjacent feeder in the bus location, and the fault location, L_{eq} is the equivalent inductor of the branches of the capacitor bank (including the bank inductor) The capacitor is our capacitor between the capacitor bank and the beginning of the bus, and C_{eq} is the equivalent capacitance of the capacitor banks. For shunt capacitor banks, a reasonable estimate of the outrush current can be calculated as follows [7]:

$$i_{pk} = \sqrt{\frac{1000}{3f}} \times \sqrt{\frac{Q_C\ kvar}{L}} \quad (26)$$

where i_{pk} is the maximum outrush current (kA), f is the frequency of the power system, Q_C is the three-phase nominal reactive power of the capacitor bank, and L is the inductance between the capacitor bank and the fault location (μH).

7. An Algorithm for Determining the Usefulness of Transient Limiting Inductors

Fig. 7 shows the flowchart of the comprehensive algorithm for determining the desirability of the limiting inductor [12]. The steps of implementing the algorithm are as follows:

Step 1: In this step, the inrush current $i_{sb}(i)$ and its oscillation frequency $f_{sb}(i)$ in the scenario of connecting a single capacitor bank for each capacitor bank are calculated using (2) and (4).

Step 2: In this step, the suitability of the calculated values is checked according to the IEC62271-100 standard. In other words, it is checked that the range of inrush current is less than 20 kiloamperes, and the frequency of its fluctuations is less than 4250 Hz.

Step 3: In this step, the inrush current $i_{b2b}(i)$ and its fluctuation frequency $f_{b2b}(i)$ in back-to-back scenarios are calculated based on (11), (12), (20), and (21).

Step 4: In this step, similar to the second step, according to the IEC standard, the suitability of the values calculated in the third step is checked.

Step 5: In this step, the inrush current $i_{outrush}(i)$ and its oscillation frequency $f_{outrush}(i)$ in the capacitor bank discharge scenario in the condition of near-fault occurrence are calculated using (22) to (25).

Step 6: In this step, similar to the second, and fourth steps, according to the IEC standard, the suitability of the values calculated in the fifth step is checked.

It is worth mentioning that in each of the second, fourth and sixth steps, according to the standard [3], the inrush current, and calculated frequency are compared with the allowed values. If the calculated current and frequency are not in the allowed range, by increasing the TLI inductance value specified under Ladd, calculations are calculated again with the new inductance and this repetition loop continues until the current and frequency are within the allowed range. Finally, Ladd is considered to be the minimum inductance required for the inductor to be optimal.

8. Simulation and Discussion

In this section, the studied network modeling report in EMTP-RV software and the evaluation of the proposed comprehensive algorithm are given.

8.1. Networks Modelling

Fig. 8 shows the single-line diagram of a studied substation including two shunt capacitor banks with a nominal power of 4.8 MW. In this substation, two capacitor banks are connected to the 33 kV bus. Also, the nominal specifications of each circuit breaker are:

- The nominal voltage of the switches is 36 kV.
- The nominal short-circuit current of the circuit breakers is equal to 25 kA.
- $\boldsymbol{L_1}$ and $\boldsymbol{L_2}$ are the inductance between the bus and the capacitor bank circuit breaker
- $\boldsymbol{L_3}$ and $\boldsymbol{L_4}$ are the inductance between the capacitor bank circuit breaker and the capacitor bank
- $\boldsymbol{L_{BUS1}}$ *and* $\boldsymbol{L_{BUS2}}$ are the inductance of the bus path between circuit breakers.

First, this network was modeled in EMTP-RV software. Then, different capacitor bank switching scenarios were simulated through the 5512 CB.

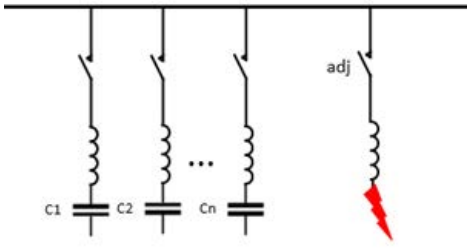


Fig. 6: System diagram to evaluate the capacitor bank outrush current [2].

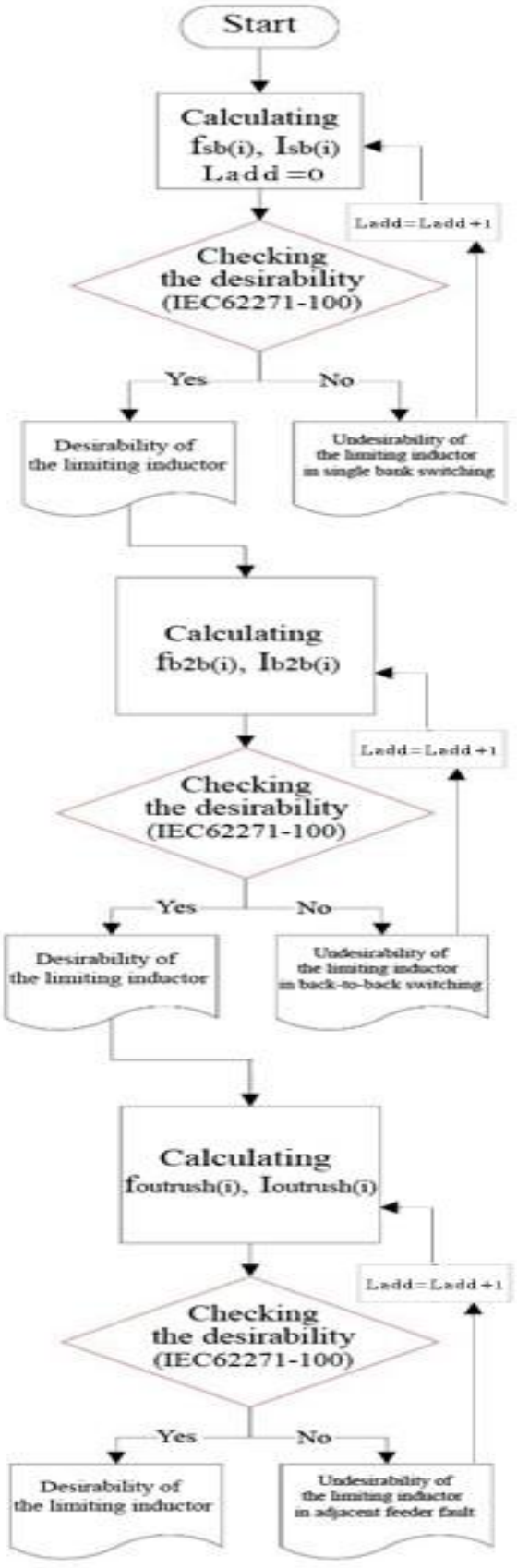


Fig. 7: Comprehensive algorithm for determining the desirability of transient limiting inductor.

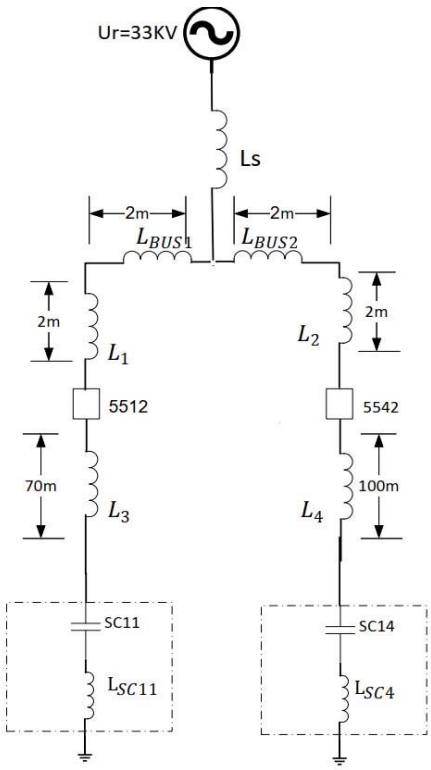


Fig. 8: Single-line diagram of 33 KV studied substation.

8.2. Comparison of EMTP-RV Results and Proposed Algorithm

In Tables 2 and 3, respectively, the results obtained from checking the suitability of the transient limiting inductor concerning the transient states of capacitor bank switching in the studied substation with the EMTP-RV software and the proposed algorithm can be seen. As can be seen, the peak current and frequency values using the proposed algorithm in Table 2 are very close to the corresponding values in Table 1.

The current waveform obtained from the transient states in the EMTP-RV software is shown in Figs. 9, 10 and 11.

Table 1: Conventional inductance values between capacitor banks [4].

Maximum rated voltage (kV)	Bus bar inductance per phase ($\frac{\mu H}{m}$)	Conventional inductance between banks* (μH)
17.5 and below	0.702	10 to 20
36	0.781	15 to 30
52	0.840	20 to 40
72.5	0.840	25 to 50
123	0.856	35 to 70
145	0.856	40 to 80
170	0.879	60 to 120
245	0.935	85 to 170

* This value does not include the inductance of the capacitor bank itself. In total, the inductance of the capacitor bank is in the order of 10 µH and 5 µH for banks with a voltage higher than 52 kV and lower than 52 kV.

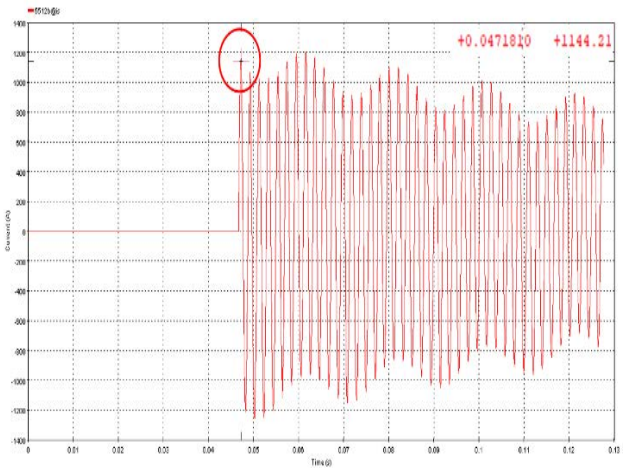


Fig. 9: The single bank switching current waveform of SC11.

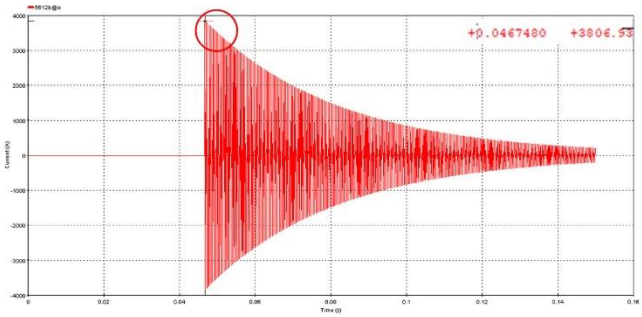


Fig. 10: The back-to-back switching current waveform of SC11 (EMTP-RV).

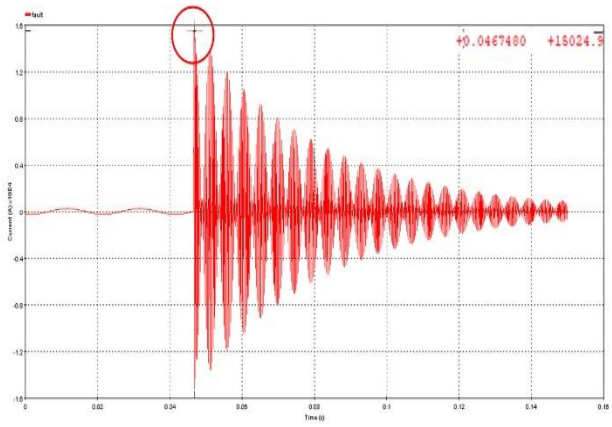


Fig. 11: Outrush current waveform (EMTP-RV).

Table 2: Evaluation Results for the network by EMTP-RV.

Scenario	Peak current (kA)	Current frequency (Hz)	Amount of inductor
Single-bank switching SC11	1.144	484	Desirable
Back-to-back switching SC11	3.806	3209	Desirable
Outrush current	15.024	3215	Desirable

Table 3: Evaluation results for the network by the proposed algorithm.

Scenario	Peak current (kA)	Current frequency (Hz)	Amount of inductor
Single bank switching SC11	1.150	486	Desirable
Back-to-back switching SC11	3.840	3231	Desirable
Outrush current	15.280	3224	Desirable

The comparison of the results of Tables 1 and 2 can be seen in Fig. 12 in a more specific way. Another point that can be mentioned in Tables 1 and 2 is the result of examining the usefulness of the transient limiting inductor, obtained with both methods of the same output in this connection.

9. Development of Software

9.1. Methodology

The production and development of a software package requires step-by-step actions that can finally be presented in the form of efficient, and standard software. Therefore, in the following, the method used in producing the software package is explained in 5 steps. These steps can be seen in Fig. 13.

9.2. Design and Implementation of Database Based on Database Management System

Using the database management system provides the possibility of editing, deleting, and adding data in the future. if the volume of input data is high, they can be saved for later use. Therefore, since substations may undergo changes in development plans and need to be updated or add new data, it is necessary to design the data in a database that can be managed or edited. Therefore, MySQL data management system has been used in the design and implementation of this software package.

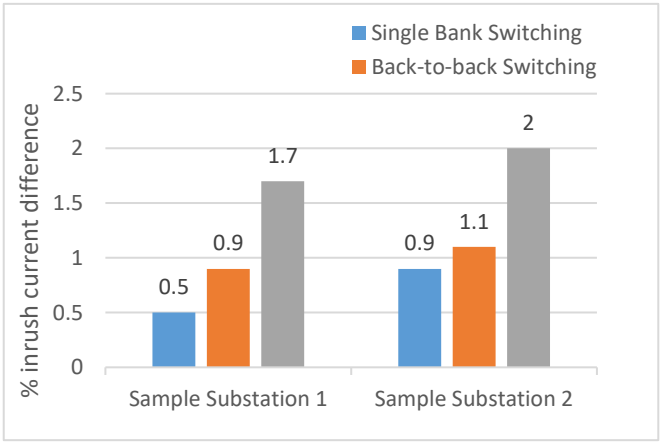


Fig. 12: The percentage difference between the transient current value in EMTP-RV software and the proposed algorithm.

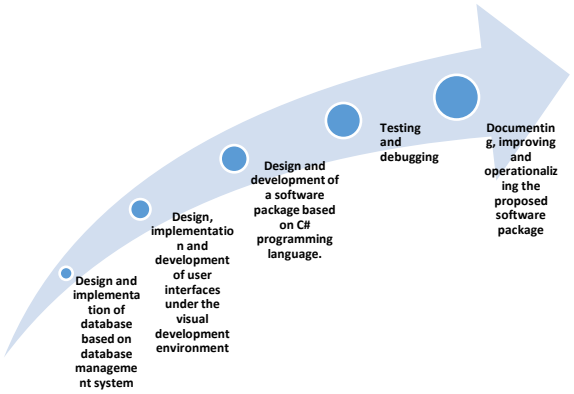


Fig. 13: Action diagram for software development to determine the desirability of transient limiting inductors for shunt capacitor banks.

Before designing the database, the processes and algorithms were checked, and then the database tables were designed according to the data and the relationship between them. The relationship between the tables was determined differently to avoid redundancy and repetition of data. One of the most fundamental challenges in developing a database is determining the exact relationship between data tables. Accurate knowledge of the nature of the data, as well as complete knowledge of the processing algorithms in which the data are used, are among the factors that influence the determination of the relationship between the data tables. Therefore, the database model has been extracted by conducting numerous investigations regarding the exact knowledge of the nature of the data and how to use the processing algorithms. Next, as an example in Fig. 14, the structure of the data table of breakers is given.

In the first field, a numeric ID is assigned to each breaker, which is unique and cannot be empty, and in the second field, a name is assigned to each breaker, which is a string type and cannot be empty. In the third field (bb_id), this breaker is assigned to a busbar whose value is numerical and cannot be empty. In the field (i_sc_b), the value of the short circuit current is of decimal type and cannot be empty.

Tables are linked through foreign keys. Like the table of circuit breakers, which is linked to the table of busbars through the bb_id field and specifies the busbar to which the circuit breaker is connected. Also, when inserting data, it is necessary to validate the type of user input data so that they do not encounter errors when inserting into the database. Like the breaker short circuit current field that cannot be empty and must enter a numerical value, otherwise it will not be allowed to enter information in the database.

9.3. Design, Implementation, and Development of User Interfaces Under the Visual Development Environment

After compiling the database to communicate between the written algorithms, the database, and the user requests, a user interface is needed, and the visual development environment has been used to create this connection. In fact, by the user interface, the required data is received from the user and stored in the database, and then, according to the user's request for processing, the required data is called from the database tables, and its report is displayed through the user interface.

In Fig. 15, there is an example of a user interface that can add, delete, and edit data by clicking on its different parts. In Fig. 15, the user can add a new substation in the software through the designed user interface. Moreover, in Fig. 16, the user can perform the desired processing on the data stored in the database by selecting the processing method, the desired station, and voltage level.

9.4. Design and Development of a Software Package based on C# Programming Language

C# programming language has been used to develop the user interface and compile algorithms as well as to communicate with the database in the visual environment. This language has several advantages, including:

1- Syntax similar to Java, C++, and C language

2- The most powerful programming language from Net Framework. Uses.

3- High security

4- Ability to reuse codes with rich libraries for use in different fields

5- Being multi-platform (Cross-Platform)

9.5. Testing and Debugging

After the initial compilation of the algorithms, receiving data from the database, and reporting the processes resulting from the implementation of the algorithms, it is necessary to create test data to test and check the performance of the software in different conditions and display possible errors to the user; In order to ensure the correct implementation of the obtained algorithms, when using the software, the user can perform the desired processing and receive a favorable report by receiving the appropriate message and correcting the data.

#	Name	Type	Collation	Attributes	Null	Default	Comments	Extra	Action
1	id	int(11)			No	None		AUTO_INCREMENT	Change Drop More
2	name	varchar(500)	utf8_persian_ci		No	None			Change Drop More
3	bb_id	int(11)			No	None			Change Drop More
4	i_sc_b	double			No	None			Change Drop More

Fig. 14: Table structure of data breakers in MySQL database

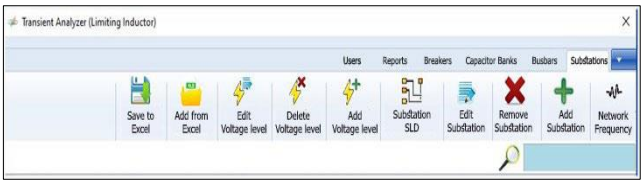


Fig. 15: Sample user interface (main page of the software).



Fig. 16: User interface example (add substation).

Testing and debugging is one of the most extended steps in software production, because the suitability of all algorithms and models used in the software is examined according to the sample data, and the system messages to the user are determined and modified with great accuracy and sensitivity; To avoid unforeseen ambiguities while using the software. This stage of developing the software package is repeated many times to fix all the tests and bugs of the software. Figs. 17 and 18 show examples of error messages in adding a station and a breaker, respectively. Fig. 19 shows the steps taken in the testing and debugging stage of the software. After preparing the initial version of the software package, the sample data has been entered into the software. Software bugs, including error notification when entering incorrect information as well as during data processing, matching the output of the coded algorithm in the software with the manually calculated results, and then the solution is determined by holding joint meetings between the computer group and the electrician. Applications are provided to report errors and modify algorithms. Moreover finally, the solutions provided in the software have been applied, and a new version has been provided. These measures have been continued until all the problems have been resolved and corrective measures have been implemented during numerous meetings.

9.6. Documenting, Improving, and Finalizing the Proposed Software Package

In order to finalize the software, user interfaces, and graphical interfaces for data entry, the selection of processing operations and reporting were reviewed. The arrangement of graphic elements, and data entry steps was modified so that the user could quickly enter the data and get the desired output from the software. The software report was modified according to the user's needs. Primary data and graphic charts were applied in the report to understand the results of the processes better. In order to improve the application of the software in organizations and its use by several users, the user management section has been added to the software, which allows the definition of new users with different accesses. This way, each user can enter data from different stations, perform processing operations, and get reports from the software.

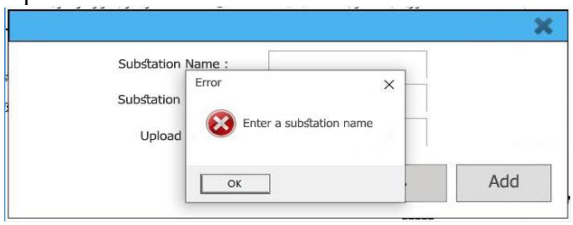


Fig. 17: Sample error message when adding a substation.

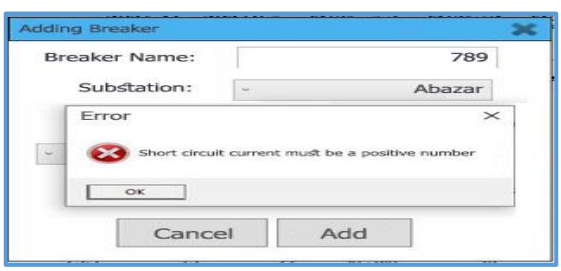


Fig. 18: Sample message when adding a breaker.

The user management section is shown in Fig. 20. It is possible to add, delete, and edit users. In the section of the main page of user management, it is possible to search among users and the time of their last login. To document and improve the use of the software, a user guide was developed. In this guide, how to work with all the menus, as well as how to enter data, perform processing operations, and report from the software, are illustrated. Figs. 21 and 22 are examples of software manual pages.

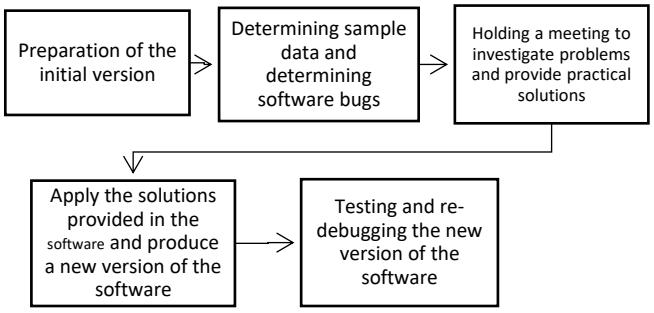


Fig. 19: Diagram of software testing and debugging procedures.

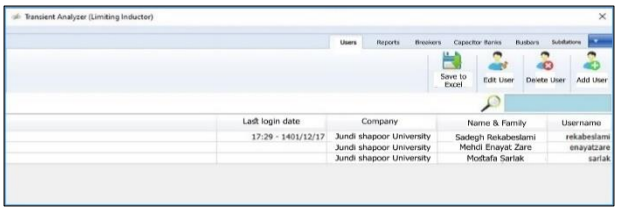


Fig. 20: User management section in Transient Analyzer software.

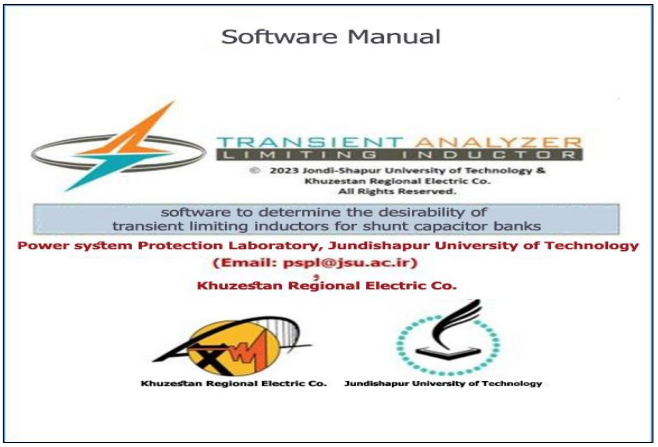


Fig. 21: Transient Analyzer software manual.

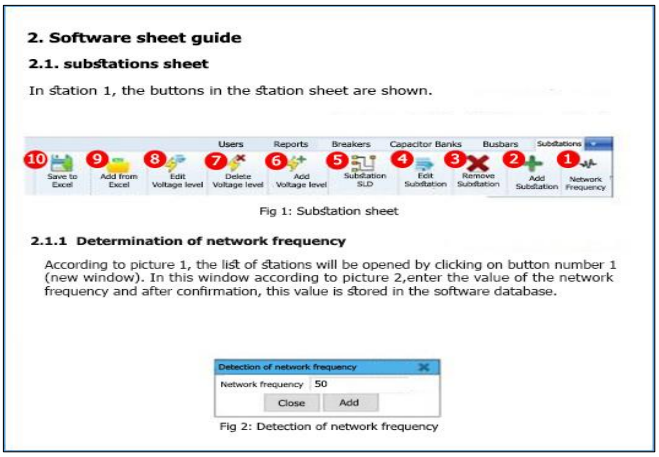


Fig. 22: Transient Analyzer software manual.

10. PRACTICAL EXAMPLE

In the following, Shadegan substation network is considered as a sample network to check the desirability of series inductors with the help of the proposed software.

10.1. Case Study

Fig. 23 shows the diagram of Shadgan substation, including a bank of shunt capacitor banks with a rated power of 4.8 MW. In this station, two capacitor banks are connected to the 33 kV bus. Also, the nominal specifications of each of the circuit breakers are:

- The nominal voltage of circuit breakers is 36 kV.
- The nominal short-circuit current of circuit breakers is equal to 25 kiloamperes.
- $\mathbf{L_1}$ and $\mathbf{L_2}$ are the inductance between the bus and the circuit breaker of the capacitor bank.
- $\mathbf{L_3}$ and $\mathbf{L_4}$ are inductance between the capacitor bank circuit breaker and the capacitor bank.
- $\mathbf{L_{BUS1}}$ and $\mathbf{L_{BUS2}}$ are the inductance of the bus path between circuit breakers.

Network information:

U_r	33 kV
L_s	The inductance of the source is equal to 7.5 mH and according to the frequency of 50 Hz, it is equivalent to 2.385 ohms.
L_1, L_2	The inductances between the bus and the circuit breaker of each capacitor bank
L_3, L_4	Inductances between capacitor bank circuit breaker and each capacitor bank
L_{BUS1} و L'_{BUS2}	Bus inductance between capacitor bank circuit breakers.
L_{sc11}, L_{sc12}	Inductance of each phase in each capacitor bank.
5512,5522	circuit breakers
	The short circuit current of the source (I_s) is equal to 8.774 kA at a voltage of 33 kV.

10.2. Investigating the Desirability of Transient Limiting Inductors of Sample Networks Using the Proposed Software

The information under Sections 1-3 is entered in the Transient Analyzer software and after all the processes are done, the software report is presented in Figs. 24 and 25. Fig. 24 shows the characteristics of the desired station, and Fig. 25 shows the results of the processing done by the developed software.

As shown in Fig. 25, the results of single capacitor bank reconnection processes are favorable according to the IEC Std62271-100 standard. However, the results of back-to-back capacitor bank connection processes are unfavorable according to the standard, and up to 78 microHenries are required for the limiting inductor. The series should be added so that the results are favorable. Also, the results of capacitor bank energy discharge processes in the conditions of near external fault occurrence are unfavorable according to the standard criteria, and it is necessary to add 78 µH to the series limiting inductor to make the results favorable. Therefore, in total, if 78 µH of inductance is added to the series inductor, the results will be favorable in all three scenarios.

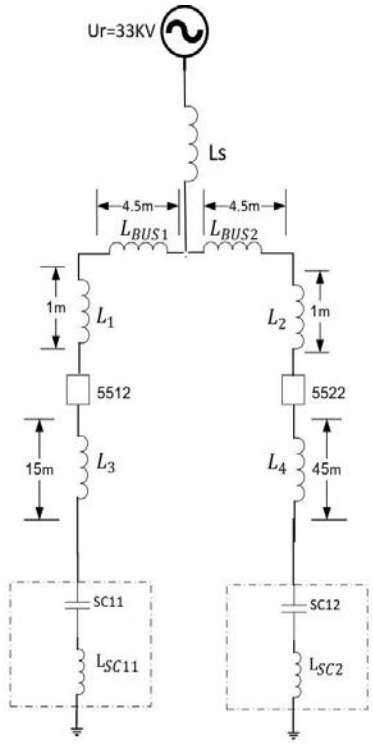


Fig. 23: Single-line diagram of 33 KV substation.

Processing results of the desirability of transient limiting inductors in shunt capacitor banks

kzrec.co.ir

1. General specifications

User specifications	Name & Family	Company	Date & Time
Manager System	Sadegh Rekabeslami	Jundi Shapoor University	1401/09/12 9:21

2. Specifications of substation

Substation	Short circuit current (A)	Short circuit Reactance (ohm)	Frequency (Hz)	Substation Position	Short circuit power (MVA)
Shadegan	-	2.383	50		-

3. Specifications of selected busbars

Busbar	Voltage level (Kv)	Adjacent breaker	Distance of adjacent feeder from busbar(m)	Short circuit current of adjacent feeder (kA)
51	33	5022	1	25
52	33	5042	1	25

4. Specifications of capacitor banks

Capacitor bank	Voltage Level (Kv)	Reactive power (MVA)	Limiting inductance (uH)
SC11	33	4.8	0
SC12	33	4.8	0

5. Specifications of circuit breakers

Breaker	Breaker Short circuit current (kA)	Distance of breaker to source (m)	up stream case	Distance to upstream case (m)	downstream case	Distance to downstream case (m)
5512	25	5.5	51 Busbar	5.5	SC11	20
5522	25	5.5	52 Basbar	5.5	SC12	14

Fig. 24: Software report - Shadgan station specifications.

6.1. Investigating the desirability of series limiting inductors at the voltage level of 33 kV

6.1.1. The results of single capacitor bank switching processes

Min Additional TLI * (uH)	Desirable limiting inductor (IEC Standard 62271-100)	Frequency (Hz)	Current Peak (KA)	Capacitor Bank	Breaker
-	Desirable	487.05	1.16	SC11	5512
-	Desirable	487.20	1.16	SC12	5522

6.1.2. The results of back-to-back capacitor bank switching processing

Min Additional TLI * (uH)	Desirable limiting inductor (IEC Standard 62271-100)	Frequency (Hz)	Current Peak (KA)	Capacitor Bank	Breaker
78	Undesirable	8.943	10.62	SC11	5512
78	Undesirable	8.943	10.62	SC12	5522

6.1.3 The results of capacitor bank energy discharge processes in near fault conditions

Min Additional TLI * (uH)	Desirable limiting inductor (IEC Standard 62271-100)	Frequency (Hz)	Current Peak (KA)	Busbar	Adjacent breaker
78	Undesirable	8.692	41.30	51	5022
78	Undesirable	8.692	41.30	52	5042

6.2. Analysis of 33 kV voltage level processes

Min Additional TLI * (uH)	Desirable limiting inductor (IEC Standard 62271-100)	Voltage level (Kv)	Substation
78	Undesirable	33	Shadegan

Fig. 25: The results of Shadgan station processing algorithms.

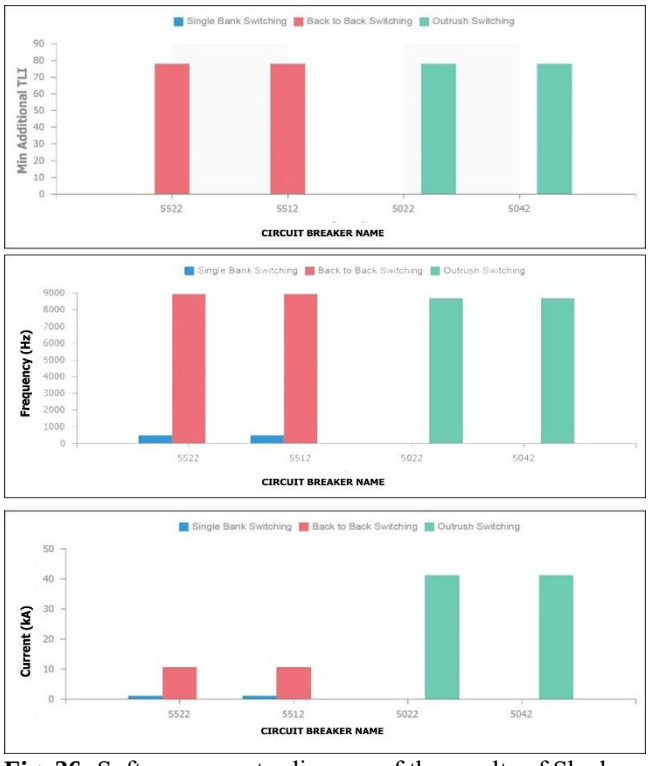


Fig. 26: Software report - diagram of the results of Shadgan station's processing algorithms.

Fig. 25 shows the report of software processing algorithms in Shadgan station. The inrush current and its frequency and minimum inductor have been compared for the suitability of conduit capacitor bank switching scenarios, back-to-back, and capacitor bank discharge in the near-fault location.

11. Conclusion

In this article, based on IEC standards for shunt capacitor banks, using nominal information of circuit breakers, capacitor banks, the distance between the installed equipment and the corresponding busbar short circuit level, a comprehensive algorithm for determining the desirability of the value of transient limiting inductors in capacitor banks was tried. Then, according to the comparison of the results of the developed algorithms with the results of the EMTP-RV software, the validation of the proposed algorithm was done, and it was observed that the difference percentage is less than 2%. Therefore, the developed proposed algorithm has good accuracy compared to EMTP-RV software. Also, the methodology of developing and producing software for determining the desirability of shunt capacitor bank series inductors was investigated. In the end, the proposed algorithm was released in a software package called ‹Transient Analyzer for ease of use.

Credit Authorship Contribution Statement

Sadegh Rekabeslami Zadeh: Conceptualization, Data curation, Formal analysis, Investigation, Methodology, Resources, Software, Validation, Roles/Writing - original draft. **Gholamali Torabi:** Data curation. **Sasan Najafi Birgani:** Conceptualization, Data curation, Formal analysis, Funding acquisition, Investigation, Methodology, Project administration, Resources, Software, Supervision, Validation, Visualization, Roles/Writing - original draft, Writing - review & editing. **Mehdi Enayat Zare:** Data curation, Formal analysis. **Mostafa Sarlak:** Conceptualization, Data curation, Formal analysis, Resources, Supervision, Writing - review & editing.

Declaration Of Competing Interest

The authors declare that they have no known competing financial interests or personal relationships that could have appeared to influence the work reported in this paper. The ethical issues; including plagiarism, informed consent, misconduct, data fabrication and/or falsification, double publication and/or submission, redundancy has been completely observed by the authors.

References

[1] L. Van der Sluis and A.L.J. Janssen, “Clearing faults near shunt capacitor banks” *IEEE Transactions on Power Delivery*, vol. 5, no. 3, pp. 1346–1354, 1990.

[2] *Transient Limiting Inductor Applications in Shunt Capacitor Banks*, The Transmission & Distribution Committee Capacitor Subcommittee with input from The Switchgear Committee, 2016.

[3] *IEEE Guide for Application of Power Apparatus Bushings*, IEEE Standard C57.19.100-1995, Aug. 1995.

[4] *IEEE Application Guide for Capacitance Current Switching for AC High-Voltage Circuit Breakers*, IEEE Standard C37.012, 2014.

[5] IEC High-Voltage Switchgear and Controlgear - Part 100: Alternating Current Circuit-Breakers, IEC 62271-100 ed2.1, 2012.

[6] *20 and 33 KV Capacitor Bank Equipment Standard*, Iran Electric Power Production and Transmission Joint Stock Company (Tavanir), Deputy Research and Technology Department, Standards Office, 2015.

[7] *IEEE Guide for Application of Shunt Power Capacitors*, IEEE Standard 1036, 2010.

[8] I*EEE Standard for Ratings and Requirements for AC High-Voltage Circuit Breakers with Rated Maximum Voltage Above 1000 V*, IEEE Standard C37.04, 2018.

[9] *IEEE Standard for AC High-Voltage Circuit Breakers Rated on a Symmetrical Current Basis - Preferred Ratings and Related Required Capabilities for Voltages Above 1000 V*, IEEE Standard C37.06, 2009.

[10] *IEEE Standard for AC High-Voltage Circuit Breakers Rated on a Symmetrical Current Basis—Preferred Ratings and Related Capabilities for Voltages above 1000V*, IEEE Standard C37.06-1, 2007.

[11] *IEEE Standard Test Procedure for AC High-Voltage Circuit Breakers Rated on a Symmetrical Current Basis*, IEEE Standard C37.09, 2009.

[12] X. Chen, and Y. Gon, "Precharge Switch: A strategy to suppress the inrush current of high voltage capacitor" in *IEEE 4th International Conference on Information Systems and Computer Aided Education*, 2021.

[13] P. A. A. Pramana; A. A. Kusuma; B. S. Munir, "Inrush current investigation of capacitor bank switching for 150kv electrical system in Indonesia," in *IEEE International Conference on High Voltage Engineering and Power Systems (ICHVEPS)*, pp. 259-263, 2017.

[14] S. Xiangzheng; G. Chunlin; and Z. Kejia, "Accurate switching strategy of shunt reactive power compensation capacitor in 220kv substation" in *IEEE Sustainable Power and Energy Conference (ISPEC)*, pp. 1612-16917, 2019.

[15] S. Rekabeslami Zadeh, G. Torabi, S. Najafi Birgani, M. Enayat Zare and M. Sarlak, "Comprehensive algorithm for determining the desirability of the amount of transient limiting," in *The 4th Conference on Applied Research in Electrical Engineering*, 2024.

BIOGRAPHY



Sadegh Rekabeslami Zadeh received the B.S. degree in electrical engineering from Shahid Chamran University of Ahvaz (SCU), Khuzestan, Iran, in 2013 and the M.S. degrees in electrical engineering from Joundi-Shapour University of Technology (JSU), Dezful, Iran, in 2023, respectively. Currently, he is Electrical Expert in Khuzestsn Steel Company. His research interests include the application of the new methods of AI in power system studies.



Gholamali Torabi received the M.S. degrees in electrical engineering from Joundi-Shapour University of Technology (JSU), Dezful, Iran, in 2019, respectively. Currently, he is Electrical Expert in Khuzestan Regional Electricity Company. His research interests include the application of the fault analysis in power transmission networks.



Sasan Najafi Birgani born in Masjed-Soleiman, Iran on February 24, 1990. Power electrical associate from Chamran technical college, Ahwaz, Khuzestan, Iran, in 2010. Bachelor of power engineering from Azad university of Masjed-Soleiman, Masjed-Soleiman, Khuzestan, Iran, in 2016. Master of power systems engineering from Jondishapour University, of Dezful Dezful, Khuzestan, Iran in 2019.He is currently an employee of local lower systems of Khuzestan, in Khuzestan, Iran, as an Expert in management and operation of electrical installations and networks.



Mehdi Enayat Zare was born on September 11th, 1981 in Dezful city, Khuzestan province, Iran. He received her Bachelor of Science (BSc.), in field of Software Engineering, from the Bu-Ali Sina University, Hamedan, Iran, in 2004. He completed her Master of Science (MSc.), in field of Software Engineering, from the Amirkabir University of Technology, Tehran, Iran, 2007. He is a faculty member of Jondi-Shapur university of technology, Dezful, Iran since 2008. His research interests lie in the area of Machine Learning, Learning Automata, Heuristic Algorithms, Agile Software Engineering, Distributed Database.



Mostafa Sarlak received the B.S. degree in electrical engineering from Khajeh Nasir Toosi University of Technology (KNTU), Tehran, Iran, in 2003 and the M.S. and Ph.D. degrees in electrical engineering from Iran University of Science and Technology (IUST), Tehran, Iran, in 2005 and 2011, respectively. Currently, he is Associate Professor in the Electrical and Computer Engineering Department, Joundi-Shapour University of Technology. His research interests include the application of pattern-recognition methods in digital power system protection and power system studies.

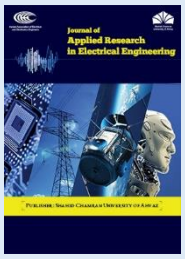
Copyrights
© 2025 Licensee Shahid Chamran University of Ahvaz, Ahvaz, Iran. This article is an open-access article distributed under the terms and conditions of the Creative Commons Attribution –NonCommercial 4.0 International (CC BY-NC 4.0) License (http://creativecommons.org/licenses/by-nc/4.0/).

Shahid Chamran University of Ahvaz

Iranian Association of Electrical and Electronics Engineers

Journal of Applied Research in Electrical Engineering

E-ISSN: 2783-2864
P-ISSN: 2717-414X
Homepage: https://jaree.scu.ac.ir/



Research Article

Deep Learning-based Underwater Object Detection and Recognition for Multi-Robot Systems

ValiMohammad Nazarzehi Had [1,*] and Zobeir Raisi [1]

[1] *Chabahar Maritime University, Chabahar, Iran*

* *Corresponding Author: v.nazarzehi@cmu.ac.ir*

Abstract: This paper introduces an innovative method for underwater object detection and recognition using a deep learning framework and autonomous underwater vehicles. The proposed method uses a deep learning framework with a network of underwater mobile robots operating within three-dimensional environments. To navigate these environments effectively, a random decentralized algorithm guides autonomous underwater vehicles (AUVs) in detecting objects within confined three-dimensional spaces. The deployment strategy involves utilizing the vertices of a cubic grid to optimize the positioning of AUVs across the search area. To enhance the object detection capabilities of mobile underwater robots within these environments and address the complexities of similar objects concealed in their surroundings, deep learning based on the YOLOv6 framework is refined to achieve improved performance and efficiency metrics. Specifically, the proposed Camouflaged Sea Edge and Attention Module (CSEA) is integrated into the YOLO framework, resulting in a substantial (8%) enhancement in mean average precision (mAP) performance, with a negligible impact (approximately 3%) on efficiency when evaluated on the publicly available TrashCan benchmark dataset. Additionally, to accelerate the training convergence and to better detect small objects within the TrashCan dataset, a distinct loss function based on Distance Intersection over Union (DIoU) is employed in the final proposed model. Several ablation studies are conducted to compare various YOLO models and evaluate the performance of the proposed CSEA module on the TrashCan dataset.

Keywords: Mobile Robots, AUVs, Distributed Control, Deep Learning, Object Detection

Article history
Received 22 October 2024; Revised 12 May 2025; Accepted 12 July 2025; Published online November 9, 2025.
© 2025 Published by Shahid Chamran University of Ahvaz & Iranian Association of Electrical and Electronics Engineers (IAEEE)

How to cite this article
V. Nazarzehi Had and Z. Raisi, "Deep learning-based underwater object detection and recognition for multi-robot systems," *J. Appl. Res. Electr. Eng.*, vol. 4, no. 1, pp. 24-33, 2025. DOI: 10.22055/jaree.2025.48211.1142

Check for updates

1. INTRODUCTION

In recent years, the progress in marine robot development has created fresh possibilities for ocean exploration. When combined with advanced machine vision techniques, self-driving underwater vehicles (AUVs) have proven very effective in studying the underwater world. Using a network of AUVs can significantly increase the speed and efficiency of certain tasks. This is especially valuable in tasks with tight deadlines or search and rescue operations. Because in tasks that require extensive sensing or data collection over a large area, multiple robots can cover more ground simultaneously. Moreover, having various robots provides redundancy. If one robot fails, others can continue the task, and this improves system reliability. In addition, multi-robot systems can be more easily scaled to handle larger workloads by adding more robots to the fleet [1].

By integrating deep learning techniques into such networks, researchers utilize these robots with the ability to autonomously process and interpret a vast array of underwater data, ranging from diverse marine species to submerged structures. Furthermore, to keep waste out of the ocean, it's beneficial to use self-operating marine robots to clear debris from the water, which depends on having a robust and accurate system for detecting objects [2].

Recently, deep learning models have demonstrated remarkable success in various applications, including object detection [3], visual place recognition [4], segmentation [5], classification [6], and video processing [7].



Fig. 1: Sample camouflaged objects in underwater images.

Deep learning architectures that are designed specifically for object detection are categorized into two-stage and one-stage frameworks. The one-stage architectures, such as YOLO [8] (You Only Look Once) and SSD [9] (Single Shot Detector), perform object detection in a single pass. On the other hand, two-stage object detection architectures, like Faster R-CNN [10] or Mask-RCNN [11], employ a two-step process. They typically involve a first stage that generates region proposals and a second stage that refines these proposals by predicting more accurate bounding boxes and object classes, enabling high-precision object detection but at the cost of increased computational complexity and slightly slower inference times, which makes them unsuitable for detecting objects in real-time in underwater environments.

With the advancement of deep learning techniques, several methods for detecting objects in underwater environments have been introduced [12-15]. While these algorithms take advantage of both the one- and two-stage deep learning frameworks to detect underwater objects, they still have difficulties in detecting challenging scenarios, including poor video quality, low visibility, contrast, and distortions in sharpness, non-uniform lighting, and reflections from suspended particles. As shown in Fig. 1 , one of the common challenges in underwater images is that the object has high similarity in hiding with its surrounding environment, which affects the final performance of the utilized detector. Moreover, the effectiveness of a group of autonomous underwater vehicles (AUVs) in searching for objects in situations where the presence of targets is uncertain and the environment is unpredictable relies on the efficiency of the search strategy.

In this paper, we extend the distributed random search algorithm presented in [16-18] by combining the proposed distributed search approach with deep learning object identification methods to improve the AUV's object detection abilities in the search environment. Using this algorithm, the AUVs move on the vertices of a cubic grid to detect objects in the entire search area. The vertices in the cubic grid will enhance the distribution of deployed autonomous underwater vehicles (AUVs). Consequently, they optimize the object detection task by efficiently spreading AUVs in the search area. In this paper, unlike the previous studies, it is assumed that the AUVs are equipped with object detection capabilities. Moreover, we discuss the pre-processing steps necessary to enhance underwater images, the architecture of convolutional neural networks tailored to underwater scenarios, the importance of annotated datasets for training, and the various challenges and ongoing research efforts in this field. We apply a newly designed module, namely CSEA, and analyze its performance on the baseline YOLOv6 [19] framework using the publicly available benchmark dataset [20]. Due to the lack of natural light and the blurry condition in underwater images, objects in the taken frames are close to the background. The main advantage of the designed CSEA module in combination with the YOLOv6 architecture is the capability to distinguish these types of objects. The main contributions of this paper can be summarized as follows:

1- This work proposes an extension to the distributed random search algorithm presented in [16-18] by integrating deep learning object detection methods, aiming to enhance the AUV's object detection capabilities in underwater search scenarios.
2- We used the YOLOv6 architecture [19] as the baseline and applied the proposed Camouflaged Sea Edge and Attention (CSEA) module to enhance the detection of camouflaged objects in underwater images.
3- To determine the most suitable YOLO architecture for underwater object detection, we trained and compared various YOLO detection models.
4- We conducted a comprehensive quantitative and qualitative ablation experiment to evaluate the performance of the proposed CSEA module when integrated with the baseline architecture.
5- To evaluate the effectiveness of our proposed model, we applied it to the well-known TrashCan dataset [20] and compared its performance with state-of-the-art (SoTA) methods, including [12-15,20].

2. Related Work

Underwater object identification has attracted remarkable research interest in recent years due to its extensive utility in fields such as marine engineering. Currently, advanced techniques for detecting underwater objects are based on deep learning frameworks, which can be summarized as follows.

2.1. Object Detection Architectures

Single Shot Detector (SSD) [9] and YOLO (You Only Look Once) [8] are well-known one-stage pipelines that aim to perform object detection and localization in a single pass through the network. These architectures divide the image into a grid of cells and predict bounding boxes and class scores directly for each cell. Typically, one-stage methods are faster due to their single-pass nature. They may need help with accurately localizing small objects or handling complex scenes with overlapping objects and often have lower accuracy compared to two-stage methods, especially on challenging datasets. Nevertheless, two-stage approaches like Faster-RCNN [21] and Mask-RCNN [22] pipelines are more accurate, especially in scenarios with small objects and complex backgrounds. These methods break the object detection process into the region proposal and object classification stages. Firstly, they produce region proposals (potential object bounding boxes) using techniques like

Region Proposal Networks (RPN). They then classify the proposed regions and refine the bounding box coordinates. However, two-stage methods are computationally more intensive due to the two-step process and may not be as applicable for applications that require real-time outputs as one-stage methods.

The one-stage and two-stage deep-learning object detection frameworks have been used in many SoTA underwater object detection algorithms [12-15] on benchmark datasets and achieved good performances. For example, Ref. [14] modified the Mask-RCNN [22] architecture by applying dilated convolution to improve the feature maps outputted from the feature pyramid network backbone, and an attention mechanism that led to adaptive learning for the network. These improvements make their proposed pipeline more suitable for detecting small garbage underwater. Ref. [20] introduced the benchmark TrashCan dataset and established a foundational detector using the Faster-RCNN [21] and Mask-RCNN [22] frameworks. This dataset and detector combination have become a significant reference point for subsequent research in trash detection, providing a standardized benchmark for evaluating detection performance and advancing the state of the art. Ref. [23] utilized the capabilities of YOLOv3 to identify underwater marine life and floating debris on the ocean's surface. Their study suggests that we can effectively use autonomous robots like drones and underwater vehicles as viable tools for the continuous monitoring and assessment of the marine environment. Ref. [24] combined the idea of deep-learning techniques and autonomous underwater vehicles (AUVs) to detect submerged objects in underwater environments effectively, which achieved promising results in underwater object detection. Ref. [24] proposed the idea of using a single autonomous underwater vehicle to identify submerged marine debris by analyzing Forward-Looking Sonar (FLS) imagery. To that effect, they first trained a deep learning Convolutional Neural Network (CNN) to perform image classification to recognize distinct objects within the FLS images. Then, the trained model is fed as an object detector by using a sliding window technique to identify and localize underwater objects. This early method highlights the capability of deep learning techniques and autonomous underwater vehicles in underwater object detection.

The above-mentioned innovative strategies represent significant contributions to the domain of detecting underwater objects using mobile robots, which forms the core focus of this paper. However, all of the mentioned studies utilized the idea of one AUV in their research. By using the potential of multiple autonomous underwater vehicles (AUVs), we can significantly enhance our ability to search and cover a wider range of underwater domains than using only one AUV, which increases efficiency, improves coverage, and enhances object detection capabilities in underwater environments.

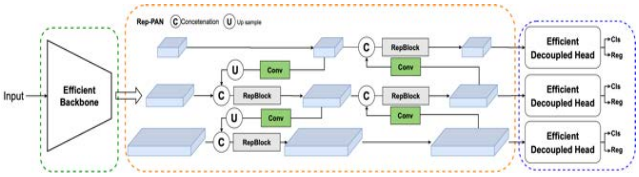


Fig. 2: The overall architecture of the baseline YOLOv6 [19].

2.2. YOLO Architectures for Object Detection

YOLO architectures [8], [25], [26] are single-stage object detection frameworks that do not require the Regional Proposal Network as used in two-stage frameworks like Faster-RCNN [21] and Mask-RCNN [22]. The YOLO architectures are also well-known for working well in multi-processing with powerful GPUs, and their networks not only reduce delays caused by hardware but also expand the range of applications in industrial settings.

After the success of the first version of YOLO introduced by [8], multiple improved versions of a framework based on YOLO have been proposed [8, 25, 26]. Inspired by ResNet and [27] Feature Pyramid Network (FPN) [28], the Ref. [26] improved the performance of the previous generation by modifying the feature extraction backbone via using a skip connection like ResNet (Darknet-53) and utilizing more prediction heads like FPN [28]. Ref. [25] improved the accuracy and inference time of the previous model by introducing a decoupled prediction head and modifying the feature extraction backbone. YOLOv6 [19] also introduced a new backbone called EfficientRep and modified the middle parts of the architecture by introducing Rep-PAN Neck, which led to a more efficient pipeline in terms of FPS and better performance regarding precision compared to the previous frameworks. It is worth mentioning that the researcher has developed other versions of YOLOs, and their performance and efficiency are slightly better in terms of Precision and FPS compared to the previous architectures. The models and their implementation of these models, such as YOLOv5 [29], YOLOR [30], YOLOv8 [31], and YOLONAS [32] can be found on GitHub.

YOLOv6 [19] is a recent architecture from the YOLO world. Its framework has several advantages in object detection; it is designed to be hardware-efficient and fast while still maintaining high accuracy, making the YOLOv6 a well-suited object detection model for a wide range of applications. Furthermore, the YOLOv6 head is an anchor-free head, which means that it does not rely on predefined anchors to predict bounding boxes. Instead, the head predicts the center and size of each object directly, which makes the YOLOv6 head faster and more efficient than anchor-based heads like Faster-RCNN [21]. Fig. 2 illustrates an overview of the YOLOv6 pipeline, which is composed of three main components: Backbone, neck, and Head, which can be summarized as follows. Firstly, the Efficient-backbone module extracts features from the input image.

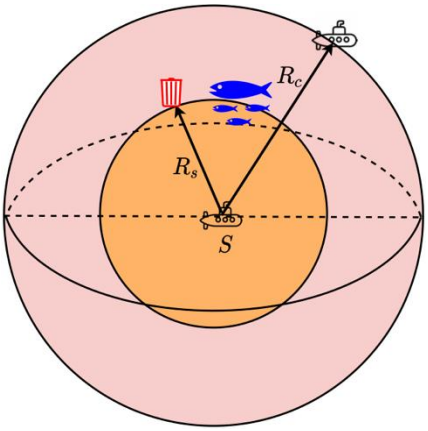


Fig. 3: The sensing and communication ranges are represented by R_s and R_c, respectively.

Then, the elements from the backbone are passed through the Rep-PAN neck to fuse them and enhance the detection features. Afterward, the combined features are passed through the anchor-free head to predict the center and size of each object. Finally, the predicted bounding boxes are post-processed to remove duplicates and filter out low-confidence detections.

Although the YOLOv6 architecture has shown remarkable performance in general object detection datasets [33], its performance may decline on challenging ocean or underwater images due to the complexity of the objects in these environments and the low-resolution images. One of the challenges that affects the performance of the baseline YOLO6 model is that the object has high similarity with its background, which is abundant underwater. These types of images, as shown in Fig. 1 make the baseline model perform poorly on these images. Inspired by the recent progress in this field and aiming to enhance the accuracy of the baseline model for these images, we incorporated a novel module known as the Camouflaged Sea Edge and Attention (CSEA) module onto the YOLOv6 architecture. This addition aids the model in more effectively identifying images of this nature.

3. METHODOLOGY

In this paper, we consider the challenge of object detection by a network of AUVs equipped with deep-learning object detection algorithms in bounded three-dimensional environments. Assume that mobile underwater robots are deployed to detect objects. Note that, in real-world scenarios, mobile robots can exhibit a diverse range of movement patterns. In this study, we specifically examine a system where mobile robots move randomly within the search area. We assume that the AUVs are using sensors with limited-range object detection capabilities, denoted as R_s. The AUVs can only identify objects located inside their detection zone, which is a sphere of radius R_s. Additionally, we consider an object as identified when it falls within the sensing range of a mobile underwater robot.

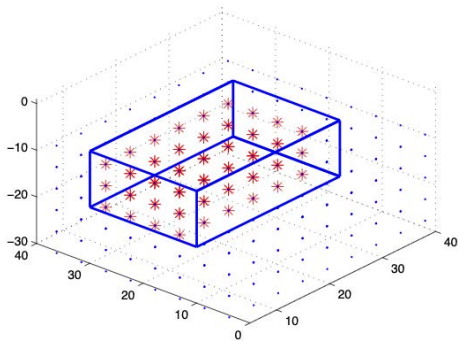


Fig. 4: The specified target region (T) is depicted as a cube, $\widehat{\mathrm{V}}$ denoted by *,V represented by '.' [17].

To guide an autonomous underwater vehicle (AUV) back to the search area, upon reaching the boundary of the search region, it is given a new random heading that steers it back into the search area. The objective of the search is to detect objects in the given search area. We also adopt a spherical communication model for each AUV, denoted as $\mathrm{R}_c > 0$, as shown in Fig. 3. This implies that AUV i can gather information about its neighbors within a sphere with a radius R_c defined by:

$$\mathrm{S}_{i,\mathrm{R}_c} = \{p \in \mathrm{R}^3; \| \left(p - p_i(\mathrm{K})\right) \| \leq \mathrm{R}_c\} \qquad (1)$$

Here, we utilize a random search algorithm based on a cubic grid to effectively disperse the autonomous underwater vehicles (AUVs) throughout the search area, enabling object detection within a confined 3D space. Consider a cubic grid that divides the target region T into uniform cubes, each having sides of length. $\frac{2\mathrm{R}_S}{\sqrt{3}}$. Denote V as the infinite set comprising the centers of all cubes within this grid. The set $\widehat{\mathrm{V}} = \mathrm{V} \cap \mathrm{T}$ is referred to as a cubic covering set for T, as depicted in Fig. 4. In the initial phase of this algorithm, the AUVs create a shared cubic grid that covers the entire search area. Subsequently, they execute the object detection task by navigating randomly among the grid vertices.

As illustrated in Fig. 5, autonomous underwater vehicles (AUVs) are represented as spheres with a sensing radius denoted as R_s, and they navigate randomly within the designated search area. Throughout the search process, these mobile underwater robots retain information about detected objects and share this data with other robots within their communication range. In the depicted scenario, AUVs 1 and 5, as well as AUV 1 and 3, fall within each other's communication ranges, facilitating the exchange of search information between them. Consequently, AUV 3 and 5 establish indirect communication through AUV 1, optimizing the search task by avoiding redundant searches for objects already detected by their counterparts. Note that, to always keep the mobile underwater robot inside the search area, the algorithm calculates how far the robot can move in the next step without going outside the boundary. If the calculated distance would take the robot beyond the search area, a new distance is chosen. This repeats until a valid distance is found, ensuring the robot stays within the designated region.

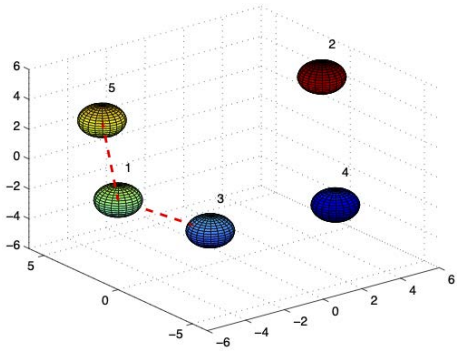


Fig. 5: Spheres denote the AUVs, -- depicts communication between the neighboring AUVs [18].

The search operation is conducted by the mobile underwater robots, which navigate randomly to the vertices of a cubic grid using random movements. Initially, it is assumed that autonomous underwater vehicles (AUVs) lack a common covering grid and a shared coordinate system. Consequently, consensus variables are employed to establish a unified covering grid, as outlined in [29]. This covering grid consists of the centers of cubes that tessellate the search area.

$$V_1 = \left(x + \alpha_1 \frac{2R_s}{\sqrt{3}}, y + \alpha_2 \frac{2R_s}{\sqrt{3}}, z + \alpha_3 \frac{2R_s}{\sqrt{3}}\right) \quad (2)$$

Vector V_1 denotes the positions of cube centers utilized to tessellate the search area. In this context, α_1, α_2, and α_3 belong to the set of integers Z. The algorithm takes the sensing range R_s and coordinates (x, y, z) as inputs, serving as a seed for the 3D grid's growth. For establishing a shared covering grid, it is assumed that each AUV possesses consensus variables $x_i(k)$, $y_i(k)$, and $z_i(k)$ within its coordinate system.

The sensing range R_s and a point $q_i(k) = \big(x_i(k), y_i(k), z_i(k)\big)$ uniquely define a 3D grid. Hence, $q_i(k)$ and R_s uniquely determine a 3D grid in T. The consensus variables $q_i(k) = [x_i(k) \quad y_i(k) \quad z_i(k)]$ along with scalar parameters α_1, α_2, α_3 and R_s describe the positions of the grid's vertices. The AUVs initiate with different values for coordination variables $x_i(0)$, $y_i(0)$, and $z_i(0)$, ultimately converging to consensus values x_0, y_0, and z_0, establishing a common coordinate system for the AUVs. Let $p_i(k)$ represent the coordinates of AUV i at time k, and $C[q, R_s]$ defines the nearest vertices of the 3D grid to point p. The following equations demonstrates the rules for updating the consensus variables and the coordinates of AUVs, which can be commutated as:

$$x_i(k+1) = \frac{x_i(k) + \sum_{j \in N_i(k)} x_j(k)}{1 + |N_i(k)|}$$
$$y_i(k+1) = \frac{y_i(k) + \sum_{j \in N_i(k)} y_j(k)}{1 + |N_i(k)|} \quad (3)$$
$$z_i(k+1) = \frac{z_i(k) + \sum_{j \in N_i(k)} z_j(k)}{1 + |N_i(k)|}$$

$$p_i(k+1) = C[q_i(k), R_s]\big(p_i(k)\big) \quad (4)$$

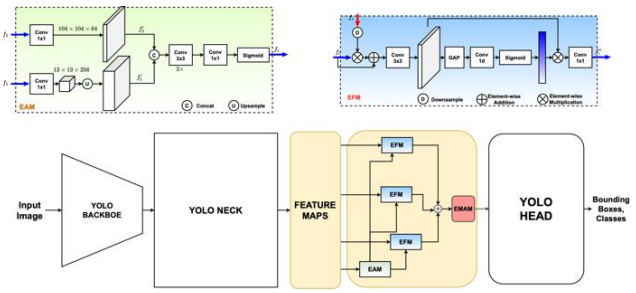


Fig. 6: The overall diagram of the proposed underwater object detection framework. The EAM (up-right) and EFM (up-left) modules were redesigned from [36] and [37], respectively.

Here, $N_i(k)$ represents the set of neighboring AUVs j (where $j \neq i$ and $j \in 1,2,\ldots,n$) within its communication range, and $|N_i(k)|$ denotes the number of neighbors at time k. Following the above equations, each underwater robot updates its consensus variables by averaging its values with those of its neighbors within its communication range. After building the common grid, the AUVs travel between grid vertices until they identify all objects using the introduced deep learning method.

3.1. Baseline Model

In this work, inspired by the YOLOv6 [19] and the camouflage object detection [34,35] architectures, we design a new framework, as shown in Fig. 6 to improve the baseline YOLOv6's (see Fig. 2) performance in underwater object detection. As seen, the network first extracts the features from the backbone, and then the extracted features to enhance the features are fed into the Rep-PAN neck to further improve the receptive field and the localization of multi-level feature maps. The resulting multi-level features are provided in the proposed module (CSEA), which consists of three main sub-blocks (more details in section 3.2) for processing to better focus on the region of interest of the object. Finally, the outputs of the CSEA features are passed through an anchor-free prediction head module that outputs the final bounding box and classes of the input image.

3.2. Camouflaged Sea Edge and Attention (CSEA) Module

Inspired by [36], after extracting multi-level features from the backbone and the neck of the YOLOv6 architecture, we integrated a new module (as shown in yellow Fig. 6) to help the model effectively distinguish the object structure and details. The integrated module is composed of three sub-blocks: edge-aware module (EAM), edge-guidance feature module (EFM), and edge mask attention module (EMAM).

The EAM sub-block combines the low and high-level features coming from the neck of YOLOv6, which effectively extracts object boundary-related edge semantics, which later help the upcoming sub-bloks to better capture edge features that are important in close to background object.

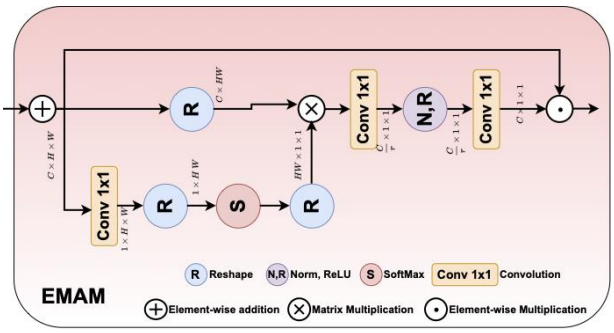


Fig. 7: The utilized Edge Mask Attention Module (EMAM) [38].

To that effect, as seen in Fig. 7, both the low-level and high-level features pass through a two 1x1 convolution layer to output an edge feature (f_e) that is obtained by concatenation and convolution operations, followed by the Sigmoid function.

The EFM sub-block works similar to an attention module in a vision transformer [37] pipeline. It enhances the representation learning in object detection by incorporating boundary-related edge cues into feature representations. This module uses a channel attention mechanism locally to improve cross-channel interaction and identify important alerts among different feature channels. The process involves element-wise multiplication between the input features (f_i) and edge features (f_e), followed by a skip-connection and a 3×3 convolution to produce fused components.

Finally, we utilize a new attention module, namely edge mask attention module (EMAM), to enable the model to obtain more contextual semantics and focus accurately on different regions of the feature maps more likely to contain objects [38]. The proposed sub-block is shown in Fig. 4. Assume F be the fused multi-level feature maps coming from the EAM and EFM sub-blocks. As shown, the global attention map ($\mathcal{G}$) in the EMAM sub-block can be computed as follows:

$$\mathcal{G} = \hat{F} \otimes \left(c_\gamma \sum_{\forall i} \frac{\exp^{c_\alpha f_i}}{\sum_{\forall j} \exp^{c_\alpha f_j}} F_i \right) \quad (5)$$

where c_α and c_γ are 1x1 convolutions that are learnable. The $\hat{F}$ is the 1-dimensional (1D) version of F. The i and j in (5) mean the enumeration for all the positions of the 2D input feature maps, and the $\otimes$ operation denotes matrix multiplication. Then to further achieve channel-wise dependencies of (5), the global attention maps transformed ($\mathcal{T}$) as follows:

$$\mathcal{T} = \sigma(c_1(R(\mathrm{L_N}(c_2(S))))) \quad (6)$$

where σ denotes the sigmoid function. c_1 and c_2 represent the trainable 1x1 convolutions. R and $\mathrm{L_N}$ show the RelU function and layer normalization, respectively.

The final output (Y) of EMAM sub-block can be calculated as follows using (5) and (6):

$$Y = \mathcal{G} \odot F \quad (7)$$

where $\odot$ shows the element-wise multiplication.

3.3. Loss Function

The head of the YOLOv6, as shown in Fig. 2, uses two loss functions for the final prediction: the classification loss that predicts the category of the object and the bounding box regression loss that outputs the coordinates of the bounding box. For the classification, an improved combination version of cross entropy and focal loss (FL) [39] called Varifocal Loss ($\mathrm{V_{fl}}$) [40] is used, which is defined as follows:

$$V_{fl}(D_i, G_j) = \begin{cases} -G_j(G_j log(D_i) + (1 - G_j) log(1 - D_i)), & G_j > 0 \\ -\alpha {D_i}^{\gamma}(1 - D_i), & G_j = 0 \end{cases} \quad (8)$$

Where D_i is the predicted class score by the model, and G_j denotes the score of the ground truth in the dataset. We use the Distance-IoU (DIoU) Loss [41] for bounding box regression. DIoU is an improved version of GIOU [42] loss, which converges faster during training and works better on small and dense object detection.

$$\mathcal{L}_{DIoU} = 1 - IoU + \frac{\rho^2(D, G)}{c^2}. \quad (9)$$

where $\rho(\cdot)$ illustrates Euclidean distance. c represents the diagonal length of the smallest bounding box that covers both detected and ground-truth bounding boxes. IoU is the intersection over a union computed as:

$$IoU = \frac{|D \cap G|}{|D \cup G|}, \quad (10)$$

where $|.|$ denotes the area, $G = (x', y', w', h')$ is the ground-truth, and $D = (x, y, w, h)$ is the predicted box. The final loss of the model, which considers both the classification of (8) and (9), can be defined as :

$$\mathcal{L} = \lambda_b \mathcal{V}_{fl} + \lambda_v \mathcal{L}_{DIoU} \quad (11)$$

where λ_b and λ_v are hyperparameters that are set to 0.8 and 1 during our implementation.

4. Experimental Results

4.1. Implementation Details

The proposed model is fine-tuned until it reaches convergence (~ 150 epochs) by using the transfer learning technique. To optimize the parameters associated with the loss functions, the AdamW optimizer [43] is employed, accompanied by the poly-learning policy. This optimization algorithm ensures that the model learns and adapts effectively throughout the training process. The training phase is carried out on a 24 GB memory of the NVIDIA RTX 3090 GPU. We set the batch size to 16 during training.

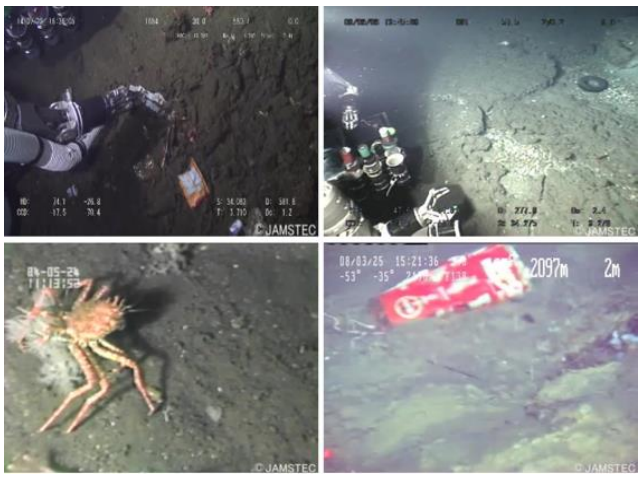


Fig. 8: Sample images of TrashCan Dataset [20].

Different augmentation strategies are applied during training, including image resizing, random rotations, and horizontal flipping. The augmentation process enables the final model to acquire a more comprehensive understanding of the TrashCan dataset and be more generalizable and robust in real-world, unseen scenarios.

4.2. TrashCan Dataset

The TrashCan dataset [20] is designed specifically for underwater object detection. The images of this dataset are collected using remotely operated underwater vehicles (ROVs), which are obtained from the J-EDI dataset [44].

The TrashCan dataset includes 7212 images of different underwater objects (22 diverse classes), mainly from the Sea of Japan. The resolution of images in this dataset changes from 480x270 pixels to 480x360 pixels, where they are annotated in the COCO dataset [33] annotation format using rectangular bounding boxes and segmentation labels. Fig. 8 illustrates some sample images of this dataset.

4.3. Evaluation Metrics

The Average Precision (AP) metric relies on precision-recall measures and works with the classes of multiple objects. It defines a positive prediction by using Intersection over Union (IOU). Precision measures the accuracy of the model for positive predictions. The Recall metric checks how many actual positive cases the model correctly recognizes. The precision (P) and Recall (R) can be calculated as follows:

$$P = \frac{TP}{TP + FP} \tag{12}$$

$$R = \frac{TP}{TP + FN} \tag{13}$$

where TP and FP denote true positives and false positives, respectively. False Negatives (FN) are the number of object regions that the model did not correctly predict.

Let G_j be the j^{th} ground-truth in the given image, and D_i be the i^{th} detection bounding box (D_i). Therefore, we can calculate the precision and recall based on the intersection over union (IoU) metric as follows:

Table 1: Comparing the proposed method's performance with SOTA methods [12-15] on the TrashCan [20] dataset. The best performance is highlighted in bold.

Model-Name	AP	AP_{50}	AP_{75}	AP_s	AP_m	AP_l
RISDU [12]	0.38	0.49	0.32	0.38	—	—
GCC-Net [13]	0.41	0.61	—	—	—	—
Hong et al. [20]	0.29	0.51	0.28	0.21	0.30	0.40
Deng et al. [14]	0.44	0.65	**0.48**	0.35	**0.48**	**0.66**
MLDeT [20]	0.42	0.63	0.46	0.37	0.42	0.57
Proposed	**0.45**	**0.66**	0.47	**0.38**	0.46	0.63

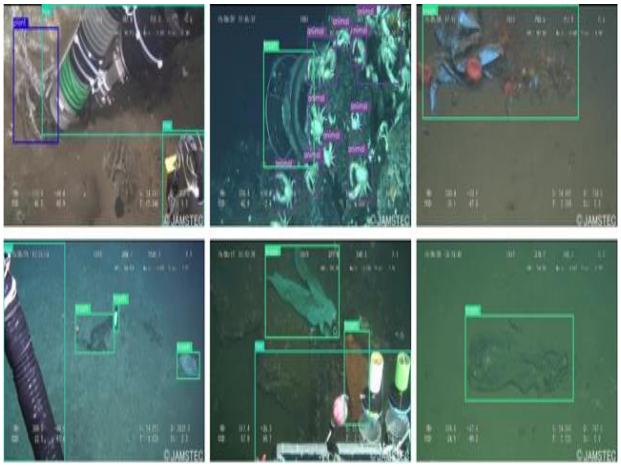


Fig. 9: Qualitative results of the proposed model on challenging samples of the TrashCan Dataset [20].

$$\text{IoU} = \frac{\text{Area}(G_j \cap D_i)}{\text{Area}(G_j \cup D_i)} \tag{14}$$

In the end, for handling multiple object categories, the mAP can be formulated as follows:

$$mAP = \frac{1}{N}\sum_{i=1}^{N} A\,P_i \tag{15}$$

where AP_i denotes the average precision of the i −th class.

4.4. Quantitative Results

In this section, we carried out a thorough evaluation of underwater object detection methods using the mean Average Precision (mAP) is a widely accepted metric in the object detection community. Table 1 presents a quantitative comparison of our proposed model with SoTA techniques on the TrashCan dataset. Our model outperforms other methods [12-15] on the TrashCan dataset, achieving the highest mAP.

4.5. Qualitative Results

Fig. 9 illustrates the qualitative results of the proposed model on some challenging images of the TrashCan dataset. As seen, the proposed model accurately detects objects in the images, which confirms the effectiveness of the proposed model.

Table 2: Comparison of the map performances of different deep learning models [19, 25, 26] on the TrashCan dataset.

Model	mAP
YOLOv3	0.33
YOOX	0.35
YOLOv6[Baseline]	**0.37**

Table 3: The effect of the utilized module on the baseline model. The best performance is highlighted in bold. "FPS" demonstrates the frames per second.

Model	Module	mAP	FPS
Baseline	-	0.37	**68**
Proposed	**CSEA**	**0.45**	65

It is worth mentioning that there are certain limitations to the proposed architecture, which may fail in some sample images. The proposed method has difficulty in the detection of low-resolution images and objects that are heavily occluded. These challenges are common and unresolved issues in the object detection community. One potential solution for addressing these challenges is augmentation techniques during training and using a higher number of instance images that contain low-resolution and occluded objects.

4.6. Ablation Study

We evaluate the performance of several SOTA deep-learning models using mean Average Precision (mAP) and Frames Per Second (FPS) metrics. To that effect, we first evaluated different YOLO models on the TrashCan dataset. As shown in Table 2, the YOLOv6 model has the best performance in terms of mAP, which makes it a good candidate as our baseline detection model for further investigation. Building upon this foundation, we applied the introduced CSEA module, which we integrated into the YOLOv6 architecture, as demonstrated in Table 3. The incorporation of the CSEA module on the baseline leads to a remarkable performance boost, signifying a substantial improvement in object detection accuracy. The successful detection of camouflage objects in Fig. 10 also confirms the effectiveness of the utilized module in the baseline architecture. We also experimented with the efficiency of our models. As seen in Table 3, the baseline model achieved a good efficiency in terms of FPS (~ 68), which confirms it can be used in real-time applications like underwater object detection using mobile robots. It can also be seen that applying the designed CSEA module does not affect the efficiency of the final model, and it obtains a close speed to the baseline model.

5. Discussion and Future Work

Deep learning models are renowned for their requirement of substantial data for training, which often leads to enhanced inference performance and more generalization capabilities on novel datasets. Our work falls into this category as well.

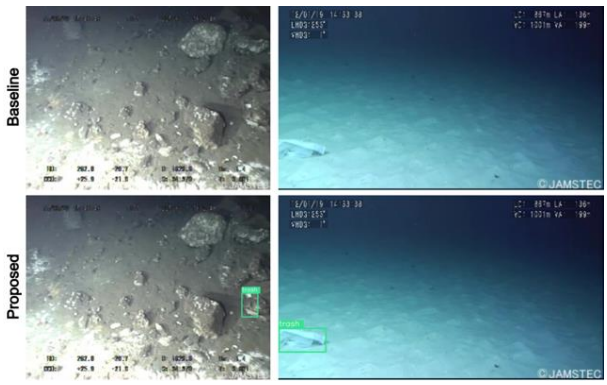


Fig. 10: Comparing qualitatively the proposed model with the baseline on objects that have a color close to the background.

As evident from the results presented in Table 1. While our proposed model achieved the SoTA performance on the TrashCan dataset, with an average precision of 0.45, these results fall short of practical application in real-world scenarios. However, this performance can be improved by utilizing a larger dataset, which could be obtained from real-world annotated datasets that are costly or can be synthetically created in limited environments to further investigate the illumination variation and generalization capability of the model, such as the pool that we intend to explore in future research. Ultimately, our objective is to apply the findings of deep learning detections to real-world autonomous underwater vehicle robots for practical and meaningful applications.

6. Conclusions

In this study, we have presented the idea of integrating distributed random search techniques with deep learning techniques to identify challenging cases in underwater images using AUVs within a 3D search environment. After experimenting with different baseline object detection frameworks, we have selected the YOLOv6 pipeline as the baseline, which has better efficiency and accuracy performance. We have designed a new module, namely Camouflaged Sea Edge and Attention Module (CSEA), and integrated it with YOLOv6 architecture to improve the detection of objects hidden in the background. We have compared our model with SoTA models on the benchmark TrashCan dataset that is designed for underwater object detection and recognition. The quantitative results have shown that the final model achieved competitive performance in comparison with SOTA methods on the TrashCan using the Average Precision metric and a real-time performance (~ 65) in terms of FPS. The CSEA module in the architecture boosted the mAP by a large margin (~ 8%) than the baseline and had a minor effect (~ 3) on the FPS. We have also provided qualitative results to show the performance of the

model and the designed CSEA module on challenging underwater images.

Credit Authorship Contribution Statement

ValiMohammad Nazarzehi Had: Investigation, Methodology, Visualization, Roles/Writing - original draft, Writing - review & editing. **Zobeir Raisi**: Conceptualization, Formal analysis, Investigation, Methodology, Software, Validation, Visualization, Roles/Writing - original draft, Writing - review & editing.

Declaration Of Competing Interest

The authors declare that they have no known competing financial interests or personal relationships that could have appeared to influence the work reported in this paper. The ethical issues; including plagiarism, informed consent, misconduct, data fabrication and/or falsification, double publication and/or submission, redundancy has been completely observed by the authors.

References

[1] V. Nazarzehi and A. V. Savkin, "Decentralized three-dimensional formation building algorithms for a team of nonholonomic mobile agents," *International Journal of Control, Automation and Systems*, vol. 17, pp. 1283–1292, 2019.

[2] J. Li, G. Zhang, C. Jiang, and W. Zhang, "A survey of maritime unmanned search system: theory, applications and future directions," *Ocean Engineering*, vol. 285, p. 115359, 2023.

[3] Z. Zou, K. Chen, Z. Shi, Y. Guo, and J. Ye, "Object detection in 20 years: A survey," *Proceedings of the IEEE*, 2023.

[4] Z. Raisi and J. Zelek," Visual place recognition from end-to-end semantic scene text features," *Frontiers in Robotics and AI,* vol. 11, p.1424883 2024.

[5] S. Minaee, Y. Boykov, F. Porikli, A. Plaza, N. Kehtarnavaz, and D. Terzopoulos, "Image segmentation using deep learning: A survey," *IEEE Transactions on Pattern Analysis and Machine Intelligence*, vol. 44, no. 7, pp. 3523–3542, 2021.

[6] W. Rawat and Z. Wang, "Deep convolutional neural networks for image classification: A comprehensive review," *Neural computation*, vol. 29, no. 9, pp. 2352–2449, 2017.

[7] M. Ghafari, A. Amirkhani, E. Rashno, and S. Ghanbari, "Smart AI-based Video Encoding for Fixed Background Video Streaming Applications," *Journal of Applied Research in Electrical Engineering*, 2023 vol. 2, no. 1, pp. 37-44.

[8] J. Redmon, S. Divvala, R. Girshick, and A. Farhadi, "You only look once: Unified, real-time object detection," in *Proc. IEEE Conf. on Comp. Vision and Pattern Recognition*, pp. 779– 788, 2016.

[9] W. Liu, D. Anguelov, D. Erhan, C. Szegedy, S. Reed, C.-Y. Fu, and A. C. Berg, "SSD: Single shot multibox detector," in *Eur. Conf. on Comp. Vision*, pp. 21–37, Springer, 2016.

[10] S. Ren, K. He, R. Girshick, and J. Sun, "Faster R-CNN: Towards Real-Time Object Detection with Region Proposal Networks," *Advances in Neural Information Processing Systems*, vol. 28, 2015.

[11] K. He, G. Gkioxari, P. Dollar, and R. Girshick, "Mask R-CNN," in *Proceedings of the IEEE International Conference on Computer Vision*, pp. 2961–2969, 2017.

[12] B. C. Corrigan, Z. Y. Tay, and D. Konovessis, "Real-time instance segmentation for detection of underwater litter as a plastic source," *Journal of Marine Science and Engineering*, vol. 11, no. 8, p. 1532, 2023.

[13] L. Dai, H. Liu, P. Song, and M. Liu, "A gated cross-domain collaborative network for underwater object detection," *arXiv preprint arXiv:2306.14141*, 2023.

[14] H. Deng, D. Ergu, F. Liu, B. Ma, and Y. Cai, "An embeddable algorithm for automatic garbage detection based on complex marine environment," *Sensors*, vol. 21, no. 19, p. 6391, 2021.

[15] D. Ma *et al.*, "Mldet: Towards efficient and accurate deep learning method for marine litter detection," *Ocean & Coastal Management*, vol. 243, p. 106765, 2023.

[16] V. Nazarzehi, A. V. Savkin and A. Baranzadeh, "Distributed 3D dynamic search coverage for mobile wireless sensor networks," *IEEE Communications Letters*, vol. 19, no. 4, pp.633-636, April 2015.

[17] V. Nazarzehi and A. V. Savkin. "Distributed self-deployment of mobile wireless 3D robotic sensor networks for complete sensing coverage and forming specific shapes," *Robotica*, vol. 36, no. 1, pp. 1-18, 2018.

[18] V. Nazarzehi and A. Baranzadeh, "A distributed bio-inspired algorithm for search of moving targets in three-dimensional spaces," in *2015 IEEE International Conference on Robotics and Biomimetics (ROBIO)*, Zhuhai, China, 2015, pp. 2507-2512.

[19] C. Li, L. Li, H. Jiang, K. Weng, Y. Geng, L. Li, Z. Ke, Q. Li, M. Cheng, W. Nie, *et al.*, "Yolov6: A single-stage object detection framework for industrial applications," *arXiv preprint arXiv:2209.02976*, 2022.

[20] J. Hong, M. Fulton, and J. Sattar, "Trashcan: A semantically segmented dataset towards visual detection of marine debris," *arXiv preprint arXiv:2007.08097*, 2020.

[21] S. Ren, K. He, R. Girshick, and J. Sun, "Faster R-CNN: Towards real-time object detection with region proposal networks," in *Proc. Adv. in Neural Info. Process. Sys.*, pp. 91–99, 2015.

[22] K. He, G. Gkioxari, P. Dollar, and R. Girshick, "Mask R-CNN," in *Proc. IEEE Int. Conf. on Comp. Vision*, pp. 2961–2969, 2017.

[23] J.-I. Watanabe, Y. Shao, and N. Miura, "Underwater and airborne monitoring of marine ecosystems and debris," *Journal of Applied Remote Sensing*, vol. 13, no. 4, Art. no. 044509, 2019.

[24] M. Valdenegro-Toro, "Submerged marine debris detection with autonomous underwater vehicles," in *2016 International Conference on Robotics and Automation for Humanitarian Applications (RAHA)*, pp. 1–7, IEEE, 2016.

[25] Z. Ge, S. Liu, F. Wang, Z. Li, and J. Sun, "Yolox: Exceeding yolo series in 2021," *arXiv preprint arXiv:2107.08430*, 2021

[26] J. Redmon and A. Farhadi, "YOLOv3: An incremental improvement," *arXiv preprint arXiv:1804.02767*, 2018.

[27] K. He, X. Zhang, S. Ren, and J. Sun, "Deep residual learning for image recognition," in *Proceedings of the IEEE conference on computer vision and pattern recognition*, pp. 770– 778, 2016.

[28] T.-Y. Lin, P. Dollar, R. Girshick, K. He, B. Hariharan, and S. Belongie, "Feature pyramid networks for object detection," in *Proceedings of the IEEE conference on computer vision and pattern recognition*, pp. 2117–2125, 2017.

[29] G. Jocher, K. Nishimura, T. Mineeva, and R. Vilarino, "Yolov5 (2020),"˜ *GitHub repository. [Online]. Available: https://github.com/ultralytics/yolov5, 2020.*

[30] C.-Y. Wang, I.-H. Yeh, and H.-Y. M. Liao, "You only learn one representation: Unified network for multiple tasks," *arXiv preprint arXiv:2105.04206*, 2021.

[31] G. Jocher, A. Chaurasia, and J. Qiu, "Ultralytics yolov8," *[Online]. Available: https://github.com/ultralytics/ultralytics*, 2023.

[32] J. Terven and D. Cordova-Esparza, "A comprehensive review of yolo: From YOLOv1 to YOLOv8 and beyond," *arXiv preprint arXiv:2304.00501*, 2023.

[33] T.-Y. Lin, M. Maire, S. Belongie, J. Hays, P. Perona, D. Ramanan, P. Dollar, and C. L. Zitnick, "Microsoft coco: Com-´ mon objects in context," in *Computer Vision–ECCV 2014: 13th European Conference,* Zurich, Switzerland, September 6-12, 2014, Proceedings, Part V 13, pp. 740–755, Springer, 2014.

[34] D.-P. Fan, G.-P. Ji, G. Sun, M.-M. Cheng, J. Shen, and L. Shao, "Camouflaged object detection," in *Proceedings of the IEEE/CVF conference on computer vision and pattern recognition*, pp. 2777–2787, 2020.

[35] H. Mei, G.-P. Ji, Z. Wei, X. Yang, X. Wei, and D.-P. Fan, "Camouflaged object segmentation with distraction mining," in *Proceedings of the IEEE/CVF Conference on Computer Vision and Pattern Recognition*, pp. 8772–8781, 2021.

[36] Y. Sun, S. Wang, C. Chen, and T.-Z. Xiang, "Boundary-guided camouflaged object detection," *arXiv preprint arXiv:2207.00794*, 2022.

[37] A. Dosovitskiy et al., "An image is worth 16x16 words: Transformers for image recognition at scale," arXiv preprint arXiv:2010.11929, 2020.

[38] Z. Raisi and J. Zelek, "Investigation of deep learning optimization algorithms in scene text detection," *International Journal of Industrial Electronics Control and Optimization*, vol. 6, no. 3, pp. 171–182, 2023.

[39] T.-Y. Lin, P. Goyal, R. Girshick, K. He, and P. Dollar, "Focal loss for dense object detection," in *Proceedings of the IEEE International Conference on Computer Vision*, pp. 2980–2988, 2017.

[40] H. Zhang, Y. Wang, F. Dayoub, and N. Sunderhauf, "Varifocalnet: An iou-aware dense object detector," in *CVF Conference on Computer Vision and Pattern Recognition (CVPR)*, pp. 8510–8519, 2020.

[41] Z. Zheng, P. Wang, W. Liu, J. Li, R. Ye, and D. Ren, "Distance-iou loss: Faster and better learning for bounding box regression," *in Proceedings of the AAAI conference on artificial intelligence*, vol. 34, pp. 12993–13000, 2020.

[42] H. Rezatofighi, N. Tsoi, J. Gwak, A. Sadeghian, I. Reid, and S. Savarese, "Generalized intersection over union: A metric and a loss for bounding box regression," in *Proceedings of the IEEE/CVF conference on computer vision and pattern recognition*, pp. 658–666, 2019.

[43] I. Loshchilov and F. Hutter, "Decoupled weight decay regularization," *arXiv preprint arXiv:1711.05101*, 2017.

[44] C. H. Lucas et. al., "Gelatinous zooplankton biomass in the global oceans: geographic variation and environmental drivers," *Global Ecology and Biogeography*, vol. 23, no. 7, pp. 701–714, 2014.

BIOGRAPHY



Valimohammad Nazarzehi Had received his Ph.D. degree in 2016 from the University of New South Wales, Australia. Currently, he is an assistant professor in the Department of Electrical Engineering, Chabahar Maritime University, Iran. His research interests include decentralized control, marine control systems, control of mobile robots, robotics, and image processing



Zobeir Raisi received his Ph.D. degree in Systems Design Engineering from the University of Waterloo, Waterloo, Canada. His graduate research focused on advanced techniques in text detection and recognition in wild images, object detection, and segmentation.

Following his Ph.D., he served as a Postdoctoral Fellow in the Department of Systems Design Engineering at the University of Waterloo, collaborating with the Vision and Image Processing Lab on several high-impact academic-industrial projects. These projects spanned areas of computer vision, image processing, and machine learning, and engaged notable partners, including Apple Inc., Baltimore Orioles Inc., and ATS Automation Inc.

Dr. Raisi's research interests are computer vision, deep learning, and artificial intelligence. He currently holds a faculty position as an Assistant Professor at Chabahar Maritime University.

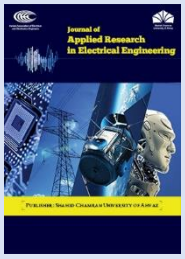
Copyrights
2025 Licensee Shahid Chamran University of Ahvaz, Ahvaz, Iran. This article is an open-access article distributed under the terms and conditions of the Creative Commons Attribution –NonCommercial 4.0 International (CC BY-NC 4.0) License (http://creativecommons.org/licenses/by-nc/4.0/).

Shahid Chamran University of Ahvaz

Iranian Association of Electrical and Electronics Engineers

Journal of Applied Research in Electrical Engineering

E-ISSN: 2783-2864
P-ISSN: 2717-414X
Homepage: https://jaree.scu.ac.ir/



Review Article

A Review on Blockchain-based Gaming: Existing Insights, Deficits, and Emerging Avenues

Patikiri Arachchige Don Shehan Nilmantha Wijesekara [1,*]

[1] *Department of Electrical and Information Engineering, Faculty of Engineering, University of Ruhuna, Galle 80000, Sri Lanka*

* *Corresponding Author: nilmantha@eie.ruh.ac.lk*

Abstract: Gaming is the notion of playing electronic games that involves users in the form of avatars or characters engaging with an interactive digital experience to achieve a specific gaming objective. Blockchains can enhance the overall gaming platform by helping to provide auditing, transparency, incentivization, security, and verification features in gaming. We analyze distinct blockchain-stemmed gaming structures, understand 11 tasks of blockchain-stemmed gaming reflection, and investigate them extensively regarding gaming- and blockchain-linked qualities. We packed an inaugural sample of 94 paper origins by extracting the papers for filtering standards chased down from E-collections, imposing a systematic and longish quality assessment scheme. Derived from the study, in blockchain-stemmed gaming, blockchain can support game auditing (C1), game incentivization (C2), gamification (C3), cooperative game play (C4), game fraud prevention and fair play (C5), game DApps with extendibility (C6), game asset ownership protection and asset transactions (C7), game user-produced elements security (C8), game credential verification (C9), game rule transparency (C10), and crypto gaming (C11). Extensive investigation discovers that in blockchain-stemmed gaming, 21.7% exploit gamification (C3), 75.6% exploit linear blockchain, and 10.8% exploit PoS consensus. As deficits, consensus approaches like proof of authority and stake, and unconventional blockchain are rarely used, while blockchain-based gaming concepts such as C1, C8, and C10 are deficient. Ultimately, we expose the advantages and asperities of the reflection of blockchain-stemmed gaming and then extend offers to shrink them.

Keywords: Gaming, Blockchain, Copyright, Fraud prevention, Auditing.

Article history
Received 30 August 2024; Revised 02 July 2025; Accepted 05 August 2025; Published online November 9, 2025.
© 2025 Published by Shahid Chamran University of Ahvaz & Iranian Association of Electrical and Electronics Engineers (IAEEE)
How to cite this article
P. A. D. S. N. Wijesekara, "A review on blockchain-based gaming: Existing insights, deficits, and emerging avenues," *J. Appl. Res. Electr. Eng.*, vol. 4, no. 1, pp. 34-55, 2025. DOI: 10.22055/jaree.2025.47893.1136

Check for updates

1. INTRODUCTION

In gaming, rules define how players deal with the game, and among them are two types of rules: formal rules that are formally defined and written for gaming and the other is informal, unwritten rules that are not formally expressed but need to be learned by the player to play the game [1]. In traditional games, game assets are owned by the game operator, while in blockchain-based gaming, assets can be owned by the players [2]. In contrast to traditional games, in which all assets are created by the game creators, user-produced elements are a new and emerging concept that allows players to produce and share their customized creations within the game environment [3]. In multi-modal multiplayer gaming environments, speech input and multimodal gestures facilitate the user to interact collaboratively within the game [4]. In character customization, players can create unique avatars by selecting different appearance options, while in a war game, weapons and equipment can be customized [5]. Game accessibility options include adjustable difficulty levels, scalable text sizes, and colorblind modes, allowing the game to be able to be played by a differently abled audience [6].

The game contains the software, content, mechanics, and design elements that define the player experience, and it can provide excitement, fear, happiness, security, insecurity, or indifference as an objective feeling to the end-users [7]. The game client communicates with the game server to exchange data like player actions, game state updates, player information, etc., while the game server is responsible for managing the game world, processing game logic, and communicating between multiple clients [8]. Authentication is critical in online games to identify the users they claim to be and provide permissions to use the game's features. In

order to achieve this process, users need to log in, and once logged in, they are provided with an authentication token [9]. Analytics can provide an insight into the player's behavior such that the game can be updated dynamically to suit the player's behavior. Research in [10] has shown that, using a multi-level game theoretical model, subordinates and principals at organizational levels should have explicit contracts for monitoring and sanctioning, where agents are players.

By simulating real-world scenarios, serious games aim to bring behavioral changes in the participants of the game subsequent to playing the game and can simulate real-world situations that may be difficult to implement in reality due to safety concerns, cost, time consumption, etc. while aiming to develop the gamer's skill [11]. On the other hand, gamification integrates game-like features such as points, badges, leaderboards, and challenges into non-game-related activities in order to motivate the desired activity [12]. Within game user research, it involves studying the interaction among players and their surroundings, using the interaction between humans and computers, studying media, and studying social science in diverse game types, not limited to entertainment games [13]. In a study that assessed the backend side of massive multiplayer online gaming, it was shown that the infrastructure-as-a-service tier performs superiorly to the platform-as-a-service tier in cloud platforms in terms of real-time latency [14]. This work surveys diverse approaches where blockchain has been utilized in numerous gaming concepts discussed above.

Blockchain is a decentralized ledger scheme that securely records transactions across a network of computers [15]. In a linear blockchain, there is a successive block continuum leveraging cryptographic hash links [16]. A non-conventional blockchain deviates from the linear blockchain, where transactions are not grouped into blocks, but individually linked to multiple previous transactions [17]. A digital signature, which is realized using public-key cryptography, is used to warrant the authenticity of transactions by using a private key for signing them and a public key to verify the signatures [18]. Smart contracts autonomously apply agreements banning the requisite for middlemen, reducing the risks of fraud and falsification, and are further strengthened by a high degree of trust thanks to blockchain's immutable features [19].

Centered around this investigation, the blockchain-stemmed gaming reflection can be ranked among the 11 tasks. First, within game auditing, the data stored in the blockchain can be utilized for auditing the game [20]. Next, within game incentivization, it includes the principle of the play-to-earn concept, or it involves trading in-game virtual assets with the aid of blockchains and tokens/cryptocurrencies [21]. Alternatively, in blockchain-driven gamification, a gamified concept is utilized along with blockchain-driven storage and collaboration to improve security and trust [22]. Further, blockchains can provide cooperative game play by facilitating the creation of cooperative game worlds, using specific cooperative consensus approaches that are based on cooperative game play, or maintaining cooperative scoring systems [23]. Next, in blockchain-stemmed game fraud prevention and fair play, game fraud like cheating is avoided using smart contracts and consensus mechanisms and also includes fair maintenance of true randomness without skewness from third parties [24]. Moreover, game DApps can be administered to perform a certain operation related to the game, such as opening a loot box with high trustworthiness [25]. Then, in blockchain-stemmed game asset ownership protection and asset transactions, game assets are typically tokenized and associated with the digital IDs of the players, and ownership regarding assets is stored on the blockchain [26]. Next, blockchains can provide transparency and accountability for game user-produced elements' security and also be utilized for game credential verification by implementing authentication and access control with the assistance of smart contracts [27]. In blockchain-stemmed game rule transparency, game rights and rules are implemented as a distributed system with the approval of peers [28]. Finally, crypto gaming refers to storing in-game resources that exist as tokens in the blockchain on top of a cryptocurrency network and trading game assets for cryptocurrency [29].

We found two review papers that have been published so far related to blockchain-based gaming. In the first paper, the authors do a systematic exploration of how blockchain has been utilized to improve educational gaming and provide insights for educational institutes [30]. In the second one, the reviewers discuss the crypto games using Ethereum as the cryptocurrency while comparing game characteristics with legal gambling perspectives [31]. However, to our perception, so far no one has done a survey on the whole blockchain-based gaming concept, discussing diverse aspects of game auditing, fraud prevention, asset ownership protection, incentivization, credential verification, rule transparency, etc. using blockchain technology. Thus, we aim to fulfill that deficiency by using this appraisal.

Fig. 1 disseminates the title listing of this inspection.

1.1. Contribution to Conventional Literature

- We separated and briefly illustrated the gaming idea (Section 3);
- An outline of the blockchain structure is exposed (Section 4);
- Analyze conventional blockchain-stemmed gaming structures (Section 5);
- Investigate extensively on the analyzed blockchain-stemmed gaming structures (Section 6);
- The advantages and asperities of blockchain-stemmed gaming are exposed (Section 7);
- Offers and coming ways for harnessing blockchain-stemmed gaming are exposed (Section 8).

2. METHODOLOGY

This study analyzes the active examinations of blockchain-stemmed gaming spread as digital files throughout history, imposing a systematic and longish mixed-method quality evaluation scheme [32].

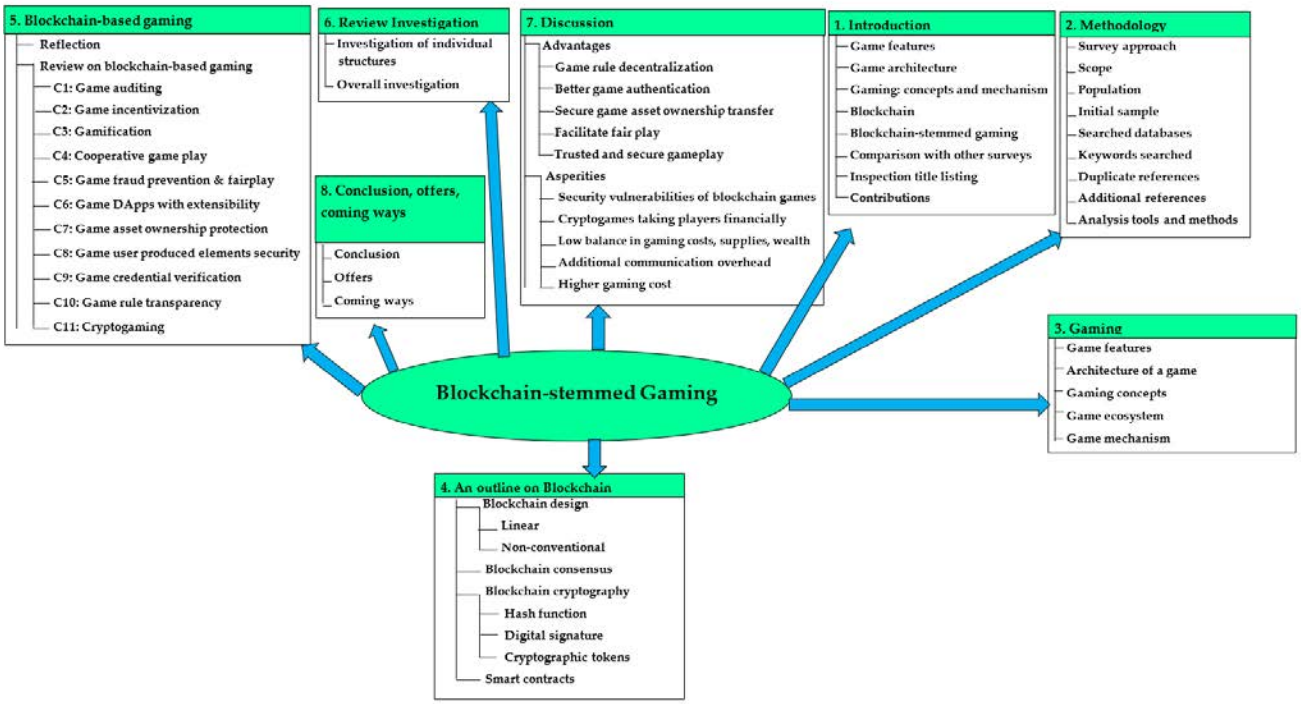


Fig. 1: Title listing of blockchain-stemmed gaming inspection.

Particularly, it evaluates a combination of the principles of gaming and blockchain. Therefore, all unprecedented research papers and cyberworld papers posted on gaming, blockchain-stemmed gaming, and blockchain characterize the scenario set in the setting of this study. However, the scenario-set sources are enigmatic to explore. Hence, imposing the pertinent investigating terms and filtering standards, we packed 97 sources from unprecedented research papers and cyberworld papers.

We chased down Google Scholar, ScienceDirect, ACM Digital Library, Wiley Online Library, MDPI, and IEEE Xplore Digital Library. The favorite investigating terms were "Gaming" OR "Blockchain-stemmed gaming" OR "Blockchain-stemmed user produced content" OR "Blockchain-maintained game rules transparency" OR "Blockchain-maintained virtual assets" OR "Blockchain-stemmed multiplayer functionality" OR "blockchain and game architectures" OR "blockchain-stemmed game monitoring and analytics" OR "Blockchain-stemmed serious games" OR "Blockchain-stemmed gamification" OR "Blockchain-stemmed game authentication" OR "Blockchain-stemmed game auditing" OR "Blockchain-stemmed game fraud prevention" OR "Blockchain and game incentivization" OR "Blockchain and game asset ownership protection" OR "blockchain and game asset reusability" OR "Blockchain".

Some factors in extracting the papers articulated the filtering standards. First, the referenced research orders English phrasing, and thereafter, it orders exceptional connection to the investigating term. Next, for elevating the reliableness of the conducted study, serial articles were supplied with a raised preference than seminar papers and non-peer-reviewed content. We didn't prioritize unprecedented research papers within a specified content producer satisfying the filtering standards; rather, we processed all content producers equivalently. The final filtering standard publishes that a specified unprecedented conceptual essay orders revelation within the time of 1975 and 2024.

The inaugural sample was moderated to 94 origins of papers; latterly, it was disclosed that 3 origins were surpluses. We quoted conceptions and illustrations employing 38 paper origins. To complement this study with prevalent studies, we at last fused 2 literature analysis papers to the assemblage of papers, shifting the universal volume of origins of papers to 134.

To study accumulated blockchain-stemmed gaming, we drew on the catalogs for study categorization. We drafted realizations drawing on Office 365 to objectively oversee study data glued to gaming- and blockchain-stemmed factors [33].

3. GAMING

3.1. Game Features

3.1.1. Rules

Rules are considered the building blocks of a game since they define how participants deal with the game and among them. There exist two types of rules in gaming according to literature. One is formal rules that are formally defined and written for gaming, and the other is informal, unwritten rules that are not formally expressed but need to be learned by the player to play the game [34]. If rules are not clearly defined, it will affect the gameplay and degrade the quality of experience felt by the player. Rules define how players move around the game and how they earn points to win the game. In [35], the authors review how gaming can be used for education by changing the play rules such that it engages the student in a hands-on learning activity.

3.1.2. Assets

Assets are different virtual properties (visual-audio components) that constitute the game, including but not limited to character models, animations, background music, sound effects, credits, items, avatars, etc. CloudyGame has been proposed as a new software architecture to share and manage various playing instances with on-demand game asset streaming on edge servers, enabling cloud gaming on the edge [36]. These contribute to improving the immersion and appeal of a game, providing a better experience for the player. The avatar customized by users has been shown as a virtual asset that captures the virtual identity of players in massive multiplayer online games [37]. In traditional games, these assets are owned by the game operator, while in blockchain-based gaming, assets can be owned by the players. Monster is a scheme that utilizes deep learning and generative artificial intelligence models with the Pixel2Mesh architecture to automatically generate 3D gaming assets that would otherwise require a graphic designer [38].

3.1.3. User-produced elements

In contrast to traditional games, in which all assets are created by the game creators, user-produced elements are a new and emerging concept that allows participants to produce and share their customized creations within the game environment. Barbarossa is a user-generated content-driven pervasive role-playing game that introduces portability to pervasive games otherwise restricted to limited environments [39]. This is different in comparison to traditional games, where the players are restricted to a specific game. Moreover, this user-generated content has the capability to be collaboratively utilized in numerous games that encourage players to create new content. In [40], the authors propose a method to learn user quality-of-perception of cloud gaming utilizing features of user-produced elements like feature words of text. Examples of user-generated content are custom levels, mods, skins, characters, etc. that are not predefined by the game developer. There are instances in which entire new games have been created due to user-generated content. Examples are "Counter Strike" and "Defense of the Ancients", which evolved from "Half Life" and "Warcraft III", respectively [41]. User-produced content can be optimally collected on game servers, where the game creators can make real-time decisions based on user statistics derived from them [42]. Data collection should not negatively affect the gaming performance and should be collected with minimal overhead; therefore, real-time optimizing systems are more appropriate for data gathering [43].

3.1.4. Multiplayer functionality

Multiplayer functionality provides the opportunity for the players to interact with each other in real-time, either cooperatively or competitively, through a network in online multi-playing games. Research in [44] points out 4 networking aspects that should be satisfied for efficient multi-playing: networking resources like bandwidth and latency, communication architectures, scalability by parameterization, and security against cheating and vandalism. The level of multi-playing can vary from simple cooperation to large-scale battles. Features such as matchmaking, leaderboards, and voice can improve the overall multiplayer experience. In [45], a ranking system has been introduced to improve the user experience for massive multiplayer games like "League of Legends". In multi-modal multiplayer gaming environments, speech input and multimodal gestures facilitate the user's ability to interact collaboratively within the game [46].

3.1.5. Customization options

Customization options predefined by the game developer allow players to personalize their gaming experience based on their own playstyle and preferences. For instance, in character customization, players can create unique avatars by selecting different appearance options. In [47], researchers show that there is less association between avatar customization and cooperation or competition in game play, while these have a resemblance to social outcomes. In a war game, weapons and equipment can be customized. These further include a customizable user interface that allows adjustments in display options, audio preferences, etc. In interactive storytelling, a user-centric approach is recommended, which provides various customization levels for optimizing the gaming experience without being limited to technology attributes or medium characteristics [48].

3.1.6. Accessibility options

Accessibility options aim to strike a balance between players' physical and cognitive abilities. A review in [49] shows that differently abled people find difficulties in games due to not receiving feedback, not having identification in in-game responses, and the inability to provide inputs from various input devices. These include adjustable difficulty levels, scalable text sizes, and colorblind modes, allowing the game to be played by a differently abled audience. To improve accessibility, game developers often use subtitles and audio descriptions. For instance, in [50], a user-friendly interface with visual cues and icons is designed for gaming that can be projected to a screen or use touchscreen technology, reducing the struggle of interacting while playing board and card games.

3.2. Architecture of a Game

3.2.1. Game client

The game client is the application program with which the players interact directly, which is installed on the player's device and responsible for rendering graphics, playing sounds, and handling user input. In a performance evaluation done by using the game Ms. Pac-Man, it has been found that frame rate and distortions of display are critical factors for gaming using thin clients, while they have different degrees of robustness to network impairments [51]. The game client communicates with the game server to exchange data like player actions, game state updates, player information, etc. The data-transfer channel among the game server and the client should meet the high-end quality of service requirements for the purpose of the game to be productive [52]. Another study done on the performance of the client in mobile cloud gaming states that they can save energy by 30%, and bitrate and framerate affect the decoder's resource consumption, with framerate having the highest effect [53].

Fig. 2 disseminates the hybrid client-server architecture that exists in multiplayer games.

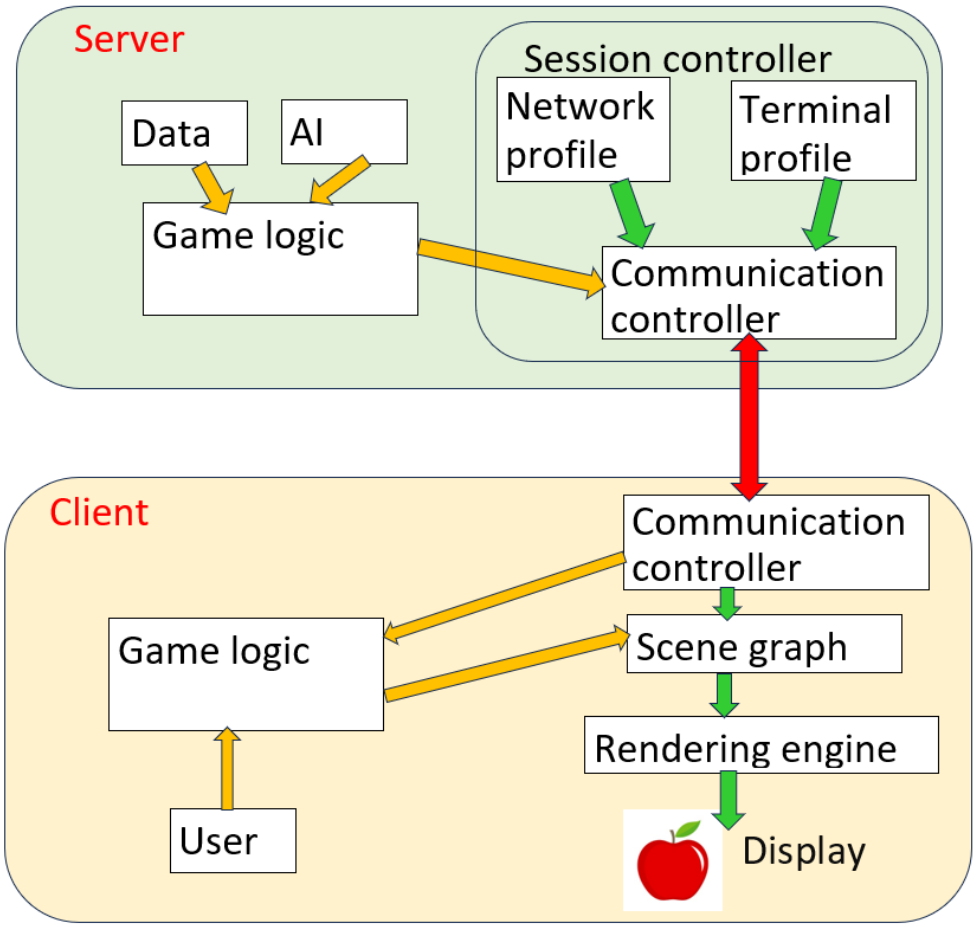


Fig. 2: Hybrid client-server architecture of multiplayer games.

3.2.2. Game server

The game server is responsible for managing the game world, processing game logic, and communicating between multiple clients. An algorithmic approach to server provisioning by using queuing theory and stochastic models in order to select server type and distribution of software has been studied in [54]. Moreover, in [55], a cloud mobile gaming approach by shifting the workload of gaming engines to cloud servers while mobile devices only provide gaming commands to servers has been used and tested for user quality of experience. Furthermore, it stores the authoritative version of the game state so as to warrant consistency among all clients. In order to prevent authentication problems and unauthorized use of copyrighted content, server abandonment should be prevented in order to protect the rights of game stakeholders [56]. Not only that, it handles physics simulation, game rule enforcement, player connections, and matchmaking. In mobile cloud gaming, the network should result in low-latency communication while also maintaining reliable communication, since gaming involves the transmission of video and audio frames [57]. Therefore, link-lifetime-based routing approaches are more suitable to be deployed in such environments that take into effect the dynamics of the mobile network while also minimizing latency [58].

3.2.3. Monitoring and analytics tools

Monitoring tools can track the performance and health of game servers in order to identify if any issues exist. Research in [10] has shown that using a multi-level game theoretical model, subordinates and principals at organizational levels should have explicit contracts for monitoring and sanctioning, where agents are players. Analytics can provide an insight into the player's behavior so that the game can be updated dynamically to suit the player's behavior. Research in [59] shows that game and learning analytics are less suitable for analytics in serious games and that serious game analytics are required to show actionable insights to retrain or remediate playing learners. Moreover, similar measures and gameplay action behavior profiles with n-grams to preserve navigation of directional paths have been evaluated for differentiation of user profiles in serious games [60].

3.3. Gaming Concepts

3.3.1. Serious games

Serious games are aimed at ambitions beyond enjoyment, like education, demonstration, training, etc. By simulating real-world scenarios, they further aim to bring behavioral changes in the participants of the game subsequent to playing the game. Serious games can simulate real-world situations that may be difficult to implement in reality due to safety

concerns, cost, time consumption, etc., while aiming to develop the player's skills [61]. Furthermore, they incorporate game mechanics and elements while aiming to achieve a specific purpose. They can be used to improve the psychological and physiological sensory motor functions and change the nutritional factors of elderly people in rehabilitation [62]. An investigation into the impact of serious games on medical training indicates that the game has motivated experienced medical students; however, it is counter-productive for new students [63]. A serious game designed for disaster preparedness of earthquakes' behavioral response and evacuation has shown that the game play has increased knowledge about evacuation and self-efficacy [64].

3.3.2. *Gamification*

Gamification is the principle of applying game design principles and elements in non-game contexts with the objective of enhancing engagement and motivation. It integrates game-like features such as points, badges, leaderboards, and challenges into non-game-related activities in order to motivate the desired activity. For instance, a study done using the Kano model shows that fitness applications that reward users based on completing workouts have a high degree of user satisfaction [65]. Furthermore, systematic reviews suggest that language learning platforms with progress tracking using virtual reality and gamification indeed help to learn foreign languages effectively, especially the English language [66].

3.3.3. *Exercise gaming*

Exercise gaming demands physical activity from the players, promoting physical fitness of the players while at the same time providing entertainment. In a study done among older adults aged more than 50 years, they preferred virtual augmented exercise gaming over traditional exercises, despite not having evidence for an association between physical fitness and game performance [67]. These often involve full-body tracking and motion controllers. "Exercise My Game" has been shown as a platform to transform a given traditional action game into a full-body motion game by mapping control input into game action and mixing input feedback with the game's interface by considering game requirements [68].

3.3.4. *Simulation gaming*

Simulation games replicate real-world systems in a virtual environment. Players can take on different roles, such as controller, manager, and designer of diverse elements like cities, vehicles, etc. A comparative study done on two flight simulation games, "Falcon 4.0" and "Microsoft Flight Simulator", shows that Falcon participants have shown short and long transfers in flight evaluation metrics, proving that the game has fortified them for common and special military activities [69]. In the planning profession, the "SimCity" game simulator has been used to provide a dynamic decision-making surrounding for students to develop problem-solving skills and crafting, despite not being a tool that helps to achieve learning outcomes in all students [70].

3.3.5. *Social games*

Social games are games that promote social interaction and are played with cooperation or competition with other players. In social games, according to [71], challenges, communication, providing gifts, meeting friends, and friends bars have been identified as techniques that improve the social aspects of social games. "World of Warcraft" has been shown as a game that has social aspects that allow players to have social relations and provide social game elements such as grouping with social networks [72].

3.3.6. *Narrative games*

Narrative games involve delivering narratives or character-driven experiences, where players make choices that influence the direction of the story, leading to various branching paths. Research has shown that game mechanics in narrative games provoke the game players to act in a way that helps in the construction of engaging stories out of the player's mind by creating tension using spatial conflicts, characterization, and moral dilemmas [73]. In the narrative game "Life is Strange", non-violent interpersonal conflicts are encouraged and allowed to be experienced by game mechanics that do not emphasize winning or losing, but rather putting into practice ethical exploration and empathy [74].

3.4. Game Ecosystem

The game ecosystem is graphically disseminated in Fig. 3.

3.4.1. *User*

Users are the individuals who interact with the game and have their own set of skills and preferences. Within game user research, it involves studying the interaction among players and their surroundings by using the interaction between humans and computers, the study of media, and social science

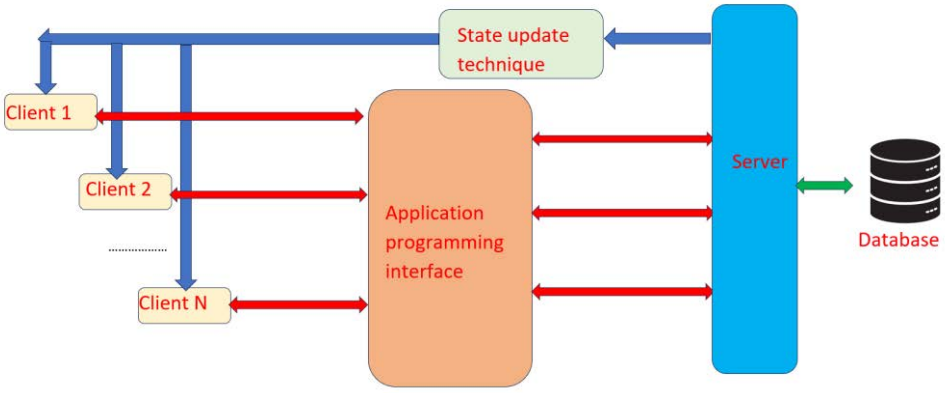


Fig. 3: Cloud-based multiplayer game ecosystem.

in diverse game types, not limited to entertainment games [75]. However, some computer game users have been reported to show addiction to it, characterized by excessive use of gaming such that it negatively interferes with common tasks, and these users have shown lower dopamine levels to gaming-related stimuli [76].

3.4.2. Interface software and device

Interface software and devices are the mediums through which users interact with the game. In [77], a hand-gesture-based interface to interact with the game in a public setting using vision algorithms to identify the complex gestures has been studied. Hardware interfaces include gaming consoles, personal computers, and mobile phones. The software interface provides the graphical and audio interfaces required to navigate menus, control characters, and interact with the game environment. However, in pervasive gaming, users are not restricted to traditional graphical user interfaces or computer screens, but are supported by tangible user interfaces in which players can grasp and move real-world objects for interaction with the game [78].

3.4.3. Backend platform

The backend platform is comprised of infrastructure and services that support online functionality and connectivity to the game, such as databases, servers, networking protocols, matchmaking algorithms, etc., enabling multiplayer gameplay, social interactions, downloadable content, etc. In a study that assessed the backend side of massive multiplayer online gaming, it was shown that the infrastructure-as-a-service tier performs superiorly to the platform-as-a-service tier in cloud platforms in terms of real-time latency [14]. Moreover, game-backend-as-a-service has been proposed with the development of gamification as a service in order to provide cross-platform game services embedding game features like leaderboards and remote storage [79].

3.4.4. Game

The game contains the software, content, mechanics, and design elements that define the player experience. A game can provide excitement, fear, happiness, security, insecurity, or indifference as an objective feeling to the end-users. In order to deliver a particular objective feeling to the user, there are numerous game categories such as action, puzzle, shooter, fight, flight, sports, strategy, etc. The author in [80] argues that gameplay and interactivity are distinct features, while gameplay is associated with emotions and player experience. Game play can consist of narratives, immersive worlds, and rewarding progression systems, while it can be aligned with a game story to enhance the player experience by enhancing immersion and improving player motivation. In [81], authors proposed machine learning to classify game events in order to discuss the relationship among diagnosed event clusters and patterns in game design to incorporate player personal profiles for analysis. Machine learning can be effectively used to classify game events and for other classification or regression problems related to gaming [82].

3.5. Game Mechanism

3.5.1. Game loop

The game loop is the backbone of the game, which is a continuous loop that runs throughout the game's lifetime. The main functions of this are input handling, updating, and rendering graphics. This loop starts by gathering input from the player, such as key strokes, joystick inputs, etc., and the game updates its internal state based on the received input by considering other factors such as physics calculations, game logic, etc., in order to render the updated state to the screen. Work in [83] proposes the simultaneous parallel operation of a graphic processing unit and a central processing unit to process game loop activities using Lua scripts to choose the best processor for a given task by considering performance over time. Moreover, this loop is iteratively run throughout the game to provide an illusion of real-time gameplay. Some have proposed the gameplay loop for educational game design using knowledge from didactics, taking into consideration curriculum and mediation, and player-centric design [84]. Thus, knowledge generation models like machine learning tools can be effectively utilized to extract knowledge from the game loop for improving game design [85].

3.5.2. Game authentication

Authentication is critical in online games to identify the users they claim to be and provide permissions to use the game's features. In order to achieve this process, users need to log in, and once logged in, they are provided with an authentication token that uniquely identifies a player session. For subsequent transactions between the game client and server, this authentication token is used for user validation. By criticizing weaknesses in single-time user authentication, continuous authentication has been realized in gaming environments with the aid of mouse movement tracking acting as credible reliability markers to authenticate users in real-time and has shown good performance compared to static authentication [86]. Some have proposed a novel interactive framework that necessitates players to pursue a gaze pattern in order to provide authentication to the game that prevents early-prepared videos or images from deceiving the authentication system [87].

3.5.3. Virtual assets

Virtual assets are items or currency within a gaming environment that are really valuable to the game players, such as weapons, armor, virtual currency, etc. However, it has been reported that some have misused virtual assets, such as virtual currencies, in multiplayer online games where cybercriminals have used them to send virtual currencies to other cyber-criminals, known as money laundering [88]. These assets are usually created by game developers using 3D modeling software and are stored in the game database along with their metadata [89]. Players may buy or sell virtual assets during gameplay in agreement with game mechanics, either using virtual or real-world currencies, allowing monetization. Recently, researchers have proposed photogrammetry, a technique to generate photorealistic 3D models, for generating 3D models in gaming systems [90].

Table 1 disseminates conventional literature on the gaming idea.

Table 1: Conventional literature on the gaming idea.

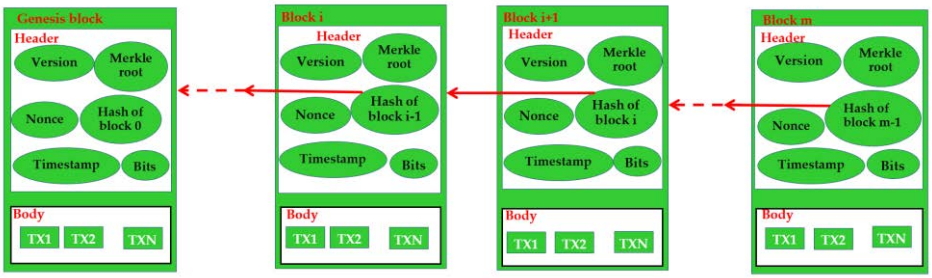
Gaming aspect	Conventional literature	Strategy	Performance
Game rules	Authentic design [35]	Changing play rules for learning	Not applicable
Game assets	CloudyGame [36]	Streaming of assets dynamically and sharing game instances	70-80% lower memory and computational resource requirement, scalable
	Virtual assets [37]	Study role of game character in massive multiplayer online games	Offer implications to business field
	Monster [38]	Deep learning with Pixel2Mesh architecture	Reduce intervention and expenditure for 3D game object construction
User generated elements	Barbarossa [39]	User generated content driven pervasive role-playing game	Improves user quality of experience
	CGQoE [40]	Predicting cloud gaming QoE using user produced elements using 14 feature words	Able to predict QoE and can analyze factors affecting it
Multiplayer functionality	Multiplayer computer games [44]	Present 4 networking aspects for efficient multi-playing	Discuss and analyze the aspects
	Sensitive matchmaking [45]	A ranking system to improve user experience	Applicable to League of legends and can be generalized
	Multimodal multiplayer tabletop gaming [46]	Players interact directly using speech and hand gestures	Multimodal gestures and speech enhance collaborative interaction
Game customization	Avatar customization [47]	Cooperative gaming and avatar customization	In game cooperation and competition have an effect on social outcomes
	Interactive storytelling [48]	Customization levels for optimizing gaming experience	Have analyzed on interactive storytelling
Game accessibility	Interaction with accessibility [50]	A user-friendly interface with visual cues and icons	Reduces the struggle for interacting for playing board and card games
Game client	Thin client gaming [51]	Evaluate performance of game Ms. Pac Man using 3 thin clients	Frame rate and distortions of display are critical factors for gaming
	Mobile cloud gaming performance [53]	Cloud gaming platform to do experiments on actual mobile clients	Save energy by 30% and bitrate and framerate affect decoder's resource consumption
Game server	Server provisioning [54]	Queuing theory and stochastic models	Computationally efficient and cost optimal
	Cloud server based mobile gaming [55]	Develop a MGUE model and a prototype to measure user experience	Validate MGUE model and characterize user experience
	Server authentication [56]	Propose ideas to prevent server abandonment	Protection measures can protect access to legally purchased items
Game monitoring and analytics	Monitoring and gaming [10]	Multi-level game theoretical model with monitoring and sanctioning	Has applied the model to the financial service industry
	Serious game analytics [59]	Analyze and discuss on the perspective of serious game analytics	Game and learning analytics are less suitable for analytics in serious game
	Evaluation of similarity measures [60]	Differentiate players based on GAD profiles using similarity measures	Similarity measures used in combination are more effective
Serious games	Prevention and rehabilitations [62]	3 criteria to evaluate effectiveness of serious games	Improve the psychological and physiological sensory motor functions of elders
	Medical training [63]	Five empirical studies to assess serious games	Motivated the experienced medical students
	Disaster preparedness [64]	Training done in Auckland city hospital using immersive virtual reality	Increased the knowledge about evacuation and self-efficacy
Gamification	Fitness application [65]	Reward users based completing workouts, Kano model for evaluation	High degree of user satisfaction
	English language learning [66]	Virtual reality and gamification	Help to learn foreign languages effectively
Exercise gaming	Virtual augmented exercise gaming [67]	Tested 3 versions of VAE	Preferred for virtual augmented exercise gaming over traditional exercises
	Exercise my game [68]	Full body motion game by mapping control input into game action	Converted Portal 2 into exergame "Sportal"
Simulation gaming	Transfer of training [69]	A study done using 3 groups: Falcon, Microsoft FS, and control	Falcon 4.0 players have shown short and long transfer in flight evaluation metrics
	SimCity [70]	Have evaluated the learning of students using SimCity	Allow students to develop problem solving skills and crafting
Social games	Social mechanics [71]	Analyze social mechanics in social games	Different mechanisms were found to encourage social activity
	World of warcraft [72]	Explore social relations and social game elements impact experience	Design suggestions to enhance user experience are proposed
Narrative games	Narrative game mechanics [73]	Conduct 3 case studies	Provoke the game players to act and create tension
	Life is strange [74]	Detailed case study of representations of how game mechanics allow playing of interpersonal conflicts	Non-violent interpersonal conflicts are encouraged
Game user	Game user research [75]	Learn about interactions between users and game	Present a case study on methods
	Game addiction [76]	Studied interactions for a motorbike riding game	Game users have shown excessive use of gaming
Game interface	Playing into wild [77]	Hand gesture-based interface	Obtained results for "Tortellino X-Perience"
	Pervasive gaming [78]	Tangible interface by physically grasping and moving	Developed framework as part of a game design course
Game backend	Multiplayer game backends [14]	Evaluate suitability of cloud platforms for developing backend of MMOG	infrastructure-as-a-service tier performs superior to platform-as-a-service tier
	GBaaS [79]	Game-backend-as-a-service for cross platform game services	Survey some GBaaS
Gameplay	Gameplay emotions [80]	Argue gameplay and interactivity as distinct features	Gameplay is associated with emotions and player experience
	PPAX [81]	Gameplay experience assessment with machine learning	Discuss relationship among events and game design patterns
Game loop	Adaptive game loop [83]	Game loop activities using Lua scripts to choose the best processor	Find the optimum processor for grouped tasks
	Educational game design [84]	Player centered design using knowledge from didactics	A case investigation of a literacy game shows the application of gameplay loop method
Game authentication	User identity [86]	Mouse dynamics for continuous authentication	Good performance compared to static authentication
	Live authentication [87].	Gaze pattern for authentication	Prevents early prepared videos or images from deceiving the authentication system
Virtual assets	Photogrammetry [90]	Generate photorealistic 3D models	Discuss possible areas of application

4. An Outline on Blockchain

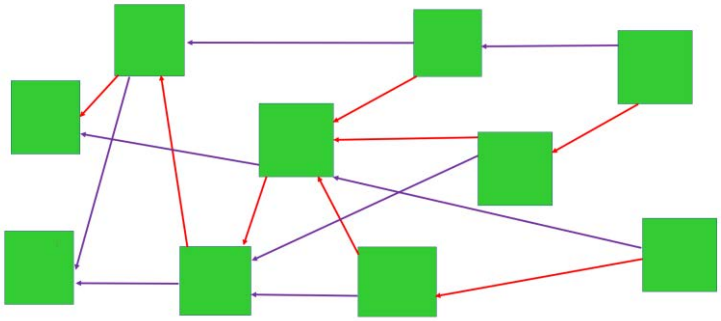
Blockchain is a dispersed ledger scheme that securely logs transactions across a network of computers [91]. The records are immutable, making it not possible to alter or delete them without the consensus of the participants, further making the blockchain transparent [92].

4.1. Design

In a linear blockchain, there is a successive block continuum leveraging cryptographic hash links [93]. A non-conventional blockchain deviates from the linear blockchain, where transactions are not grouped into blocks but individually linked to multiple previous transactions [94]. This structure makes them scalable and has a high throughput,



(a)



(b)

Fig. 4: Blockchain designs (a) Linear, (b) Non-conventional (Graphchain).

as transactions can be processed concurrently. There exist also hybrid structures that combine the features of linear and non-conventional blockchains [95].
Fig. 4 disseminates linear and non-conventional blockchain architectures.

4.2. Consensus

Consensus is the mechanism by which blockchains reach agreement on the validity of transactions in order to maintain their integrity [96]. In traditional consensus approaches, miners compete to solve a complex puzzle, and the first to solve it gets the opportunity to add the next block [97]. Other consensus approaches include those based on the number of coins held and ability to stake, the holding of high reputation and authority, the ability to allocate disk space, etc. [98].

4.3. Cryptography

Cryptographic algorithms are utilized to maintain the security and tamper-proof nature of transactions, unlike data aggregation [99]. In hash functions, input data produces a fixed-size character string, which is used to ensure data integrity and create unique identifiers for blocks [100]. A digital signature, which is realized using public-key cryptography, is used to warrant the authenticity of transactions by using a private key for signing the transactions and a public key to verify the signatures [101]. Cryptographic tokens are used to represent assets, ownership, and ownership transfer in decentralized applications [102].

4.4. Smart Contracts

In smart contracts, terms of agreement are directly written into the code that can execute itself when predefined conditions are met [103]. Thus, these can be used to automate the execution of agreements, eliminating the need for intermediaries, reducing the risks of fraud and manipulation, and further strengthening the high degree of trust thanks to blockchain's immutable features [104].

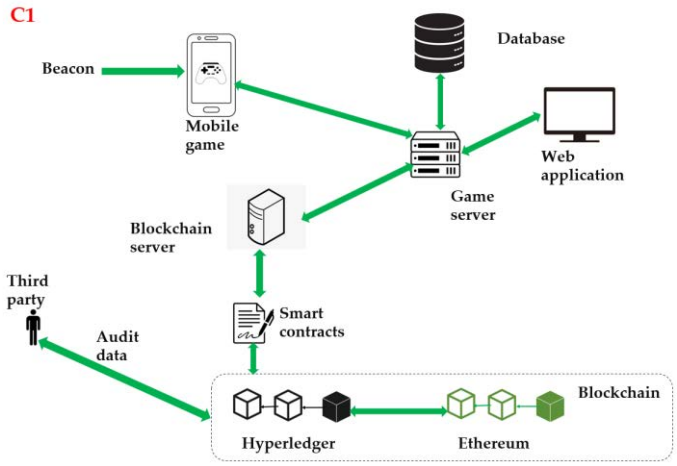
5. BLOCKCHAIN-BASED GAMING

5.1. Reflection

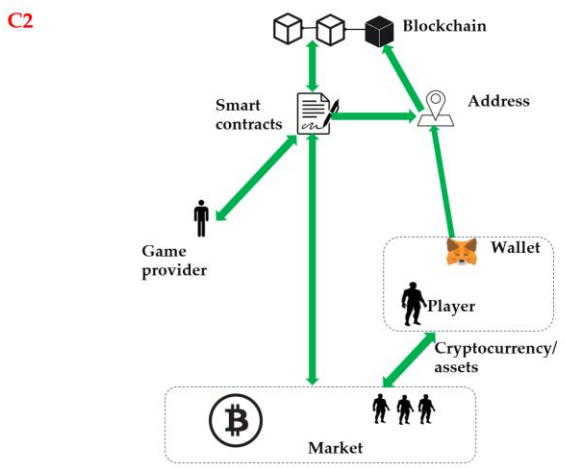
Centered around this investigation, the blockchain-stemmed gaming reflection can be ranked into the nether 11 tasks**.**

- Game auditing (C1)
- Game incentivization (C2)
- Gamification (C3)
- Cooperative game play (C4)
- Game fraud prevention and fair play (C5)
- Game DApps with extendibility (C6)
- Game asset ownership protection and asset transactions (C7)
- Game user-produced elements security (C8)
- Game credential verification (C9)
- Game rule transparency (C10)
- Crypto gaming (C11)

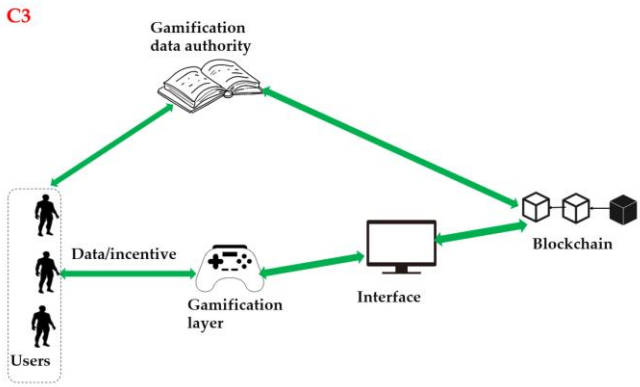
Fig. 5 illuminates the reflection of blockchain-stemmed gaming.


C1
Beacon
Mobile game
Database
Web application
Game server
Blockchain server
Third party
Audit data
Smart contracts
Blockchain
Hyperledger
Ethereum

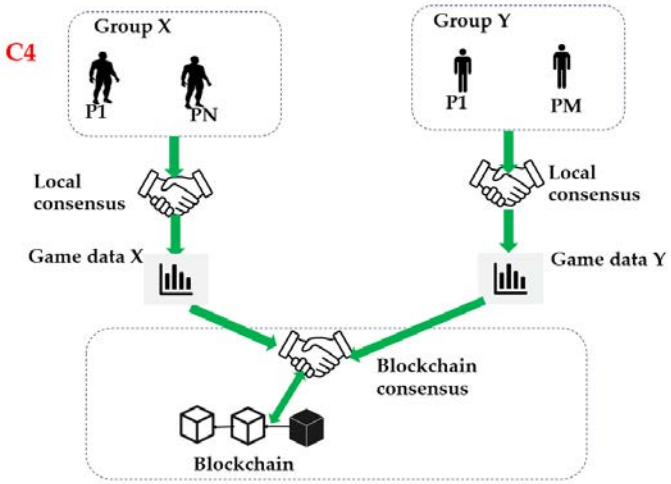
(a)


C2
Blockchain
Smart contracts
Address
Game provider
Wallet
Player
Cryptocurrency/ assets
Market

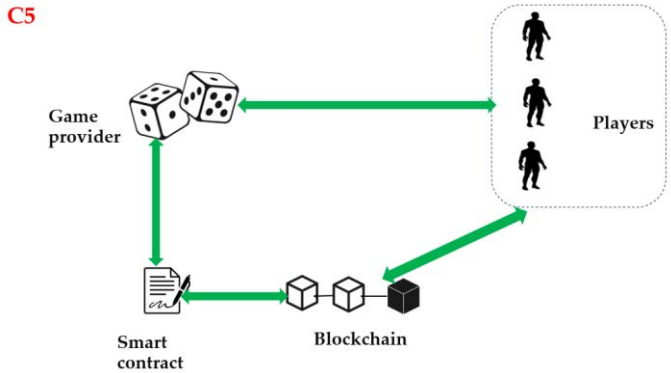
(b)


C3
Gamification data authority
Data/incentive
Gamification layer
Interface
Blockchain
Users

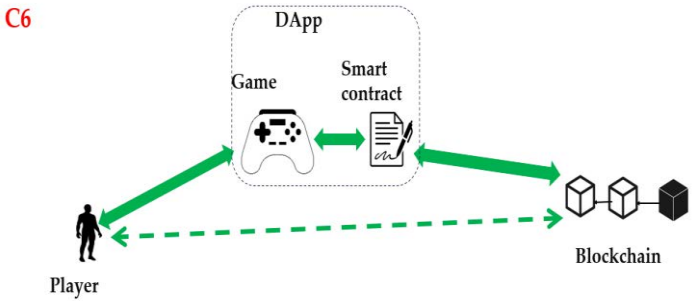
(c)


C4
Group X
P1
PN
Group Y
P1
PM
Local consensus
Local consensus
Game data X
Game data Y
Blockchain consensus
Blockchain

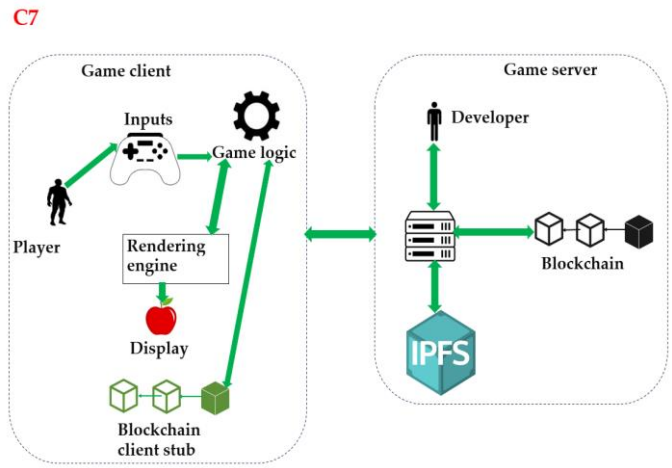
(d)


C5
Game provider
Players
Smart contract
Blockchain

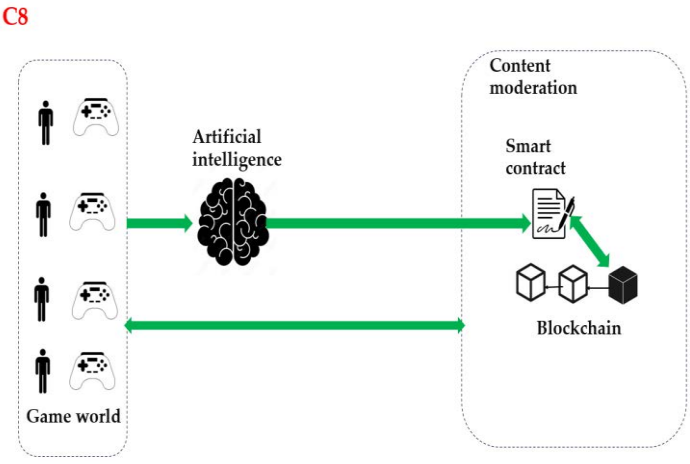
(e)


C6
DApp
Game
Smart contract
Player
Blockchain

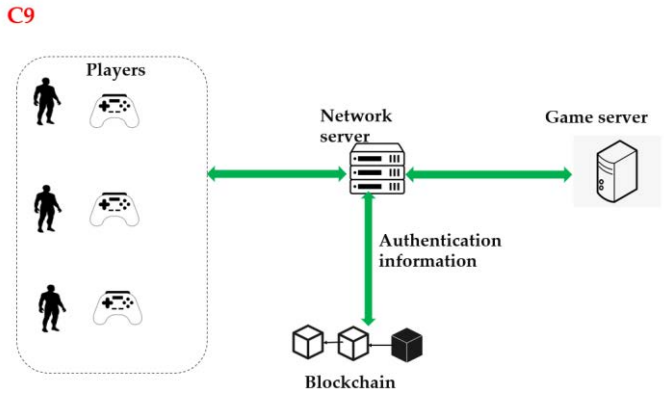
(f)



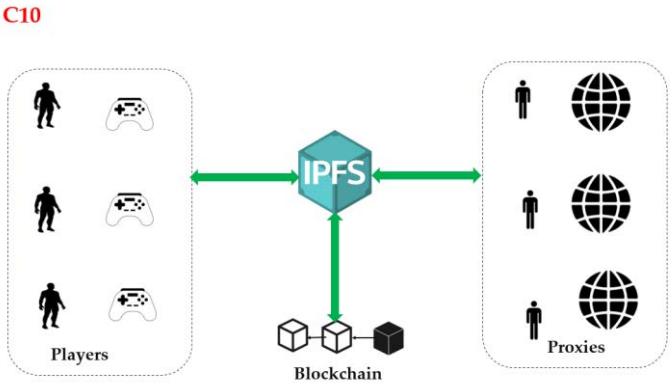
(g)



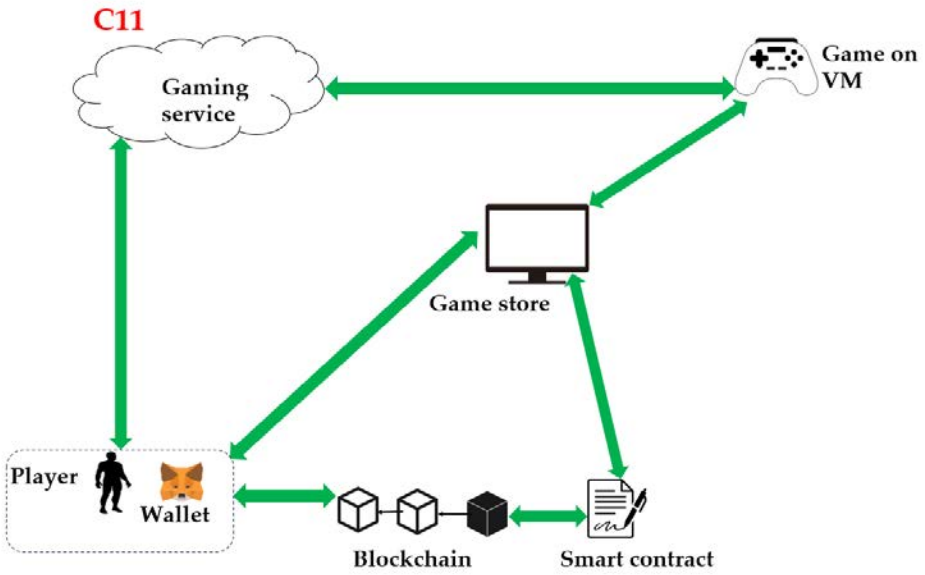
(h)



(i)



(j)



(k)

Fig. 5: Reflection of blockchain-stemmed gaming (a) C1, (b) C2, (c) C3, (d) C4, (e) C5, (f) C6, (g) C7, (h) C8, (i) C9, (j) C10, (k) C11.

5.2. Review on Blockchain-based Gaming

5.2.1. Game auditing

For an IoT scavenger hunting mobile game that facilitates users to interact with real-world locations where player-received rewards are stored on the blockchain as Non-Fungible Tokens (NFTs) that can be subsequently utilized for trading virtual assets in a secure and auditable manner [20].

5.2.2. Game incentivization

In [105], blockchain (permissioned and permissionless) is applied in the internet of things in order to attract customers and retain them through in-game asset improved monetization by using personalized advertisements, where permissioned blockchain has resulted in improved throughput and delay performance while public blockchain has facilitated transparency and immutability. In blockchain-based gaming, the dealings between the game supplier and gamers can be modeled as a two-stage Stackelberg game where the virtual game resources are associated with the player's address and traded them using a second exchange market, where the model decides the game provider's optimal pricing scheme and the player's optimal utility while also considering blockchain gas fees [21]. In play-to-earn blockchain games where users play to earn cryptocurrencies in the form of digital labor, blockchain is utilized to reconfigure the capital-labor relationship, facilitating the financialization of labor; however, there is a precarity associated with volatile earnings and insecure contractual employment [106].

5.2.3. Gamification

Researchers have used a serious gaming strategy to gamify crowdsensing in a metropolitan water framework where the gamified environment provides entertainment while crowdsensing achieves water-linked problems where a distance-limited multi-depot vehicle routing problem has been evaluated, while the Hyperledger blockchain supplies the overall trust among stakeholders in crowdsensing [22]. Knowledge is modeled as triples, and knowledge retrieved from users is validated and included in the knowledge base by using a gamified crowdsourcing approach where users are rewarded for relying on their assistance for the knowledge verification procedure, and blockchain is availed to archive the user logs securely [107]. In order to increase human involvement in crowdsourcing for fake news identification, gamification has been blended with smart contracts to deploy the platform rules transparently with elevated trust [108]. Some have used gamification to increase user participation in vehicle parking, where the users report free spaces and obtain free parking time in return as a reward, while blockchain has been utilized to implement the process in a distributed and decentralized manner with collaboration [109]. In [110], the authors show how blockchain can be utilized in educational gamification to achieve security and transparency while also achieving the desired educational objectives. Similarly, GamiChain is an online education model that uses gamification for learning and playing, while blockchain is utilized to implement security in the system by creating a distributed storage algorithm in the blockchain [111]. Research in [112] depicts two problems in blockchain-based gaming systems, which are non-functioning user participation and unsustainability in the growth of assets, and proposes a generic stealth gamification model that contains a gamified layer in the decentralized applications to interface with the blockchain. Similarly, "Healthcare Game Blockchain" is a platform developed for game developers, healthcare providers, and patients to create serious games related to healthcare that can be used for patient treatment and healthcare analytics using big data analytics, where blockchain is utilized to improve the data sharing security on the platform [113].

5.2.4. Cooperative gaming

In research [114], reciprocal crowdsourcing is introduced, which is a decentralized cooperative crowdsourcing technique driven by blockchain to elevate trust among the participants who do collaborative work, where a blockchain game known as "Cell Evolution" is used to build cooperative game worlds. In order to reduce drawbacks in conventional consensus in peer-to-peer blockchain games without changing the game architecture, proof-of-play is a new consensus approach that has minimum intervention with game play, providing a decentralized architecture for gaming [115]. Moreover, this consensus approach has been utilized in peer-to-peer online games to generate an anti-cheating technique by providing positive rewards for players who act as intended and having other measures to tackle long-range attacks [23]. Alternatively, another research proposes a new consensus approach to be deployed in blockchain-based gaming known as proof-of-achievement that focuses on the number of activities accomplished within the game to achieve the consensus that is optimum for blockchain-based gaming [116]. In [117], blockchain is proposed for data sharing to maintain a secured scoring system for multiplayer games, which has been tested using the Unity game engine and Ethereum blockchain, where the score data transaction process is affected by blockchain gas-related variables.

5.2.5. Game fraud prevention and fair play

By utilizing the assistance of smart contracts and blockchain, the research in [24] customizes games with the least modification to game clients to manage game status at the servers by consensus mechanisms to check modifications to player assets, minimizing dishonesty and distributed refusal of service attacks in multiplayer online games. Similarly, "GiNA" is an approach for online peer-to-peer games to improve the security and authenticity of data communication by using a smart contract-rooted blockchain packet transfer for sensitive data, an off-chain encrypted packet transfer, and an Ethereum-compatible currency known as "GiCoin" to buy and sell assets [118]. Driven by the fact that games such as gambling games need to have a true random number generator without being manipulated by a centralized authority, research in [119] shows how blockchain can be utilized to achieve the preceding purpose of making the gameplay fair. Moreover, some propose a game-theoretic approach to protect randomness in blockchain-based games where agents bet on random event outcomes to align the incentives with low skewness [120]. Similarly, in another research, authors propose blockchain as a solution to manage the private random state in online multiplayer gaming in a decentralized

manner, thanks to its transparency and immutability features [121].

5.2.6. Game DApps with extendibility

The study in [122] proposes a methodology for creating decentralized apps with blockchain for blockchain-based crypto-collectible games that presents the specifications and application design process and finally compares them with guidelines. In research [25], authors propose smart contracts running on blockchain to implement loot boxes in video games and design a DApp that demonstrates the buying and unclosing of loot boxes, which has yielded improved transparency and trustworthiness compared to the traditional technique.

5.2.7. Game asset ownership protection and asset transactions

In a study that has implemented a mobile game using blockchain resource tokens and self-executing contracts, it was shown that the blockchain introduced features like trust and transparency, providing genuine asset ownership, have resulted positively towards gameplay by improving self-engagement and player retention [123]. Transaction Certification Authority is a distributed ledger scheme that provides an immutable and cryptographic framework for managing the generation and ownership transfer of digital assets by tracking transactions and maintaining a record of asset ownership [26].

"GameBlockchain" is a scheme that enables secure transactions leveraging non-fungible tokens, is open source, and provides the opportunity for game stakeholders to create and exchange game assets in a secure approach by recording critical operations on the blockchain [124]. A representation of blockchain gaming assets is utilized to enhance the data exchange in gaming and provide distributed data storage to be used by decentralized apps [125]. In a multiplayer tourism serious game, a visualized transaction scheme is implemented using the Ethereum blockchain by integrating it with the game engine to handle simulation of transactions among various characters in the game, and in this system, the gas price variable has affected the transaction process speed [126]. Furthermore, research in [127] demonstrates how blockchain can be utilized to reward users using fungible and non-fungible tokens in a 2D-game where metadata and token images are recorded in the IPFS.

5.2.8. Game user-produced elements

In [128], artificial intelligence and blockchain are combined to detect hate speech in user-generated content of online games known as "MetaHate" in the metaverse, where gradient boost-based AI detects hate speech while blockchain provides transparency and accountability.

5.2.9. Game credential verification

Work in research [27] shows how an alternative security mechanism can be deployed when the confidential security key is misplaced by using smart contracts for depositing game digital assets into them, accompanied by a set of authentication inquiries that can be deployed in cyber games to access players' accounts without the secret key. In order to avoid players' data from being manipulated, work in [129] proposes a decentralized LoRA WAN with a gateway system to secure the states in the game network, a hashing algorithm to tackle privacy, and smart contracts to cater to delay requirements and user authentication.

5.2.10. Game rule transparency

In research [28], in order to transfer the sole proprietorship of game rights and rules from game creators to a distributed approach and to prevent the game creators from changing the rules arbitrarily and asset prices, reward mechanisms, etc., a decentralized computation and token administration scheme using the Ethereum blockchain is proposed for game networks.

5.2.11. Crypto gaming

CryptoKitties is the first widely recognized blockchain-based crypto game. In CryptoKitties, a study has investigated the value construction scarcity among CryptoKitties token owners presented in the form of virtual cats and blockchain-proven ownership using DappRadar and Etherscan analytics [29]. In a cloud gaming system rooted in tokens, "CryptoArcade" is a system that utilizes cryptocurrency to provide a resource-aware pricing technique that prevents quality of service degradation while players further use smart contracts to trade tokens prior to gaming [130]. Similarly, "CloudArcade" is a token-driven cloud gaming scheme to provide resource-aware silent payments that use payment channels to improve the system's performance to protect users' payments on floating prices [131].

6. Review Investigation

6.1. Investigation of Individual Structures

Table 2 emphasizes the extensive investigation of blockchain-stemmed gaming structures in view of gaming qualities, blockchain qualities, and posted time.

6.2. Overall Investigation

Fig. 6 illuminates the dissemination of blockchain-stemmed gaming in view of gaming qualities, blockchain qualities, and posted time. As illuminated from Fig. 6a, C3 (blockchain-stemmed gamification) has the highest proportion (21.7%) of BC-stemmed gaming reflection, after C7 (16.2%), C4 (13.5%), C5 (13.5%), C11 (8.1%), C2 (8.1%), C6 (5.4%), C9 (5.4%), C1 (2.7%), C8 (2.7%), and C10 (2.7%). Likewise, in BC-stemmed gaming, 75.6% of schemes apply a linear blockchain, while 21.6% have a generic design and 2.8% have a non-conventional design, as illuminated in Fig. 6b. Furthermore, as illuminated from Fig. 6c, the majority of schemes (21.6%) have been created to apply unspecified consensus, succeeded by PoW (19.0%), PoW/PoS (13.5%), PoS (10.8%), and so forth. Ultimately, when examining the fluctuation of schemes associated with BC-stemmed gaming, as illuminated from Fig. 6d, it is apparent that the reflection has been launched by 2018, raised until 2021, condensed until 2023, and observed an increment in 2024.

Table 2: Investigation of blockchain-stemmed gaming structures

Reflection	Proposal	Blockchain design	Blockchain consensus	Smart contracts	Additional features	Performance	Year
Game auditing (C1)	Scavenger Hunt [20]	Linear	PBFT	Yes	BLE beacons, NFT	Estimate maximum active players	2020
Game incentivization (C2)	Mobile gaming [105]	Linear	PoS, PBFT	Yes	Cross game asset transfers	Improved throughput, delay performance	2021
	Loot box market [21]	Linear	PoS	Yes	Two-stage Stackelberg game	Game provider should adopt a conservative pricing scheme	2022
	Playing for keeps [106]	Linear	PoS	Yes	Play to Earn	Reflect an ongoing financialization of labor in gaming	2024
Gamification (C3)	Crowdsensing water [22]	Linear	PBFT	Yes	Vickrey–Clarke–Groves auction model	High trust in gamified scenario	2021
	Knowledge content validation [107]	Linear	PoW	Similar approach	Contribution-based rewarding	Validate knowledge content successfully	2021
	Fake news detection [108]	Generic	Generic	Yes	Octalysis	Increase public intention to use the platform	2021
	Gamified smart parking [109]	Linear	DPoS	No	Beacon information collection	Save time and money for parking	2019
	Student centered learning [110]	Generic	Generic	No	Gamification model	RPG game model suitable for increasing user motivation	2021
	GamiChain [111]	Linear	PoW/PoS	Yes	Agile development methods, IPFS	Support Merdeka campus program	2022
	Gamification in blockchain [112]	Linear	PoW/PoS	Yes	Gamification model	No performance analysis presented	2018
	Healthcare games [113]	Non-conventional	PoA	Yes	Big data analysis, patient tracking and treatment	User interface design and implementation approach provided	2023
Cooperative game play (C4)	Cell evolution [114]	Linear	PoD	Yes	Reciprocal crowdsourcing	Increased engagement due to full control of what is owned	2020
	Proof of play [115]	Linear	Proof-of-play	No	A new block writing procedure	Minimum game intervention and overhead	2019
	P2P game [23]	Linear	Proof-of-play	No	Anti-cheating mechanism	Proof of play is advantageous over PoW	2023
	Proof of achievement [116]	Linear	Proof-of-achievement	No	None	Optimized performance for blockchain games	2019
	Scoring system [117]	Linear	PoW	Yes	Unity game engine	Score data process affected by gas related variables	2021
Game fraud prevention and fair play (C5)	Real-time cheat prevention [24]	Linear	Simple majority	Yes	Optimization strategies	Minimize cheating and DDoS attacks	2018
	GiNA [118]	Linear	PoS	Yes	GiCoin, off-chain encrypted packet transfer	Improved game security and authenticity	2021
	Random number generation [119]	Linear	MBFT	Yes	Random number generation algorithm	Effective algorithm and good performance	2019
	Game theoretic randomness [120]	Linear	PoW	No	Game theory	Only slight skewness in distribution of random events	2019
	Private random state [121]	Linear	PoW	Yes	Six key entities, incentivization	Maintain prolonged random state	2020
Game DApps with extendibility (C6)	Secure DApp [122]	Linear	PoW	Yes	Consider application life cycle	Discuss several guidelines for smart contracts	2020
	Loot boxes [25]	Linear	PoW/PoS	Yes	Decision theory	Analyze DApp's accuracy, security, cost	2021
Game asset ownership protection and asset transactions (C7)	Blockchain game features [123]	Linear	DPoS	Yes	Blockchain asset tokens	Improve self-engagement and player retention	2022
	Digital game asset management [26]	Generic	Generic	No	None	Track ownership transfer of assets	2021
	GameBlockchain [124]	Linear	Custom	Yes	NFT	Able to create and trade assets	2022
	Video game data exchange [125]	Generic	Generic	Yes	Hashing	No performance analysis	2019
	Tourism serious game [126]	Linear	PoW	Yes	Multiplayer transaction system	Gas price variable has affected the transaction process speed	2020
	Mage Runner [127]	Linear	PoS	Yes	IPFS, tokens	A basic implementation is demonstrated	2024
Game user produced elements security (C8)	MetaHate [128]	Generic	Generic	Yes	Artificial intelligence	86.01% accuracy	2024
Game credential verification (C9)	Online game authentication [27]	Generic	Generic	Yes	Security questions	Security questions can cope with malicious behavior	2021
	Delay management [129]	Generic	Generic	Yes	LoRA WAN, hashing	Solve delay and untrusted network users	2018
Game rule transparency (C10)	Decentralized computing and NFT [28]	Linear	PoW/PoS	Yes	Decentralized computation, NFT, IPFS	Proxy based computation takes less time than game server	2020
Crypto gaming (C11)	CryptoKitties [29]	Linear	PoW/PoS	Yes	Breeding the queen bee concept	Investigated the value construction scarcity	2021
	CryptoArcade [130]	Generic	Generic	Yes	Prospect theory, cryptocurrency	Avoid QoE degradation, EUT players are more probable to buying	2022
	CloudArcade [131]	Linear	PoW	Yes	Cryptocurrency, resource-aware pricing	Good generality on QoE-driven application	2020

7. DISCUSSION

7.1. Advantages

7.1.1. Game rule decentralization

In traditional games, the game rules are defined by the game creators, and they have sole proprietorship over them. In blockchain-based games, the game creators lose the sole proprietorship, and game rights and rules are implemented as a distributed system with the approval of peers. This can indeed prevent game creators from having sole centralized control over in-game asset prices, rules, and reward mechanisms. On the other hand, blockchain-based gaming is player-driven, meaning that centralized authority is nullified by the decentralized blockchain approach, preventing manipulation by the central authorities. Indeed, in these systems, it facilitates the players and developers to interact and come to an agreement regarding rules, prices, reward mechanisms, etc.

7.1.2. Better game authentication

Smart contracts that execute upon meeting certain conditions can be deployed in blockchain-based gaming systems to reinforce game authentication and access control. Moreover, they can also be used as a secondary mechanism for game players to authenticate themselves if the primary mechanism, such as the private key, is lost. Due to blockchain, identity theft and impersonation can be minimized, as player identities can be stored as digital immutable IDs in the blockchain.

Blockchains replace traditional game authentication with decentralized authentication without needing intermediaries, reducing centralized authentication vulnerabilities such as hacking attacks. Blockchain-based gaming also caters to cross-platform authentication, where players access their accounts and game assets across multiple games and platforms.

7.1.3. Secure game asset ownership transfer

In ownership assignment, the digital identifier of the game player is associated with in-game assets. Trusted asset ownership protection can lead to higher player retention since players feel more protected about their asset ownership. In blockchain-based games, ownership regarding assets can be recorded on the blockchain so that it cannot be tampered with once recorded, preventing third parties from claiming false ownership. In these systems, the game assets are typically represented in the form of NFTs on the blockchain that are unique to each asset and easily verifiable, allowing players to have true ownership and control over the assets. This facilitates users to easily trade assets, and in those instances, the transfer of ownership will be recorded on the blockchain, providing ownership of the asset to the new owner.

7.1.4. Facilitate fair play

Cheating is a form of misconduct in computer gaming where players may take secondary measures, avoiding or overriding game rules, to win the game. Due to blockchain, the game servers can monitor the game status by using consensus approaches to check modifications to player assets, preventing cheating. Moreover, cryptographic techniques can be incorporated for off-chain storage along with in-chain storage of sensitive data to enable fair play. Moreover, in order to maintain true randomness in gaming, blockchain can be deployed, preventing manipulation or biasedness from centralized third parties and facilitating fair play, like in the case of gambling. Furthermore, in multiplayer online games, the private random state can be maintained owing to the immutable and transparent features of the blockchain. Finally, consensus approaches can also be incorporated to reward good players and punish players who cheat.

7.1.5. Trusted and secure gameplay

In cooperative game worlds, trust is an important parameter that can be protected due to the characteristic features of blockchain. In such instances, crowdsourcing can be implemented with the aid of blockchain, facilitating trusted collaboration. Moreover, novel consensus approaches suitable to be deployed in blockchain-based games, such as proof-of-play and proof-of-achievement that reward players based on game progress and achieve collective approval, can be effectively utilized to increase the security and trustworthiness of the game. Moreover, in multiplayer games, blockchains can enable tamper-proof recording of the scoring system, preventing third parties from manipulating the score and improving the trust and security of the gameplay.

7.2. Asperities

7.2.1. Security vulnerabilities of blockchain games

A case study shows that even though blockchain games are relatively more secure than non-blockchain-based gaming solutions, they can still have security vulnerabilities [132]. Specifically, smart contracts that are deployed on blockchain are known to have vulnerabilities where attackers can hijack the contract, such as in the event of calling a “fallback” function. These vulnerabilities can exist in different layers, ranging from virtual machine design to Solidity language. If an intruder obtains entrance to the private wallet of a blockchain and if two-step verification does not exist, he can further penetrate into the game server and may take control of game assets. Furthermore, due to these vulnerabilities, attacks like cookie replay, injection, cross-site scripting, brute force attacks to crack authentication, etc.

7.2.2. Crypto games imaging players as financialized subjects

According to a study conducted on crypto games, they are known to imagine players as financialized subjects using risk and investment as solutions to economic problems [133]. This can shift the focus of gaming experiences from objective feelings like entertainment, fear, etc. to opportunities for making profit. This can further destabilize the cryptocurrency market as players tend to be engaged in trading and business activities rather than playing and enjoying the game. Moreover, players with high financial capability may get the opportunity to buy rare assets and win the game, while fluent players who are less economically capable may not get that opportunity and thus may lose the game. This practice can lead to pay-to-win implementation scenarios where game developers design the game so that players who spend money are more capable of winning.

7.2.3. Low balance in gaming costs, supplies, and wealth

Relying on a study done regarding the rise and fall of CryptoKitties, it has been found that the imbalance in the game supply of assets, gaming cost, and revenue, and the

hiatus among wealthy and penniless gamers, has contributed towards the downfall of the game [134]. When the game costs do not tally with the supplies and wealth, it can create an

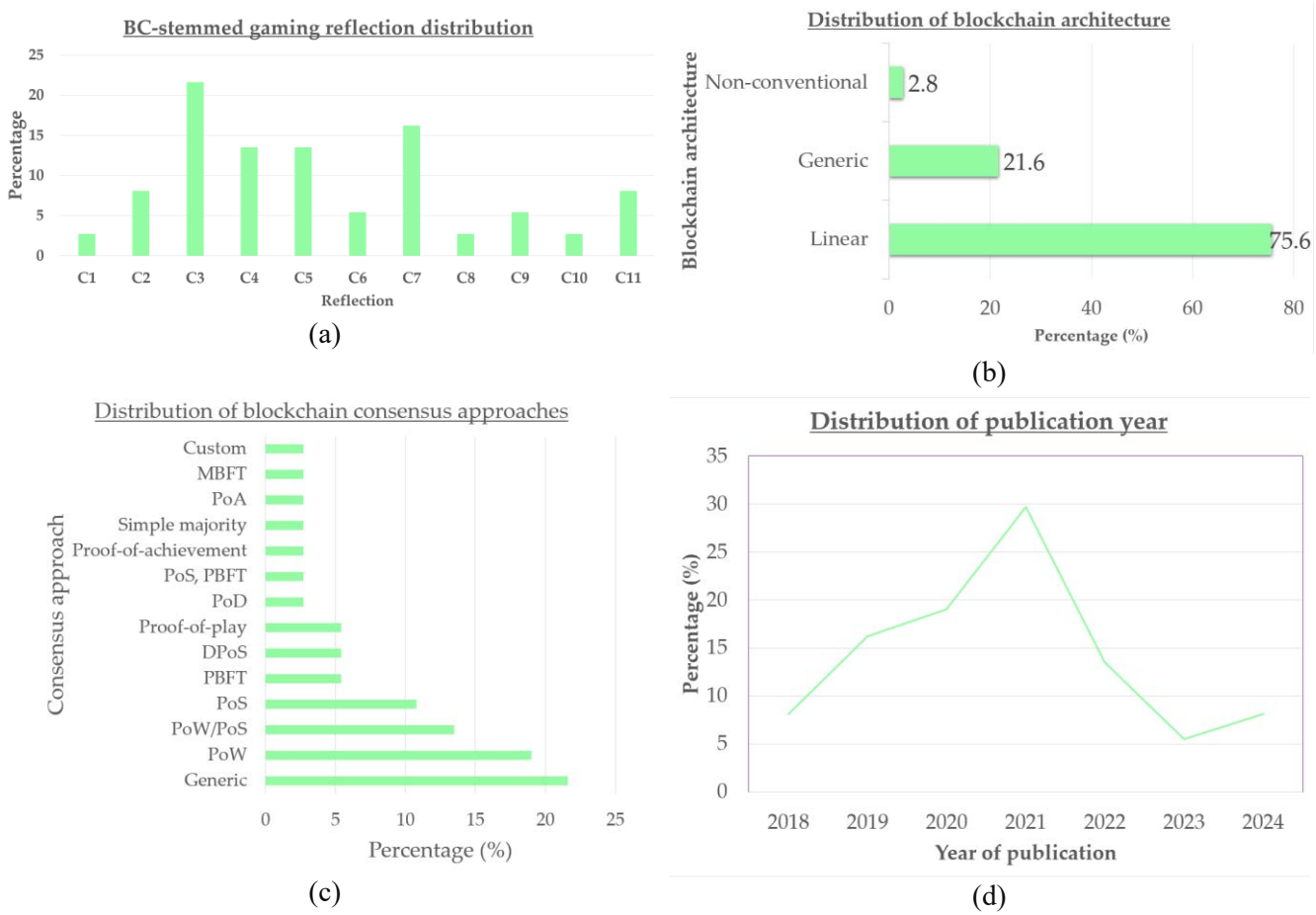


Fig. 6: Overall investigation (a) BC-stemmed gaming reflection, (b) BC design, (c) BC consensus, (d) Distribution time.

economic imbalance where the higher-wealth players may get an advantage over the low-wealth ones. Moreover, if the costs of achieving in-game assets are very low, it can negatively affect gaming by diminishing the player's long-term engagement within the game. On the other side, if the in-game assets or currency are much higher than the demand, it can lead to asset inflation, making them less valuable and making it challenging for players to achieve game goals.

7.2.4. Additional communication overhead in gaming

In multi-player online games, there is a huge load of information transmitted among the players and game servers. When blockchain is incorporated into such a scenario, the communication burden is even greater, as it causes additional communication for distributed transaction creation, verification, and consensus processes. Due to this, it can result in increasing the overall latency of the system, degrading the real-time effect of gaming and the quality of service. Moreover, this can further result in a requirement for higher communication bandwidth to maintain the quality of service. Thus, users with slower internet connections will be easily penalized.

7.2.5. Higher gaming cost

Owing to the incorporation of blockchain, the gaming cost has naturally increased. One of the reasons for this is the increase in communication overhead, which makes communication more expensive compared to traditional gaming. The other main cost is the blockchain transaction cost since every blockchain transaction causes transaction fees known as gas fees in the Ethereum blockchain. These costs are avalanched in games that involve a high degree of in-game asset transfers and interactions, like massive multiplayer online games. Thus, this higher cost can limit players from engaging in blockchain-based games compared to traditional gaming.

8. Conclusion, Offers, and Coming Ways

In this investigation, we investigated gaming features, the architecture of a game, gaming concepts, the game ecosystem, and game mechanisms**.** Afterwards, with an outline of the blockchain structure, we investigated blockchain-stemmed gaming**.** Centered around this investigation, we understood blockchain-stemmed gaming reflection within 11 tasks: game auditing (C1), game incentivization (C2), gamification (C3), cooperative game play (C4), game fraud prevention and fair

play (C5), game DApps with extendibility (C6), game asset ownership protection and asset transactions (C7), game user-produced elements' security (C8), game credential verification (C9), game rule transparency (C10), and crypto gaming (C11). Likewise, we extensively investigated the selected articles regarding 11 tasks of reflection, gaming- and blockchain-linked qualities. Finally, we exposed the advantages and asperities to the reflection of blockchain-stemmed gaming.

This inspection improves the conventional literature by presenting conducive knowledge connected with blockchain-stemmed gaming**.** This can guide the chances for the investigators to derive the conventional tides and differences in blockchain-stemmed gaming to fund subsequent research.

Centered around the asperities identified, the following offers can be extended to shrink them.

- The smart contract codes deployed in blockchain games need to be properly audited before actual implementation to detect any vulnerabilities that exist within the code. Specifically, auditors need to check for every possible situation of inputs and conditions that the code may run in order to detect the vulnerabilities. Further, they need to do formal verification, code feature matching, and symbolic execution.
- Blockchain-based games should not be designed entirely using a pay-to-win model, even though in crypto games it involves trading in-game assets among players. The game design should be aligned such that higher fluent players tend to win the game rather than those who buy in-game assets. In order to reduce this gap, the performance gains gained through game assets can be reduced.
- The blockchain games should maintain a good balance between gaming costs, supplies, and wealth because it determines the success of the game. The game needs to be engineered with the scarcity of assets principle in mind, where there is a scarcity of assets and players engage in different activities to earn assets and ultimately win the game. The game designers should avoid setting in-game asset values too high or too low and should set an optimum price after a feasibility study to match the player's wealth and skills.
- In order to overcome the difficulty of high communication overhead due to blockchain, system designers can think of alternative blockchain architectures and consensus mechanisms that incur lower communication overhead than a traditional linear blockchain deploying proof-of-work consensus. Moreover, robust communication techniques with data compression can also aid in reducing the communication overhead. Moreover, transactions can be offloaded from the blockchain while keeping only references in the blockchain to reduce communication overhead.
- To reduce gaming costs, in-game assets can be tokenized, allowing players to own their digital items, which can allow them to trade assets over multiple game platforms, reducing the costs of acquiring in-game assets. Deviating from the pay-to-win model, play-to-earn mechanics can be implemented in the blockchain-based game design, allowing players to engage in the game and rewarding them based on their positive engagement, allowing them to earn to rectify the gaming costs.

First, a coming way to develop blockchain-based gaming is by researching consensus techniques that are specifically designed for gaming environments. Moreover, since this reflection of blockchain-based gaming has been known for security vulnerabilities, especially those related to smart contracts, they could be tested against quantum computer attacks and designed to resist quantum computer threats as well. Moreover, scholars may propose robust blockchain architectures designed for gaming purposes that have a lower communication overhead with alternative distributed storages along with blockchain.

CREDIT AUTHORSHIP CONTRIBUTION STATEMENT

Patikiri Arachchige Don Shehan Nilmantha Wijesekara: Conceptualization, Data curation, Formal analysis, Investigation, Methodology, Resources, Software, Validation, Visualization, Roles/Writing - original draft, Writing - review & editing.

DECLARATION OF COMPETING INTEREST

The authors declare that they have no known competing financial interests or personal relationships that could have appeared to influence the work reported in this paper. The ethical issues; including plagiarism, informed consent, misconduct, data fabrication and/or falsification, double publication and/or submission, redundancy has been completely observed by the authors.

References

[1] A. Ensslin, "Computer gaming," in *The Routledge Companion to Experimental Literature*, pp. 497-511, 2012.

[2] P. *Bourke* and J. Shier, "Space Filling: A new algorithm for procedural creation of game assets," in *Proceedings of the 5th annual international conference on computer games multimedia & allied technology*, pp. 1-5, 2013.

[3] C. S. Brunt, A. S. King, and J. T. King, "The influence of user-generated content on video game demand," *Journal of Cultural Economics*, vol. 44, pp.35-56, 2020.

[4] N. Ducheneaut and R. J. Moore, "The social side of gaming: a study of interaction patterns in a massively multiplayer online game," in *Proceedings of the 2004 ACM Conference on Computer Supported Cooperative Work*, pp. 360-369, 2004.

[5] V. McArthur, "The UX of avatar customization," in *Proceedings of the 2017 CHI Conference on Human Factors in Computing Systems*, pp. 5029-5033, 2017.

[6] D. Archambault, T. Gaudy, K. Miesenberger, S. Natkin, and R. Ossmann, "Towards generalised accessibility of computer games," in *Third International Conference on Technologies for E-Learning and Digital Entertainment,* pp. 518-527, 2008.

[7] P. Sweetser, and P. Wyeth, "GameFlow: a model for evaluating player enjoyment in games," *Computers in Entertainment (CIE)*, vol. 3, no. 3, pp.3-3, 2005.

[8] Y. Deng, Y. Li, R. Seet, X. Tang, and W. Cai, "The server allocation problem for session-based multiplayer cloud

gaming," *IEEE Transactions on Multimedia*, vol. 20, no. 5, pp.1233-1245, 2017.

[9] S. R. Yamane, "Secure online game play with Token: A case study in the design of multi-factor authentication device," in *Second International Conference on Human Centered Design,* pp. 597-605, 2011.

[10] S. Mizrahi, and Y. Minchuk, "Performance management in a decentralized setting: Monitoring and gaming in the financial services industry," *Managerial and Decision Economics*, vol. 38, no. 6, pp.742-753, 2017.

[11] K. Martinez, M. I. Menéndez-Menéndez, and A. Bustillo, "A new measure for serious games evaluation: gaming educational balanced (GEB) model," *Applied Sciences*, vol. 12, no. 22, Art. no.11757, 2022.

[12] F. F. H. Nah, V. R. Telaprolu, S. Rallapalli, and P. R. Venkata, "Gamification of education using computer games," in *15th International Conference on Human Interface and the Management of Information. Information and Interaction for Learning, Culture, Collaboration and Business,* pp. 99-107, 2013.

[13] S. Lim, and B. Reeves, "Computer agents versus avatars: Responses to interactive game characters controlled by a computer or other player," *International Journal of Human-Computer Studies*, vol. 68, no. 1-2, pp.57-68, 2010.

[14] N. Kasenides, and N. Paspallis, "Multiplayer game backends: A Comparison of commodity cloud-based approaches," in *European Conference on Service-Oriented and Cloud Computing*, pp. 41-55, 2020.

[15] L. Marchesi, M. Marchesi, R. Tonelli, and M. I. Lunesu, "A blockchain architecture for industrial applications," *Blockchain: Research and Applications*, vol. 3, no. 4, Art. no. 100088, 2022.

[16] P. A. D. S. N. Wijesekara, "Ethical Knowledge Sharing Leveraging Blockchain: An Overview," *Science, Engineering, and Technology*, vol. 4, no. 1, pp. 112-136, 2024.

[17] D. Pennino, M. Pizzonia, A. Vitaletti, and M. Zecchini, "Blockchain as IoT Economy enabler: A review of architectural aspects," *Journal of Sensor and Actuator Networks*, vol. 11, no. 2, Art. no. 20, 2022.

[18] P. A. D. S. N. Wijesekara, "A Literature Review on Access Control in Networking Employing Blockchain," *Indonesian Journal of Computer Science*, vol. 13, no. 1, pp. 734-768, 2024.

[19] A. Kosba, A. Miller, E. Shi, Z. Wen, and C. Papamanthou, "Hawk: The blockchain model of cryptography and privacy-preserving smart contracts," in *2016 IEEE Symposium on Security and Privacy,* pp. 839-858, 2016.

[20] A. Manzoor, M. Samarin, D. Mason, and M. Ylianttila, "Scavenger hunt: Utilization of blockchain and IoT for a location-based game," *IEEE Access*, vol. 8, pp.204863-204879, 2020.

[21] Y. Jiang, S. Fan, and W. Cai, "Economic analysis of loot box market in blockchain games," in *Proceedings of the Fourth ACM International Symposium on Blockchain and Secure Critical Infrastructure*, pp. 35-46, 2022.

[22] A. Predescu, D. Arsene, B. Pahonțu, M. Mocanu, and C. Chiru, "A serious gaming approach for crowdsensing in urban water infrastructure with blockchain support," *Applied Sciences*, vol. 11, no. 4, Art. no.1449, 2021.

[23] F. Wu, H. Y. Yuen, H. Chan, V. C. Leung, and W. Cai, "Facilitating serverless match-based online games with novel blockchain technologies," *ACM Transactions on Internet Technology*, vol. 23, no. 1, pp.1-26, 2023.

[24] S. Kalra, R. Sanghi, and M. Dhawan, "Blockchain-based real-time cheat prevention and robustness for multi-player online games," in *Proceedings of the 14th International Conference on Emerging Networking Experiments and Technologies*, pp. 178-190, 2018.

[25] A. Carvalho, "Bringing transparency and trustworthiness to loot boxes with blockchain and smart contracts," *Decision Support Systems*, vol. 144, Art. no. 113508, 2021.

[26] G. Ragnoni, "System and Methods for Blockchain-Inspired Digital Game Asset Management," in *5th AIROYoung Workshop and AIRO PhD School 2021 Joint Event on Optimization and Data Science: Trends and Applications,* pp. 181-188, 2021.

[27] M. Boroń, and A. Kobusińska, "Alternative authentication with smart contracts for online games," in *2021 IEEE 46th Conference on Local Computer Networks*, pp. 415-418, 2021.

[28] K. B. Muthe, K. Sharma, and K. E. N. Sri, "A blockchain based decentralized computing and NFT infrastructure for game networks," in *2020 Second International Conference on Blockchain Computing and Applications*, pp. 73-77, 2020.

[29] A. Serada, T. Sihvonen, and, J. T. Harviainen, "CryptoKitties and the new ludic economy: How blockchain introduces value, ownership, and scarcity in digital gaming," *Games and Culture*, vol. 16, no. 4, pp.457-480, 2021.

[30] G. Jaferian, D. Ramezani, E. Polyak, and M. Wagner, "Exploring blockchain's horizons in educational gaming," *INTED2024 Proceedings*, pp.5050-5058, 2024.

[31] O. J. Scholten, N. G. J. Hughes, S. Deterding, A. Drachen, J. A. Walker, and D. Zendle, "Ethereum crypto-games: Mechanics, prevalence, and gambling similarities," in *Proceedings of the Annual Symposium on Computer-Human Interaction in Play*, pp. 379-389, 2019.

[32] P. A. D. S. N. Wijesekara, "An Overview on Blockchain-based Social Media," *Science, Engineering and Technology*, vol. 5, no. 1, pp. 213-247, 2025.

[33] P. A. D. S. N. Wijesekara, and Y. K. Wang, "A Mathematical Epidemiological Model (SEQIJRDS) to Recommend Public Health Interventions Related to COVID-19 in Sri Lanka," *COVID*, vol. 2, no. 6, pp. 793-826, 2022.

[34] L. N. Taylor, "Gaming ethics, rules, etiquette, and learning," in *Handbook of Research on Effective Electronic Gaming in Education*, pp. 1057-1067, 2009.

[35] D. O. Manusos, "Authentic design in gaming changing the rules of play," *Technology and Engineering teacher*, vol. 72, no. 8, p.8, 2013.

[36] A. Bhojan, S. P. Ng, J. Ng, and W. T. Ooi, "CloudyGame: Enabling cloud gaming on the edge with dynamic asset streaming and shared game instances," *Multimedia Tools and Applications*, vol. 79, pp.32503-32523, 2020.

[37] T. Manninen, and T. Kujanpää, "The value of virtual assets: the role of game characters in MMOGs," *International Journal of Business Science & Applied Management (IJBSAM)*, vol. 2, no. 1, pp.21-33, 2007.

[38] M. Brocchini, M. Mameli, E. Balloni, L. D. Sciucca, L. Rossi, M. Paolanti, E. Frontoni, and P. Zingaretti, "Monster: a deep learning-based system for the automatic generation of gaming assets," in *International Conference on Image Analysis and Processing*, pp. 280-290, 2022.

[39] V. Kasapakis, and D. Gavalas, "User-generated content in pervasive games," *Computers in Entertainment (CIE)*, vol. 16, no. 1, pp.1-23, 2017.

[40] S. Li, T. Wen, H. Yan, and X. Qin, "Prediction of Quality of Experience (QoE) of Cloud-Gaming Through an Approach to Extracting the Indicators from User Generated Content (UGC)," in *International Conference on Human-Computer Interaction*, pp. 253-262, 2023.

[41] H. Duan, Y. Huang, Y. Zhao, Z. Huang, and W. Cai, "User-generated content and editors in video games: Survey and vision," in *2022 IEEE Conference on Games*, pp. 536-543, 2022.

[42] P. A. D. S. N. Wijesekara, K. L. K. Sudheera, G. G. N. Sandamali, and P. H. J. Chong, "Data gathering optimization in hybrid software defined vehicular networks," in *Proceedings of the 20th Academic Sessions*, p. 59, 2023.

[43] P. A. D .S. N. Wijesekara, K. L. K. Sudheera, G. G. N. Sandamali, and P. H. J. Chong, "An optimization framework for data collection in software defined vehicular networks," *Sensors*, vol. 23, no. 3, pp. 1600, 2023.

[44] J. Smed, T. Kaukoranta, and H. Hakonen, "Aspects of networking in multiplayer computer games," *The Electronic Library*, vol. 20, no. 2, pp.87-97, 2002.

[45] M. Myślak, and D. Deja, "Developing game-structure sensitive matchmaking system for massive-multiplayer online games," in *2014 International Workshops on Social Informatics,* pp. 200-208, 2015.

[46] E. Tse, S. Greenberg, C. Shen, and C. Forlines, "Multimodal multiplayer tabletop gaming," *Computers in Entertainment*, vol. 5, no. 2, p.12, 2007.

[47] I. Dolgov, W. J. Graves, M. R. Nearents, J. D. Schwark, and C. B. Volkman, "Effects of cooperative gaming and avatar customization on subsequent spontaneous helping behavior," *Computers in Human Behavior*, vol. 33, pp.49-55, 2014.

[48] B. Bostan, and T. Marsh, "The 'interactive'of interactive storytelling: Customizing the gaming experience," in *9th International Conference on Entertainment Computing,* pp. 472-475, 2010.

[49] M. Tyagi, C. Choudhary, and R. Majumdar, "A study on gaming engines accessibility," *Advances in Interdisciplinary Engineering: Select Proceedings of FLAME 2018*, pp.33-41, 2019.

[50] T. S. Rothdeutsch, "Interaction with Accessibility on Digital Gaming Platform," *Rochester Institute of Technology*, 2022.

[51] Y. C. Chang, P. H. Tseng, K. T. Chen, and C. L. Lei, "Understanding the performance of thin-client gaming," in *2011 IEEE International Workshop Technical Committee on Communications Quality and Reliability*, pp. 1-6, 2011.

[52] P. A. D. S. N. Wijesekara, W. M. A. K. Sangeeth, H. S. C. Perera, and N. D. Jayasundere, "Underwater Acoustic Digital Communication Channel for an UROV," in *Proceedings of the 5th Annual Research Symposium*, p. E17, 2018.

[53] C. Y. Huang, P. H. Chen, Y. L. Huang, K. T. Chen, and C. H. Hsu, "Measuring the client performance and energy consumption in mobile cloud gaming," in *2014 13th Annual Workshop on Network and Systems Support for Games*, pp. 1-3, 2014.

[54] Y. Li, Y. Deng, X. Tang, W. Cai, X. Liu, and G. Wang, "Cost-efficient server provisioning for cloud gaming," *ACM Transactions on Multimedia Computing, Communications, and Applications,* vol. 14, no. 3s, pp.1-22, 2018.

[55] S. Wang, and S. Dey, "Modeling and characterizing user experience in a cloud server based mobile gaming approach," in *2009 IEEE Global Telecommunications Conference*, pp. 1-7, 2009.

[56] M. Warren, "Server authentication and its role in controlling access to copyrighted works in software and video games," *Available at SSRN 3014660*, 2017.

[57] P. A. D. S. N. Wijesekara, and S. Gunawardena, "A machine learning-aided network contention-aware link lifetime- and delay-based hybrid routing framework for software-defined vehicular networks," *Telecom*, vol. 4, no. 3, pp. 393-458, 2023.

[58] P. A. D. S. N. Wijesekara, K. L. K. Sudheera, G. G. N. Sandamali, and P. H. J. Chong, "Machine Learning Based Link Stability Prediction for Routing in Software Defined Vehicular Networks," in *Proceedings of the 20th Academic Sessions*, p. 60, 2023.

[59] C. S. Loh, Y. Sheng, and D. Ifenthaler, "Serious games analytics: Theoretical framework," *Serious games analytics: Methodologies for performance measurement, assessment, and improvement*, pp.3-29, 2015.

[60] C. S. Loh, I. H. Li, and Y. Sheng, "Comparison of similarity measures to differentiate players' actions and decision-making profiles in serious games analytics," *Computers in Human Behavior*, vol. 64, pp. 562-574, 2016.

[61] T. Susi, M. Johannesson, and P. Backlund, "Serious games: An overview," *University of Skövde*, pp. 1-24, 2007.

[62] J. Wiemeyer, and A. Kliem, "Serious games in prevention and rehabilitation—a new panacea for elderly

people?," *European Review of Aging and Physical Activity*, vol. 9, pp.41-50, 2012.

[63] M. Dankbaar, "Serious games and blended learning; effects on performance and motivation in medical education," *Perspectives on medical education*, vol. 6, pp.58-60, 2017.

[64] Z. Feng, V. A. González, R. Amor, M. Spearpoint, J. Thomas, R. Sacks, R. Lovreglio, and G. Cabrera-Guerrero, "An immersive virtual reality serious game to enhance earthquake behavioral responses and post-earthquake evacuation preparedness in buildings," *Advanced Engineering Informatics*, vol. 45, Art. no. 101118, 2020.

[65] S. Yin, X. Cai, Z. Wang, Y. Zhang, S. Luo, and J. Ma, "Impact of gamification elements on user satisfaction in health and fitness applications: A comprehensive approach based on the Kano model," *Computers in Human Behavior*, vol. 128, p.107106, 2022.

[66] R. D. Pinto, B. Peixoto, M. Melo, L. Cabral, and M. Bessa, "Foreign language learning gamification using virtual reality—a systematic review of empirical research," *Education Sciences*, vol. 11, no. 5, Art. no. 222, 2021.

[67] P. Van Schaik, J. Blake, F. Pernet, I. Spears, and C. Fencott, "Virtual augmented exercise gaming for older adults," *CyberPsychology & Behavior*, vol. 11, no. 1, pp.103-106, 2008.

[68] B. Walther-Franks, D. Wenig, J. Smeddinck, and R. Malaka, "Exercise my game: Turning off-the-shelf games into exergames," in *12th International Conference on Entertainment Computing,* pp. 126-131, 2013.

[69] H. J. Korteling, A. S. Helsdingen, and R. R. Sluimer, "An empirical evaluation of transfer-of-training of two flight simulation games," *Simulation & Gaming*, vol. 48, no. 1, pp.8-35, 2017.

[70] J. Gaber, "Simulating planning: SimCity as a pedagogical tool," *Journal of Planning Education and Research*, vol. 27, no. 2, pp.113-121, 2007.

[71] M. Consalvo, "Using your friends: Social mechanics in social games," in *Proceedings of the 6th International Conference on Foundations of Digital Games*, pp. 188-195, 2011.

[72] A. Rapp, "Social game elements in world of warcraft: Interpersonal relations, groups, and organizations for gamification design," *International Journal of Human–Computer Interaction*, vol. 34, no. 8, pp.759-773, 2018.

[73] T. Dubbelman, "Narrative game mechanics," in *9th International Conference on Interactive Digital Storytelling,* pp. 39-50, 2016.

[74] F. Jonsson, and L. Eklund, "Narrative and Mechanical Integration Playing with Interpersonal Conflicts in Life Is Strange," In *Representing Conflicts in Games,* pp. 191-207, 2022.

[75] H. Desurvire, and M. S. El-Nasr, "Methods for game user research: studying player behavior to enhance game design," *IEEE Computer Ggraphics and Applications*, vol. 33, no. 4, pp.82-87, 2013.

[76] A. M. Weinstein, "Computer and video game addiction—a comparison between game users and non-game users," *The American journal of drug and alcohol abuse*, vol. 36, no. 5, pp.268-276, 2010.

[77] M. Roccetti, G. Marfia, and A. Semeraro, "Playing into the wild: A gesture-based interface for gaming in public spaces," *Journal of Visual Communication and Image Representation*, vol. *23*, no. 3, pp.426-440, 2012.

[78] B. Jung, A. Schrader, and D. V. Carlson, "Tangible interfaces for pervasive gaming," in *Proceedings of the 2nd International Conference of the Digital Games Research Association. Changing Views: Worlds in Play*, pp. 16-20, 2005.

[79] R. A. P. de Queirós, "A survey on game backend services," *Gamification-Based E-Learning Strategies for Computer Programming Education*, pp.1-13, 2017.

[80] J. Frome, "Interactive works and gameplay emotions," *Games and Culture*, vol. 14, no. 7-8, pp.856-874, 2019.

[81] B. Cowley, I. Kosunen, P. Lankoski, J. M. Kivikangas, S. Järvelä, I. Ekman, J. Kemppainen, and N. Ravaja, "Experience assessment and design in the analysis of gameplay," *Simulation & Gaming*, vol. 45, no. 1, pp.41-69, 2014.

[82] H. M. D. P. M. Herath, W. A. S. A. Weraniyagoda, R. T. M. Rajapaksha, P. A. D. S. N. Wijesekara, K. L. K. Sudheera, and P. H. J. Chong, "Automatic assessment of aphasic speech sensed by audio sensors for classification into aphasia severity levels to recommend speech therapies," *Sensors*, vol. 22, no. 18, pp. 6966, 2022.

[83] M. Joselli et. al., "An adaptative game loop architecture with automatic distribution of tasks between cpu and gpu," *Computers in Entertainment*, vol. 7, no. 4, pp.1-15, 2010.

[84] A. Czauderna, and E. Guardiola, "The gameplay loop methodology as a tool for educational game design," *Electronic Journal of e-Learning*, vol. 17, no. 3, pp. 207-221, 2019.

[85] P. A. D. S. N. Wijesekara, and S. Gunawardena, "A comprehensive survey on knowledge-defined networking," *Telecom*, vol. 4, no. 3, pp. 477-596, 2023.

[86] M. S. Handoko, "Unlocking user identity: a study on mouse dynamics in dual gaming environments for continuous authentication," Master's alternative plan paper, *Minnesota State University,* pp. 1-71*,* 2023.

[87] Q. Wang, L. Deng, H. Cheng, H. Fan, X. Du, and Q. Yang, "Live Gaze-Based Authentication and Gaming System," in *5th International Conference on Human Aspects of Information Security, Privacy and Trust,* pp. 239-250, 2017.

[88] A. Moiseienko, and K. Izenman, "Gaming the system: Money laundering through online games," *RUSI Newsbrief*, vol. 39, no. 9, pp. 1-5, 2019.

[89] P. A. D. S. N. Wijesekara, "Deep 3D Dynamic Object Detection towards Successful and Safe Navigation for Full Autonomous Driving," *Open Transportation Journal*, vol. 16, no. 1, pp. e187444782208191, 2022.

[90] C. Solanki, and D. J. Mathew, "3D Game Asset Generation of Historical Architecture Through

Photogrammetry," in *Encyclopedia of Computer Graphics and Games*, pp. 20-23, 2024.

[91] P. A. D. S. N. Wijesekara, "A Survey on Blockchain-Based Routing in Communication Networks," *Indonesian Journal of Electrical Engineering and Informatics*, vol. 13, no. 1, pp. 196-225, 2025.

[92] J. Song, P. Zhang, M. Alkubati, Y. Bao, and G. Yu, "Research advances on blockchain-as-a-service: Architectures, applications and challenges," *Digital Communications and Networks*, vol. 8, no. 4, pp.466-475, 2022.

[93] P. A. D. S. N. Wijesekara, "Blockchain and Artificial Intelligence for Big Data Analytics in Networking: Leading-edge Frameworks," *Journal of Engineering Science & Technology Review*, vol. 17, no. 3, pp. 125-143, 2024.

[94] Z. Zhang, M. Zhang, Y. Li, B. Fan, and L. Jiang, "Directed acyclic graph blockchain for secure spectrum sharing and energy trading in power IoT," *China Communications*, vol. 20, no. 5, pp. 182-197, 2023.

[95] P. A. D. S. N. Wijesekara, "Load Balancing in Blockchain Networks: A Survey," *International Journal of Electrical and Electronic Engineering & Telecommunications*, vol. 13, no. 4, pp. 260-276, 2024.

[96] S. Verma, D. Yadav, and G. Chandra, "Introduction of formal methods in blockchain consensus mechanism and its associated protocols," *IEEE Access*, vol. 10, pp.66611-66624, 2022.

[97] P. A. D. S. N. Wijesekara, "A Review of Blockchain-Rooted Energy Administration in Networking," *Indonesian Journal of Computer Science*, vol. 13, no. 2, pp. 1607-1642, 2024.

[98] P. A. D. S. N. Wijesekara, "Intrusion Detection Using Blockchain in Software-Defined Networking: A Literature Review," *Journal of Engineering Science & Technology Review*, vol. 18, no. 1, pp. 57-79, 2025.

[99] C. Seneviratne, P. A. D. S. N. Wijesekara, and H. Leung, "Performance analysis of distributed estimation for data fusion using a statistical approach in smart grid noisy wireless sensor networks," *Sensors*, vol. 20, no. 2, pp. 567, 2020.

[100] P. A. D. S. N. Wijesekara, "A Review on Deploying Blockchain Technology for Network Mobility Management," *International Transactions on Electrical Engineering and Computer Science*, vol. 3, no. 1, pp. 1-33, 2024.

[101] A. Alahmadi, S. Çalkavur, P. Solé, A. N. Khan, M. A. Raza, and V. Aggarwal, "A new code based signature scheme for blockchain technology," *Mathematics*, vol. 11, no. 5, p.1177, 2023.

[102] P. A. D. S. N. Wijesekara, "Network Virtualization Utilizing Blockchain: A Review" *Journal of Applied Research in Electrical Engineering*, vol. 3, no. 2, pp. 136-158, 2024.

[103] D. He, R. Wu, X. Li, S. Chan, and M. Guizani, "Detection of vulnerabilities of blockchain smart contracts," *IEEE Internet of Things Journal*, vol. 10, no. 14, pp. 12178 – 12185, 2023.

[104] P. A. D. S. N. Wijesekara, and S. Gunawardena, "A review of blockchain technology in knowledge-defined networking, its application, benefits, and challenges," *Network*, vol. 3, no. 3, pp. 343-421, 2023.

[105] I. Pittaras, N. Fotiou, V. A. Siris, and G. C. Polyzos, "Beacons and blockchains in the mobile gaming ecosystem: A feasibility analysis," *Sensors*, vol. 21, no. 3, Art. no. 862, 2021.

[106] G. K. S. Tan, "Playing for keeps: Digital labor and blockchain precarity in play-to-earn gaming," *Geoforum*, vol. 151, Art. no. 104009, 2024.

[107] H. Bu, and K. Kuwabara, "Validating knowledge contents with blockchain-assisted gamified crowdsourcing," *Vietnam Journal of Computer Science*, vol. 8, no. 04, pp.471-491, 2021.

[108] W. S. Wang, and L. C. Lee, "Development of a fake news checking crowdsourcing platform consisting of smart contracts combined with gamification," in *2021 IEEE International Conference on Consumer Electronics-Taiwan,* pp. 1-2, 2021.

[109] J. C. Ferreira, A. L. Martins, F. Gonçalves, and R. Maia, "A blockchain and gamification approach for smart parking," in *Second EAI International Conference on Intelligent Transport Systems, From Research and Development to the Market Uptake,* pp. 3-14, 2019.

[110] Q. Aini, N. Lutfiani, and M. S. Zahran, "Gamification based on blockchain technology to enhance student centered learning," *CCIT Journal*, vol. 14, no. 1, pp.100-110, 2021.

[111] Q. Aini, N. Azizah, R. Salam, N. P. L. Santoso, and S. Millah, "iLearning education based on gamification blockchain," *Indonesian Journal of Electrical Engineering and Computer Science*, vol. 26, no. 1, pp.531-538, 2022.

[112] R. M. Parizi, and A. Dehghantanha, "On the understanding of gamification in blockchain systems," in *2018 6th international conference on Future Internet of Things and Cloud Workshops,* pp. 214-219, 2018.

[113] S. Chen, Q. Cao, and Y. Cai, "Blockchain for healthcare games management," *Electronics*, vol. 12, no. 14, Art. no. 3195, 2023.

[114] K. Xin, S. Zhang, X. Wu, and W. Cai, "Reciprocal crowdsourcing: building cooperative game worlds on blockchain," in *2020 IEEE International Conference on Consumer Electronics,* pp. 1-6, 2020.

[115] H. Y. Yuen, F. Wu, W. Cai, H. C. Chan, Q. Yan, and V. C. Leung, "Proof-of-play: A novel consensus model for blockchain-based peer-to-peer gaming system," in *Proceedings of the 2019 ACM International Symposium on Blockchain and Secure Critical Infrastructure*, pp. 19-28, 2019.

[116] K. Komiya, and T. Nakajima, "Increasing motivation for playing blockchain games using proof-of-achievement algorithm," in *First International Conference on HCI in Games,* pp. 125-140, 2019.

[117] Y. M. Arif, M. N. Firdaus, and H. Nurhayati, "A scoring system for multiplayer game base on blockchain

technology," in *2021 IEEE Asia Pacific Conference on Wireless and Mobile,* pp. 200-205, 2021.

[118] N. Patel, A. Shukla, S. Tanwar, N. Kumar, and J. J. Rodrigues, "Gina: A blockchain-based gaming scheme towards ethereum 2.0," in *2021 IEEE International Conference on Communications*, pp. 1-6, 2021.

[119] M. Du, Q. Chen, L. Liu, and X. Ma, "A blockchain-based random number generation algorithm and the application in blockchain games," in *2019 IEEE International Conference on Systems, Man and Cybernetics*, pp. 3498-3503, 2019.

[120] D. Kraft, "Game-theoretic randomness for blockchain games," *arXiv preprint arXiv:1901.06285*, pp. 1-19, 2019.

[121] R. Harkanson, C. Chiu, Y. Kim, and J. Y. Jo, "A framework for decentralized private random state generation and maintenance for multiplayer gaming over blockchain," in *2020 IEEE 44th Annual Computers, Software, and Applications Conference,* pp. 483-488, 2020.

[122] N. Trojanowska, M. Kedziora, M. Hanif, and H. Song, "Secure decentralized application development of blockchain-based games," in *2020 IEEE 39th International Performance Computing and Communications Conference*, pp. 1-8, 2020.

[123] I. Paajala, J. Nyyssölä, J. Mattila, and P. Karppinen, "Users' perceptions of key blockchain features in games," *Future Internet*, vol. 14, no. 11, Art. no. 321, 2022.

[124] C. Paduraru, R. Cristea, and A. Stefanescu, "Enhancing the security of gaming transactions using blockchain technology," in *Proceedings of the 37th IEEE/ACM International Conference on Automated Software Engineering*, pp. 1-8, 2022.

[125] L. Besançon, C. F. Da Silva, and P. Ghodous, "Towards blockchain interoperability: Improving video games data exchange," in *2019 IEEE International Conference on Blockchain and Cryptocurrency,* pp. 81-85, 2019.

[126] Y. M. Arif, R. P. Pradana, H. Nurhayati, S. M. S. Nugroho, and M. Hariadi, "A blockchain-based multiplayer transaction for tourism serious game," in *2020 International Conference on Computer Engineering, Network, and Intelligent Multimedia*, pp. 138-143, 2020.

[127] A. Bhand, R. Bhand, and M. Mali, "MAGE RUNNER: The game using blockchain technology," *Journal of Innovations in Business Industry*, vol. 2, no. 2, pp. 59-78, 2024.

[128] H. Sanghvi et. al., "MetaHate: AI-based hate speech detection for secured online gaming in metaverse using blockchain," *Security and Privacy*, vol. 7, no. 2, Art. no. e343, 2024.

[129] I. Ali, and N. Javaid, "Delay management and security for states and actions involves gaming network based on the blockchain, *COMSATS University Islamabad*, pp. 1-7, 2018.

[130] S. Fan, J. Zhao, R. Zhao, Z. Wang, and W. Cai, "CryptoArcade: A cloud gaming system with blockchain-based token economy," *IEEE Transactions on Cloud Computing*, vol. 11, no. 3, pp. 2445–2458, 2022.

[131] J. Zhao, Y. Chi, Z. Wang, V. C. Leung, and W. Cai, "Cloudarcade: A blockchain empowered cloud gaming system," in *Proceedings of the 2nd ACM International Symposium on Blockchain and Secure Critical Infrastructure*, pp. 31-40, 2020.

[132] T. Min, and W. Cai, "A security case study for blockchain games," in *2019 IEEE Games, Entertainment, Media Conference,* pp. 1-8, 2019.

[133] B. Egliston, and M. Carter, "Cryptogames: The promises of blockchain for the future of the videogame industry," *New Media & Society*, Art. no. 14614448231158614, 2023.

[134] X. J. Jiang, and X. F. Liu, "Cryptokitties transaction network analysis: The rise and fall of the first blockchain game mania," *Frontiers in Physics*, vol. 9, Art. no. 57, 2021.

Biography



Patikiri Arachchige Don Shehan Nilmantha Wijesekara obtained his first-class honors B.Sc. Engineering degree specializing in Electrical and Information Engineering in 2017 from the University of Ruhuna. He has received 6 academic awards for his bachelor's degree, including 2 gold medals and 1 scholarship. He has published his research works in reputed journals and holds an H-index of 13. He received a Ph.D. degree from the same university in computer networking. He has been recruited as a lecturer at the University of Ruhuna since 2018. His research interests include networking, machine learning, and blockchain.

Copyrights
© 2025 Licensee Shahid Chamran University of Ahvaz, Ahvaz, Iran. This article is an open-access article distributed under the terms and conditions of the Creative Commons Attribution –NonCommercial 4.0 International (CC BY-NC 4.0) License (http://creativecommons.org/licenses/by-nc/4.0/).

Shahid Chamran University of Ahvaz

Iranian Association of Electrical and Electronics Engineers

Journal of Applied Research in Electrical Engineering

E-ISSN: 2783-2864
P-ISSN: 2717-414X
Homepage: https://jaree.scu.ac.ir/



Research Article

Performance Evaluation of a PV-Based Multilevel Inverter with Improved THD and Efficiency

Parimalasundar Ezhilvannan[1,*], Kumar Reddy Cheepati[2], and Suresh Krishnan[3]

[1] *Electrical and Electronics Engineering, Mohan Babu University, Tirupati, India*

[2] *Electrical and Electronics Engineering, KSRM College of Engineering, Kadapa, India*

[3] *Electrical and Electronics Engineering, Christ University, Bangalore, India*

* *Corresponding Author: parimalpsg@gmail.com*

Abstract: This work presents the design, simulation, and performance evaluation of a three-phase multilevel inverter (MLI) system integrated with photovoltaic (PV) technology for grid-connected applications. The proposed system consists of a photovoltaic array, a Maximum Power Point Tracking (MPPT) controller based on the Perturb and Observe (P&O) algorithm, a DC-DC boost converter for voltage regulation, and a cascaded H-bridge multilevel inverter equipped with an LC filter to reduce output distortions. The entire system is modeled and analyzed using MATLAB/Simulink. Simulation results reveal that the system delivers a peak power output of 3000 W, maintains a regulated DC bus voltage of 800 V, and produces a stable three-phase AC output voltage of 400 V (RMS). The proposed inverter topology effectively reduces the Total Harmonic Distortion (THD) of the output waveform to 2.8% by optimizing the switching strategy using sinusoidal pulse width modulation (SPWM), significantly outperforming the 6.5% THD observed in conventional two-level inverter systems. Additionally, the system achieves an improved conversion efficiency of 96%, up from the typical 92%, through effective MPPT operation and low-loss inverter design. These improvements ensure superior power quality and reliable grid synchronization. The study underscores the viability of multilevel inverters in enhancing the performance of PV systems and promoting the efficient utilization of renewable energy sources for grid integration.

Keywords: DC-DC Converter, Grid Integration, Multilevel Inverter, Photovoltaic System, Three Phase System, THD.

Article history
Received 08 March 2025; Revised 02 August 2025; Accepted 01 October 2025; Published online 30 December 2025.
© 2025 Published by Shahid Chamran University of Ahvaz & Iranian Association of Electrical and Electronics Engineers (IAEEE)
How to cite this article
P. Ezhilvannan, K. R. Cheepati, and S. Krishnan, "Performance evaluation of a PV-based multilevel inverter with improved THD and efficiency," *J. Appl. Res. Electr. Eng.*, vol. 4, no. 1, pp. 56-68, 2025.
DOI: https://doi.org/10.22055/jaree.2025.49215.1182

Check for updates

NOMENCLATURE

ns	Number of switches in conduction per cycle
fs	Switching frequency
Iavg, Irms	Average and RMS current
Eon, Eoff	Energy lost during turn-on and turn-off
Vdc	DC link voltage
Iload	Load current
Qrr	Reverse recovery charge
Qg	Gate charge
Vg	Gate drive voltage

1. INTRODUCTION

The growing global energy demand and the urgent need for sustainable alternatives have significantly accelerated the transition toward renewable energy sources. Among these, solar photovoltaic (PV) systems have become a prominent solution due to their wide availability, minimal environmental impact, and long-term reliability. Their integration with modern infrastructure, especially the electrical grid and electric vehicle (EV) charging stations, has received increasing attention, as it enables clean energy utilization and reduces reliance on fossil fuels. However, achieving optimal system performance presents persistent challenges in energy conversion efficiency, energy storage management, and grid synchronization. A conventional PV system typically

comprises a PV array, a Maximum Power Point Tracking (MPPT) controller, a DC-DC converter, energy storage units, and an inverter for DC to AC conversion. MPPT controllers are critical in extracting maximum energy from PV panels, particularly under fluctuating irradiance and temperature conditions. The DC-DC boost converter increases the panel voltage to meet the input requirements of the inverter and the connected grid or load. To maintain stable operation, battery banks serve as energy buffers. For AC power delivery and grid connectivity, MLIs are often preferred due to their ability to produce stepped output voltages that enhance power quality, reduce total harmonic distortion (THD), and improve overall system efficiency. Pulse-width modulation (PWM) techniques further support inverter control, allowing reliable operation under varying load demands [1-3].

The rising adoption of EVs has created a parallel demand for sustainable charging infrastructure. Traditional charging stations predominantly rely on grid electricity, which may still be derived from non-renewable sources. Integrating PV-based systems with EV charging stations offers a sustainable alternative that lowers operational costs and carbon emissions. Such integration ensures uninterrupted charging through grid support while utilizing solar energy during daylight hours. The effectiveness of PV systems depends heavily on environmental factors such as sunlight intensity, shading, and temperature. To address these variations, MPPT algorithms are employed to consistently maximize energy capture. Conventional MPPT methods such as Perturb and Observe (P&O) and Incremental Conductance (IC) are widely implemented due to their simplicity and ease of deployment [4-7]. However, their performance declines under rapidly changing environmental conditions. Recent advances have introduced intelligent MPPT techniques based on fuzzy logic, neural networks, and artificial intelligence. These methods offer faster response and improved tracking accuracy in dynamic settings. In parallel, conventional boost converters used in DC-DC stages often experience high voltage stress and switching losses, limiting system efficiency. To mitigate these issues, researchers have proposed advanced converter designs, including interleaved and cascaded configurations, which enhance voltage gain and reduce ripple. In this context, the current study implements a high-efficiency DC-DC boost converter integrated with a filter to ensure voltage stability and suppress noise. At the core of power delivery lies the inverter stage. Among multilevel inverter topologies, the diode-clamped, flying capacitor, and cascaded H-bridge configurations are the most extensively studied. The diode-clamped multilevel inverter (DCMLI) uses clamping diodes to generate multiple voltage levels, resulting in improved output quality. However, it encounters issues such as voltage imbalance and increased complexity in diode arrangement, which limit its scalability. The flying capacitor multilevel inverter (FCMLI) replaces diodes with capacitors to achieve stepped output voltages. While this approach offers better voltage balancing, it requires a large number of capacitors, increasing the system's size and cost. The cascaded H-bridge multilevel inverter (CHBMLI), due to its modular structure and ease of implementation, has become popular in PV systems. It achieves high voltage levels using series-connected H-bridge cells, each powered by an independent DC source. Nevertheless, its reliance on isolated power supplies poses challenges in practical implementation. PWM strategies are essential in shaping inverter output. Sinusoidal PWM (SPWM) provides a straightforward technique for harmonic reduction, while Space Vector PWM (SVPWM) enhances DC bus utilization and inverter efficiency. Selective Harmonic Elimination (SHE) is another widely explored method that suppresses low-order harmonics by solving nonlinear equations, thereby improving waveform quality. Hybrid modulation strategies that combine these methods are gaining traction to optimize performance. When MLIs are integrated into grid-connected PV systems, they enhance energy extraction, reduce THD, and facilitate smooth power injection. Studies indicate that THD values can be reduced below 3%, aligning with IEEE 519 power quality standards. In addition, MLIs are increasingly used in EV charging stations, where they enable efficient DC-AC conversion and support bidirectional power flow in vehicle-to-grid (V2G) applications [8-11].

Ongoing research in MLI development focuses on minimizing component count, enhancing fault tolerance, and embedding artificial intelligence-based control methods to improve reliability and operational intelligence. However, as voltage levels increase, the circuit complexity rises, demanding more switching devices, diodes, or capacitors. This growth not only escalates the cost and control overhead but also complicates modulation strategies and real-time operation. In diode-clamped inverters, voltage imbalance among capacitors can lead to system instability. Similarly, in flying capacitor inverters, maintaining balanced voltage levels across capacitors is crucial, as imbalances may cause overvoltage stress on power devices and reduce component lifespan [12-15]. Although voltage balancing techniques such as redundant switching states and feedback control have been proposed, they increase system complexity and sensor requirements. Even though MLIs reduce switching stress relative to two-level inverters, higher-level designs introduce more semiconductors, leading to increased conduction losses. While optimized PWM strategies such as SVPWM and SHE help mitigate these losses, their computational demands make real-time processing more challenging. The adoption of wide-bandgap semiconductors such as Silicon Carbide (SiC) and Gallium Nitride (GaN) offers a promising route to reduce switching losses, but their high cost remains a limiting factor for widespread deployment. Furthermore, the growing number of components increases the likelihood of system faults and necessitates robust detection and mitigation strategies. These include redundant power paths, fault-tolerant control algorithms, and system reconfiguration. However, these solutions require additional hardware and increase the computational burden, making them less suitable for cost-sensitive applications [15-18].

Managing THD and electromagnetic interference (EMI) is another critical concern. Although MLIs inherently reduce THD by generating stepped waveforms, improper modulation or variable loads can reintroduce harmonics. High-frequency switching also contributes to EMI, potentially affecting nearby electronic systems. Filters—both passive (LC, LCL) and active—are essential to maintain compliance with standards such as IEEE 519 and IEC regulations. Passive filters, though commonly used, add bulk and may cause resonance issues, while active filters provide dynamic harmonic compensation at the cost of increased control

complexity and expense. The performance of MLIs in renewable energy applications is further influenced by fluctuating power input, particularly in PV and wind systems. Stable operation in such dynamic conditions necessitates intelligent control systems, including AI-based algorithms and predictive control models. Maintaining synchronization with the grid is particularly critical, as deviations in phase, voltage, or frequency can result in power instability or disconnection. Phase-Locked Loops (PLLs) are widely employed for synchronization, but their accuracy can degrade under grid disturbances such as voltage sags or frequency shifts. Adaptive PLLs and Model Predictive Control (MPC) approaches have been explored to address these issues, yet their implementation increases design complexity. Ultimately, while MLIs hold considerable promise for enhancing the efficiency and quality of renewable energy systems, several practical challenges hinder their widespread adoption. These include the complexity of component coordination, cost of implementation, computational demands of control strategies, and the need for compliance with stringent power quality standards. Overcoming these challenges is essential for the continued development of high-performance, grid-compatible PV and EV charging systems [19-24].

The following are the objectives of the PV integrated three phase grid system:

- The research aims to design and implement a PV-based energy system that efficiently integrates with the utility grid. The system incorporates a three-phase multilevel inverter to ensure seamless energy conversion and delivery, reducing reliance on conventional power sources.
- The study focuses on enhancing the performance of the DC-DC boost converter by improving its efficiency and minimizing power losses. By selecting appropriate switching devices and control strategies, the converter steps up the PV output voltage with high efficiency while maintaining voltage stability.
- The implementation of a three-phase multilevel inverter aims to reduce THD in the output waveform, improving power quality. Pulse-width modulation techniques are employed to achieve a near-sinusoidal AC output, ensuring grid compliance.
- The research utilizes the Perturb and Observe (P&O) MPPT algorithm to maximize power extraction from the PV array under varying environmental conditions. Real-time optimization of the duty cycle ensures that the system operates at peak efficiency.

2. Three Phase Multilevel Inverter With Grid System

Figs. 1 through 10 collectively illustrate the design, operation, and modulation of a two-stage grid-connected PV system integrated with a three-phase MLI for efficient renewable energy conversion and EV charging applications. Fig. 1 presents the block diagram of the proposed two-stage PV system. The PV array generates direct current (DC) electricity, which is optimized using a MPPT algorithm. The harvested power is then processed through a DC-DC boost converter to elevate the voltage to the desired level required by the inverter. This high-voltage DC power is fed into a three-phase MLI, which transforms it into alternating current (AC) suitable for grid connection and EV charging. A filter stage is incorporated after the inverter to mitigate THD, thereby enhancing power quality, energy efficiency, and system stability. Fig. 2 elaborates on the integration scheme of the PV system with a three-phase utility grid using a filtering mechanism. Fig. 3 illustrates the conventional five level MLI. The PV-generated DC is first conditioned by a high-efficiency boost converter and then converted to AC through a three-phase MLI. The inverter produces stepped voltage waveforms that reduce harmonic distortion. The output is further refined using a three-phase filter that eliminates high-frequency harmonics, ensuring smooth and high-quality power delivery to the grid. This setup supports bidirectional power flow, making it suitable for vehicle-to-grid (V2G) operations and smart grid scenarios. Fig. 4 illustrates the circuit design of a reduced-switch five-level MLI topology. This inverter configuration generates five distinct output voltage levels: +2Vdc, +Vdc, 0V, -Vdc, and -2Vdc. By using a minimal number of power switches, this design reduces switching losses and complexity while maintaining high output quality. The inverter operates with an optimized switching sequence controlled by PWM signals, enabling efficient power conversion and reduced component count, which is ideal for compact and cost-effective renewable energy systems. Figs. 5, 6, and 7 display the inverter's stepped output waveforms corresponding to specific voltage levels. Fig. 4 shows the waveform for the +2Vdc state, where the inverter connects the load to the highest DC potential, contributing to peak AC voltage. Fig. 6 depicts the +Vdc state, representing an intermediate voltage level that provides smoother transitions during positive waveform cycles. Fig. 7 illustrates the 0V state, a neutral condition that helps maintain waveform symmetry and balance during AC signal transitions. These voltage states collectively improve power quality by reducing the rate of voltage change and limiting high-frequency harmonics. Fig. 9 highlights the -2Vdc output state, achieved when the inverter switches connect the load to the lowest DC potential. This state, together with the positive and intermediate levels, forms a complete set of voltage steps that contribute to a near-sinusoidal output, significantly reducing THD and EMI. Finally, Fig. 10 shows the generation of Pulse Width Modulation (PWM) pulses used to control the switching states of the five-level inverter. These PWM signals determine the precise timing for switch activation, ensuring accurate voltage generation, harmonic suppression, and grid synchronization. This modulation technique enhances overall system performance, making the inverter suitable for high-efficiency PV-grid integration and EV charging applications. The proposed system employs a reduced-switch five-level CHBMLI topology. This choice offers a favourable trade-off between performance and complexity. Compared to diode-clamped and flying capacitor inverters, the reduced-switch CHBMLI requires fewer components, resulting in lower switching losses and simpler modulation. Additionally, it produces high-quality stepped waveforms, contributing to a significant reduction in THD. However, limitations include the need for precise voltage balancing and increased control complexity under dynamic loading, which are addressed in this design using optimized PWM and filter integration.

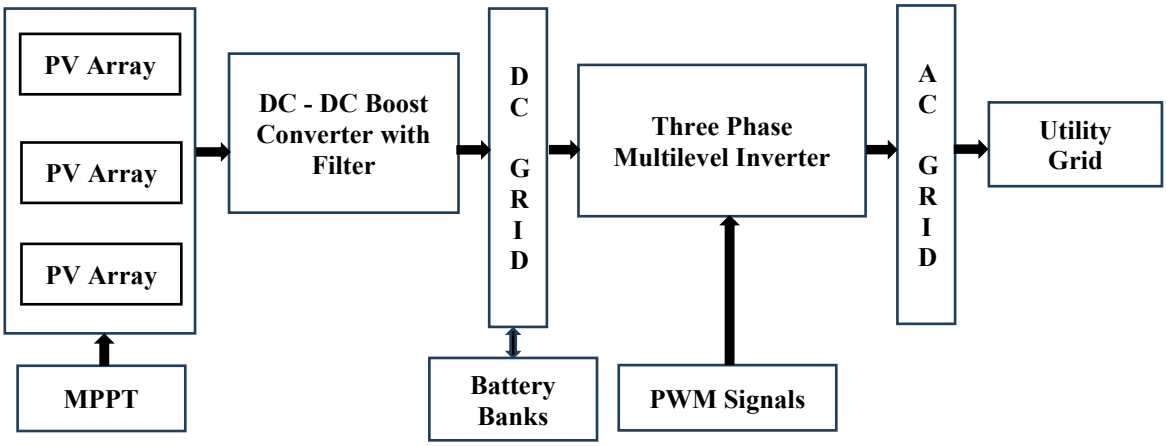


Fig. 1: PV to grid system through three phase MLI.

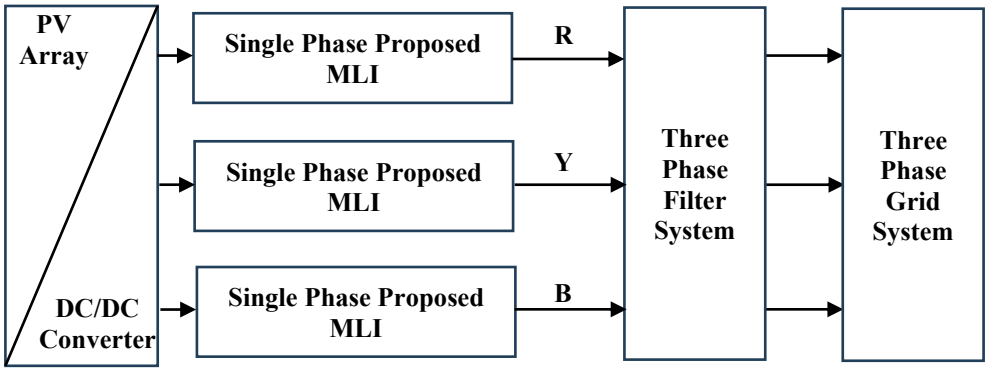


Fig. 2: PV with three phase grid system with filter.

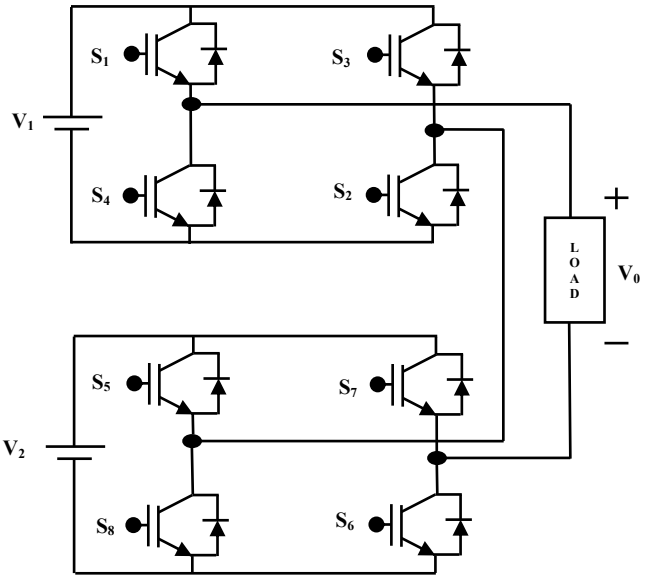


Fig. 3: PV conventional single phase five level inverter topology.

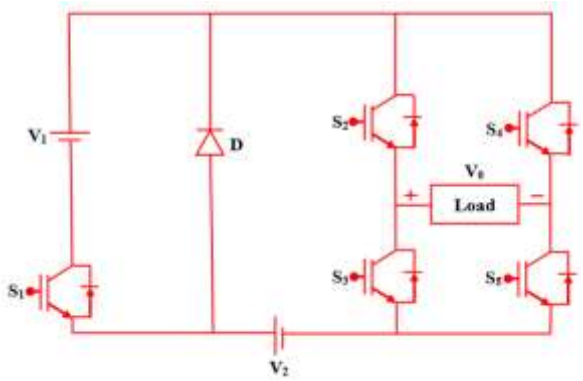


Fig. 4: Reduced switch five level output MLI.

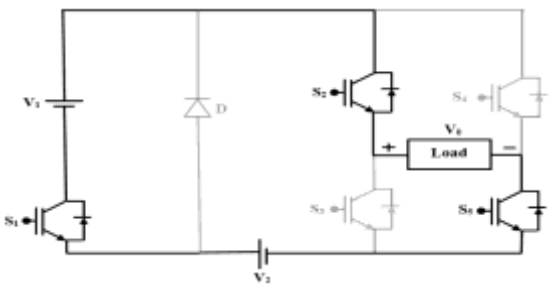


Fig. 5: +2Vdc Output voltage.

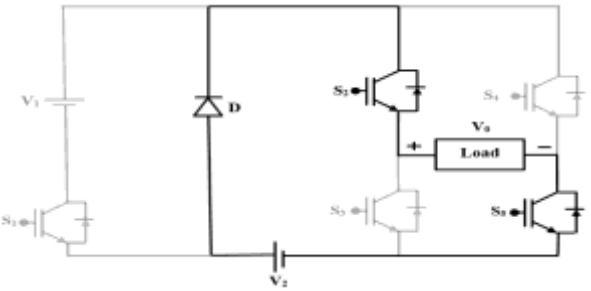


Figure 6: +Vdc Output voltage.

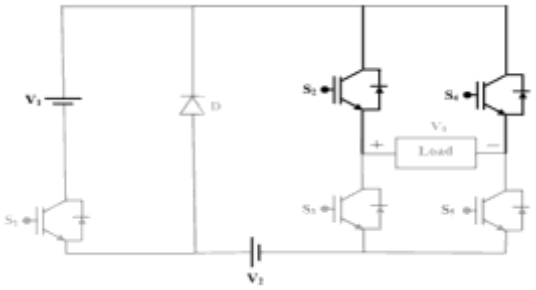


Fig. 7: 0Vdc Output voltage.

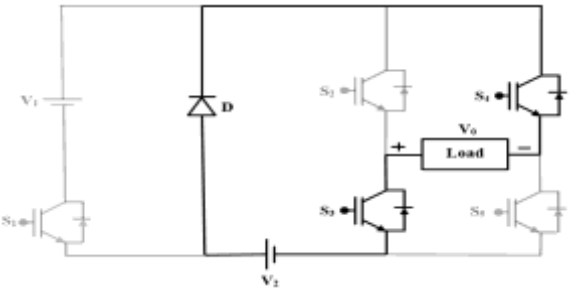


Fig. 8: -Vdc Output voltage.

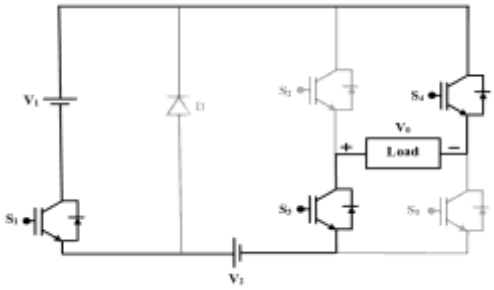


Fig. 9: -2Vdc Output voltage.

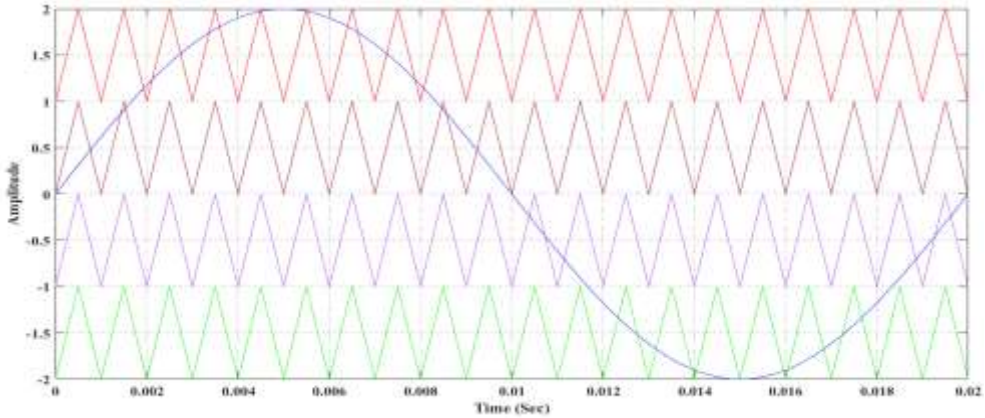


Fig. 10: PWM Pulse generation of five level inverter.

3. MPPT AND POWER LOSS ANALYSIS

Maximum Power Point Tracking is a crucial technique used in photovoltaic (PV) systems to maximize energy extraction under varying environmental conditions, such as changes in solar irradiance and temperature. The MPPT algorithm, as illustrated in the provided flowchart, continuously measures the voltage (V) and current (I) of the PV system, subsequently computing the power output (P) by multiplying these values (P = V × I). The core principle of the algorithm is to dynamically adjust the duty cycle of a DC-DC boost converter to track the maximum power point (MPP), ensuring optimal efficiency. The flowchart describes a Perturb and Observe (P&O) method, one of the most commonly implemented MPPT techniques. Initially, the algorithm measures the power at the current time step, P(k), and compares it with the previous power value, P(k-1). If the power remains unchanged, no adjustments are made. However, if a power increase is detected (P(k) > P(k-1)), the algorithm further examines whether the voltage has also increased. If the voltage has risen (V(k) > V(k-1)), the duty cycle is increased (D = D + ΔD), pushing the system further along the P-V curve in search of the MPP. Conversely, if the voltage has decreased (V(k) < V(k-1)), the duty cycle is reduced (D = D - ΔD) to move the operating point back toward the MPP. Similarly, if a power decrease is detected (P(k) < P(k-1)), the algorithm determines whether the voltage has increased or decreased and adjusts the duty cycle accordingly to maintain operation at or near the peak power point. By continuously cycling through this process, the MPPT controller ensures that the PV system operates at the most efficient point, adapting to fluctuations in environmental conditions. Fig. 12, which presents the power-voltage (P-V) characteristics of a PV array, further illustrates the significance of MPPT in energy harvesting. The curve demonstrates how power output varies with voltage, with a clear peak corresponding to the MPP. If the system operates to the left of this peak, an increase in voltage leads to higher power output, whereas if the system is to the right of the peak, increasing voltage results in power loss. The MPPT controller continuously adjusts the operating voltage to remain at the peak of the curve, preventing energy loss and maximizing power generation. This technique is critical for ensuring that PV systems achieve high efficiency, particularly in large-scale solar installations where even minor improvements in energy harvesting translate to significant gains in electricity production. Without MPPT, PV systems would be unable to dynamically respond to environmental changes, leading to suboptimal performance and energy losses. As solar energy adoption continues to grow globally, advanced MPPT algorithms, such as incremental conductance and fuzzy logic-based methods, are being explored to further improve performance, efficiency, and adaptability in diverse operating conditions. The implementation of MPPT not only enhances renewable energy utilization but also contributes to the broader goal of sustainable and efficient energy generation.

The conduction loss of Insulated Gate Bipolar Transistor (IGBT) can be calculated in the following Eq. (1) [5],

$$P_{\text{Cond,IGBT}} = \frac{1}{T}\int_0^T \left[V_f I(t) + R_{\text{on}} I^2(t)\right] dt \quad (1)$$

The conduction loss of diode can be calculated in the following equation [5].

$$P_{\text{Cond,D}} = \frac{1}{T}\int_0^T \left[V_f I_D(t) + R_D I_D^2(t)\right] dt \quad (2)$$

For an m-level inverter (m=5), the conduction losses per switching device depend on the duty cycle which is calculated in (3) [5].

$$P_{\text{Cond}} = n_s \cdot f_s \cdot V_f I_{\text{avg}} + n_s \cdot R_{\text{on}} I_{\text{rms}}^2 \quad (3)$$

Switching losses occur due to finite turn-on and turn-off times, which is calculated in (4) and further energy lost during turn-on and turn-off can be calculated in (5) and (6) [5].

$$P_{\text{sw}} = \sum_{i=1}^{n_s} \left(E_{\text{on},i} + E_{\text{off},i}\right) f_s \quad (4)$$

$$E_{\text{on}} = \frac{1}{2} V_{\text{dc}} I_{\text{load}} t_{\text{on}} \quad (5)$$

$$E_{\text{off}} = \frac{1}{2} V_{\text{dc}} I_{\text{load}} t_{\text{off}} \quad (6)$$

Diode reverse recovery losses occur due to stored charge removal can be calculated using (7) [12].

$$P_{\text{rec}} = \frac{1}{2} Q_{\text{rr}} V_{\text{dc}} f_s \quad (7)$$

These include control circuit losses, driver circuit losses, and gate drive power are calculated using (8) [12].

$$P_{\text{aux}} = P_{\text{driver}} + P_{\text{control}} \quad (8)$$

For an IGBT gate drive, which is calculated in Eq. (9) [12],

$$P_{\text{driver}} = Q_g V_g f_s \quad (9)$$

Equation (10) provides the total power loss in a five-level inverter based on switching characteristics and device parameters [12].

$$P_{\text{total}} = \sum \Big[n_s \left(V_f I_{\text{avg}} + R_{\text{ou}} I_{\text{rms}}^2\right) + n_s f_s \frac{1}{2} V_{\text{dc}} I_{\text{load}} (t_{\text{ou}} + t_{\text{off}}) + n_d \frac{1}{2} Q_{\text{rr}} V_{\text{dc}} f_s + Q_g V_g f_s \Big] \quad (10)$$

4. RESULTS AND DISCUSSION

Fig. 13 illustrates the current-voltage (I-V) characteristics of the PV array. The curve shows how the PV current varies with voltage under different solar irradiance levels. The short-circuit current (Isc) and open-circuit voltage (Voc) define the extreme operating points of the system. MPPT techniques adjust the voltage to ensure maximum power extraction, enhancing system efficiency. Fig. 14 presents the DC-link capacitor voltage profile in the PV system. The capacitor stabilizes the DC bus voltage by filtering ripples and transients before supplying power to the multilevel inverter. Maintaining a steady DC bus voltage ensures efficient power conversion and minimizes voltage fluctuations affecting inverter performance. Fig. 15 shows the three-phase output voltage of the inverter before filtering. The stepped waveform contains high-frequency harmonics due to the switching operation of the multilevel inverter. The unfiltered output may cause grid disturbances; hence, a filtering system is necessary to smoothen the waveform and meet grid quality standards. Fig. 16 depicts the variation in three-phase output current when the load changes. The inclusion of a filter ensures stable current delivery with minimal distortions, improving power quality. The current

waveform remains consistent, reducing harmonics and improving efficiency for grid integration and EV charging applications. Fig. 17 illustrates how the grid-connected inverter responds to variations in load current. When the load demand fluctuates, the inverter adjusts its output to maintain stable grid integration. The system ensures seamless power delivery without voltage imbalances or excessive harmonic distortions. Fig. 18 presents the THD analysis of the inverter's output voltage and current with a filtering circuit. The filter significantly reduces harmonic distortion, ensuring compliance with IEEE 519 standards. The proposed system achieves a THD below 3%, improving power quality and grid stability. Fig. 18 compares the THD of the conventional and proposed MLI systems. The conventional system exhibits a higher THD (~6.5%), while the proposed MLI achieves a reduced THD (~2.8%). This improvement enhances power quality, making the system more suitable for grid-connected applications. Fig. 19 illustrates THD analysis of conventional and proposed MLI system. Fig. 20 presents the efficiency comparison between the conventional and proposed methods. The conventional system operates at ~92% efficiency, while the proposed method achieves ~96%. The enhanced efficiency is due to optimized switching control, reduced power losses, and improved MPPT performance, making the system ideal for renewable energy applications. Table 1 illustrates the parameters of PV connected three phase grid system. Fig. 21 illustrates the SWOT analysis of proposed inverter. Table 2 illustrates the performance analysis of conventional and proposed inverter.

Table 1: Performance parameters of three phase grid connected grid system.

Parameters	Values
PV system peak power	3000 W
PV system peak current	5.5 A
DC capacitor output voltage	800 V
Three-Phase output voltage (without filter)	230 V (Peak)
Three-Phase output current (with filter)	~10 A
Grid connected current variation	0–12 A
THD output voltage (with filter)	2.80%
THD output current (with filter)	2.50%
THD of conventional MLI	6.50%
THD of proposed MLI	2.80%
Efficiency of conventional method	92%
Efficiency of proposed method	96%
Output power (Conventional)	2800 W
Output power (Proposed)	3000 W
Power quality improvement	30–40% reduction in THD

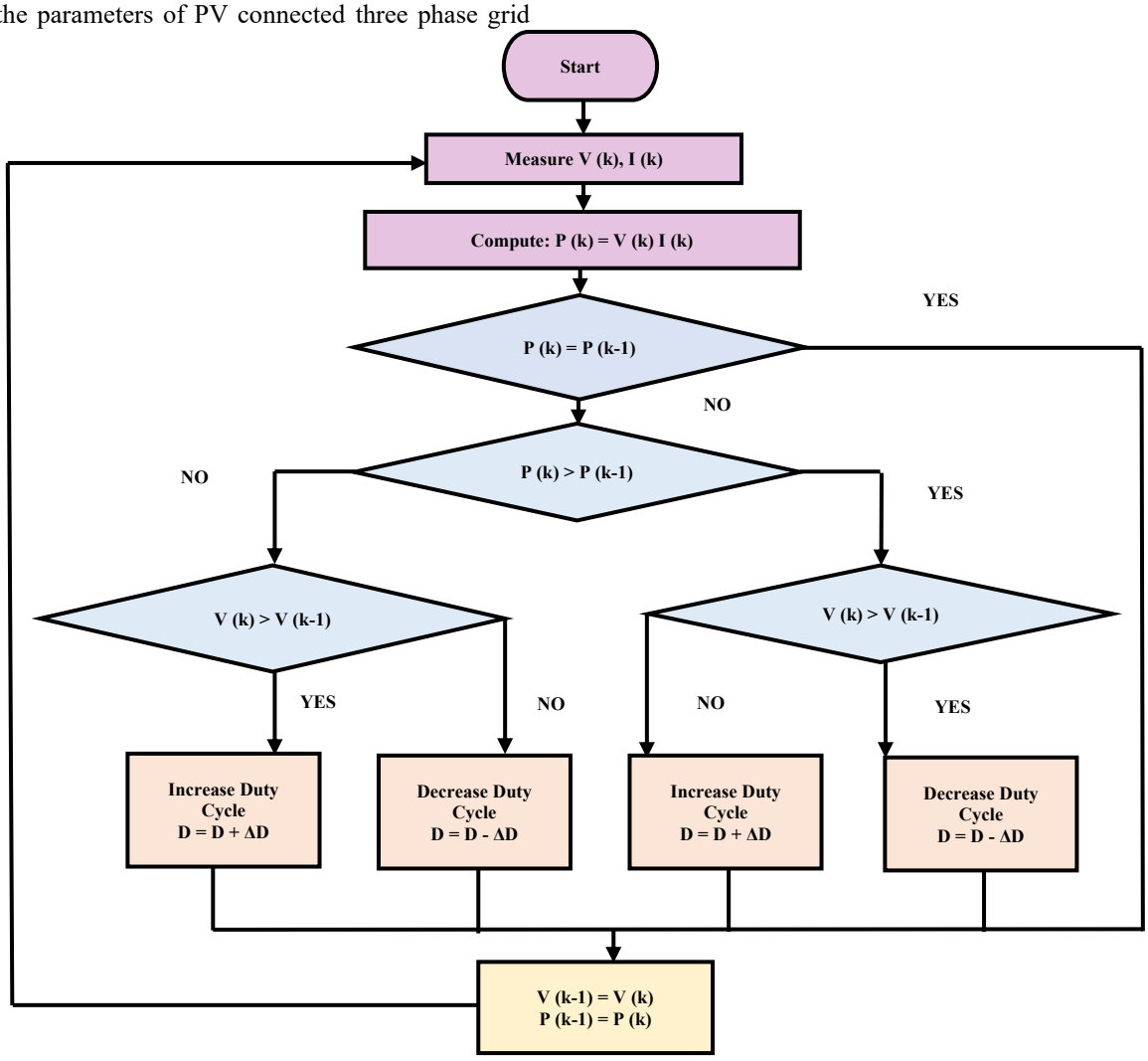


Fig. 11: Maximum power point tracking system for PV system.

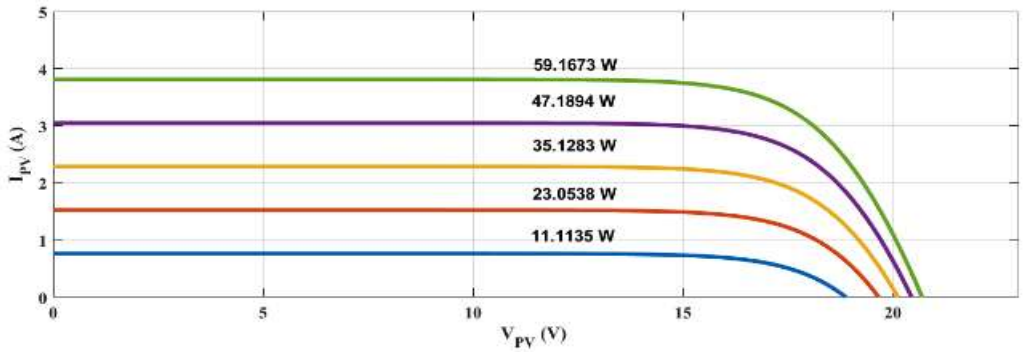


Fig. 12: P-V Characteristics of PV system.

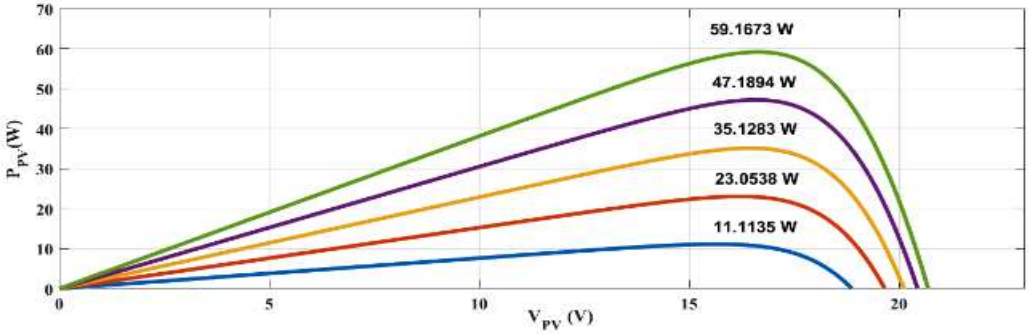


Fig. 13: I-V Characteristics of PV system.

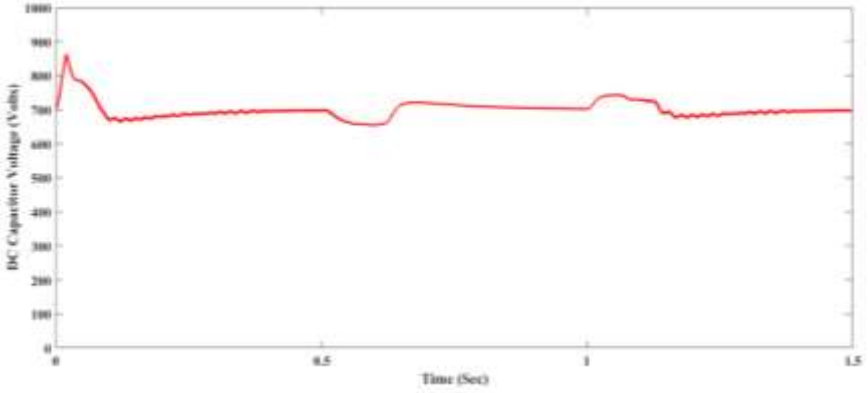


Fig. 14: DC capacitor output voltage for DC bus system.

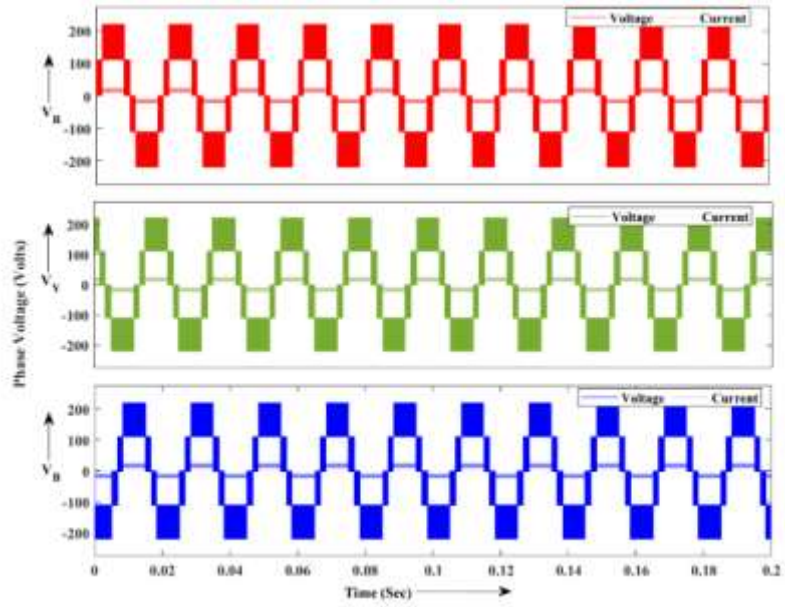


Fig. 15: Three phase output voltage without filter.

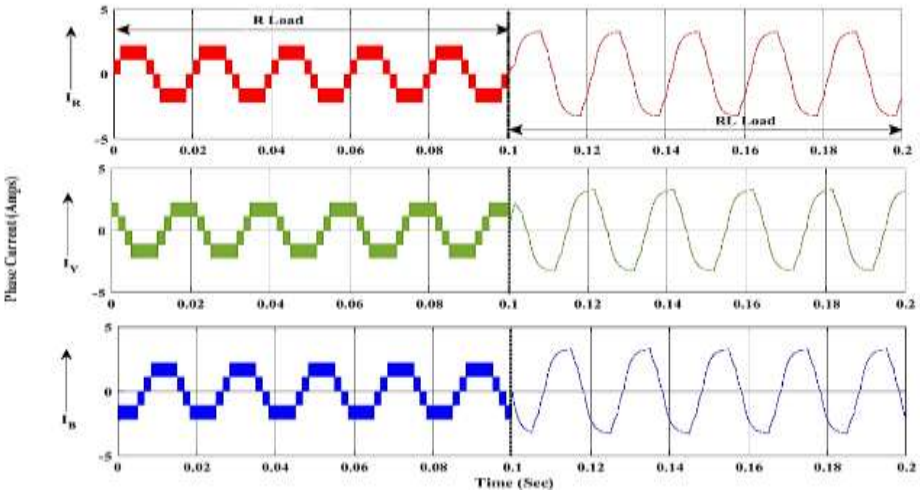


Fig. 16: Three phase output current change in load with filter.

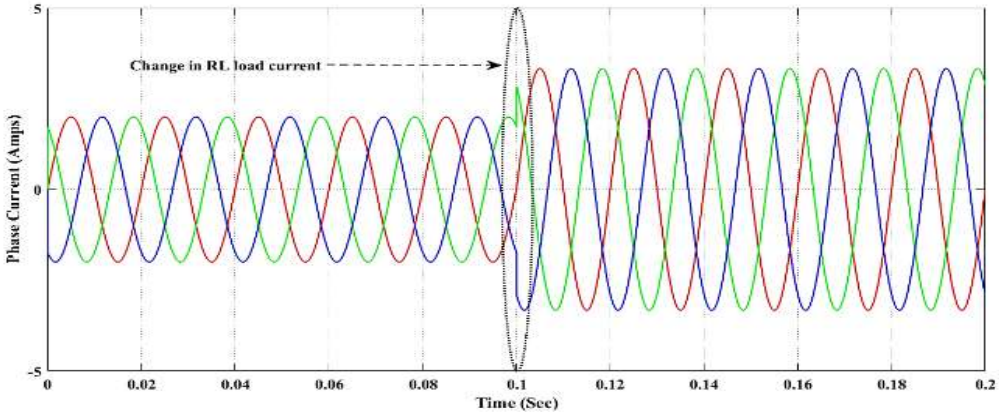


Fig. 17: Grid connected current due to change in load current.

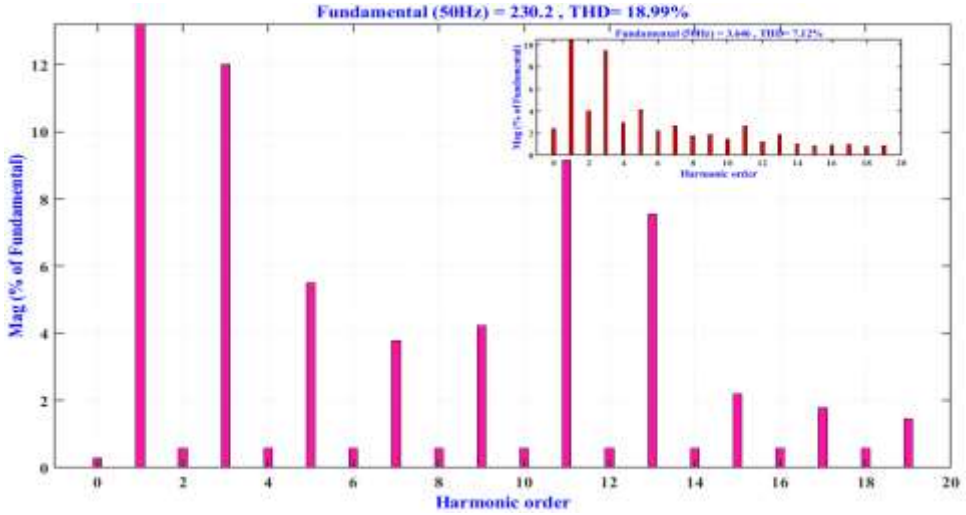


Fig. 18: THD analysis output voltage and current with filter circuit.

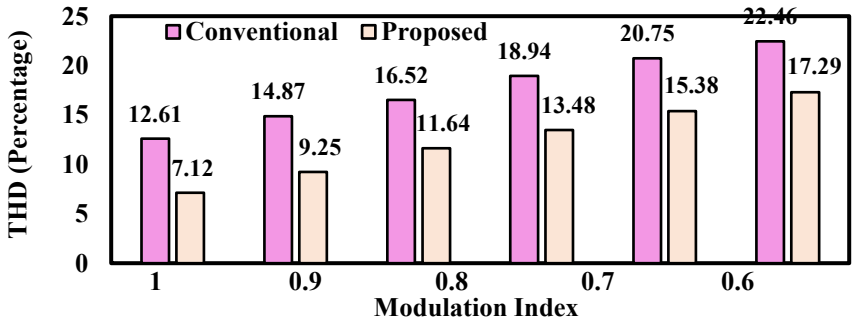


Fig. 19: THD analysis of conventional and proposed MLI system.

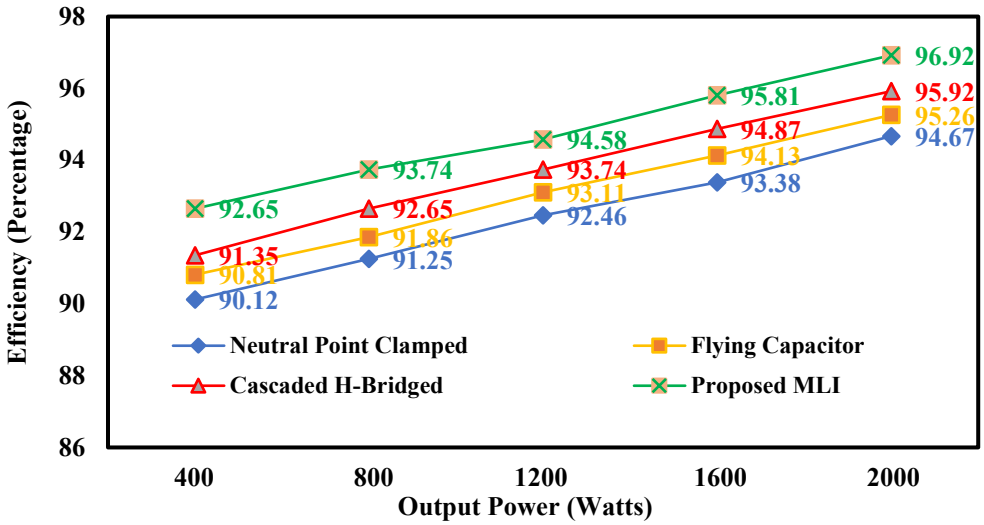


Fig. 20: Efficiency analysis of proposed and conventional methods.

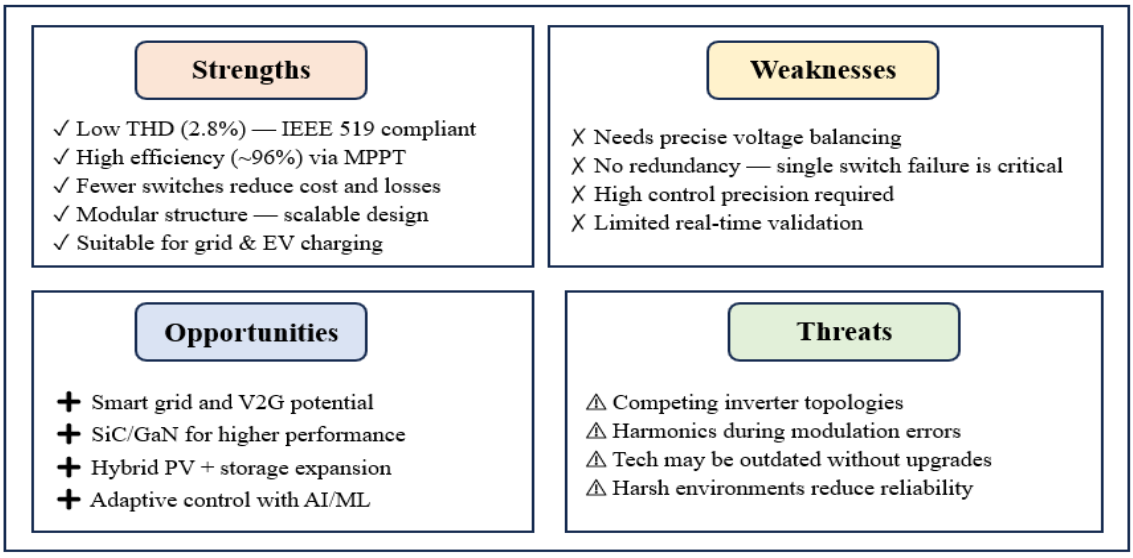


Fig. 21: SWOT analysis of proposed five level inverter.

Table 2: Comparative analysis of conventional and proposed five level MLI.

Criteria	Proposed CHBMLI System	Diode-Clamped MLI (DCMLI)	Flying Capacitor MLI (FCMLI)	Conventional Two-Level Inverter
Switch count	Reduced (8 switches for 5-level output)	High (requires clamping diodes per level)	High (requires multiple capacitors)	Minimal (2 or 3 per phase)
Output quality (THD)	Low THD (2.8% with filter)	Moderate (3.5–5% typical)	Low (but needs balancing control)	High THD (>7%)
Efficiency	High (~96%)	Moderate (~90–93%)	Moderate (~92–94%)	Moderate (~90–92%)
Cost	Moderate (fewer switches and no need for isolation)	High (more components and complex diodes)	High (costly capacitors and balancing circuit)	Low (simpler but low performance)
Complexity	Moderate (PWM with reduced switches)	High (voltage balancing + diode network)	High (complex control for capacitor balancing)	Low (simple PWM control)
Modularity	High (cascaded H-bridge structure)	Low	Low	Low
Reliability	Improved with fewer components	Susceptible to diode imbalance failures	Capacitor degradation under thermal stress	Moderate, but low resilience to THD or grid issues

Figs. 22 and 23 depict the hardware implementation and real-time performance output of the proposed five-level CHBMLI integrated with a PV system. The experimental setup consists of a PV emulator, MPPT controller, a high-efficiency DC-DC boost converter, and the CHBMLI configured with reduced switch topology. The inverter is constructed with a total of eight switches and multiple isolated DC sources to generate five distinct output voltage levels effectively reducing switch count and improving conversion efficiency.



Fig. 22: Hardware setup of proposed five level MLI.

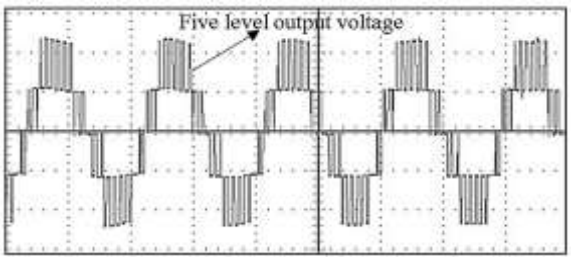


Fig. 23: Real time five level output voltage.

Fig. 23 presents the oscilloscope capture of the real-time inverter output voltage waveform, clearly demonstrating the expected stepped nature. The waveform validates the system's capability to synthesize a near-sinusoidal AC output with minimal harmonic distortion. The five-level output ensures lower dv/dt stress, contributing to reduced electromagnetic interference (EMI) and improved power quality. The experimental results closely match the simulation analysis, with THD levels observed below 3%, aligning with IEEE 519 standards which is analysed in Fig. 24. This validates the robustness and practicality of the hardware implementation for grid-connected renewable applications, particularly in EV charging stations where high efficiency and power quality are critical. The setup confirms real-time feasibility of the proposed topology with reliable modulation and control strategies.

5. Conclusion

The proposed PV-based three-phase MLI system has been successfully designed and analyzed for grid and EV charging applications. The simulation results validate the system's ability to improve energy conversion efficiency, power quality, and grid stability. The implementation of an MPPT-controlled DC-DC boost converter effectively maximizes power extraction, ensuring an optimal DC bus voltage of 800 V. The MLI topology minimizes harmonic distortion, reducing THD to 2.8%, which significantly improves grid compatibility. Compared to conventional inverters, the proposed system enhances efficiency to 96% and reduces power losses, making it a more reliable and cost-effective solution. The study also highlights the advantages of integrating PV energy with the grid, offering a sustainable and uninterrupted power supply. However, further research can focus on optimizing the MLI structure to reduce the number of switches and improve cost-effectiveness. Additionally, real-time implementation and experimental validation of the system would provide deeper insights into its practical feasibility. Overall, the proposed system presents a promising approach for enhancing the reliability and

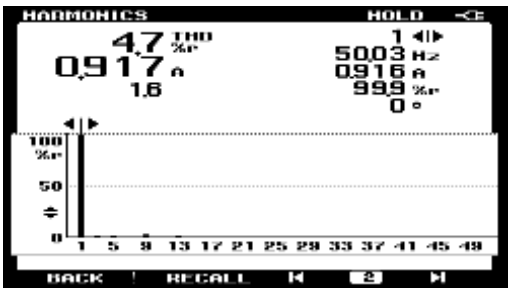


Fig. 24: THD analysis of five level inverter.

efficiency of renewable energy-based power conversion systems, paving the way for improved EV charging infrastructure and smart grid applications.

Acknowledgments

This work was supported by the Sree Vidyanikethan Educational Trust (SVET), Tirupati, Andhra Pradesh, India.

Credit Authorship Contribution Statement

Parimalasundar Ezhilvannan: Conceptualization, Data curation, Formal analysis, Investigation, Methodology, Resources, Software, Supervision, Validation, Visualization, Writing - original draft, Writing - review & editing. **Kumar Reddy Cheepati**: Conceptualization, Data curation, Formal analysis, Methodology, Resources, Software, Supervision, Validation, Writing - original draft, Writing - review & editing. **Suresh Krishnan:** Conceptualization, Data curation, Formal analysis, Funding acquisition, Investigation, Methodology, Software, Supervision, Validation, Visualization, Writing - original draft, Writing - review & editing.

Declaration Of Competing Interest

The authors declare that they have no known competing financial interests or personal relationships that could have appeared to influence the work reported in this paper. The ethical issues; including plagiarism, informed consent, misconduct, data fabrication and/or falsification, double publication and/or submission, redundancy has been completely observed by the authors.

References

[1] M. A. Hosseinzadeh, M. Sarebanzadeh, C. F. Garcia, E. Babaei, J. Rodriguez, and R. Kennel, "Reduced multisource switched-capacitor multilevel inverter topologies," *IEEE Transactions on Power Electronics*, vol. 37, no. 12, pp. 14647-14666, Dec. 2022.

[2] Z. Zhang, J. Yao, and A. Ioinovici, "Switched-Capacitor multilevel inverter with input source-load common ground for applications supplied by green energy," *IEEE Transactions on Circuits and Systems II: Express Briefs*, vol. 71, no. 1, pp. 186-190, Jan. 2024.

[3] J. He, Y. Ye, and X. Wang, "ZVS and inrush charging current suppression design for switched-capacitor multilevel inverters," *IEEE Transactions on Power Electronics*, vol. 38, no. 9, pp. 10611-10616, Sept. 2023.

[4] V. Sirohi, T. S. Saggu, J. Kumar, and B. Gill, "Implementation of a novel multilevel inverter topology with minimal components—an experimental study," *IEEE Canadian Journal of Electrical and Computer Engineering*, vol. 47, no. 1, pp. 7-14, winter 2024.

[5] G. Kampitsis, E. I. Batzelis, A. Kolokasis, E. Matioli, and B. C. Pal, "A generalized phase-shift PWM Extension for improved natural and active balancing of flying capacitor multilevel inverters," *IEEE Open Journal of Power Electronics*, vol. 3, pp. 621-634, 2022.

[6] C. I. Odeh, A. Lewicki, and M. Morawiec, "A simplified SPWM scheme for a compact 3-level dual-output inverter," *IEEE Transactions on Circuits and Systems II: Express Briefs*, vol. 71, no. 9, pp. 4351-4355, Sept. 2024.

[7] A. Khoshsaadat, and M. Abedini, "A new topological method for output voltage clamping of immittance-based constant current load resonant converters," *J. Appl. Res. Electr. Eng.*, vol. 3, no. 1, pp. 33–39, 2024.

[8] Z. A. Alqarni, "Design of active fault-tolerant control system for multilevel inverters to achieve greater reliability with improved power quality," *IEEE Access*, vol. 10, pp. 77791-77801, 2022.

[9] K. Suresh and E. Parimalasundar, "A modified multi level inverter with inverted SPWM control," *IEEE Canadian Journal of Electrical and Computer Engineering*, vol. 45, no. 2, pp. 99-104, Spring 2022.

[10] K. V. Vasuda, L. K. Johny, and J. Mathew, "Effective DC link utilization of multilevel dual inverter with single source in the maximal distention mode," *IEEE Access*, vol. 12, pp. 26212-26221, 2024.

[11] X. Zheng, J. Yao, Z. Xu, and A. Ioinovici, "Multioutput switched-capacitor multilevel inverter with intrinsic elimination of the photovoltaics induced leakage current and high boost factor," *IEEE Transactions on Industrial Electronics*, vol. 70, no. 6, pp. 5850-5861, June 2023.

[12] I. A. Hassanvand, J. Ebrahimi, and M. Abasi, "Voltage regulation in low voltage distribution networks using reactive power capability of photovoltaic inverters and pid consensus algorithm," *J. Appl. Res. Electr. Eng.*, vol. 3, no. 2, pp. 159–167, 2024.

[13] A. Awadelseed, A. Lewicki, and A. Iqbal, "Single-Phase 15-level switched-capacitor boost multilevel inverter topology for renewable energy applications," *IEEE Access*, vol. 12, pp. 90782-90793, 2024.

[14] Y. Wang, F. Liu, S. Chen, G. Shen, and Q. -G. Wang, "Prediction errors analysis and correction on FCS-MPC for the cascaded h-bridge multilevel inverter," *IEEE Transactions on Industrial Electronics*, vol. 69, no. 8, pp. 8264-8273, Aug. 2022.

[15] M. Abedini and M. Abasi, "Optimization of PSS and UPFC controllers to enhance stability by using a combination of fuzzy algorithm and shuffled frog leaping algorithm," *J. Appl. Res. Electr. Eng.*, vol. 3, no. 2, pp. 168–176, 2024.

[16] G. Kampitsis, E. I. Batzelis, P. D. Mitcheson, and B. C. Pal, "A clamping-circuit-based voltage measurement system for high-frequency flying capacitor multilevel inverters," *IEEE Transactions on Power Electronics*, vol. 37, no. 10, pp. 12301-12315, Oct. 2022.

[17] N. K. Prah II, E. Twumasi, and E. A. Frimpong, "Combined economic emission dispatch in a grid-connected microgrid using an improved mayfly algorithm," *J. Appl. Res. Electr. Eng.*, vol. 2, no. 2, pp. 112–119, 2023.

[18] Salem, H. Van Khang, I. N. Jiya, and K. G. Robbersmyr, "Hybrid Three-phase transformer-based multilevel inverter with reduced component count," *IEEE Access*, vol. 10, pp. 47754-47763, 2022.

[19] E. Silva, A. M. Alzamora, M. T. A. Êvo, and H. de Paula, "Design for reliability of DC-link capacitors for multilevel inverter topologies operating in hostile environments," *IEEE Transactions on Industry Applications*, vol. 60, no. 4, pp. 5882-5892, July-Aug. 2024.

[20] V. S. K. Prasadarao, S. Peddapati, and B. Kumar, "A voltage-boosting seven-level switched capacitor multilevel inverter with reduced device count," in *IEEE Journal of Emerging and Selected Topics Power Electronics*, vol. 12, no. 1, pp. 743-753, Feb. 2024.

[21] M. D. Siddique, M. Seyedmahmoudian, S. Mekhilef, and A. Stojcevski, "Open-Circuit fault-tolerant high-gain multilevel inverter topology with minimum of 2/3 level in postfault condition," *IEEE Transactions on Power Electronics*, vol. 39, no. 10, pp. 12013-12017, Oct. 2024.

[22] Jakhar, N. Sandeep, and A. K. Verma, "A five-level X-type boosting inverter with reduced stored energy of switched-capacitors," *IEEE Transactions on Circuits and Systems II: Express Briefs*, vol. 71, no. 3, pp. 1476-1480, March 2024.

[23] H. Aghaei, E. Babaei, and M. B. B. Sharifian, "Two compact three-phase multilevel inverters for low-voltage applications," *IEEE Transactions on Power Electronics*, vol. 38, no. 1, pp. 647-656, Jan. 2023.

[24] S. Mondal *et al.*, "A switched-capacitor based single-phase transformerless inverter for grid integration," *IEEE Transactions on Applied Superconductivity*, vol. 34, no. 8, pp. 1-5, Nov. 2024, Art no. 5001005.

BIOGRAPHY



Parimalasundar Ezhilvannan received a Ph.D. in Electrical Engineering from Anna University, Chennai, in 2016. Currently serving as a Professor in the Department of Electrical and Electronics Engineering at Mohan Babu University, Tirupati, India. Earned an M.E. in Power Electronics and Drives from PSG College of Technology, Coimbatore, in 2009, and a B.E. in Electrical and Electronics Engineering from the Government College of Engineering, Bargur, in 2007. Has over 15 years of teaching and research experience, primarily focused on power electronics, electrical drives, and energy-efficient systems. Research interests include universal converters and controllers, hybrid electric vehicles, and multilevel inverter technologies. Published numerous research papers in reputed international journals and conferences. Actively serves as a reviewer for several indexed journals and maintains strong

collaborations with both academic and industrial partners. Committed to advancing smart and sustainable power electronic systems through innovative research and interdisciplinary engagement.



Kumar Reddy Cheepati earned his Ph.D. in Electrical and Electronics Engineering from JNTU Kakinada in 2021. He is currently an Associate Professor at KSRM College of Engineering (Autonomous), Kadapa, Andhra Pradesh. He completed his M.Tech in Maintenance Engineering from SJCE, Mysore (now JSS Technical University) in 2011 and B.E. from St. Joseph's College of Engineering, Chennai in 2009. With over 10 years of teaching experience, he previously served at Sree Vidyanikethan Engineering College, Tirupati, and Navodaya Institute of Technology, Raichur. Dr. Cheepati has published several papers in Scopus, SCI, and ESCI-indexed journals and has presented at international IEEE conferences. His research focuses on predictive control techniques for shunt active filters in compliance with IEEE 519-2014. He holds a patent on a "Clutch Lever Restriction Assembly" and actively reviews for journals such as EPSR, JCSC, and Circuit World. He is regularly invited for academic and research engagements



Suresh Krishnan received a Ph.D. in Electrical Engineering from Anna University, Chennai, in 2017. Currently, serving as an Associate Professor in the Department of Electrical and Electronics Engineering at Christ University, Bangalore. Earned an M.E. in Power Electronics and Drives from Sona College of Technology, Salem, in 2012, and a B.E. in Electrical Engineering from Anna University, Chennai, in 2008. Research interests include universal converters and controllers, hybrid electric vehicles, and DC–AC converter systems. Published several research papers in reputed international journals and presented at key conferences focusing on power electronics and renewable energy integration. Contributions have been acknowledged in academic and applied domains, particularly in the advancement of electric vehicle technologies and efficient power conversion architectures. Actively involved in reviewing scholarly articles and participating in technical committees across various IEEE and Scopus-indexed platforms. Dedicated to advancing both teaching and research in modern power electronics systems.

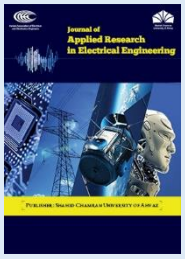
Copyrights
© 2025 Licensee Shahid Chamran University of Ahvaz, Ahvaz, Iran. This article is an open-access article distributed under the terms and conditions of the Creative Commons Attribution –Non-Commercial 4.0 International (CC BY-NC 4.0) License (http://creativecommons.org/licenses/by-nc/4.0/).

Shahid Chamran University of Ahvaz

Iranian Association of Electrical and Electronics Engineers

Journal of Applied Research in Electrical Engineering

E-ISSN: 2783-2864
P-ISSN: 2717-414X
Homepage: https://jaree.scu.ac.ir/



Research Article

Power Resource Allocation in Downlink NOMA Systems Using Joint Sum-Rate and Bit-Error-Rate Optimization

Mohammad Hasheminejad[1], Mohsen Sheikh-Hosseini[2,*]

[1] *Department of Electrical Engineering, University of Jiroft, Jiroft, Iran*

[2] *Department of Computer and Information Technology, Institute of Science and High Technology and Environmental Sciences, Graduate University of Advanced Technology, Kerman, Iran*

* *Corresponding Author: m.sheikhhosseini@kgut.ac.ir*

Abstract: The Nonorthogonal Multiple Access (NOMA) technique is one of the key enablers of next-generation cellular communications, facilitating the sharing of the same resources among users. The effectiveness of NOMA relies heavily on implementing a robust power allocation strategy that considers diverse influential factors. To address this challenge, we propose an innovative multi-objective power allocation scheme for downlink NOMA systems using the Multi-Objective Particle Swarm Optimization (MOPSO) algorithm. This approach simultaneously optimizes users' sum data rates and average bit error rates (BERs). The performance of the proposed method is analyzed in comparison to two benchmark approaches of Fixed Power Allocation (FSPA) and Greedy Algorithm-based Power Allocation (GAPA). The results confirm that, although our method offers comparable performance to these approaches regarding energy efficiency and sum data rate, it provides remarkable BER gain compared to these benchmarks.

Keywords: Non-Orthogonal Multiple Access (NOMA), Multi-Objective Particle Swarm Optimization (MOPSO), Power Allocation Algorithm, Sum Data Rate, Bit Error Rate (BER).

Article history
Received 06 October 2024; Revised 12 August 2025; Accepted 01 October 2025; Published 30 December 2025.
© 2025 Published by Shahid Chamran University of Ahvaz & Iranian Association of Electrical and Electronics Engineers (IAEEE)
How to cite this article
M. Hasheminejad, and M. Sheikh-Hosseini, "Power resource allocation in downlink NOMA systems using joint sum-rate and bit-error-rate optimization," *J. Appl. Res. Electr. Eng*., vol. 4, no. 1, pp. 69-75, 2025.
DOI: https://doi.org/10.22055/jaree.2025.48107.1141

Check for updates

1. INTRODUCTION

The continuous evolution of wireless technologies has led to the development of advanced cellular networks such as 5G, beyond 5G, and 6G, which promise transformative capabilities in connectivity, speed, and reliability [1-3]. However, these networks face significant challenges, including signal degradation due to channel impairments and path loss, particularly in high-frequency bands [3-5]. In the context of 5G, advanced paradigms such as cooperative communications, Device-to-Device communications, and full-duplex communication have been proposed to enhance coverage, capacity, and energy efficiency [6, 7]. Furthermore, key enablers such as massive Multiple-Input Multiple-Output (MIMO) systems, millimeter-wave communications, and ultra-dense networks (UDNs) address the limitations of conventional networks [6-8]. UDNs, by deploying a dense network of small cells, significantly improve coverage and capacity in high-demand environments. To manage this density efficiently, network slicing within virtualization frameworks allows the dynamic creation of multiple virtual networks, or "slices," each tailored to meet a specific requirement to ensure that the diverse traffic demands are met with optimized resource allocation [9].

Additionally, advanced access techniques like Non-Orthogonal Multiple Access (NOMA) have emerged as a promising technology for 5G and beyond, offering superior resource management compared to traditional orthogonal multiple access (OMA) methods [10-12]. Unlike conventional OMA schemes like TDMA, FDMA, and CDMA, NOMA allows sharing of the same resources across time, frequency, and code domains, distinguishing users by different power levels [12-14]. To ensure reliable

communication and system efficiency, the power allocation is done based on the values of the user channel gains. In particular, in the case of downlink NOMA, the available power is distributed in descending order of channel gains, enabling data recovery through Successive Interference Cancellation (SIC) at the receivers [15, 16].

Existing research on NOMA performance analysis encompasses a range of strategies aimed at enhancing various aspects, including spectral efficiency, energy efficiency, user fairness, and overall network reliability and capacity [17]. To this end, artificial intelligence tools, including various optimization techniques, have garnered significant interest in the design and optimal resource management of the NOMA scheme. The joint optimization of power allocation and channel assignment in NOMA systems is considered NP-hard due to the combinatorial nature of the problem, which involves a large search space and complex interactions between variables [15, 16, 18-22]. This difficulty arises from the need to simultaneously determine the optimum power levels for users and assign channels in a way that maximizes system performance metrics such as throughput or fairness, while also satisfying Quality of Service (QoS) constraints and system power constraints. This optimization problem is further complicated by the need to consider the decoding order for SIC and, in some cases, additional factors such as reflection coefficients in Reconfigurable Intelligent Surface (RIS)-assisted systems [8, 22]. Optimization techniques are also explored in the context of integrating NOMA with MIMO technologies, addressing resource management challenges, and implementing advanced signal processing for effective NOMA schemes [22]. Additionally, the implementation of SIC is a key factor in NOMA performance, with research indicating that optimized power allocation can significantly improve system throughput [24]. Moreover, the effects of imperfect receivers on NOMA performance have been investigated, highlighting the importance of robust SIC mechanisms [25].

The recent literature on power allocation optimization of NOMA systems has presented various strategies to enhance system performance. Reference [26] introduces a power allocation scheme for uplink NOMA systems, optimizing sum throughput under constraints using the Karush-Kuhn-Tucker conditions, showing improved throughput over OMA systems. Reference [27] extends the optimization to downlink NOMA systems, employing Lyapunov optimization to address long-term network utility maximization, overcoming the non-convex nature of the problem with a dynamic programming-based algorithm. Reference [28] proposes a dynamic power allocation strategy for uplink NOMA, which outperforms fixed power allocation, especially at low Signal-to-Noise Ratios (SNRs). In particular, reference [24] focuses on the downlink NOMA with SIC, where the proposed power allocation algorithm significantly improves system throughput compared to OMA. Reference [29] develops two power allocation strategies for downlink NOMA based on channel state information and predefined QoS, demonstrating superior performance to OMA. Reference [30] studies downlink NOMA power allocation using a genetic algorithm-based approach, achieving near-optimal performance with reduced complexity. Reference [31] analyzes NOMA in heterogeneous cloud radio access networks, proposing a joint optimization of user association, scheduling, and power allocation, showing improvements in rate, interference mitigation, and fairness. Reference [32] compares three power allocation schemes for NOMA, with full search power allocation yielding the best performance despite its complexity. Lastly, reference [33] explores a sub-optimal power allocation algorithm for 5G NOMA systems with hybrid beamforming, enhancing data flow with a low-complexity iterative technique.

Multi-objective optimization algorithms can enhance power allocation in uplink and downlink NOMA by simultaneously addressing various objectives such as maximizing throughput, energy efficiency, and fairness among users. These algorithms can provide a balance between conflicting objectives as existing works have applied various optimization techniques to address the trade-offs inherent in NOMA systems [12, 26-28].

This research aims to use multi-objective optimization tools to improve the efficiency of the power allocation algorithm in downlink NOMA systems. To be more precise, unlike most of the existing studies which often allocate power through optimizing one performance metric, we implement a Multi-Objective Particle Swarm Optimization (MOPSO) technique that simultaneously optimizes both the sum data rates of the users and the mean BER. The MOPSO algorithm is an extension of the classical Particle Swarm Optimization (PSO) method, which itself was inspired by the collective social behavior observed in fish schools and bird flocks. PSO is a population-based optimization technique in which particles iteratively adjust their positions within the search space, guided by both their own experiences and those of neighboring particles, to identify optimal solutions [34, 35]. MOPSO adapts this concept to address problems involving multiple conflicting objectives by maintaining a diverse set of solutions that approximate the Pareto front. Consequently, MOPSO combines the simplicity and efficiency of PSO with the capability to effectively tackle multi-objective optimization problems [36].

The novelties and contributions can be itemized as:

- **Novel Approach:** Unlike most proposed NOMA power allocation methods that focus solely on sum rate or BER, our approach optimizes both criteria simultaneously.
- **General Framework:** We present a flexible framework that can be adapted to various network conditions and user requirements, enhancing power allocation strategies.
- **Performance Improvement:** We conduct a comprehensive performance analysis under diverse scenarios, validating the robustness of our proposed power allocation method and highlight its advantage in terms of different key performance metrics.

The rest of this paper is organized as follows: the next section includes the signal model, problem statement, and the details of the proposed MOPSO algorithm. The third section outlines the experimental setup and discusses the results obtained. Finally, the fourth section provides a conclusion summarizing the study's key findings.

2. SUGGESTED POWER ASSIGNMENT APPROACH

2.1. System and Signal Model

Fig. 1 represents the schematic of the power-domain downlink NOMA system consisting of one base station (BS) and K users, each with one antenna. In this system, the BS divides the available power between users according to their channel gains and transmits a superimposed signal over the common channel. On the users' side, the SIC receiver is employed to remove interference and decode their data.

The model of received signal at the k^{th} user terminal will be:

$$\begin{aligned} y_k &= h_k X + n_k = h_k \sum_{k=1}^{K} \sqrt{p_k}\, x_k + n_k \\ &= h_k \left[\sum_{i=1}^{k-1} \sqrt{p_i}\, x_i + \sqrt{p_k} x_k + \sum_{i=k+1}^{K} \sqrt{p_i}\, x_i\right] + n_k \end{aligned} \quad (1)$$

in which $h_k = g_k / \sqrt{1 + d_k^{\alpha}}$ models the effective channel between the k^{th} user and the BS, where d_k stands for the distance between these two, g_k is the small-scale fading of the environment with Rayleigh distribution, and α is the path loss factor of this environment. n_k represents the noise sample at the k^{th} user terminal and follows additive white Gaussian noise (AWGN) with zero mean and variance N_0.

The parameter $X = \sum_{k=1}^{K} \sqrt{p_k}\, x_k$ represents the superposed signal of the BS terminals to be transmitted over the channel. In this formulation, p_k is the allocated power to the k^{th} user and x_k denotes the desired signal of this user which is a complex symbol of a digital modulator with the constraint of $\mathrm{E}[|x_k|^2] = 1$. As mentioned earlier, the BS assigns p_k to different users according to the values of the channel gains $|h_k|^2$. Actually, if the channel gains are sorted so that $|h_1|^2 < |h_2|^2 < \cdots < |h_K|^2$, the BS divide the available power between different users so that $p_1 > p_2 > \cdots > p_K$. This power allocation approach granitizes the reliable data recovery at the user terminals using process described in the sequel.

To recover x_k from y_k at the k^{th} user terminal, the interfering signals of all previous users, i.e., (x_1, x_2,…, x_{k-1}), are first removed in a sequential manner using maximum likelihood (ML) detector and SIC. Then, by considering the signals of the remaining users (x_{k+1}, x_{k+2},…, x_K) as interference, the ML detection is carried out to recover x_k with the below signal to interference plus noise (SINR) ratio.

$$\gamma_k = \frac{|h_k|^2 p_k}{|h_k|^2 \sum_{i=k+1}^{K} p_i + N_0} \quad (2)$$

2.2. Problem Statement and Formulation

As outlined before, this research aims to optimally allocate power resources between different users of the downlink NOMA systems by modeling this problem as a constrained multi-objective optimization problem and solving it using MOPSO. Our two objective functions are the sum of the achievable data rates and the average bit error rate of the users, where the former can be modeled using the well-known formula of information theory as

$$\begin{aligned} R &\overset{\text{def}}{=} f_1(\gamma_1, \ldots, \gamma_K) = \sum_{k=1}^{K} R_k \\ &= \sum_{k=1}^{K} \log_2(1 + \gamma_k) \\ &= \sum_{k=1}^{K} \log_2\left(1 + \frac{|h_k|^2 p_k}{N_0 + |h_k|^2 \sum_{i=k+1}^{K} p_i}\right) \end{aligned} \quad (3)$$

where R_k is the achievable data rate of k^{th} user.
In the case of the second objective function, the average BER of the system, i.e., P_e, can be formulated as

$$\begin{aligned} P_e &\overset{\text{def}}{=} f_2(\gamma_1, \ldots, \gamma_K) = \frac{1}{K} \sum_{k=1}^{K} P_{e,k} \\ &= \frac{1}{K} \sum_{k=1}^{K} f_k(\gamma_1, \ldots, \gamma_K) \end{aligned} \quad (4)$$

in which $P_{e,k}$ represents the average BER of k^{th} user. Unlike R_k, $P_{e,k}$ not only depends on its corresponding SINR γ_k, but also is a function of previous SINRs $(\gamma_1, \ldots, \gamma_{k-1})$ due to the error propagation caused by imperfect SIC at the $(x_1, \ldots, x_{k-1})$ terminals. Moreover, finding an exact expression for $f_k(\gamma_1, \ldots, \gamma_k)$ is not straightforward. Therefore, the analysis of P_e is much more complex or even impossible. As it is common, herein, we use Monte-Carlo simulation to compute this objective function. It is important to note that optimizing the first function involves maximization, while the second function needs to be minimized. Considering the relevant constraints, the proposed, multi-objective optimization problem in this research can be formulated as follows:

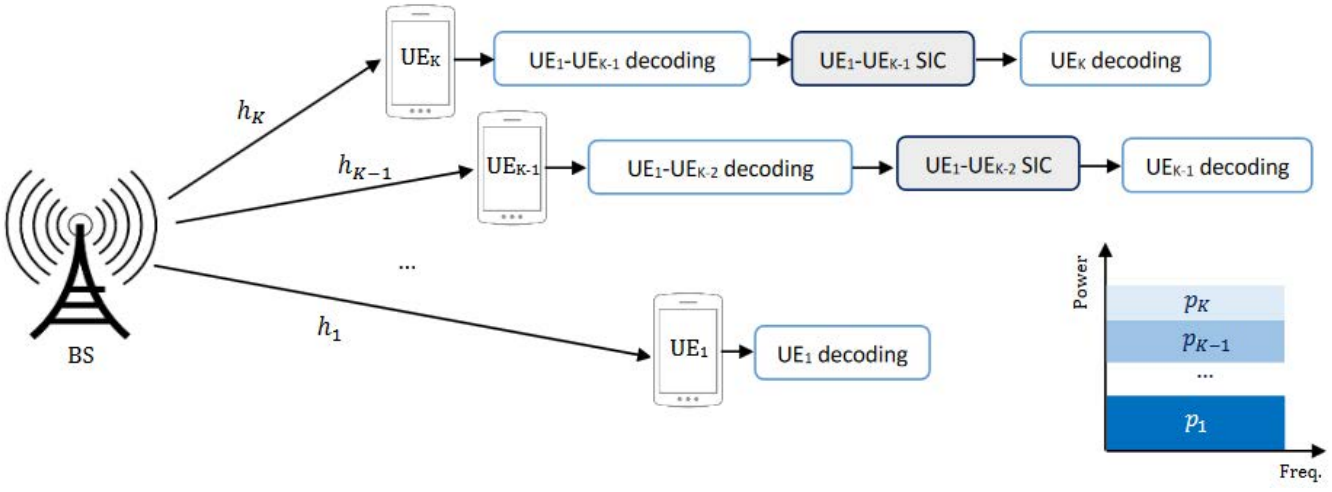


Fig. 1: A shematic of the downlink NOMA scheme with K uers [37].

$$\begin{cases} \min\limits_{p_1,\dots,p_K} & (P_e, -R), \\ subject\ to & \begin{cases} \sum_{k=1}^{K} p_k = P \\ p_1 > p_2 > \cdots > p_K \\ P_{e,k} \geq BER_{th} \end{cases} \end{cases} \quad (5)$$

where P it the total power available at the BS terminal, therefore, the constraint of $\sum_{k=1}^{K} p_k = P$ must be satisfied. In addition, BER_{th} represents a threshold which guarantees the minimum reliability required by users.

2.3. The Multi-Objective PSO Approach

The multi-objective PSO algorithm will be employed to find the optimal power allocation $\mathbf{p} = [p_1, \dots, p_K]$ that balances the two objectives. The PSO process can be described as follows:

a. Initialization:

- Each particle ($\boldsymbol{p}_i$) is a power vector that contains k elements, where each element relates to a user. The velocity vector of each particle ($\mathbf{V}_i$) represent the rate of change of a particle's power in the search space.
- Randomly initialize a swarm of particles, where each particle represents a potential solution (power allocation vector).
- Initialize each particle's position $\mathbf{p}_i$, and velocity $\mathbf{V}_i$.

b. Fitness Evaluation:

- For each particle, evaluate the fitness based on the two objectives:
- Calculate the sum rate R, and the BER for the given power allocation.
- Use a weighted approach or Pareto dominance to evaluate the performance of each particle.

c. Update Rules:

- Update the velocity and position of each particle based on its personal best position and the global best position found by the swarm.
- The updated equations are as follows:

$$\mathbf{V}_i(t+1) = \omega \mathbf{V}_i(t) + c_1 r_1 \left(\mathbf{p}_{i,\text{best}} - \mathbf{p}_i(t)\right) + c_2 r_2 \left(\mathbf{p}_{\text{global}} - \mathbf{p}_i(t)\right) \quad (6)$$

$$\mathbf{p}_i(t+1) = \mathbf{p}_i(t) + \mathbf{V}_i(t+1) \quad (7)$$

d. Termination:

- The algorithm iterates until a stopping criterion is met (e.g., a maximum number of iterations or convergence of the swarm).

2.4. Computational Complexity Analysis

The computational complexity of the proposed MOPSO algorithm can be characterized in terms of the key problem parameters. N denote the total number of users, G the group size, P the number of particles in the swarm, and I the maximum number of iterations. For a given particle, evaluating the objective functions (sum-rate and BER) involves computing the SINR, sum-rate, and BER for all groups. Under a fixed grouping strategy, this requires $O(N)$ operations per evaluation. Thus, the total complexity of MOPSO is approximately $O(P \times I \times N)$, where $P \times I$ represents the total number of candidate solutions evaluated. In following simulation settings ($P = 50$, $I = 100$), this yields 5,000 evaluations, which is tractable for NOMA scenarios with up to 12 users and results in MATLAB runtimes below two seconds on a standard desktop. Therefore, the computational cost of the proposed method is negligible compared to the substantial performance gains reported in the subsequent section.

3. Experimental Setting and Results

This section aims to evaluate the performance of the proposed Multi-Objective PSO Approach for optimizing NOMA grouping. To this end, well-known MOSPO n technique is adopted. The downlink NOMA system is implemented in MATLAB software so that a BS is located in the center of the cell with a radius of 50m, and the users are scattered randomly and uniformly inside this cell. Moreover, a Rayleigh fading channel of three taps and a path loss exponent of $\alpha = 2$ are included. The SNR per bit (E_b/N_0) changes from 0 to 40 (dB). The BPSK modulation is considered for the BS terminal and SIC receiver at the users' stations. In the simulations, two scenarios are considered for the number of users; these are $K = 6$ and $K = 12$, and a user grouping of size two is assumed in each scenario. Moreover, Fixed Power Allocation (FSPA) and Greedy Algorithm-based Power Allocation (GAPA) are utilized as benchmark methods to evaluate the performance of our proposed approach, labeled as "MOPA" in the subsequent figures, which is based on MOPSO under settings specified in Table 1. Fig. 2 and Fig. 3 represent the sum date rate results for the NOMA systems of $K = 6$ and $K = 12$, respectively. Notes, since the group size is set equal to two, it is worthing to emphasize that the number of groups in the scenarios of $N = 6$ and $N = 12$ will be three and six, respectively. The sum rate results in Fig. 2 and Fig. 3 are obtained by summing the data rates across all groups. Similarly, the spectral efficiency and BER results in the subsequent figures are derived by averaging over values of the corresponding metric over all groups. The comparison presented in these Fig. 2 and Fig. 3 reveals that, while the overall sum rate performance of the three methods is relatively similar, the FSPA method demonstrates a slight advantage over the other two. Fig. 4 and Fig. 5 illustrate the results for the energy efficiency, where the former stands for the $K = 6$ users and the latter has $K = 12$ users. As can be seen, Fig. 4 shows that the three methods perform similarly in the 6-user scenario. However, as the number of users increases to 12, the proposed method described in this study exhibits a significant performance improvement compared to the other two methods, as shown in Fig. 5.

Eventually, the BER results of both $N = 6$ and $N = 12$ scenarios are compared in Fig. 6. As seen, the advantage of the proposed method becomes evident in its substantial improvement in BER compared to the other two methods. This superiority arises from the inclusion of BER as one of the objective functions in the proposed MOPSO method, a critical consideration that is absent in the other methods. Given the pivotal role of BER in ensuring communication reliability, the proposed method's effectiveness is clearly demonstrated.

Table 1: Parameter setting of the MOPSO.

Parameter	Setting
Particle count	50
Maximum iterations	100
Weight of inertia	0.7
Factor of cognitive learning (c1)	1.5
Factor of social learning (c2)	1.5
Maximum speed	2
Elite fraction	0.7
Objectives functions	Sum-Rate and BER
Size of archive	20
Factor of exploration	0.2
Factor of exploitation	0.2

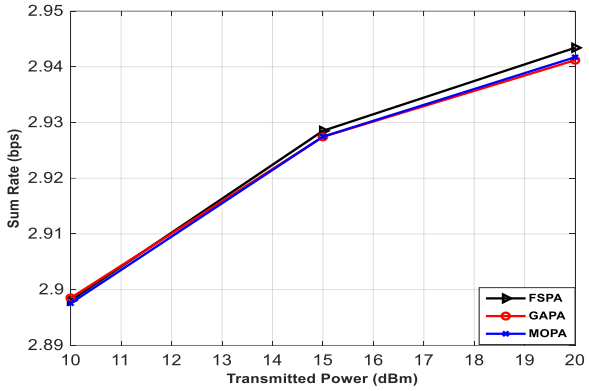


Fig. 2: Sum date rate results for the NOMA system of $K = 6$ users.

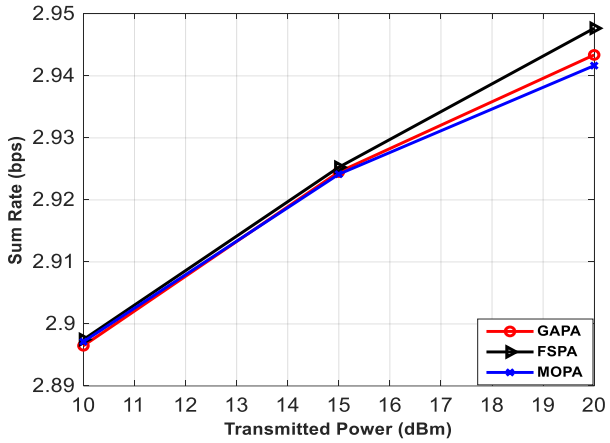


Fig. 3: Sum date rate results for the NOMA system of $K = 12$ users.

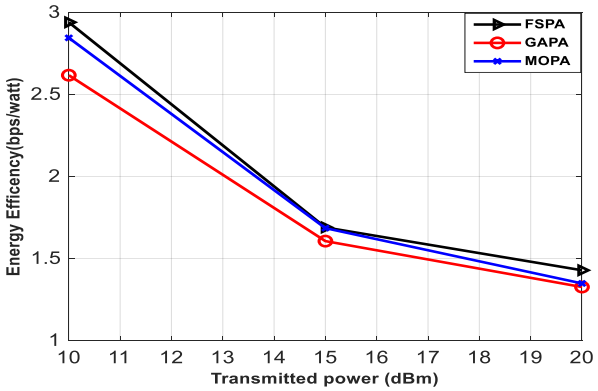


Fig. 4: Energy efficiency results for the NOMA system of $K = 6$ users.

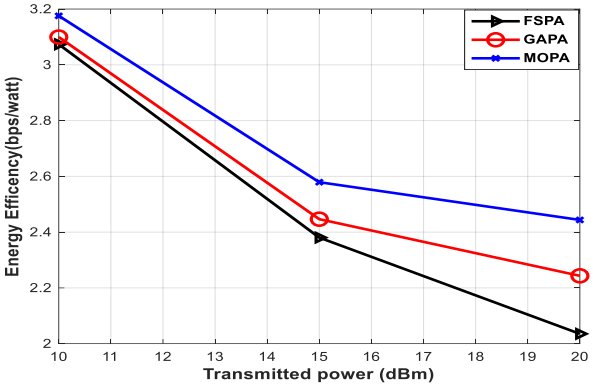


Fig. 5: Energy efficiency results for the NOMA system of $K = 6$ users.

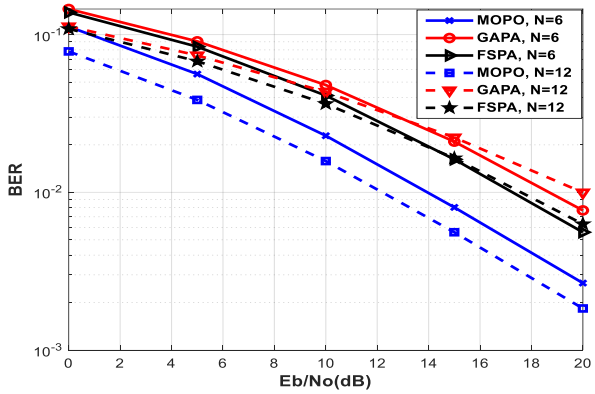


Fig. 6: BER results for the NOMA systems of $K = 6$ and $K = 12$ users.

4. Conclusion

In this paper, a novel MOPSO-based method is proposed for power allocation in downlink NOMA systems, effectively addressing the dual objectives of minimizing BER and maximizing the sum rate. The method identifies the optimal Pareto front for power allocation by categorizing users based on channel gain, enabling a balanced trade-off between these two key performance metrics. This study is particularly noteworthy as it simultaneously considers both BER and sum rate, diverging from conventional approaches that often prioritize one metric to the other. The proposed solution outperforms two benchmark methods, Fixed Power Allocation (FSPA) and Greedy Algorithm-based Power Allocation (GAPA), in terms of BER. Additionally, the comparative analysis demonstrates that the proposed method achieves performance comparable to these benchmarks in terms of spectral efficiency and sum rate.

Acknowledgment

This research was supported by University of Jiroft under the grant No 5812-02-03.

Credit Authorship Contribution Statement

Mohammad Hasheminejad: Conceptualization, Methodology, Software, Validation, Writing - review & editing. **Mohsen Sheikh-Hosseini**: Conceptualization, Methodology, Supervision, Validation, Writing - review & editing.

DECLARATION OF COMPETING INTEREST

The authors declare that they have no known competing financial interests or personal relationships that could have appeared to influence the work reported in this paper. The ethical issues; including plagiarism, informed consent, misconduct, data fabrication and/or falsification, double publication and/or submission, redundancy has been completely observed by the authors.

REFERENCES

[1] C.-X. Wang *et al.*, "On the Road to 6G: Visions, Requirements, Key Technologies, and Testbeds," *IEEE Commun. Surv. Tutorials*, vol. 25, no. 2, pp. 905–974, 2023.

[2] M. Sheikh-Hosseini, F. Rahdari, H. Ghasemnezhad, S. Ahmadi, and M. Uysal, "A comparative performance evaluation of OFDM, GFDM, and OTFS in impulsive noise channels," *IEEE Open J. Commun. Soc.*, pp. 1–1, 2024.

[3] M. Chafii, L. Bariah, S. Muhaidat, and M. Debbah, "Twelve scientific challenges for 6G: Rethinking the foundations of communications theory," *IEEE Commun. Surv. Tutorials*, vol. 25, no. 2, pp. 868–904, 2023.

[4] T. Yenealem and R. Getachew, "Selection and tuning propagation path loss model for Hawassa city, Ethiopia at 1800 MHz frequency," *J. Appl. Res. Electr. Eng.*, vol. 2, no. 2, pp. 127–135, 2023.

[5] M. Basiri Abarghouei and R. Saadat, "Full-Duplex device-to-device relays in a novel hybrid and adaptive joint relaying network: Symbol error analysis and optimum power allocation," *J. Appl. Res. Electr. Eng.*, vol. 2, no. 2, pp. 194–205, 2024.

[6] S. Kumar, A. S. Dixit, R. R. Malekar, H. D. Raut, and L. K. Shevada, "Fifth generation antennas: a comprehensive review of design and performance enhancement techniques," *IEEE Access*, vol. 8, pp. 163568–163593, 2020.

[7] B. Sadeghi, and S. M. S. Sadough, "IRS-Assisted visible light communication for improved monitoring of patient vital signals in hospital environment," *J. Appl. Res. Electr. Eng.*, vol. 3, no. 2, pp. 240–249, 2025.

[8] F. Rahdari, M. Sheikh-Hosseini, and M. Jamshidi, "Edge user performance improvement by intelligent reflecting surface-assisted NOMA system," *J. Electr. Comput. Eng. Innov.*, pp. 275–282, 2024.

[9] P. A. D. S. N. Wijesekara, "Network virtualization utilizing blockchain: A review," *J. Appl. Res. Electr. Eng.*, vol. 3, no. 2, pp. 136–158, 2024.

[10] T. O'Shea and J. Hoydis, "An introduction to deep learning for the physical layer," *IEEE Trans. Cogn. Commun. Netw.*, vol. 3, no. 4, pp. 563–575, Dec. 2017.

[11] R. Shafin, L. Liu, V. Chandrasekhar, H. Chen, J. Reed, and J. C. Zhang, "Artificial intelligence-enabled cellular networks: A critical path to beyond-5G and 6G," *IEEE Wirel. Commun.*, vol. 27, no. 2, pp. 212–217, Apr. 2020.

[12] C. Zhang, P. Patras, and H. Haddadi, "Deep learning in mobile and wireless networking: A survey," *IEEE Commun. Surv. Tutorials*, vol. 21, no. 3, pp. 2224–2287, 2019.

[13] M. Eisen, C. Zhang, L. F. O. Chamon, D. D. Lee, and A. Ribeiro, "Learning optimal resource allocations in wireless systems," *IEEE Trans. Signal Process.*, vol. 67, no. 10, pp. 2775–2790, May 2019.

[14] J. Kaur, M. A. Khan, M. Iftikhar, M. Imran, and Q. Emad Ul Haq, "Machine learning techniques for 5G and beyond," *IEEE Access*, vol. 9, pp. 23472–23488, 2021.

[15] L. Salaun, C. S. Chen, and M. Coupechoux, "Optimal Joint subcarrier and power allocation in NOMA is strongly NP-Hard," in *2018 IEEE International Conference on Communications (ICC)*, May 2018, pp. 1–7.

[16] G. Liang, Q. Zhu, J. Xin, Y. Feng, and T. Zhang, "Joint user-channel assignment and power allocation for non-orthogonal multiple access relaying networks," *IEEE Access*, vol. 7, pp. 30361–30372, 2019.

[17] V. Vishalakshi and G. Shivsharanappa Biradar, "A taxonomy on power optimization techniques for fifth-generation heterogenous non-orthogonal multiple access networks," *Int. J. Electr. Comput. Eng.*, vol. 14, no. 2, pp. 1616–1624, Apr. 2024.

[18] J. Cui, Z. Ding, and P. Fan, "Beamforming design for MISO non-orthogonal multiple access systems," *IET Commun.*, vol. 11, no. 5, pp. 720–725, Mar. 2017.

[19] L. Lei, D. Yuan, C. K. Ho, and S. Sun, "Joint optimization of power and channel allocation with non-orthogonal multiple access for 5G cellular systems," in *2015 IEEE Global Communications Conference (GLOBECOM)*, Dec. 2015, pp. 1–6.

[20] J. Zhu, J. Wang, Y. Huang, S. He, and X. You, "Multichannel resource allocation for downlink non-orthogonal multiple access systems," in *GLOBECOM 2017 - 2017 IEEE Global Communications Conference*, Dec. 2017, pp. 1–6.

[21] J. Zhu, J. Wang, Y. Huang, S. He, X. You, and L. Yang, "On optimal power allocation for downlink non-orthogonal multiple access systems," *IEEE J. Sel. Areas Commun.*, pp. 1–1, 2017.

[22] J. Zuo, Y. Liu, Z. Qin, and N. Al-Dhahir, "Resource Allocation in Intelligent Reflecting Surface Assisted NOMA Systems," *IEEE Trans. Commun.*, vol. 68, no. 11, pp. 7170–7183, Nov. 2020.

[23] Y. Liu, H. Xing, C. Pan, A. Nallanathan, M. Elkashlan, and L. Hanzo, "Multiple-Antenna-Assisted non-orthogonal multiple access," *IEEE Wirel. Commun.*, vol. 25, no. 2, pp. 17–23, Apr. 2018.

[24] T. Manglayev, R. C. Kizilirmak, and Y. H. Kho, "Optimum power allocation for non-orthogonal multiple access (NOMA)," in *2016 IEEE 10th International Conference on Application of Information and Communication Technologies (AICT)*, Oct. 2016, pp. 1–4.

[25] U. Sharma, P. Singh, and M. Awasthi, "Non-Orthogonal Multiple Access (NOMA) for 5G radio technology," in *Proceedings of Third Doctoral Symposium on Computational Intelligence*, 2023, pp. 523–532.

[26] H. Zuo and X. Tao, "Power allocation optimization for uplink non-orthogonal multiple access systems," in *2017 9th International Conference on Wireless Communications and Signal Processing (WCSP)*, Oct. 2017, pp. 1–5.

[27] W. Bao, H. Chen, Y. Li, and B. Vucetic, "Joint rate control and power allocation for non-orthogonal multiple access systems," *IEEE J. Sel. Areas Commun.*, vol. 35, no. 12, pp. 2798–2811, Dec. 2017.

[28] X. Wang, T. Xu, T. Zhou, and H. Hu, "Dynamic power allocation strategy for uplink non-orthogonal multiple access systems," *Comput. Commun.*, vol. 184, pp. 36–41, Feb. 2022.

[29] M. M. El-Sayed, A. S. Ibrahim, and M. M. Khairy, "Power allocation strategies for non-orthogonal multiple access," in *2016 International Conference on Selected Topics in Mobile & Wireless Networking (MoWNeT)*, Apr. 2016, pp. 1–6.

[30] W. F. Alghasmari and L. Nassef, "Optimal power allocation in downlink Non-Orthogonal Multiple Access (NOMA)," *Int. J. Adv. Comput. Sci. Appl.*, vol. 12, no. 2, 2021.

[31] R. Rai, H. Zhu, and J. Wang, "Coordinated scheduling and power control for Non-Orthogonal Multiple Access (NOMA) enabled H-CRAN," in *2020 IEEE 91st Vehicular Technology Conference (VTC2020-Spring)*, May 2020, pp. 1–5.

[32] W. F. Alghasmari and L. Nassef, "Power allocation evaluation for downlink Non-Orthogonal Multiple Access (NOMA)," *Int. J. Adv. Comput. Sci. Appl.*, vol. 11, no. 4, 2020.

[33] N. Alzubaidi and I. S. Hubri, "Non-Orthogonal Multiple Access (NOMA) dynamic power allocation in 5G networks," *Wasit J. Eng. Sci.*, vol. 10, no. 2, pp. 111–118, Jul. 2022.

[34] Ni. K. Prah II, E. Twumasi, and E. A. Frimpong, "Combined economic emission dispatch in a grid-connected microgrid using an improved mayfly algorithm," *J. Appl. Res. Electr. Eng.*, vol. 2, no. 2, pp. 112–119, 2023.

[35] E. Farahmand and A. Mahani, "A novel energy-efficient weighted multi-level clustering protocol," *J. Appl. Res. Electr. Eng.*, vol. 1, no. 1, pp. 69–78, 2022.

[36] Coello, Carlos A. Coello, Gregorio Toscano Pulido, and Maximino Salazar Lechuga, "Handling multiple objectives with particle swarm optimization," *IEEE Trans. Evol. Comput.,* vol. 8, no. 3, 256-279, 2004.

[37] F. Rahdari and M. Sheikh-Hosseini, "Nonlinear symbolic regression for bit error rate prediction of NOMA systems in 5G cellular communications," *Eng. Appl. Artif. Intell.*, vol. 127, Art. no. 107344, Jan. 2024.

BIOGRAPHY



Mohammad Hasheminejad is an accomplished Assistant Professor at the University of Jiroft in the Kerman province, Iran, specializing in Telecommunication Engineering. Having earned a PhD in 2016, from university of Birjand, in the field of Telecommunication Engineering, he has since been an active researcher with a keen interest in data science, artificial intelligence, and robotics. Proficient in MATLAB and Python programming, Dr. Mohammad Hasheminejad has made significant contributions to the field and has been recognized with three awards as one of the best researchers in 2023 at the University of Jiroft. With a strong publication record and a dedication to advancing the frontiers of technology.



Mohsen Sheikh-Hosseini received his B.S. degree in Electrical Engineering from Shahid Bahonar University of Kerman, Iran, in 2007. He completed his M.Sc. and Ph.D. in Telecommunications Engineering from Ferdowsi University of Mashhad, Iran, in 2009 and 2014, respectively. He is currently a faculty member at the Department of Computer and Information Technology, Graduate University of Advanced Technology, Kerman, Iran. His research interests include communications theory, focusing on designing emerging physical layer waveforms, performance analysis of impulsive noise channels, and the application of AI in telecommunications. He is also interested in both wireless and wireline telecommunications technologies, particularly cellular communications, power line communications (PLC), and smart grid communications.

Copyrights
© 2025 Licensee Shahid Chamran University of Ahvaz, Ahvaz, Iran. This article is an open-access article distributed under the terms and conditions of the Creative Commons Attribution –Non-Commercial 4.0 International (CC BY-NC 4.0) License (http://creativecommons.org/licenses/by-nc/4.0/).

Shahid Chamran University of Ahvaz

Iranian Association of Electrical and Electronics Engineers

Journal of Applied Research in Electrical Engineering

E-ISSN: 2783-2864
P-ISSN: 2717-414X
Homepage: https://jaree.scu.ac.ir/



Research Article

Constrained MIMO Reference-Based Offline Steady–State (RBOSS) NMPC for PMSM using Voltage Source Inverter

Stephen Ofori[1,*], Francis Boafo Effah[1], Daniel Opoku[1]

Department of Electrical and Electronic Engineering, Kwame Nkrumah University of Science and Technology, Kumasi, Ghana

**Corresponding Author: oforistephen1@outlook.com*

Abstract: This research introduces a constrained MIMO Reference-Based Offline Steady-State (RBOSS) Nonlinear Model Predictive Control (NMPC) approach for Permanent Magnet Synchronous Motors (PMSM) to address the overlooked aspect of starting conditions in current and speed multi-objective controllers. By employing an offline predictive optimization technique, the study aims to improve the starting condition for the optimization process, thus facilitating faster convergence. The RBOSS NMPC precomputes steady-state values of PMSM motors across a range of reference speeds, which are then used as starting conditions via a lookup table during online optimization. The approach significantly reduces computational burden by 30% compared to the usual successive linearization technique; it also enhances performance parameters such as rise time and settling time while optimizing current usage. This method demonstrates potential adaptability to other nonlinear systems, marking a significant advancement in NMPC controller optimization techniques and suggesting further exploration to expand its applicability.

Keywords: Permanent Magnet Synchronous Motors (PMSM), Nonlinear Model Predictive Control (NMPC), Reference Based Offline Steady-State (RBOSS), Optimization, Starting conditions, Computational burden.

Article history
Received 15 August 2024; Revised 16 May 2025; Accepted 02 October 2025; Published online 30 December 2025.
© 2025 Published by Shahid Chamran University of Ahvaz & Iranian Association of Electrical and Electronics Engineers (IAEEE)
How to cite this article
S. Ofori, F. B. Effah, and D. Opoku, "Constrained MIMO Reference-Based Offline Steady–State (RBOSS) NMPC for PMSM using voltage source inverter," *J. Appl. Res. Electr. Eng.*, vol. 4, no. 1, pp. 76-85, 2025.
DOI: https://doi.org/10.22055/jaree.2025.47745.1131

Check for updates

1. INTRODUCTION

Since its inception in the 1960s, permanent magnet synchronous motors (PMSM) have been adapted and used in several heavy industrial applications and the automobile industry [1]. The PMSM is an electrical motor which runs at synchronous speed with the rotating magnetic field produced by the applied (fixed frequency) AC source. Its voltages are regulated by a controller and Voltage Source Inverter (VSI) to achieve varying speed ranges. It has numerous beneficial applications in milling, electric vehicles (EVs), aerospace, etc. [2]. Control of PMSM was previously achieved using V/F control, Field Oriented Control (FOC), and recently, Fuzzy Logic, Model Predictive Control (MPC) [3]. FOC being the most commonly used control technique had numerous limitations, e.g., slow rise and settling times, which led to the development of Linear MPC. Linear MPC was developed to address the limitations of FOC but required a linear model of the dynamic equation representing the physical PMSM model. Though, it had numerous standardised theories which facilitated its results analysis, the linearised model of the actual nonlinear model used was an inaccurate representation of the real model for a single prediction step since the actual nonlinear model of the PMSM had numerous local solutions and required several iterations and starting points to produce the desired control value. This led to the development of NMPC. NMPC is the current state of the art in control algorithms, especially utilized in the chemical industry for its numerous benefits such as: its ability to handle uncertainties, disturbances, and effective control of nonlinear systems [4]. NMPCs are of three types. First, the traditional NMPC: this used the actual nonlinear model for every prediction step but had the limitation of result analysis difficulty. Second, the Successive Linearization NMPC: This was an improvement of the traditional NMPC but had limitations of computational burden. Finally, the Explicit NMPC which also had the limitation of computational complexity due to the use of large data size, is application specific and requires large data and large memory allocation [5-7]. Several techniques have been developed to individually combat these limitations. For instance, reference [8] developed a

constrained optimization implicit NMPC control technique to significantly improve the stability of the speed, but had a slow settling time. Reference [9] proposed a nonlinear MPC strategy based on input-output feedback linearization (IOFL) to drive the state or manipulated variable to a steady-state and prevent further overshoot of the state and control variables when at a steady–state. With the intent to reduce computational burden and achieve efficiency, this technique exhibited an unstable quadrature voltage and was inefficient in dealing with transient behaviors. Reference [10] employed an Explicit MPC of PMSMs based on multi-point linearization to also combat computational burden, but used a few operational points for the linearization which had a significant impact on the stability of operating points far from the used operating points. Other literatures such as [11], also used the concept of double MPC online. These reviewed documents suggest that the problem of computational burden still exists and current utilization has a close relationship with stability, therefore, the desired controllable parameters such as speed or torque, are required to be controlled in parallel with the current using a multi–objective optimization [12] and also, use a closer grid of operating points to pre-compute the starting conditions required to converge to the solution faster [13].

This paper aimed to develop a multi-objective Constrained multi-input multi-output (MIMO) Reference Based Offline Steady-State (RBOSS) NMPC for Permanent Magnet Synchronous Motors (PMSMs) using a Voltage Source Inverter (VSI); to improve speed tracking performance of the successive linearization technique and ensure utilization and stability in real-time while reducing the online computational burden. The strategy adapted to achieve the results of this research work was first to develop an offline algorithm to efficiently pre-compute the steady–state values of ranges of speed setpoints. This is used to determine: 1. the speed setpoint constraint and 2. Initial condition of the online optimization of the current and speed parameters. Secondly, I proceeded to use the offline steady-state values for the linearization of a PMSM model in an online NMPC optimizer, which uses a multi-objective moving horizon cost function to predict future state and control values. This offline computed steady-state values used in the online optimization of a MIMO PMSM nonlinear system of equations as a look-up table to determine future states accurately is the novel approach employed to ensure stable and faster control at various speed ranges.

The rest of this paper is organized in this manner: Section 2 provides a brief overview and theoretical concept of the domain of study of NMPC as employed in PMSM control. Section 3 introduces the proposed strategy which seeks to reduce computational burden online while ensuring stability in the controllable parameters. Section 4 is devoted to simulation works using MATLAB/Simulink based on the principles outlined in Section 3; accessing the results to validate the efficacy of the proposed strategy. Section 5 finalized the article with a summary of key findings, observations and future trends of study.

2. CONCEPT OF NMPC IN PMSM

In PMSM's, the interaction between two magnetic fields first generated by a permanent magnet and secondly, the stator, when a rated AC source is applied, results in a torque that causes the rotor to turn synchronously with the stator's rotating field. The two main types are the Surface Mount and Interior PMSM. In the Surface Mount, the permanent magnets are mounted on the surface of the rotor to provide a uniform air gap; it has a simple structure. In the Interior PMSM, the permanent magnets are embedded within the rotor, providing better protection against demagnetization and allowing for more efficient operation at higher speeds. It offers several advantages such as: high efficiency, better power density, quiet operation and less maintenance [14]. The governing equations of the PMSM are as follows:

$$\frac{dI_d}{dt} = \frac{V_d}{L_d} - \frac{I_d R}{L_d} + \frac{I_q L_q \omega_e}{L_d} \quad (1)$$

$$\frac{dI_q}{dt} = \frac{V_q}{L_q} - \frac{I_q R}{L_q} - \frac{\lambda_m \omega_e}{L_q} - \frac{I_d L_d \omega_e}{L_q} \quad (2)$$

$$\frac{d\omega_e}{dt} = \frac{pp}{2J}\left(T_e - T_l - \frac{2B\omega_e}{pp}\right) \quad (3)$$

$$T_e = \left(\frac{3}{2}\right) \cdot pp \cdot \left(\lambda_m I_q + \left(L_d - L_q\right) I_d I_q\right) \quad (4)$$

The major drawback of this motor is its dependence on the source voltage and frequency for its running speed. Since AC sources are of a constant frequency of 50/60 Hz at 120, 220 or 415V in a single / three phase system respectively, a controller is required to alter certain motor parameters such as voltage or frequency to attain the desired stability or controllable parameters such as speed, torque or current setpoint. The general block diagram of using NMPC in PMSM control is illustrated in Fig. 1. In this figure $V_d, V_q, I_d, I_q, L_d, L_q, R, \omega_e, \lambda_m, pp, T_l, T_e, J$ are the d – and q – axis stator voltages, current, inductance, flux linkages, stator resistance, electrical velocity, max. magnetic flux linkage, pair poles, electrical angle, load torque, electromagnetic torque and inertia [15]. In a tracking application such as the speed tracking shown in Fig. 1, the process begins with the use of a PI controller to generate a reference quadrature current, I_q proportional to the reference controllable parameter, i.e., speed, while the direct current I_d is set to zero reference for surface mount PMSM. This serves the purpose of d – q reference frame alignment for start – up. For torque control purpose, it is generated using another suitable controller from the flux linkage [16].

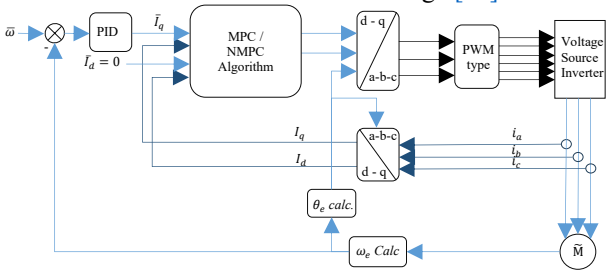


Fig. 1: General block diagram of using NMPC in PMSM control.

The NMPC is a closed loop control strategy that uses a cost function subject to the dynamic model to determine the error and cost within a prediction horizon, N_p, between a sensed three – phase converted d – q current from the motor (using the park transform) and the generated reference d – q current to compute for a new optimised control value. This control value is converted from d – q to three phase using the inverse park transform which is later used to generate a three – phase PWM signal for a three – phase inverter. The inverter uses the PWM signal to control the voltage and frequency of the PMSM according to the error signal generated by the NMPC to reach the desired setpoint [17].

3. PROPOSED RBOSS NMPC METHOD

The general control scheme of the proposed RBOSS NMPC is illustrated in Fig. 2. In this scheme, three major steps are followed.

a. PMSM Modelling, linearization and discretization.

b. Reference-based offline steady-state computation:

   i. Develop an algorithm based on the successive linearization NMPC using the L1-norm cost function.

   ii. Use the developed offline algorithm to compute the steady-state values of a carefully selected grid of speeds.

c. Online NMPC: Develop an online NMPC algorithm based on successive linearization technique using the MHE cost function following the steps below:

   i. Use the recently measured parameter to linearize the PMSM nonlinear model.

   ii. Substitute the recently measured parameter, x_k into the discrete linear model to obtain the next state.

   iii. Substitute the current state, x_k reference state, r_k, and predicted state, $\hat{x}_{k+1|k}$ into the MHE cost function.

   iv. Use the computed offline steady-state values as starting condition to solve the problem online using SQP optimizer. This penalizes the cost across a prediction horizon based on the assigned weight.

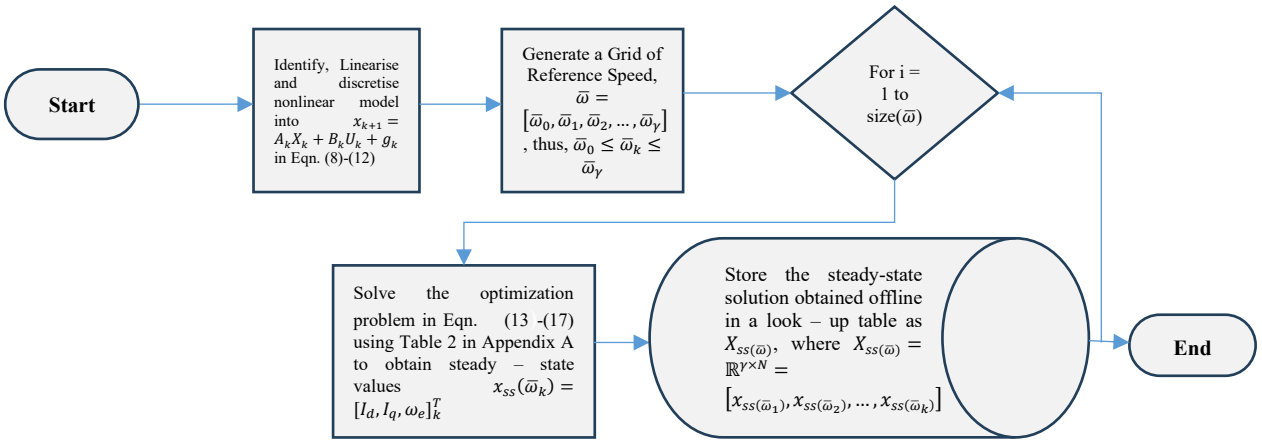


Fig. 2: A flow chart for Computation of Offline Steady – State Values for PMSM.

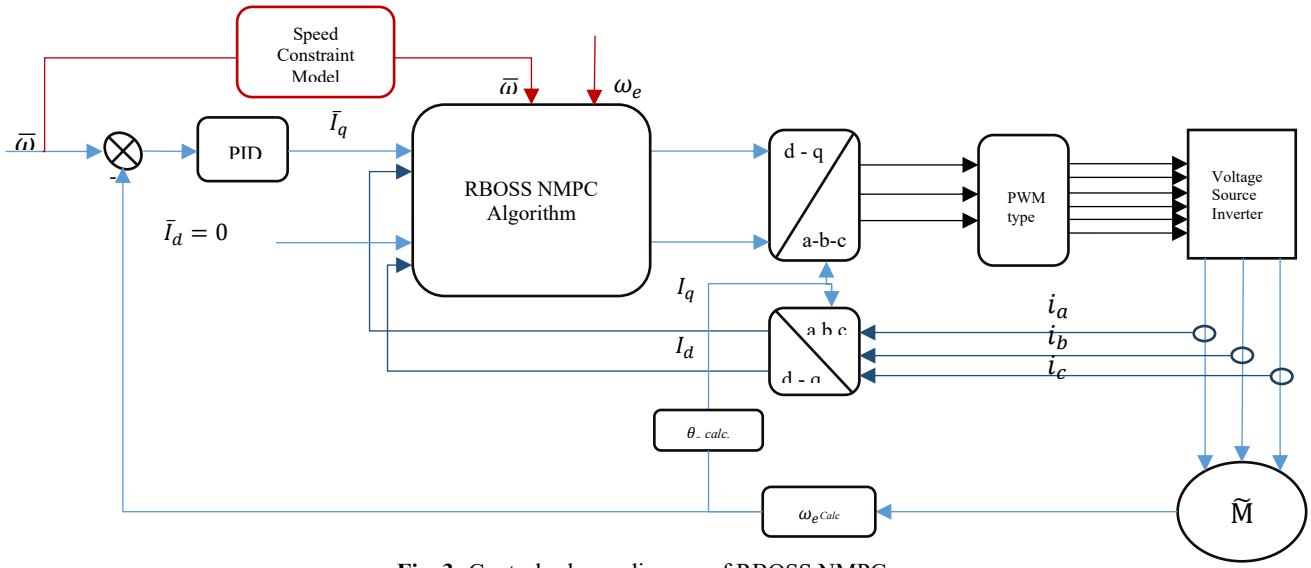


Fig. 3: Control scheme diagram of RBOSS NMPC.

3.1. PMSM Modelling, Linearisation, and Discretization

Equations (1) - (4) are put in the following form by substitutions:

$$\frac{dI_d}{dt} = \frac{V_d}{L_d} - \frac{I_d R}{L_d} + \frac{I_q L_q \omega_e}{L_d} \tag{5}$$

$$\frac{dI_q}{dt} = \frac{V_q}{L_q} - \frac{I_q R}{L_q} - \frac{\lambda_m \omega_e}{L_q} - \frac{I_d L_d \omega_e}{L_q} \tag{6}$$

$$\frac{d\omega_e}{dt} = \frac{3 I_q \lambda_m pp^2}{2J} - \frac{T_l pp}{J} - \frac{B \omega_e}{J} \tag{7}$$

The system above is linearised and discretised using the Forward Euler method in order to put the system in state-space form, $F = A_k X_k + B_k U_k + g_k$ where:

$$A_k = \begin{bmatrix} 1 - \frac{R_s \cdot \Delta T}{L_d} & \frac{L_q \cdot \Delta T \cdot \omega_e}{L_d} & \frac{I_q \cdot L_q \cdot \Delta T}{L_d} \\ -\frac{L_d \cdot \Delta T \cdot \omega_e}{L_q} & 1 - \frac{R_s \cdot \Delta T}{L_q} & -\Delta T \cdot \left(\frac{\lambda_m}{L_q} + \frac{I_d \cdot L_d}{L_q}\right) \\ 0 & \frac{3 \cdot \Delta T \cdot \lambda_m \cdot pp^2}{2 \cdot J} & 1 - \frac{B \cdot \Delta T}{J} \end{bmatrix} \tag{8}$$

$$X_k = \begin{bmatrix} I_d \\ I_q \\ \omega_e \end{bmatrix} \tag{9}$$

$$B_k = \begin{bmatrix} \frac{\Delta T}{L_d} & 0 \\ 0 & \frac{\Delta T}{L_q} \\ 0 & 0 \end{bmatrix} \tag{10}$$

$$U_k = \begin{bmatrix} V_d \\ V_q \end{bmatrix} \tag{11}$$

$$g_k = \begin{bmatrix} -\frac{(I_q \cdot L_q \cdot w_e)}{L_d} \\ \frac{I_d \cdot L_d \cdot w_e}{L_q} \\ -\frac{T_l \cdot pp}{J} \end{bmatrix} \tag{12}$$

$A_k = \mathbb{R}^{n \times n}$ is the state matrix, $X_k = \mathbb{R}^n$ is a vector of state variables, $B_k = \mathbb{R}^{n \times m}$ is the control matrix, $U_k = \mathbb{R}^m$, $g_k = \mathbb{R}^{n \times r}$ is the inherent disturbance of the PMSM dynamic model, and k, is the current discrete time step. In the discretized model above, the disturbance is additive and has r = 1.

3.2. Reference Based Offline Steady - State Computation

The offline steady-state values are computed using a grid of reference speeds, $\bar{\omega}$ separated by an interval decided by the controller's designer as in (15) and stored for later use in an online NMPC algorithm. It is obtained by solving an offline optimization problem in (13) subject to (14)-(17) to obtain the I_q mapped to each speed setpoint in the grid of speeds. $I_d = 0$, for all speed ranges as shown in (16);

$$\min_{\substack{x_0, x_1, \ldots x_P \\ u_0, u_1, \ldots u_{M-1}}} J_{\bar{\omega}_k}(X_{\bar{\omega}_k}, U_{\bar{\omega}_k}) = \sum_{i=1}^{P} \left\| X_{\bar{\omega}_{k+i}} \right\|_Q^2 + \sum_{i=0}^{M-1} \left\| U_{\bar{\omega}_{k+i}} \right\|_R^2 \tag{13}$$

Subject to

$$x_{\bar{\omega}_{k+1}} = f\left(x_{\bar{\omega}_k}, u_{\bar{\omega}_k}, \mu\right) \tag{14}$$

where

$$\bar{\omega}_k \in \bar{\omega} \tag{15}$$

$$I_d = 0, \ \forall \bar{\omega} \tag{16}$$

$$-V_{dc} \leq U_{\bar{\omega}_{k+i}} \leq V_{dc} \tag{17}$$

where:

$X_{\bar{\omega}_k} \in \mathbb{R}^n$ is the measured state at the current reference speed,

$U_{\bar{\omega}_k} \in \mathbb{R}^m$ is the control value at the current reference speed,

$Q = diag(n) > 0$, is a positive definite diagonal matrix of dimension n,

$R = diag(p) \geq 0$ is a semi-positive definite diagonal matrix of dimension m, and

$\bar{\omega} = \mathbb{R}^{\gamma} = \{\bar{\omega}_0, \bar{\omega}_1, \bar{\omega}_2, \ldots, \bar{\omega}_{\gamma}\}$ is a vector of reference speeds.

All steady-state I_q values computed must be within a chosen control voltage range of $-V_{dc}$ to V_{dc} as in (17). The offline steady-state computation and optimization process are performed using the steps simplified in Fig. 3.

3.3. Online NMPC

During the online computation, the pre-computed steady-state values are used as a starting condition for an online NMPC optimisation problem across a prediction and control horizon, N_p and N_c .The algorithm is simplified in Fig. 4. The optimisation problem to be solved online is formulated as follows in (18) - (21).

$$\min_{\substack{x_0, x_1, \ldots x_P \\ u_0, u_1, \ldots u_{M-1}}} J_k(r_k, \hat{X}_k, U_{k-1}, U_k) = \sum_{i=1}^{P} \left\| \hat{e}_{k+i|k} \right\|_Q^2 + \sum_{i=0}^{M-1} \left\| \Delta X_{k+i|k} \right\|_{Q_{ex}}^2 + \sum_{i=0}^{M-1} \left\| \Delta U_{k+i|k} \right\|_R^2 \tag{18}$$

Subject to:

$$x_{k+i|k} = f(x_k, u_k, x_{ss(\bar{\omega}_k)}) \tag{19}$$

$$-V_{dc} \leq U_{k+i|k} \leq V_{dc} \tag{20}$$

$$x_0 = x_k \tag{21}$$

where:

$\hat{e}_{k+i|k} = \hat{X}_{k+i|k}^T - r_{k+i|k}^T = \left[\hat{I}_d, \hat{I}_q, \hat{\omega}\right]_{k+i|k}^T - \left[\bar{I}_d, \bar{I}_q, \bar{\omega}\right]_{k+i|k}^T$ is the tracking error between the optimal predicted states, $\hat{X}$ and the reference state, r.

$\Delta X_{k+i|k} = \hat{X}_{k+i|k}^T - X_{k+i|k}^T = \left[\hat{I}_d, \hat{I}_q, \hat{\omega}\right]_{k+i|k}^T - \left[I_d, I_q, \omega\right]_{k+i|k}^T$ is the prediction error between current prediction, $\hat{X}$ and previous state measurement, X.

$\Delta U_{k+i|k} = \left[V_d, V_q\right]_{k|k}^T - \left[V_d, V_q\right]_{k-1|k}^T$ is the control effort and Q_{ex} is the weight for the prediction error.

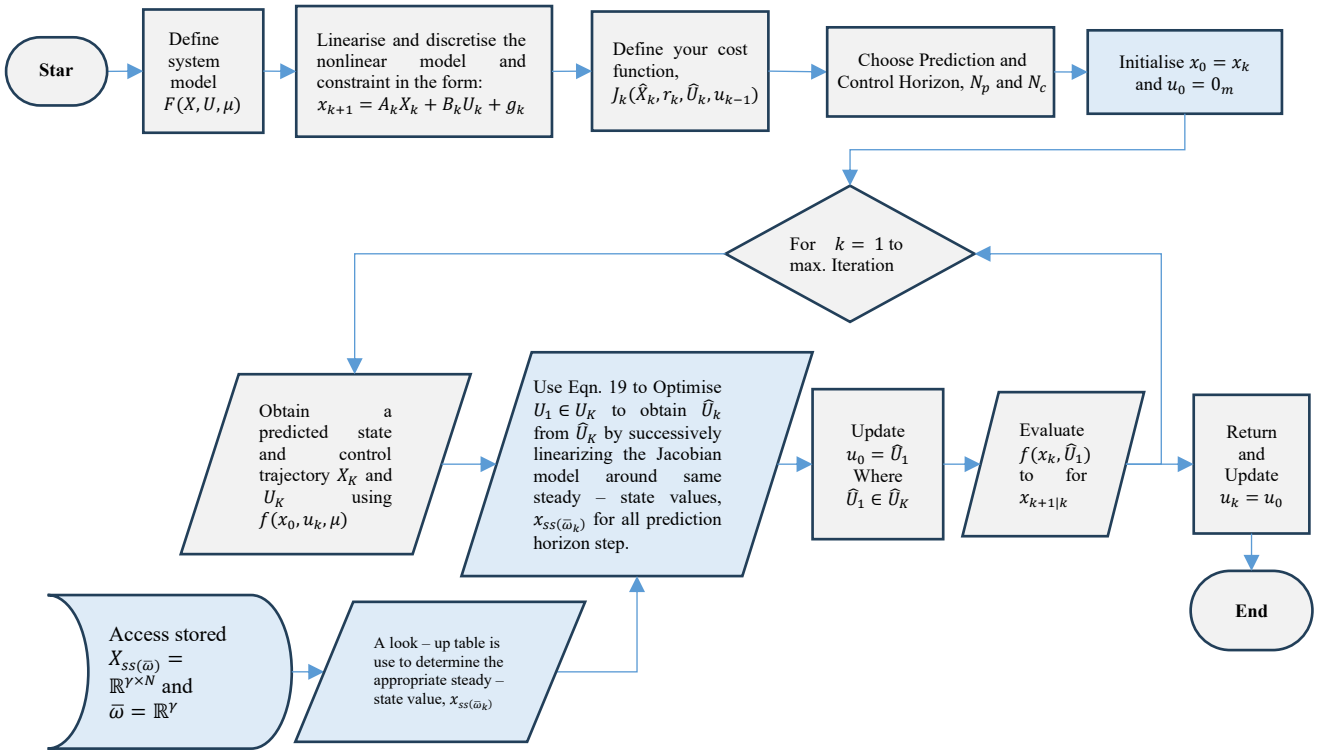


Fig. 4: A Flowchart for online NMPC optimization for PMSM.

4. Simulations and Results Analysis

All simulations were performed under fixed simulation sample time step $\Delta T = 2.5e-06$ in MATLAB/SIMULINK for 1 s for each speed setpoint from zero to high-speed of 2000 rpm while maintaining other data at the default settings.

For benchmarking purposes, the Successive Linearization NMPC technique was used to compare the proposed RBOSS NMPC model's performance.

4.1. Simulations

The model parameters in Table 1 were used for the simulation of the two controller types. Table 2, Table 3 and Table 4 are the tuning parameters for the offline optimization, the online NMPC, and the PI controller used, respectively.

4.2. Results and Analysis

In this section, results are presented for the performance of all the controllers at transient periods at high, medium and low speeds. Finally, a result of the simulation profile to compare RBOSS and successive linearization NMPC is given and compared.

4.2.1. Speed characteristics at transient

Fig. 5 shows the speed comparison between the different controllers at both high and low speeds during transient periods.

The key controller for benchmarking the performance of RBOSS is the successive linearization NMPC. Fig. 5a shows that the RBOSS has a faster rise time and better characteristics at low speeds. A general summary of results

Table 1: PMSM model parameters.

Parameter	Value(s)
Stator Resistance, R_s	0.0485 Ω
Sampling Period, ΔT	5×10-6 s
D - q inductances, $L_d = L_q$	3.95 mH
Rotor flux linkage, λ_m	0.1194 Wb
Pair Poles, PP	4
Rotor Inertia, J	0.0027 Kg·m2
Damping Factor, B	0.00115 Nm·s·rad-1
Load Torque, T_l	1 Nm

Table 2: Tuning parameters of offline optimisation.

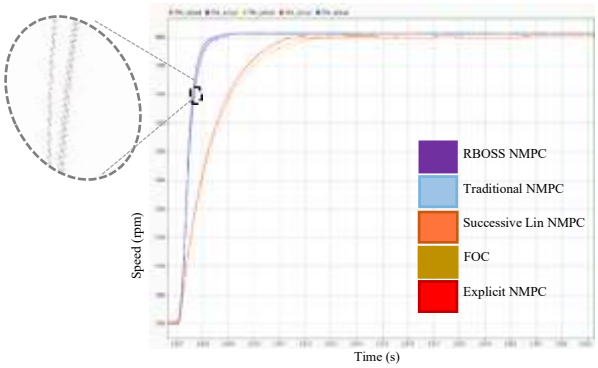
Parameter	Value(s)
Grid of reference speed' state, $\bar{\omega}$	{0, 1, 2, …, 2000} rpm
DC voltage, Vdc	230V
Prediction Horizon, P	4
Control Horizon, M	3
Weight of State, Q	diag (1000, 5, 1000)
Weight of Control input, R	diag (0.1, 0.1)
Solver type used	Sequential Quadratic Programming

Table 3: Tuning parameters of online NMPC.

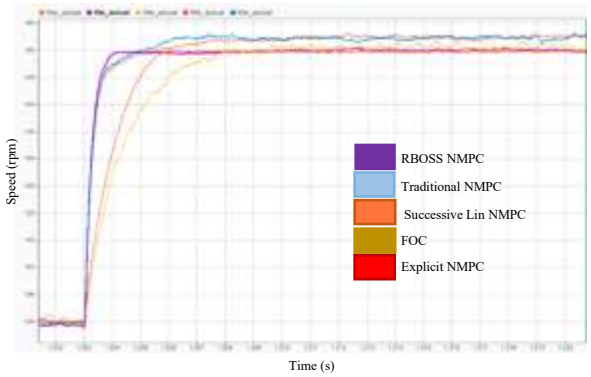
Parameters	Values
Prediction Horizon, Np	4
Control Horizon, Nc	3
Weight of Tracking Error, Q	diag ([3.20, 3.20, 50])
Weight of Prediction Error, Q_{ex}	diag ([1, 1, 1])
Weight of Control Input, R	diag ([0.05, 0.005])

Table 4: Tuning parameters of PI *c*ontroller.

	Outer (speed)	Inner (I_d)	Inner (I_q)
P	0.0514	5.1398	5.1398
I	0.554	5086.399	5086.399



(a)



(b)

Fig. 5: Transient period comparison of all controllers at (a) high speeds and (b) low speeds.

or performance metrics comparison of all the controllers by signal statics and bilevel measurement has been presented in the Appendix. It gives a summary of the comparison between FOC, Implicit NMPC, RBOSS NMPC and Explicit NMPC using its bilevel measurement and signal characteristics.

It is seen that the RBOSS achieved significant improvement in some metrics over the Successive Linearization technique. The percentage of improvement is shown in Table 5. In regards to Fig. 5a, RBOSS at low speeds exhibit better characteristics due to the provision of a good and optimized initial condition, thus, owing to the use of optimized pre-computed offline steady-state values, further impacting other performance metrics. The explicit variant, Explicit NMPC, derived from the reference based offline steady-state NMPC achieved a better rise time and no steady-state error compared to the field-oriented controller.

The statics show that some metrics such as overshot and Torque ripple T_e, remained constant, while reference I_q current generated by the PI controller and the sensed motor I_q currents increased. This is a required character to ensure a faster rise and settling times. Furthermore, it is clear from

Table 5: Percentage of change between Successive Linearisation and RBOSS

step response is a speed @ 1500 to 2000 rpm	**Percentage of Change (%)**
Rise Time	-0.019
Settling Time	-0.04
Overshoot	0
Steady – state error	-0.82
Peak to Peak Iq Current	+7.12
Peak to Peak Iq ref Current	+59.3
Peak to Peak Id current	-19.2
Peak to Peak, Te ripple	-67.36

the metrics of all the controllers in Table 5 that, generally, a reduced current utilization by I_q leads to an increased reference I_q and motor I_q currents. This behavior is largely seen in the RBOSS NMPC as a (19%) reduced I_d current leading to an increase in the reference I_q and motor I_q by approximately 7% and 59% respectively but largely depends on the tuning weight of the controllers.

4.2.2. Speed characteristics at steady–state

Figs. 6a and 6b show a graph of high- and low–speed performance at settled (steady-state) periods. The performance validation metrics of these graphs are included in as visual inspection makes it difficult to interpret. In addition to the metrics, it is observed that the RBOSS exhibit a strong robustness of the controlled variables, I_d, I_q, and ω_e. As shown in Fig. 7, at very low speeds for a step change from zero to 50 rpm the trackability of RBOSS is better than all the controllers.

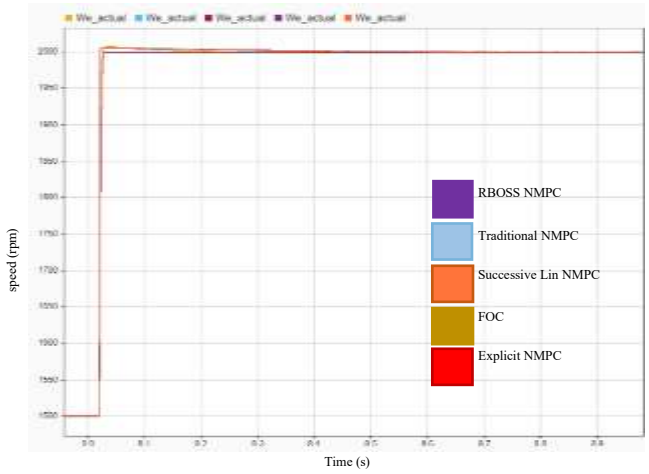
4.2.3. Current characteristics for speed ranges from 0 to 2000 rpm

In reference to the motor I_q current in Fig. 8, every speed range exhibited unique current behavior. It is seen that at very low speeds all I_q shows a poor irregular (nonlinear performance); while it is more evident in the Traditional NMPC, RBOSS performs better at low speeds from 0 – 150 rpm in Fig. 8 than the Successive Linearization technique.

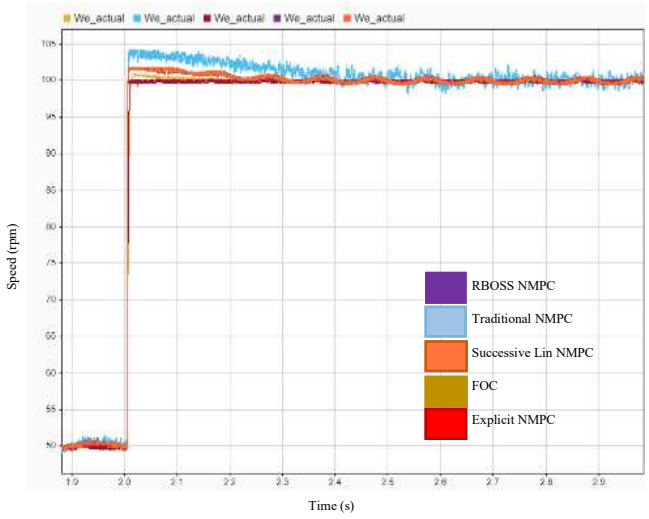
It is further observed that the current reduces as the speed approaches the reference speed in the low to mid–speed range; which is not the same for the maximum or high-speed range. The current used in high-speed range seems fairly constant. Sharp spikes in between speed changes in the current graph are a result of the trade-off in fast rise time and control effort. Generally, more weight on the control effort prioritizes archiving reduced current spikes at the expense of speed rise time.

4.2.4. Simulation time and Simulink profiling

A Simulink profile was performed on the two controllers namely Successive Linearization and the RBOSS NMPC techniques to check the computational burden of the various controllers (see Figs. 9 and 10). A comparison between the two figures from the Simulink profiler to check the computational burden shows that a good starting or initial condition helped reduce the computational time by a percentage of 30 (30%) for a 0.5 seconds simulation and 8%



(a)



(b)

Fig. 6: Steady-state period comparison of all controllers at (a) high speeds and (b) low speeds.

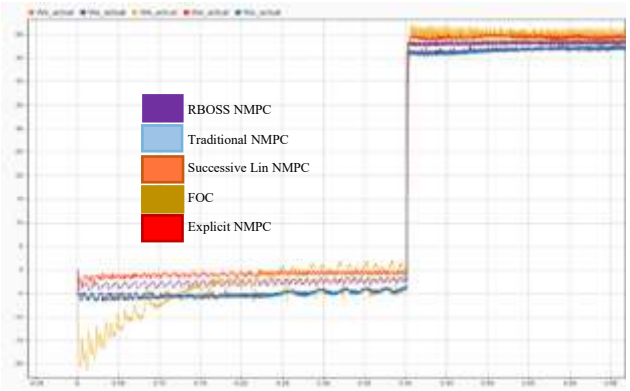


Fig. 7: Steady-state period comparison of all controllers at very low speeds.

for 0.1 seconds simulation. Table 6 and Table 7 show the comparison between profiling of simulation for 0.01s and 0.05s transient times, respectively.

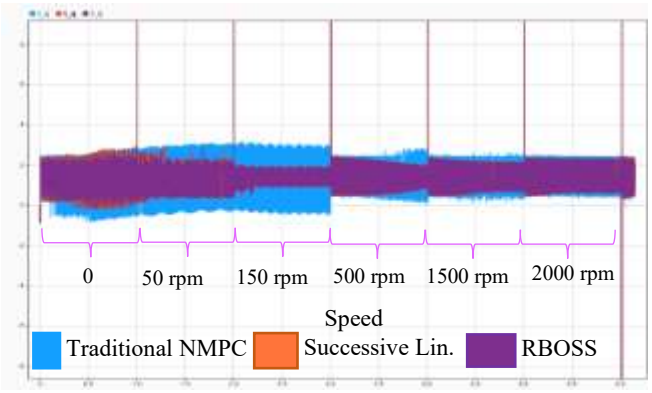


Fig. 8: Graph of I_q current for Traditional, Successive Lin., and RBOSS NMPC at various speeds.

4.2.5. General observations

The following are a few and the most necessary observations of the work

1. Sample Time: A lesser sample time made the controller greatly responsive to slight nonlinearities and small step change in reference.
2. The Type of Discretization: The Forward Euler Method was used due to its fast computation, but was less accurate compared to Tustin Forward and Tustin Backward discretization methods.
3. A long prediction horizon caused high computational complexity and was unsuitable for a fast-changing nonlinear dynamic systems such as PMSM. Hence, a prediction and control horizon of 4 and 3 were used respectively.
4. Since the PMSM dynamic equation was known, an offline symbolic Jacobian was obtained and used as the online model. This facilitated a fast runtime unlike obtaining the Jacobian online symbolically during runtime.
5. Due to the use of zeros as the initial control input value for the offline computations of the RBOSS steady–state, the use of previous control input to better the online computations during runtime lead to an increase in computational complexity due to high number of iterations. It is required that, the initial control input must correlate with that used in the offline computations.
6. The RBOSS approach required that the steady-state of all future references be precomputed offline using the nonlinear equation and an appropriate cost function. This adds extra labour hours in the design of the controller; but eliminates the need for extra online speed–torque MPC optimisation as done in the cascaded MPC schemes.
7. The tuning of the various NMPC controllers was time-consuming using the try-and-error method. Also, the obtained weight values were suitable for a specific reference point. The reference point chosen was suitable for the maximum speed to be controlled by the controller; this leads to a low computational efficiency for low speeds.

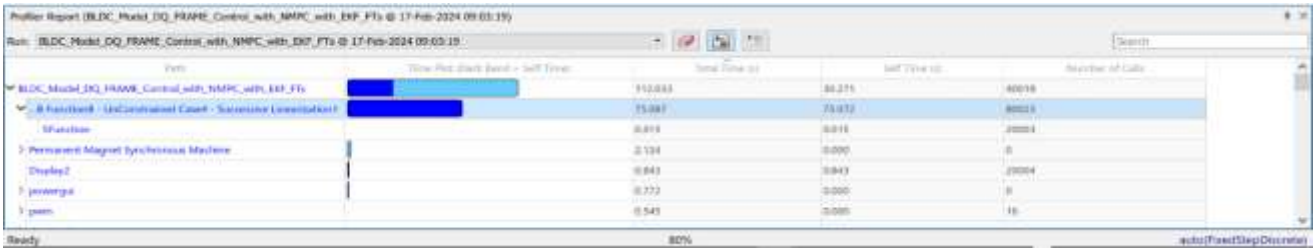


Fig. 9: Successive Linearization Simulink profile for 0.01s of simulation.

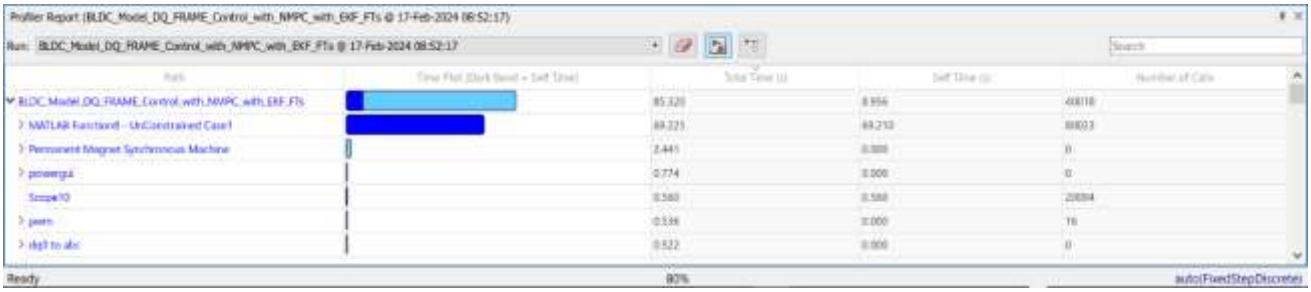


Fig. 10: RBOSS Simulink profile for 0.01s of simulation.

Table 6: Profile of 0.01s of simulation for computational burden/time check (in transient periods)

	Successive Lin.	RBOSS NMPC
Self – Time (s)	75.072	69.21
Total Time Taken	112.033	85.320
Number of Function Calls	80023	80023
Percentage of Change	8 %	

Table 7: Profile of 0.05s of simulation for computational burden/time check (in transient periods)

	Successive Lin.	RBOSS NMPC
Self-Time (s)	100.324	70.591
Total Time Taken	115.649	82.324
Number of Function Calls	80010	80010
Percentage of Change	29.6 %	

1. Conclusion

In conclusion, a MIMO reference-based offline steady-state NMPC, RBOSS NMPC has been proposed to tackle the issues of computational burden. The result has proven to be better in reducing computational burden by 8 - 29%, has a fairly better rise time (0.019%), better trackability/less steady–state error (0.82%), reduced torque ripples (by 67%) and a reduced magnitude of I_d current while maintaining other characteristics constant. Furthermore, it has been proven that a multi-objective NMPC optimization technique with a receding Horizon Cost function helps eliminate the cascaded MPC scheme which adds extra tuning burden. The explicit variant of the RBOSS NMPC resulted in better tracking and a fairly similar settling time to RBOSS but a slow rise time and a few spikes due to the small size of data used to replicate the output of RBOSS NMPC and the lack of better data pre-processing. Using higher data size was limited by computational power constraints. Also, it was required that offline steady-state values be computed and stored in a look-up table for referencing mapped to the reference speed of the current time step. It uses the same reference offline steady–state value as the initial optimization condition for all prediction steps, unlike the successive linearization technique which uses the current estimate of the speed at every prediction step making it computationally expensive for implicit NMPCs as the current estimate of the current state and control values may be far from the most optimal local solution.

Credit Authorship Contribution Statement

Stephen Ofori: Conceptualization, Data curation, Formal analysis, Investigation, Methodology, Resources, Software. **Francis Boafo Effah:** Formal analysis, Investigation, Methodology, Project administration, Supervision, Validation, Writing - original draft, Writing - review & editing. **Daniel Opoku:** Formal analysis, Investigation, Methodology, Supervision, Validation, Writing - original draft, Writing - review & editing.

Declaration Of Competing Interest

The authors declare that they have no known competing financial interests or personal relationships that could have appeared to influence the work reported in this paper. The ethical issues; including plagiarism, informed consent, misconduct, data fabrication and/or falsification, double publication and/or submission, redundancy has been completely observed by the authors.

References

[1] F. Blaschke, “The principle of field orientation as applied to the new transvector closed-loop control system for rotating field machines,” *Adjust. Speed AC Drive Syst.*, pp. 217–220, 1972.

[2] J. Gao, J. Zhang, M. Fan, Z. Peng, Q. Chen, and H. Zhang, “Model predictive control of permanent magnet synchronous motor based on state transition constraint method,” *Math. Probl. Eng.*, vol. 2021, Art. no. 3171417, 2021.

[3] F. Amiri and M. Hassan Moradi, “Designing of the controller for shipboard microgrid based on linear

matrix inequality," *J. Appl. Res. Electr. Eng.*, vol. 1, no. 2, pp. 175–185, Jul. 2022.

[4] M. Tofighi-Milani, S. Fattaheian-Dehkordi, and M. Fotuhi-Firuzabad, "A new peer-to-peer energy trading model in an isolated multi-agent microgrid," *J. Appl. Res. Electr. Eng.*, vol. 1, no. 1, pp. 33–41, Jan. 2022.

[5] G. Cimini, V. Fossi, G. Ippoliti, S. Mencarelli, G. Orlando, and M. Pirro, "Model predictive control solution for permanent magnet synchronous motors," in *Proc. Industrial Electron. Conf.*, pp. 5824–5829, 2013.

[6] C. R. Gade and W. Razia Sultana, "Control of permanent magnet synchronous motor using MPC–MTPA control for deployment in electric tractor," *Sustain.*, vol. 14, no. 19, 2022.

[7] W. S. Levine, *Handbook of model predictive control,* Springer Nature Link.

[8] X. Jiang, M. Xie, A. Ji, Y. Yang, M. Fan, and R. Chen, "Implicit model predictive control with continuous control set of PMSM drive systems," in *2020 IEEE 9th Int. Power Electron. Motion Control Conf.*, pp. 185–190, 2020.

[9] X. Kong and X. Liu, "Efficient nonlinear MPC on permanent magnet synchronous motor," in *29th Chinese Control Decis. Conf.*, pp. 4644–4647, 2017.

[10] Q. Guo, T. Pan, J. Liu, and S. Chen, "Explicit model predictive control of permanent magnet synchronous motors based on multi-point linearization," *Trans. Inst. Meas. Control*, vol. 43, no. 12, pp. 2872–2881, 2021.

[11] X. Huang, H. Pan, and K. Yuan, "Speed and current control of PMSM based on double MPC," in *Proc. 2020 7th Int. Forum Electr. Eng. Autom.*, pp. 300–304, 2020.

[12] R. Krishnan, *Permanent magnet synchronous and brushless DC motor drives*, 1st ed. Blacksburg, Virginia, USA: CRC Press LLC, 2010.

[13] F. Nikfar and D. Konstantinidis, "Solving dynamical systems with path-dependent nonlinearities using MATLAB ODE solvers," in *NCEE 2014 - 10th U.S. National Conference on Earthquake Engineering: Frontiers of Earthquake Engineering*, 2014.

[14] M. Găiceanu, "Advanced control of the permanent magnet synchronous motor," *Electr. Mach. Smart Grids Appl. - Des. Simul. Control*, 2018.

[15] M. Schwenzer, M. Ay, T. Bergs, and D. Abel, "Review on model predictive control: an engineering perspective," *Int. J. Adv. Manuf. Technol.*, vol. 117, no. 5–6, pp. 1327–1349, 2021.

[16] L. Grüne and J. Pannek, *Nonlinear model predictive control: theory and algorithm,* Springer-Verlag London Limited, 2011.

[17] T. Mrovec, P. Simonik, O. Wolf, and M. Koreny, "Control algorithms and application software of electric drive for remotely controlled vehicle," pp. 1–5, 2019.

BIOGRAPHY



Stephen Ofori received the BSc. Electrical and Electronic Engineering degree at University of Mines and Technology, Tarkwa in 2019, the MPhil. in Power Systems Engineering from Kwame Nkrumah University of Science and Technology, Kumasi, Ghana in 2024. He works as an Engineer in the mining industry and currently the QC Engineer at ArcelorMittal Liberia. His research interest includes power electronics, advanced control systems, renewable energy systems, artificial intelligence and optimisation.



Francis Boafo Effah received the BSc. Electrical and Electronic Engineering degree at the Kwame Nkrumah University of Science and Technology (KNUST), Kumasi, in 2001, the MSc in Electrical Engineering from the University of Nottingham, UK, in 2009, and the PhD in Electrical and Electronic Engineering from the University of Nottingham, UK, in 2014. He is working in the Department of Electrical and Electronic Engineering of KNUST, Kumasi, as a senior lecturer and is currently the head of the department. His research interests include the control and modulation of power converters, the application of power converters in power systems, and electrical technologies for sustainable and renewable energy systems.

APPENDIX

Table 8: General summary of controllers' performance metrics.

Step response is a speed change from 1500 to 2000 rpm	**RBOSS NMPC**	**Successive Lin. NMPC.**	**Traditional NMPC**	**Explicit NMPC**	**FOC**
Rise Time (ms)	0.59349	0.59462	0.64002	3.81800	3.82800
Settling Time (ms)	0.75509	0.75536	0.78453	4.65900	4.89500
Overshoot (%)	0.47900	0.47900	1.45700	0.49800	1.53100
Steady – state error (%)	5.50700	5.55200	6.65500	0.00000	8.08000
Peak to Peak Iq Current (A)	3.99300	3.70900	5.98100	5.61600	1.95100
Peak to Peak Iq ref Current (A)	0.18570	0.11650	0.56580	0.17700	0.06156
Peak to Peak Id current (A)	3.09900	3.84900	6.07400	5.88100	1.94700
Peak to Peak, Te ripple (Nm)	2.67000	3.96400	4.28400	4.02300	1.36400

Copyrights
© 2025 Licensee Shahid Chamran University of Ahvaz, Ahvaz, Iran. This article is an open-access article distributed under the terms and conditions of the Creative Commons Attribution –NonCommercial 4.0 International (CC BY-NC 4.0) License (http://creativecommons.org/licenses/by-nc/4.0/).



Shahid Chamran University of Ahvaz

Iranian Association of Electrical and Electronics Engineers

Journal of Applied Research in Electrical Engineering

E-ISSN: 2783-2864
P-ISSN: 2717-414X
Homepage: https://jaree.scu.ac.ir/



Research Article

Compact Two-Stage CMOS Operational Amplifier with Enhanced Gain and Bandwidth via Cascode and Negative Capacitance Techniques

MohammadMehdi Derakhshannia[1], Mohsen Shakiba[1,*], and Maryam Shakiba[1,*]

[1]Electrical and Computer Engineering, Jundi-Shapur University of Technology, Dezful, Iran

** Corresponding Authors: Mohsen Shakiba (shakiba_jsu@yahoo.com) and Maryam Shakiba (shakiba@jsu.ac.ir)*

Abstract: In this research, a two-stage CMOS amplifier has been developed, characterized by high gain, extensive frequency bandwidth, and a compact chip area. The design incorporates a negative capacitor unit, a flipped voltage follower, a cascode configuration in the first stage, and a small MOSFET-based capacitor. The use of negative capacitance effectively diminishes the parasitic capacitance from the previous stage, resulting in a notable improvement in gain bandwidth. The flipped voltage follower functions as a voltage buffer within the circuit and utilizes pole-zero cancellation techniques to improve frequency bandwidth. This design enhances the amplifier's performance by effectively managing stability and response characteristics. Additionally, modifications to the input stage of the operational amplifier through a cascode structure yield a significantly high-gain amplifier. The first stage's cascode arrangement for the MOSFET drivers, along with an active load that has high output resistance, accounts for the majority of the circuit's gain. By eliminating passive capacitors and substituting them with small MOSFET-based capacitors, the proposed design effectively reduces chip area while boosting gain bandwidth. The design and simulation processes were carried out using Cadence IC Design Virtuoso software based on standard TSMC 0.18 µm CMOS technology. The results indicate that the amplifier achieves a DC gain of 80 dB, a bandwidth of 1.3 GHz, and a phase margin of 84 degrees.

Keywords: Two-stage CMOS amplifier, Flipped voltage follower, Cascode structure, Negative capacitance MOSCAP.

Article history
Received 24 December 2024; Revised 06 December 2025; Accepted 08 December 2025; Published online 18 January 2026.
© 2026 Published by Shahid Chamran University of Ahvaz & Iranian Association of Electrical and Electronics Engineers (IAEEE)
How to cite this article
M. M. Derakhshannia, Mo. Shakiba, and Ma. Shakiba, "Compact two-stage CMOS operational amplifier with enhanced gain and bandwidth via cascode and negative capacitance techniques," *J. Appl. Res. Electr. Eng.*, vol. 4, no. 1, pp. 86-93, 2025. DOI: 10.22055/jaree.2025.48628.1147

Check for updates

1. INTRODUCTION

The operational amplifier (Op-amp) serves as a fundamental component in nearly all signal processing systems, typically employed within a feedback loop to ensure stable and predictable gain with minimal noise. Its differential and mathematical operational capabilities have facilitated analog computations and automation within mixed-signal environments. However, Op-amps that utilize bipolar junction transistors (BJTs) tend to consume more power 1, rendering them unsuitable for many modern application-specific integrated circuits (ASICs) [1]. In contrast, Op-amps based on metal-oxide-semiconductor field-effect transistors (MOSFETs) are becoming increasingly significant in contemporary signal processing architectures due to their potential for low-power operation. Nevertheless, their performance is often hindered by a lower transconductance to drain current ratio ($g_m/I_d < 28$) compared to the g_m/I_d ratio of approximately 40 for BJTs, along with issues such as poor matching and low output impedance in the strong inversion region [2, 3].

The compensation techniques employed in operational amplifiers often require considerable chip area and involve more intricate designs compared to the traditional dominant pole approach (pole splitting) commonly used in classical op-amp architectures [4,5]. Historically, the Miller effect has been utilized to create a large capacitance at the output of the high-gain differential first stage. However, a feed-forward path is also present, introducing a positive zero that affects phase characteristics similarly to a pole, which can reduce the phase margin. Typically, a nulling resistor is added in series with the compensating capacitor to adjust the location of this zero, which further increases chip area usage [6-9].

Compensation techniques utilizing a current buffer, specifically through a common gate transistor, are highly effective in enhancing the gain-bandwidth product and power supply rejection ratio (PSRR) performance. These methods allow for smaller minimum allowable values of the compensation capacitor (CC), which provides greater flexibility in balancing noise performance against power consumption. A reduced CC facilitates improved design options, enabling engineers to optimize the operational amplifier's performance while maintaining low power usage [10].

In Miller and current buffer compensation techniques, the compensation capacitor usually adds a load to the output node. However, when a voltage buffer is incorporated into the feedback loop, the compensation capacitor reduces this loading effect on the output node. Additionally, the low impedance at the output node enhances effective feedback. This compensation approach exhibits high accuracy, as it primarily depends on the matching tolerances between transconductance and capacitance. Furthermore, compensation techniques that utilize a nulling resistor alongside a voltage buffer yield the same compensation capacitor and maintain an equivalent gain-bandwidth product [11-13]. Practical voltage buffers can be created using a common-drain (CD) transistor. This paper introduces a proposed compensation technique that employs a variant of the flipped voltage follower (FVF). In many applications, FVFs exhibit better performance than traditional CD configurations due to their remarkably low output impedance. The FVF cell enables the circuit to attain a wide range of transconductance while preserving good linearity throughout the input range. This capability is crucial for applications requiring precise control over frequency response and signal processing. This capability is essential for maintaining consistent performance across various operating conditions [14, 15]. The schematic of a PMOS version of the FVF is illustrated in Fig. 1. The FVF consists of a PMOS input transistor (M_{FVF}), a transistor (M_2) with shunt feedback. Also, the proposed compensation technique involves a transistor (M_{bias}) that is used to create the bias current [14]. This configuration is essential for ensuring stable operation of the circuit. While the FVF is capable of sourcing high currents, its ability to sink current is somewhat limited. The internal feedback loop plays a crucial role in reducing the output impedance $1/gm_{FVF}$ of the control transistor by the loop gain gm_2r_{oFVF}. Consequently, the output impedance of the FVF is given by:

$$R_{out} = \frac{1}{g_{mFVF}(g_{m2}r_{oFVF})} \quad (1)$$

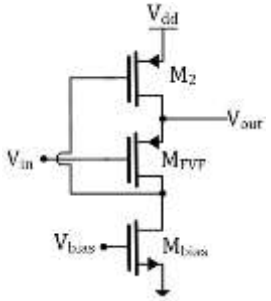


Fig. 1: Schematic representation of the Flipped Voltage Follower (FVF).

As shown in Fig. 1, which depicts the FVF. This circuit can achieve a high slew rate while maintaining low quiescent current consumption. Additionally, a MOS capacitor (MOSCAP)-based frequency compensation method minimizes die area usage, effectively eliminating passive elements that occupy space on the die. Consequently, the die area can be fully allocated to MOSFETs. In high-frequency applications, where parasitic capacitance can adversely affect performance, the incorporation of negative capacitance significantly reduces it for the preceding stage. This approach is essential for maintaining signal integrity and enhancing the overall efficiency of the circuit. The discussed paper employs a MOSCAP configured as a negative capacitance in conjunction with a voltage buffer, enhancing both the slew rate and the unity gain frequency of multistage CMOS circuits. In this setup, the first stage is designed with active negative capacitance, which plays a crucial role in optimizing circuit performance. This innovative use of negative capacitance effectively reduces the adverse effects of parasitic capacitances through partial cancellation, leading to significant improvements in both unity gain frequency and phase response. The equation for bandwidth (BW) of an operational amplifier driving a parallel combination of load resistance R1 and parasitic capacitance C_1 is given by:

$$BW = \frac{1}{2\,\pi\,C_1\,R_1} \quad (2)$$

To enhance bandwidth, reducing the value of C_1 through techniques such as negative capacitance is effective. Negative capacitance can counteract the effects of parasitic capacitance, effectively lowering the total capacitance seen by the amplifier and allowing for a higher bandwidth.

The practical circuit described utilizes a MOSCAP as a negative capacitance, replacing the traditional negative capacitor (C_N) to enhance performance metrics in multistage CMOS circuits. In this configuration, the components R_2 and C_2 are indicative of the output resistance and parasitic capacitance, respectively, which significantly affect the frequency response of the circuit [15].

The design of the proposed amplifier focuses on effectively managing both the load capacitance associated with the amplifying stage and the input capacitance related to the Negative Capacitance Generator (NCG) circuit. This dual consideration is crucial for ensuring optimal performance and stability of the amplifier in various applications. The MOSCAP functions as a negative capacitor by connecting the amplifier's output to the gain A, effectively creating a negative capacitance. By incorporating the NCG circuit into the amplifier's output node, the bandwidth is extended and can be expressed mathematically as:

$$C_N = C_N(1 - A_V) \quad (3)$$

The total capacitance is given by:

$$C_{tot} = C_N \,||(C_1 + C_2) \quad (4)$$

The bandwidth P can be calculated as:

$$P = \frac{1}{C_{tot}\, R} \tag{5}$$

The introduction of a NCG into a circuit significantly influences its frequency response by creating new poles and zeros. To optimize the performance of the NCG, it is essential to ensure that the magnitude of the zero is much greater than that of the poles. This condition allows the zero to be effectively neglected, which enhances the bandwidth of the circuit [16, 17].

This paper is organized as follows: Section 2 of the discussion focuses on the transfer function, the determination of pole-zero characteristics, and the criteria for stability in operational amplifier circuits. The results in this section clearly demonstrate that the proposed compensation technique improves phase margin and extends bandwidth, as elaborated in Section 3. Section 4 outlines widely accepted figures of merit (FOMs) used to compare the performance of different designs. In this section, we delve into the performance of the proposed circuit in comparison to existing state-of-the-art designs. The analysis focuses on key performance metrics such as gain, bandwidth, slow rate, and input/output characteristics. Finally, Section 5 concludes with a summary of the proposed methodology and suggests directions for future research [18, 19].

2. Proposed Two-Stage Amplifier

The proposed two-stage amplifier is meticulously designed to achieve an adequate GBW and a high phase margin, which are essential for efficient performance in various applications. The circuit extends the unity gain frequency and enhances operational speed while satisfying stability requirements.

The proposed circuit employs three frequency compensation techniques: the FVF, MOSCAP, and NCG block. The block diagram of this configuration is illustrated in Fig. 3, while its transistor-level implementation is detailed in Fig. 4. The proposed two-stage amplifier, as illustrated in Fig. 3, consists of two gain stages connected in series, with a Feedback Voltage (FVF) block and a MOSCAP serving as the Cc placed between nodes A and B. This configuration is critical for ensuring stability and enhancing performance. The FVF block operates as a voltage buffer, implemented using transistors M_{10}–M_{12}, while the MOSCAP serves as the *Cc*.

This configuration effectively enhances both linearity and speed within the circuit. The proposed circuit utilizes a MOSCAP not only as the compensation capacitor but also to enhance the phase margin of the amplifier. Additionally, a feedback MOSCAP, denoted as C_N, plays a crucial role in bandwidth enhancement. The inclusion of the MOSCAP allows for the elimination of passive elements from the circuit, thereby reducing die area occupation.

Furthermore, the input stage of the proposed operational amplifier has been modified using a cascode structure, resulting in a very high-gain amplifier. The first stage employs a cascode structure for the MOSFET drivers and

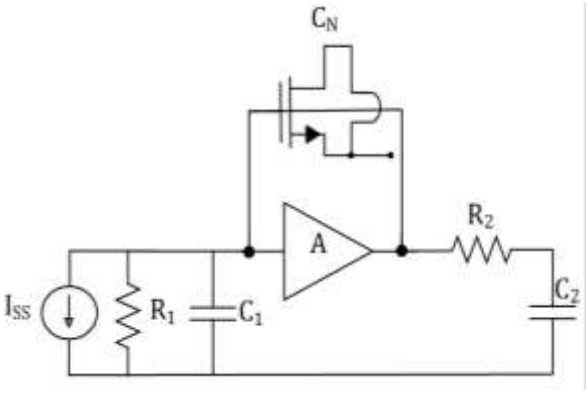


Fig. 2: Generation of negative capacitance utilizing a MOSCAP.

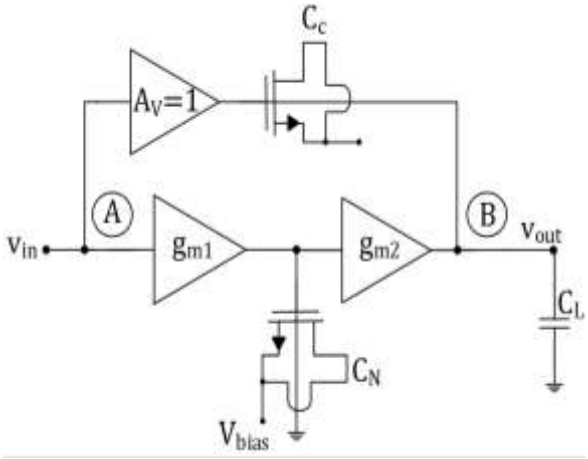


Fig. 3: Schematic representation of the proposed circuit's block diagram.

an active load with high output resistance, which contributes significantly to the overall gain of the circuit. The NCG circuit also plays a crucial role by maximizing the zero in the circuit's transfer function, leading to an increase in gain-bandwidth product (GBW). The output stage of the proposed amplifier is configured as a common source amplifier, utilizing and NMOS transistor (M_{13}) and a PMOS transistor (M_{14}). This configuration is widely recognized for its effectiveness in providing high gain and good linearity in signal amplification. The equivalent circuit for small signal analysis of the proposed compensation technique is illustrated in Fig. 5. In this configuration, the input stage is characterized by an output resistance r_{o1}, output capacitance C_1 and transconductance g_{m1}. The small signal model facilitates the evaluation of the amplifier's performance by allowing for linear analysis around a specific operating point. The first stage is loaded with a NCG, which produces a negative capacitance that effectively mitigates the effects of parasitic capacitance from the first stage. The final stage of the amplifier is configured as a common source amplifier, which includes an output resistance r_{o2}, total equivalent load capacitance C_L and transconductance g_{m2}.

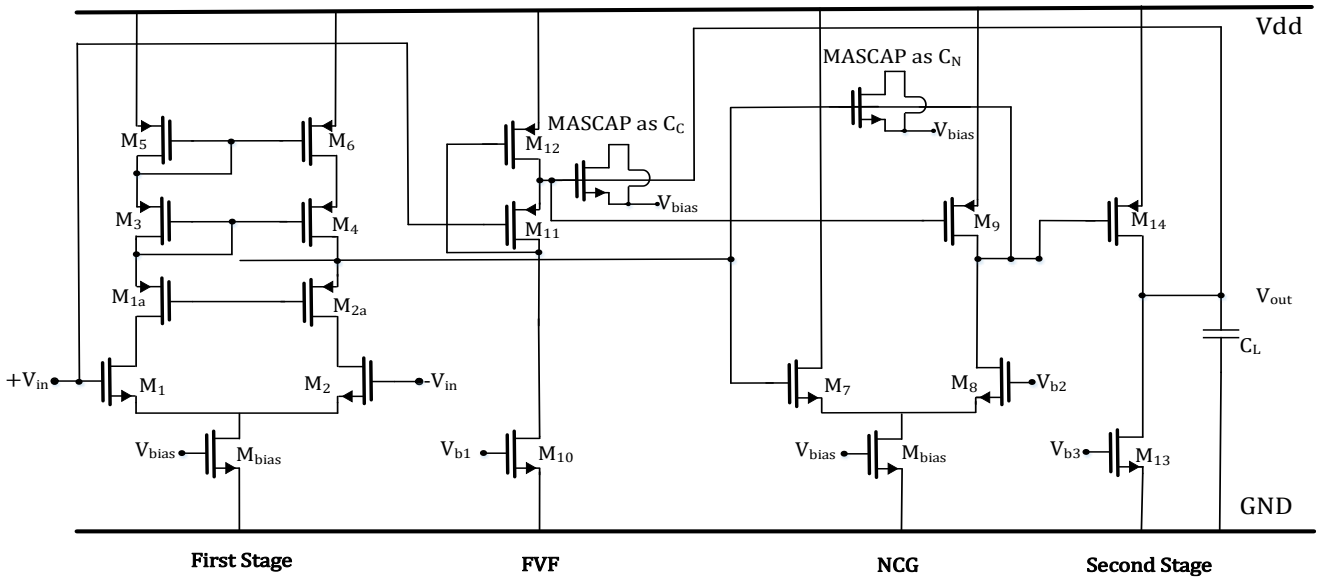


Fig. 4: Implementation of the proposed compensation technique at the transistor level.

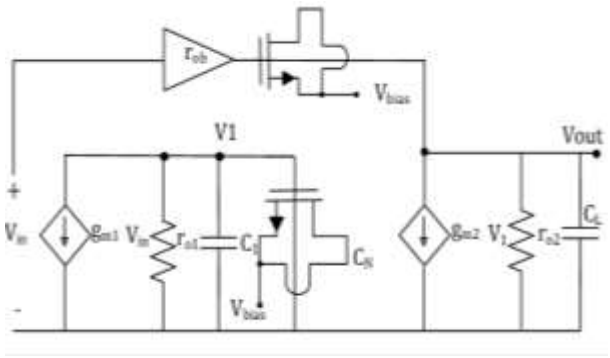


Fig. 5: Equivalent circuit for small signal analysis of the proposed compensation technique.

This configuration is known for its ability to provide significant voltage gain and is widely used in analog circuit designs. The voltage buffer, represented by the FVF cell, connects nodes A and B, with its output impedance denoted as r_{ob}. The FVF is a specialized buffer circuit known for its low-power and low-voltage operation, making it particularly suitable for modern analog and mixed-signal applications.

The small-signal transfer function of compact two-stage CMOS operational amplifier can be expressed as a second-order equation, which is crucial for analyzing the amplifier's frequency response and stability. This transfer function typically takes the form:

$$A_V = \frac{(C_C r_{o1} + C_C r_{ob})s}{\left((C_1 + C_C)r_{o1} + (C_C + C_L)r_{ob} + C_N\right)S^2} \quad (6)$$

$$\frac{+g_{m1}g_{m2}}{+\left((C_1 + C_C)(C_C + C_L)r_{o1}r_{ob}\right)S + \left(\frac{1}{(r_{o1}r_{ob})}\right)}$$

The transfer function of the proposed compact two-stage CMOS operational amplifier can be characterized by its poles, zeros, GBW, and phase margin (PM). The relevant equations for these parameters are defined as follows:

The first pole is defined as:

$$P_1 = \frac{1}{\left((C_1 + C_C)r_{o1} + (C_C + C_L)r_{ob} + C_N\right)} \quad (7)$$

The second pole is given by:

$$P_2 = \frac{1}{\left((C_1 + C_C)(C_C + C_L)r_{o1}r_{ob}\right)} \quad (8)$$

The zero is defined as:

$$\Im = (C_C r_{o1} + C_C r_{ob}) \quad (9)$$

The gain-bandwidth product is calculated as:

$$GBW = \frac{g_{m1}g_{m2}r_{o1}r_{ob}}{\left((C_1 + C_C)r_{o1} + (C_C + C_L)r_{ob} + C_N\right)} \quad (10)$$

The phase margin is determined by:

$$PM = 180 - tan^{-1}\left(\frac{GBW}{P_1}\right) - tan^{-1}\left(\frac{GBW}{P_2}\right) \quad (11)$$

The effective capacitance at the output of the first stage, represented as $C_1+C_N(1-A)$, is indeed reduced, which plays a significant role in improving the performance of the amplifier. Additionally, the small output impedance rob of the FVF contributes positively to frequency compensation. As a result, the

poles defined in (7) and (8) are positioned farther from the unity gain frequency, thereby extending the overall bandwidth of the amplifier.

3. Simulation Results

The proposed compact two-stage CMOS operational amplifier presented here introduces a method for frequency compensation in a two-stage CMOS circuit utilizing negative capacitance through a MOSCAP and the FVF. This approach effectively enhances the performance of the amplifier by addressing stability issues and improving bandwidth. Additionally, the implementation of a cascode structure in the first stage significantly enhances the amplifier's gain. Implementation of the proposed compensation technique at the transistor level, illustrated in Fig. 4, has been simulated using the Cadence Virtuoso 6.17 simulation tool with TSMC CMOS 0.18 µm process parameters. The maximum bias current in the circuit is 1.22 mA and supply voltage is set to 1.8 V. All transistors are working in saturation mode and their aspect ratios and other circuit component values are mentioned in Tables 1 and 2, respectively. The slew rate of proposed circuit is very high as the output voltage of the given circuit changes rapidly with respect to time. The simulated transient response with a 1 pF load for rising and falling edge is shown in Fig. 6 and slew rate (±) measured is 155 V/µS. The overshoot and 1 % settling time (average) of the circuit is calculated as 0.860 µV and 1.72 µS respectively. The average slew rate is 155 V/µS which is very high as compared to other reported techniques [16, 21-23].

The AC analysis of the proposed amplifier was conducted for various values of load capacitance (C_L), and the results are illustrated in Fig. 7. This simulation is essential for analyzing how different load capacitances affect the amplifier's frequency response, stability, and overall performance. The performance of the amplifier remains robust across different load capacitor values. Specifically, the amplifier achieves GBW of 1.45 MHz, 1.41 MHz, and 7.48 MHz with corresponding PM of 81°, 84°, and 107° for load capacitances of 0.1 pF, 1 pF, and 10 pF, respectively.

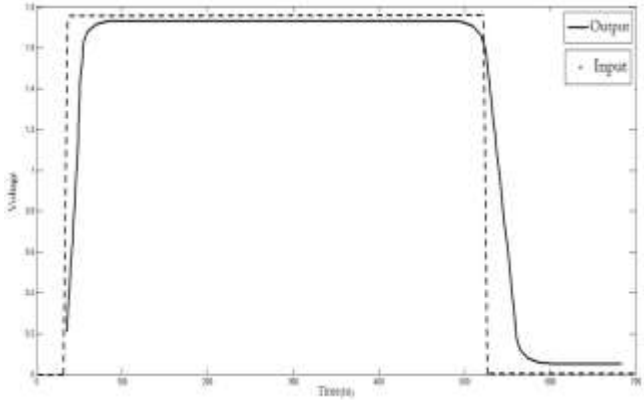


Fig. 6: The step response of the proposed amplifier with a load capacitance of 1 pF.

Table 1: MOSFETs dimensions.

MOSFET	$W(\mu m)/L(\mu m)$	MOSFET	$W(\mu m)/L(\mu m)$
M_1 and M_2	56/180	M_{10}	68/180
M_3 and M_4	70/180	M_{11} and M_{12}	40/180
M_5 and M_6	77/180	M_{13}	20/180
M_7 and M_8	73/180	M_{14}	40/180
M_9 and M_{99}	75/180	M_{1a} and M_{2a}	70/180

Table 2: Circuit parameters and corresponding numerical values.

Parameter	Simulated results	Unit
Gain	80	dB
Gainbandwidth product	1.4	GHz
Current Total	1220	µA
Supply Voltage	1.8	V
Technology	18	µm
Phase margin	84	(°)
Slew rate	155	(V/µS)
CL(pF)	1	Pf
Cc(pF)	0.001	Pf
FOM1	866	-
FOM2	93	-
Power	1.620	mW

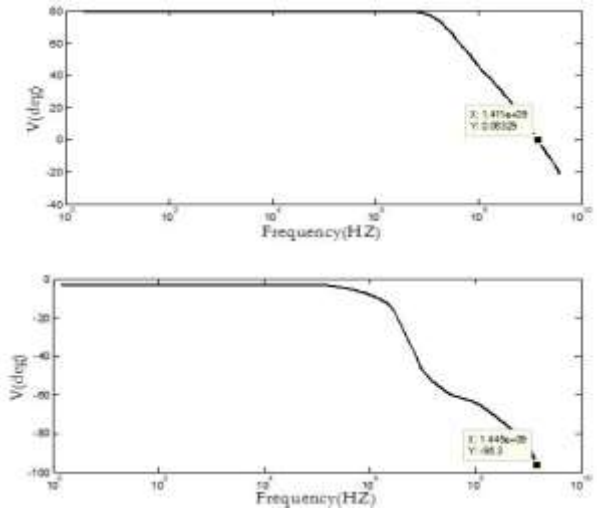


Fig. 7: Gain and phase characteristics of the proposed circuit with a load capacitance of C_L=0.1 pf.

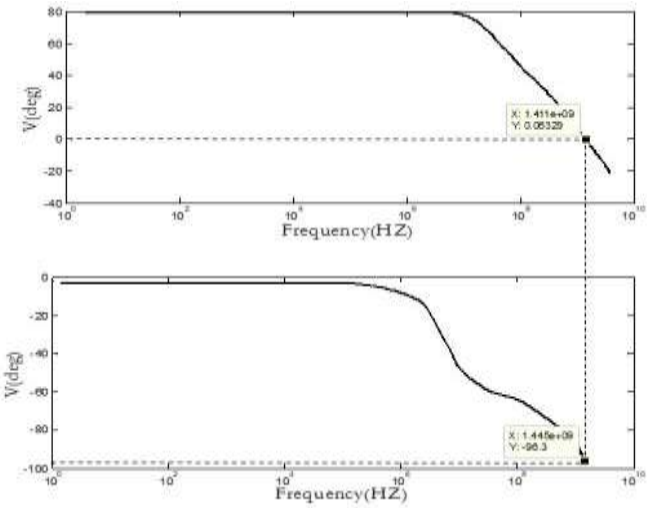


Fig. 8: Gain and phase characteristics of the proposed circuit with a load capacitance of C_L=1 pf.

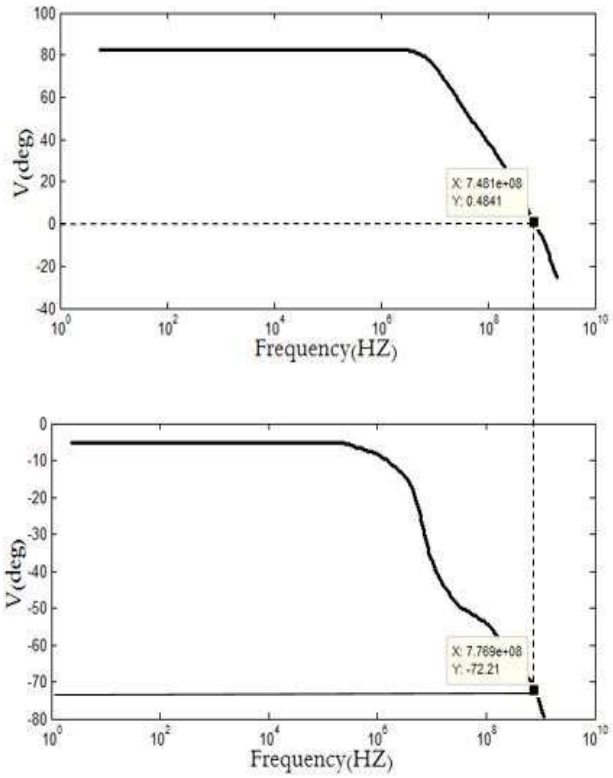


Fig. 9: Gain and phase characteristics of the proposed circuit with a load capacitance of C_L=10 pf.

The output voltage swing of the proposed circuit (Fig. 10), which ranges from 0.2 V to 1.50 V, demonstrates an improvement over the first stage cascode circuit. This enhancement in output voltage swing can be attributed to several factors: In the proposed circuit, two MOSCAPs are utilized in place of passive capacitors for negative capacitance and compensation purposes. This design choice leads to a significant reduction in chip area, as demonstrated by the equivalent circuit analysis. The calculated chip area using MOSCAPs is 3669 µm², compared to 4527 µm² when using traditional passive capacitors.

4. DISCUSSION

The proposed compensation technique has been evaluated against established topologies using two key FOM: FOMS for small-signal behavior and FOML for large-signal behavior. These figures of merit are defined as follows:

FOMS (Small Signal Behavior):

$$FOM_S = (GBW * C_L)/Iss \quad (12)$$

FOML (Large Signal Behavior):

$$FOM_L = (GBWdemonstrates * SLOW * C_L)/Iss \quad (13)$$

The proposed circuit for bandwidth extension a significant improvement in performance compared to existing techniques, as summarized in Table 3. While it requires a considerable number of transistors, it achieves an optimal

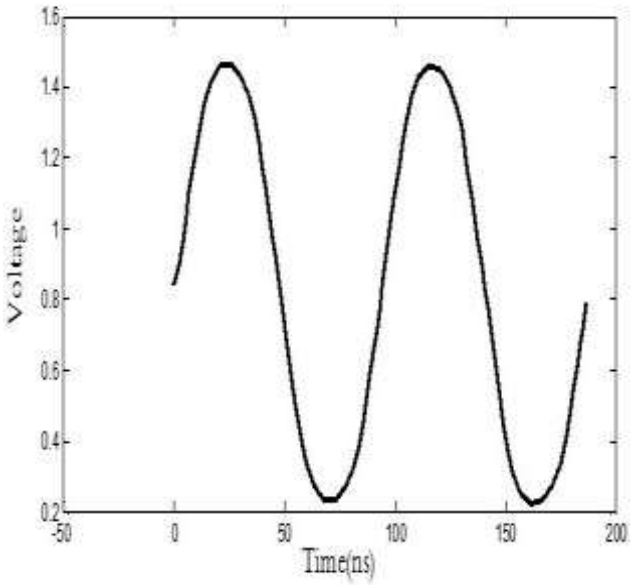
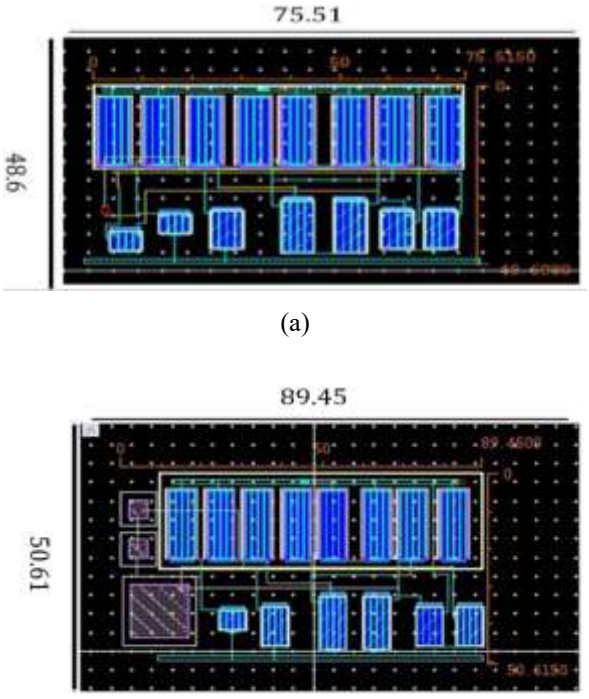


Fig. 10: Output voltage swing of proposed circuit.



(a)

(b)

Fig. 11: Layout of proposed circuit (a) with MOSCAP (b) without MOSCAP.

combination of GBW, transconductance (GM), and PM. The high slew rate and elevated values of PM and GM indicate enhanced stability. Additionally, the calculated FOM values show substantial improvements over previously reported methods [16, 21-23]. Notably, the load capacitance utilized in the proposed circuit does not influence the FOMs, which is a crucial advantage. The cascode op-amp configuration employed contributes to a higher DC gain. Overall, this circuit is characterized by its simplicity and capability to operate effectively at very high frequencies.

Table 3: Performance comparison whit some other research.

	DC gain (dB)	Load (pF)	Power (mW)	GBW (GHz)	Compensation Capacitor(pF)	Slew rate (V/µS)	P.M (°)	FOM1	FOM2
[21]	58.59	15	--	0.81	0.001	5.3	60.7	160	--
[22]	67	30	2.588	0.29	3.5	13.8	51	351	45
[23]	54	2.5	1.9	0.55	0.009	17.33	94.9	--	--
[16]	61	1	1.620	1.2	5.6	148	73	740	90
Proposed circuit	80	1	1.740	1.4	0.001	155	84	864	93

5. Conclusion

In this research, a two-stage CMOS amplifier has been designed with the goals of achieving high DC gain, wide frequency bandwidth, and a compact chip area. To enhance the amplifier's gain, a cascode configuration was implemented in the first stage. This structure effectively increases the DC gain while maintaining stability. A compensation capacitor was utilized to improve the frequency response of the amplifier. The FVF serves as a practical voltage buffer in this compensation technique, benefiting from its very low output impedance, which enhances overall performance. The incorporation of negative capacitance reduces the parasitic capacitance from the preceding stage, leading to significant improvements in GBW. The addition of a NCG introduces new poles and zeros at high frequencies, optimizing bandwidth by maximizing the zero while ensuring it is considerably larger than the poles. The use of MOSCAPs for frequency compensation minimizes die area by eliminating passive components. This allows the die area to be fully allocated to MOSFETs, resulting in a reduced chip area of 3669 µm². Simulations were conducted using Cadence IC Design Virtuoso software with TSMC 0.18 µm CMOS technology. Key performance metrics include: Slew Rate: ±155 V/µs, Overshoot: 0.86 µV, Settling Time: 1.72 µs, GBW values of 1.45 MHz, 1.41 MHz, and 7.48 MHz with corresponding phase margins of 81°, 84°, and 107° for load capacitances of 0.1 pF, 1 pF, and 10 pF, respectively. Output Voltage Swing: Ranges from 0.2 V to 1.40 V. The amplifier's performance was evaluated under varying load capacitance conditions, demonstrating that the load capacitance does not adversely affect the figures of merit.

Credit Authorship Contribution Statement

MohammadMehdi Derakhshannia: Formal analysis, Resources, Software, Visualization, Writing - review & editing. **Mohsen Shakiba:** Conceptualization, Methodology, Project administration, Resources, Software, Supervision. **Maryam Shakiba:** Conceptualization, Investigation, Methodology, Resources, Validation, Writing - original draft, Writing - review & editing.

Declaration Of Competing Interest

The authors declare that they have no known competing financial interests or personal relationships that could have appeared to influence the work reported in this paper. The ethical issues; including plagiarism, informed consent, misconduct, data fabrication and/or falsification, double publication and/or submission, redundancy has been completely observed by the authors.

References

[1] T. H. Lee, ‘‘IC Op-Amps Through the Ages’’, Stanford University: Handout # 18, EE214, Fall 2002.

[2] W. Sansen, “Analog design essentials,” *The international series in engineering and computer science*, vol. 859, Dordrecht: Springer, 2006.

[3] F. Silveira, D. Flandre, and P. Jespers, “A gm/ID based methodology for the design of CMOS analog circuits and its application to the synthesis of a silicon-on-insulator micro power OTA,” *IEEE Journal of Solid-State Circuits*, vol. 31, no. 9, pp. 1314–1319, 1996.

[4] D. M. Binkley, B. J. Blalock, and J. M. Rochelle, “Optimizing drain current, inversion level, and channel length in analog CMOS design,” *Analog Integrated Circuits and Signal Processing Journal*, vol. 47, pp. 137–163, 2006.

[5] P. E. Allen, and D. R. Holberg, “CMOS analog circuit design,” 2nd ed., New York: Oxford University Press, 2002.

[6] T. H. Lee, “Tales of the continuum: A subsampled history of analog circuits,” *IEEE Solid-State Circuits Newsletter*, vol. 12, no. 4, 38–51, 2007.

[7] D. A. Johns and K. Martin, “Analog integrated circuit design,” New York: John Wiley & Sons, 1997.

[8] J. Solomon, “The monolithic op amp: A tutorial study,” *IEEE Journal of Solid State Circuits*, vol. CS-9, no. 6, pp. 314–332, 1974.

[9] P. R. Gray, P. Hurst, S. Lewis, and R. Meyer, *Analysis and design of analog integrated circuits*. 5th ed., New Jersey: John Wiley & Sons, 2009.

[10] P. Vajpayee, "An ultra-high gain low power two stage CMOS op-amp based on inverse aspect ratio self cascode structures," *Analog Integr. Circ. Sig. Process.*, vol. 81, pp. 349–359, 2014.

[11] D. Marano, G. Palumbo, S. Pennisi, "A new advanced RNMC technique with dual-active current and voltage buffers for low-power high-load three-stage amplifiers," in *Proc. ISCAS 2009*, pp.25-28, 24-27 May 2009.

[12] G. A. Rincon-Mora, *Analog IC design with Low-Dropout Regulators (LDOs)*, McGraw Hill Professional, Mar 2009.

[13] R. J. Baker, *CMOS circuit design, layout, and simulation.* 3rd Edition.

[14] R. G. Carvajal et al., "The flipped voltage follower: a useful cell for low-voltage low-power circuit design," *IEEE Transactions on Circuits and Systems I: Regular Papers*, vol.52, no.7, pp.1276-1291, July 2005.

[15] *D. J. Comer et al, "Bandwidth extension of high-gain CMOS stages using active negative capacitance,"* in *2006 13th IEEE international conference on electronics, circuits and systems*, IEEE, 2006.

[16] U. Bansal, M. Gupta, and U. Singh, "Frequency compensation of two stage CMOS circuit using negative capacitance and flipped voltage follower," *Analog Integrated Circuits Signal Processing*, vol. 90, pp. 175–188, 2017.

[17] B. B. Daryan, H. Khalesi, V Ghods, and A. Izadbakhsh, "Multi-stage CMOS amplifier frequency compensation using a single MOSCAP," *Analog Integrated Circuits and Signal Processing*, vo. 103, pp. 237–246, 2020.

[18] M. Ghaemmaghami and S. Reyhani, "Design of a tunable 4th order OTA-C band-pass filter for use in front-end of ADC**,** *Journal of Applied Research in Electrical Engineering*, vol. 2, no. 2, pp. 152-157, July 2023.

[19] A. Khoshsaadat and M. Abedini, "A new topological method for output voltage clamping of immittance-based constant current load resonant converters**,"** *Journal of Applied Research in Electrical Engineering*, **v**ol. 3, no. 1, pp. 33-39, Jan. 2024.

[20] A. Mirvakili, and V. J. Koomson, "Passive frequency compensation for high gain-bandwidth and high slew-rate twostage OTA," *Electronics Letters*, vol. 50, no. 9, pp. 657–659, 2014.

[21] G. Moradi, M. R. Alamdar, and S. Izadpanah Tous, "Hybrid frequency compensation to improve unity-gain bandwidth of low-voltage low-power CMOS operational amplifiers," *Majlesi Journal of Telecommunication Devices*, vol. 7, no. 2, June 2018.

[22] H. Faraji Baghtash and K. Monfaredi, "A novel active feedback frequency compensation scheme for two-stage OTA," *Iranian Journal of Electrical and Electronic Engineering*, vol. 15, no. 3, Sep. 2019.

[23] S. H. Pakala, M. Manda, P. R. Surkanti, A. Garimella, and P. M. Furth, "Voltage buffer compensation using flipped voltage follower in a two-stage CMOS op-amp," in *2015 IEEE 58th International Midwest Symposium on Circuits and Systems(MWSCAS)*.

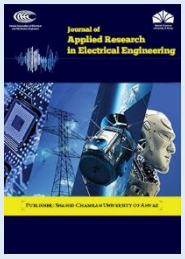
Copyrights
© 2026 Licensee Shahid Chamran University of Ahvaz, Ahvaz, Iran. This article is an open-access article distributed under the terms and conditions of the Creative Commons Attribution –NonCommercial 4.0 International (CC BY-NC 4.0) License (http://creativecommons.org/licenses/by-nc/4.0/).

Shahid Chamran University of Ahvaz

Iranian Association of Electrical and Electronics Engineers

Journal of Applied Research in Electrical Engineering

E-ISSN: 2783-2864
P-ISSN: 2717-414X
Homepage: https://jaree.scu.ac.ir/



Research Article

Texture Classification Using Deep Learning and Enhanced Local Binary Pattern

Behzad Abbasi[1,*], Majid Ghandchi[1], Sirous Tannaz[2], Javad Ostadieh[3], and Saeed Barghandan[1]

[1] *Department of electrical engineering, Ahar branch, Islamic Azad University, Ahar, Iran*

[2] *Department of electrical engineering, Urmia branch, Islamic Azad University, Urmia, Iran*

[3] *Department of electrical engineering, Khoy branch, Islamic Azad University, Khoy, Iran*

* *Corresponding Author: abbasi_behzad63@yahoo.com*

Abstract: Image texture classification is crucial in machine vision and image processing. The primary step in this classification process involves extracting features from the image. Numerous techniques have been developed for feature extraction from textured images; however, local binary patterns (LBP), in both their original and enhanced forms, stand out due to their simplicity in implementation and their ability to extract effective features that yield high classification accuracy. Experts widely recognize that deep neural networks excel at classifying images and extracting detailed features. Building on the strengths of these methods, this study introduces a new model that merges deep learning with enhanced local binary patterns. This model has been tested on the Outex and CUReT datasets. The experimental results indicate that combining deep learning with an improved local binary pattern method significantly enhances the accuracy of texture image classification. According to these results, the classification accuracy of this new model surpasses that of previous methods.

Keywords: Classification, Deep learning, Texture images, Local binary pattern, Enhanced local binary pattern.

Article history
Received 09 July 2024; Revised 20 April 2025; Accepted 06 August 2025; Published online xxx.
© 20xx Published by Shahid Chamran University of Ahvaz & Iranian Association of Electrical and Electronics Engineers (IAEEE)
How to cite this article
B. Abbasi, M. Ghandchi, S. Tannaz, J. Ostadieh, and S. Barghandan, "Texture classification using deep learning and enhanced local binary pattern," *J. Appl. Res. Electr. Eng.*, vol. 4, no. 1, pp. 94-105, 2025.
DOI: 10.22055/jaree.2025.47391.1124

Check for updates

1. INTRODUCTION

Texture classification is a crucial component of texture analysis, aimed at categorizing an unknown sample image into one of several predefined texture classes. Natural images often display variations in scale, illumination, viewpoint, and rotation, prompting texture classification methods to cover a broader spectrum of natural texture attributes. As a result, many approaches have been developed, falling into four primary categories: statistical, structural, model-based, and signal processing. Each category employs different techniques to extract features from texture images, tailored to the method used and the specific textures being analyzed. This research introduces a new model for texture image classification that integrates deep learning with an enhanced version of the local binary pattern (LBP). There have been numerous advancements in LBP methods, with some focusing on extracting distinct texture features through various pattern samples, and others enhancing noise resistance with different encoding or threshold strategies. This paper concentrates on the former approach, aiming to achieve high accuracy by extracting effective texture features and merging them with deep neural networks. Computer vision, a broad field of study, involves extracting and interpreting information from images and videos through computational algorithms. It addresses multiple challenges such as detection, segmentation, motion estimation, and image retrieval. Technological advances and the availability of extensive datasets have broadened its application scope. This paper specifically explores the combination of enhanced local binary patterns and deep learning methods for detecting and segmenting texture images. The goal is to extract relevant features from texture images and integrate them with convolutional neural networks (CNNs) for optimal texture

classification. The subsequent sections will discuss the refined versions of LBP methods tailored for texture classification, highlighting the unique challenges associated with handling texture databases. Here we delve into the literature review in this topic:

CNN, has become a dominant approach in texture analysis, object detection, and pattern recognition. [1] explored deep learning techniques for texture and dynamic texture analysis, demonstrating their effectiveness in capturing complex patterns in image data. Similarly, [2] investigated CNNs for object detection, re-identification, and recognition, highlighting their robustness in handling large-scale visual datasets. In real-world applications, CNNs have been employed for road defect detection, as seen in [3], where a CNN-based system was designed to detect potholes, improving road safety assessments. Another critical application is surface crack detection, where [4] proposed a shallow CNN architecture to enhance computational efficiency while maintaining high accuracy. Traditional texture descriptors, such as Local Binary Patterns (LBP), have been widely used in texture classification. [5] conducted a comparative study between LBP and deep texture descriptors, revealing that deep learning methods often outperform traditional approaches in robustness. Further improvements to LBP were introduced by [6], who proposed a completed modeling approach for better texture classification. [7] extended this idea with the Completed Local Binary Count (CLBC), enhancing rotation-invariant texture analysis. Peng Yang and colleagues have developed a descriptor that they use jointly for these challenges. They apply a complex Dual-tree Complex Wavelet Transform (DTCWT) to the base image to create an image pyramid. This pyramid is then merged with the Local Binary Pattern (LBP) in the DTCWT domain to formulate a method known as LBPDTCWT (Local Binary Pattern Dual-tree Complex Wavelet Transform), which is capable of generating robust texture features. By combining these features, their method has shown potential to surpass other approaches in empirical tests on benchmark datasets [8]. Tang Song and team introduced a fixed-scale descriptor called Sorted Local Gradient Pattern (SLGP) for classifying textures. Initially, they developed two complementary local gradient patterns, LGP Center (LGP CR) and Ring-to-Ring (LGP RR), to capture the rich gradient information in an image. Experiments on three texture databases indicate that this descriptor achieves superior classification results under affine transformations and both linear and nonlinear grayscale variations [9]. Creating effective features is a fundamental task in computer vision, yet finding a balance between discriminative power and robustness is challenging. Jianbai Yu and associates introduced a method named PRICoLBP, which shows resilience against changes in rotation and illumination. Previous methods have shown that enhancing spatial uniformity can improve the discriminative power of features. Despite their efficacy, existing uniformity-based features often overlook robustness against geometric and photometric variations. To address this gap, Jianbai Yu and colleagues explored the resistance to transformations that maintain spatial uniformity, leading to the development of a concept called Pairwise Transform Invariance (PTI). They introduced an approach known as PRICoLBP (Pairwise Rotation Invariant Co-Occurrence Local Binary Pattern), which integrates these novel features with rotationally invariant binary patterns to enhance robustness [10]. Local binary patterns (LBP) are recognized as potent descriptors for texture classification, but traditional LBP and its variants sometimes struggle with limited performance under restricted rotational angles. To mitigate this, Kiqiu Kwa and team developed a new local texture descriptor based on principal curvatures, called PCLBP. This descriptor combines the strengths of LBP with principal curvatures (PC) at the texture surface to improve robustness, employing a multi-resolution approach and a cross-scale encoding strategy to adjust three proportional parameters. The simplified PCLBP method is highly discriminative, invariant to changes in illumination and rotation, and offers computational simplicity [11]. Given that variations in illumination and rotation significantly affect the accuracy of texture image classification, Wei Wang and colleagues have proposed a new descriptor named Geometric Completed Local Binary Pattern (GCLBP). Drawing on the principles of continuous rotation invariance and illumination robustness from geometric curvature information, this descriptor uses principal curvatures (PC) computed for all pixels to represent the magnitude of image gradients, primarily substituting the primary gradient information in CLBP [12]. Traditional LBP descriptors, while widely used in texture analysis, are sometimes limited in capturing fully discriminative information as they rely solely on the sign bit differences within a local region. To enhance LBP's performance, Jiebin Pan and his team developed a novel texture classification descriptor called feature-based local binary pattern (FbLBP). In FbLBP, the difference vector is divided into sign and magnitude components; the sign describes the local binary pattern, while the magnitude is characterized by mean and variance features. This method is less sensitive to illumination changes and uses a local adaptive threshold to convert these features into binary codes, making it highly efficient and parameter-free for application across various databases [13]. The KNN classifier was employed for feature classification based on the distribution of extracted features. The proposed mapping methods were tested on an enhanced local binary pattern (ELBP) variant. The developed ELBP showed higher accuracy than traditional ELBP and other advanced local binary patterns. Moreover, the proposed mapping approaches improve the rotational robustness of local binary patterns, especially for larger neighborhoods. In terms of computational complexity, the new ELBP provides fewer features, significantly enhancing processing speed [14]. Rakesh Mehta et al. introduced a highly efficient and rotationally robust texture descriptor called Dominant Rotation Local Binary Pattern (DRLBP). This descriptor achieves rotation invariance by computing it based on a reference within a local region, ensuring simplicity. This reference allows quick computation of local binary patterns while maintaining comprehensive structural information. The proposed method not only preserves the complete structural information of local binary patterns but also stores additional value-based information, increasing discriminative power. Feature selection involves learning common patterns from training images and filtering out redundant, non-informative features [15]. Effective texture image identification leverages multiple visual cues from the image appearance. Local Binary Pattern (LBP) and its variants have been successful in texture description. However, due to LBP features being discrete indicators of

patterns rather than numerical values, integrating them with other distinctive features into a unified descriptor is challenging. To address the non-numerical nature of LBP patterns, Jiaopeng Hong et al. propose a numerical variant called Different Local Binary Pattern (LBPD). LBPD measures the difference of a local binary pattern from the mean structure of a specific region in the image. It is straightforward, rotationally robust, and computationally efficient. For improved performance, LBPD is combined with other distinctive cues using a covariance matrix. The proposed descriptor, Covariance-Local Binary Pattern Difference (COV-LBPD), efficiently captures the intrinsic correlations between LBPD and other features compactly. This approach aims to enhance the robustness and discriminative power of texture classification systems [16]. Jianhua Guo et al. proposed a comprehensive modeling of the Local Binary Pattern (LBP) operator and developed an enhanced framework called Completed Local Binary Pattern (CLBP) for texture classification. A local region centered on each pixel is indicated, and its Local Difference Sign Magnitude Transform (LDSMT) is demonstrated. The central pixels represent the grayscale level of the image and are transformed into a binary code, known as CLBP_C or CLBP_Center, using a global threshold. LDSMT divides local image differences into two complementary components: CLBP_Sign and CLBP_Magnitude, which are proposed for encoding. CLBP_S relates to the local binary pattern section and retains more information about the local structure compared to CLBP_M, indicating that the simple LBP operator can effectively extract texture features. By combining the features CLBP_S, CLBP_M, and CLBP_C in joint or composite distributions, significant improvements in rotationally robust texture classification can be achieved. This approach enhances the robustness of texture classification against rotation [6]. Texture image classification is crucial in computer vision research. To effectively capture texture patterns, a distinctive feature such as Local Binary Pattern (LBP) is essential. LBP is resistant to uniformity changes and grayscale variations, and its fast computation makes it popular in various texture analysis applications. However, LBP is sensitive to noise. To reduce noise effects and enhance pattern discrimination, a triple local pattern approach called Local Ternary Pattern (LTP) has been proposed. Unlike the binary encoding of LBP, LTP uses a ternary encoding scheme, making it better at tolerating noise and significantly enhancing discrimination. These advantages improve LTP's classification accuracy. This paper thoroughly examines feature extraction for robust local pattern recognition as an integer decomposition problem, formulated as a generalized version of the Bachet de Meziriac Weight Problem (BMWP). Based on this generalization, Sheng Yang et al. proposed a Local n-ary Pattern (LNP), specifically parameterized for n=2, where LBP serves as a specific case. LTP is not a specific instance of LNP. Both LBP and LTP are recognized for their success as benchmark methods for evaluating LNP performance. The proposed LNP significantly improves texture classification accuracy compared to LBP and shows considerable enhancement over LTP [17]. While LBP is sensitive to noise and LTP partially mitigates this issue, both methods perform similarly when dealing with corrupted image patterns. To address this, Jianfeng Ren et al. proposed a Noise-Resistant Local Binary Pattern (NRLBP) to preserve local structures in noisy images. Small pixels, vulnerable to noise, are first encoded as an indeterminate state and then assigned a value based on other LBP bits. Essentially, they created an error correction mechanism to recover distorted image patterns [18]. A local region in an image can be defined using its central pixel and the differences with its neighboring pixels. To effectively distinguish structures of various textures, Nishant Srivastava et al. propose a method called Noise-Invariant Structure Pattern (NISP), which uses the central pixel along with local and global information of an image. Instead of the central pixel, a computed threshold is used to add the central pixel and the mean intensity in calculating the local binary pattern code. For incorporating quantitative information, binary patterns are generated by taking thresholds related to the central pixel and local/global contrasts. Additionally, for incorporating adjacency information of a specific pixel, binary patterns are generated using global mean thresholds. The proposed method is insensitive to noise because the central pixel is not directly used as a threshold [19]. Local Binary Pattern (LBP) is considered one of the most efficient texture features with high performance. However, the traditional LBP method is highly sensitive to image noise and lacks the capability to capture information within larger structures. To address these issues, Li Liu and colleagues introduced a robust extension of LBP called Median Robust Extended Local Binary Pattern (MRELBP) for texture classification. This proposed model differs from traditional local binary patterns by utilizing regional medians instead of raw image intensities. A multi-scale local binary pattern descriptor is computed by comparing regional medians on a novel sampling pattern, effectively capturing both fine-grained and coarse-grained texture information [20]. Ticheng Song et al. propose a noise-robust descriptor for texture classification using a set of Local Contrast Patterns (LCP) through global metrics. To manage image noise, directional and non-directional difference masks are designed to compute three types of contrasts: directional, non-directional, and maximum. For pixel-level feature description, these responses are separately quantized and encoded based on various global metrics in specific patterns. The resulting patterns (LCPs) are collectively encoded to form the final representation of the proposed texture model [21]. Local Binary Pattern (LBP) is sensitive to noise and suffers from limited range detection capabilities. Despite significant advances, most types of LBP still exhibit constraints related to noise sensitivity, high dimensionality, and computational inefficiency. Addressing these issues, Jibin Pan et al. propose an adaptive local descriptor resilient to noise named Diamond Sampling Structure Based Local Adaptive Binary Pattern (DLABP). The objective is to achieve efficiency, simplicity, and speed through a structure-based sampling approach [22].

Research in texture detection often focuses on the challenging task of identifying materials under irregular conditions, a scenario rarely met by algorithms. In this work, Mircha Simpoy et al. undertake the first study to describe identifiable texture features and materials in disarray, utilizing a newly derived database from the surface tissue repository. They propose a novel texture descriptor named FV-CNN (Fisher Vector Pooling of a Convolution Neural Network), which integrates feature vectors from a convolutional neural network bank. FV-CNN is considered significantly advanced in texture detection, effortlessly

transferring across domains without the need for feature adaptation as in fully connected layers of convolutional neural networks. Moreover, FV-CNN can seamlessly combine multiscale information and describe regions of arbitrary shapes and sizes [23]. Cancer ranks among the most perilous diseases for human health. Extensive efforts have been made in radiology advancements and tools such as tumor tomography or CT (computed tomography) imaging for early cancer detection. One of the primary objectives is to distinguish malignant cancer from benign ones. In recent years, deep learning, particularly convolutional neural networks, has aided medical science in cancer identification. Deep learning algorithms invariably require large databases. However, collecting such a vast volume of images with pathological information, especially in medical imaging, particularly for cancer imaging, remains challenging. Therefore, strategies for effective learning from small databases through deep neural network models are essential. To advance this goal, Shou Zhang et al. investigate two deep neural network models with a substantial focus on expanding training samples from two proven pathological small databases for distinguishing malignant from benign cancers [24]. Designing texture features with high discriminative power and robustness under various conditions poses a significant computer vision challenge with numerous applications, including material recognition and analysis of satellite or aerial images. Historically, most texture description approaches relied on dense statistical distributions and local features. However, recent approaches for texture detection and classification in remote sensing images predominantly utilize convolutional neural networks (CNNs). The practical operation during the training of these CNN models involves using RGB channels as inputs, trained on extensive labeled datasets. In this paper, Rao Mohammad Anwar et al. present TEX-Net, a convolutional neural network model with localized binary pattern encoding. TEX-Net is trained using encoded images to map textures based on learned local binary pattern information. Additionally, they propose two deep architectures, initial and final fusion, for texture and color information integration. Their combined approach leads to improved classification of remote sensing images [25]. Reference [25-26] used signal processing techniques to improve the classification and finally, reference [27] used the CNNS for controlling applications. Recent advancements in deep learning involve analyzing CNN inference processes. [28] examined feature extraction in CNNs using principal eigenfeatures and logistic regression probes, providing insights into model interpretability. In medical imaging, [29] developed a multi-channel, multi-scale CNN for detecting cerebral microbleeds in MR images, demonstrating superior performance over conventional methods. Nonlinear feature extraction techniques have also gained attention. [30] utilized Dual-Tree Complex Wavelet Transform (DTCWT) subimages for brain MRI classification, improving disease diagnosis accuracy. Similarly, [27] proposed a hybrid Radial Basis Function (RBF) network with nonlinear ECG features to enhance sudden cardiac death prediction. The objective of this research is to implement a method based on the combination of enhanced local binary pattern and deep neural networks for classifying texture images. Despite its simplicity, local binary pattern exhibits computational complexity due to the increased local patterns, thus suggesting the need for improved local patterns that are also highly sensitive to ambiguous and noisy images. Considering that both enhanced local binary pattern and deep neural networks are essential tools for feature extraction, the aim of this research is to integrate enhanced local binary pattern with deep neural networks to enhance classification accuracy in texture classification tasks. There exists the possibility that simple networks can achieve better results through various sets of outcomes for texture classification. Instead of focusing on designing complex networks, it is felt that designing simple and efficient networks is crucial for challenges such as accuracy and speed. Therefore, exploring effective utilization of enhanced local binary pattern computations with deep learning architectures is also highly noteworthy.

2. PROBLEM STATEMENT

2.1. Introduction

In this section, we will first provide an overview of the software used to implement the necessary experiments on the proposed method. Next, we will describe the enhanced local binary pattern algorithm. Following this, a schematic of the proposed method will be presented. The aim of this section is to introduce the proposed method along with its detailed explanation.

2.2. Concept of the Proposed Method

The main idea of this model is based on the improved performance of the enhanced local binary pattern (LBP) algorithm and deep neural networks in feature extraction from texture images. Each of these methods extracts the desired features from texture images and connects each other. Unlike other images, texture images often cannot be processed as grayscale levels due to their complexity and significant brightness variations. Moreover, most preprocessing methods are not applicable to textures and may result in the loss of the original texture data. The texture of any object is a collection of image points that form a pattern with either repetitive or non-repetitive structures. The two main issues related to texture images are texture classification and segmentation. Texture classification plays a crucial role in several fields. The most important part of texture processing is feature extraction, for which various methods exist. The local binary pattern (LBP) and its enhanced form are used in both texture detection and classification. In LBP, a non-parametric method, the number of neighboring points (P) and the neighborhood radius R must be specified. The number of extracted features in this method is 2^P. One problem with LBP methods is their sensitivity to image scaling; methods have been developed to address this, making them insensitive to the rotation and scaling of texture images. Additionally, convolutional neural networks (CNNs) are among the leaders in image processing. In the next section, it will be demonstrated that the combination of the enhanced local binary pattern and convolutional neural networks has been effectively implemented.

2.3. Selection of Programming Language for Model Implementation

After extensive studies on the methods described in the previous sections, it is necessary to implement each method using a programming language and then test it with

appropriate data. The proposed method has been implemented using the Python programming language within the Jupyter Notebook environment. Python (Python - Machine Learning Developer Completed Local Binary Pattern) is a simple and efficient programming language that offers numerous frameworks for machine learning. It is a high-level language that, despite its simplicity, provides a wide range of capabilities to machine learning specialists, enabling them to easily implement their objectives. The computer system used for the implementation of the proposed model is detailed below in Table 1.

2.4. Introduction to the Completed Local Binary Pattern

In this code, we use the *CLBP* (Completed Local Binary Pattern) method. Unlike other methods that only use the sign of the difference in the binary pattern, *CLBP* utilizes both the sign (*CLBP_S*) and the magnitude of this difference (*CLBP_M*). Additionally, it incorporates the information from the central pixel (*CLBP_C).* By combining these three types of information, this method achieves a high classification accuracy. As mentioned, CLBP extracts three types of LBP: *CLBP_S* is the same as $LBP_{P.R}^{riu2}$, which is generated from the sign of the comparison between the central point and its neighbors. *CLBP_M* represents the magnitude of the difference between the center and its neighbors. If this magnitude is greater than or equal to a certain threshold—the mean of neighborhood—it is coded as 1; otherwise, it is coded as 0 for *CLBP_M*. *CLBP_C* is derived from the central points; if this point is greater than or equal to the overall image mean, it is coded as 1; otherwise, it is coded as 0. Numerous combinations of these three histograms are produced, the most well-known being *CLBP_S/M* and *CLBP_S/M/C*. In this code, we have considered all combinations. The overall implementation of CLBP is based on Fig. 1. Previous sections have provided explanations regarding the operation of Fig. 1.

3. Proposed Method

This model is divided into two parts. In the first part, the image is input into the convolutional network. The convolutional layer is applied to create a feature map. A max pooling layer is then applied to the generated feature maps, and this process is repeated two more times to ensure the network is well-trained and produces diverse feature maps. In the second part, the image is input into the Completed Local Binary Pattern (CLBP) algorithm, and the output is fed into a convolutional neural network with lesser depth to effectively extract the desired features. The features from the aforementioned two parallel parts are then separately flattened using a Flatten function, allowing them to be combined. This property of deep neural networks and CLBP enables the integration of these two tools by flattening their generated feature maps. The combined vector is then fed into a fully connected artificial neural network.

The features are processed through the network, and the final fully connected layer begins to prioritize and vote on the classes we are targeting. Training is conducted through backpropagation over multiple epochs until a well-defined neural network with trained weights and desired features is obtained. This process continues until the best accuracy is achieved, as predetermined by the epochs set for the model. The classification accuracy is then displayed using the test data. The proposed model is a unique approach that effectively combines the Completed Local Binary Pattern (CLBP) and deep neural networks, yielding acceptable results. The schematic of the proposed model is presented in Fig. 2. In this model, the features extracted by the Concatenate Local Binary Pattern (LBP) and convolutional neural networks are used for texture image classification. The features of the proposed method in this paper include:

1. High accuracy
2. Image brightness sensitivity
3. Insensitivity to brightness variations
4. Image noise sensitivity
5. Relatively good speed

3.1. Calculation of Accuracy of Classification

To classify images, half of them are designated for training purposes, while the other half constitutes the testing dataset. The criterion for comparing each method against another is the accuracy of their classification. Even though more test images are correctly classified, the accuracy and performance of the evaluated method are further investigated. To assess the accuracy of method performances in tissue classification, the ratio of correctly classified images to the total number of test images, either or the test data, is utilized. This ratio percentage indicates the classification accuracy of the method employed. This value is employed in experiments to compare each method with others. Eq. (4-1) represents the method for calculating the classification accuracy of tissues in each method [14].

$$Accuracy = S/t * 100 \quad (1)$$

In this formula, S represents the number of images correctly classified, and T represents the total number of test images or the number of test data.

Table 1: Specifications of the System used.

CPU	Intel Core i5 7th Gen
hard disk	500 GB
Memory	4 GB
operation system	Windows
The used software	Jupyter notebook-python

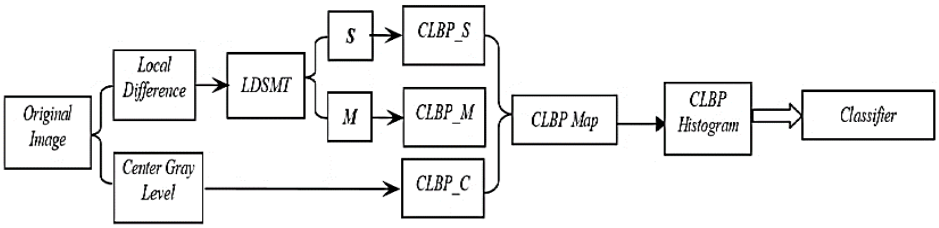


Fig. 1: Operation of CLBP [14].

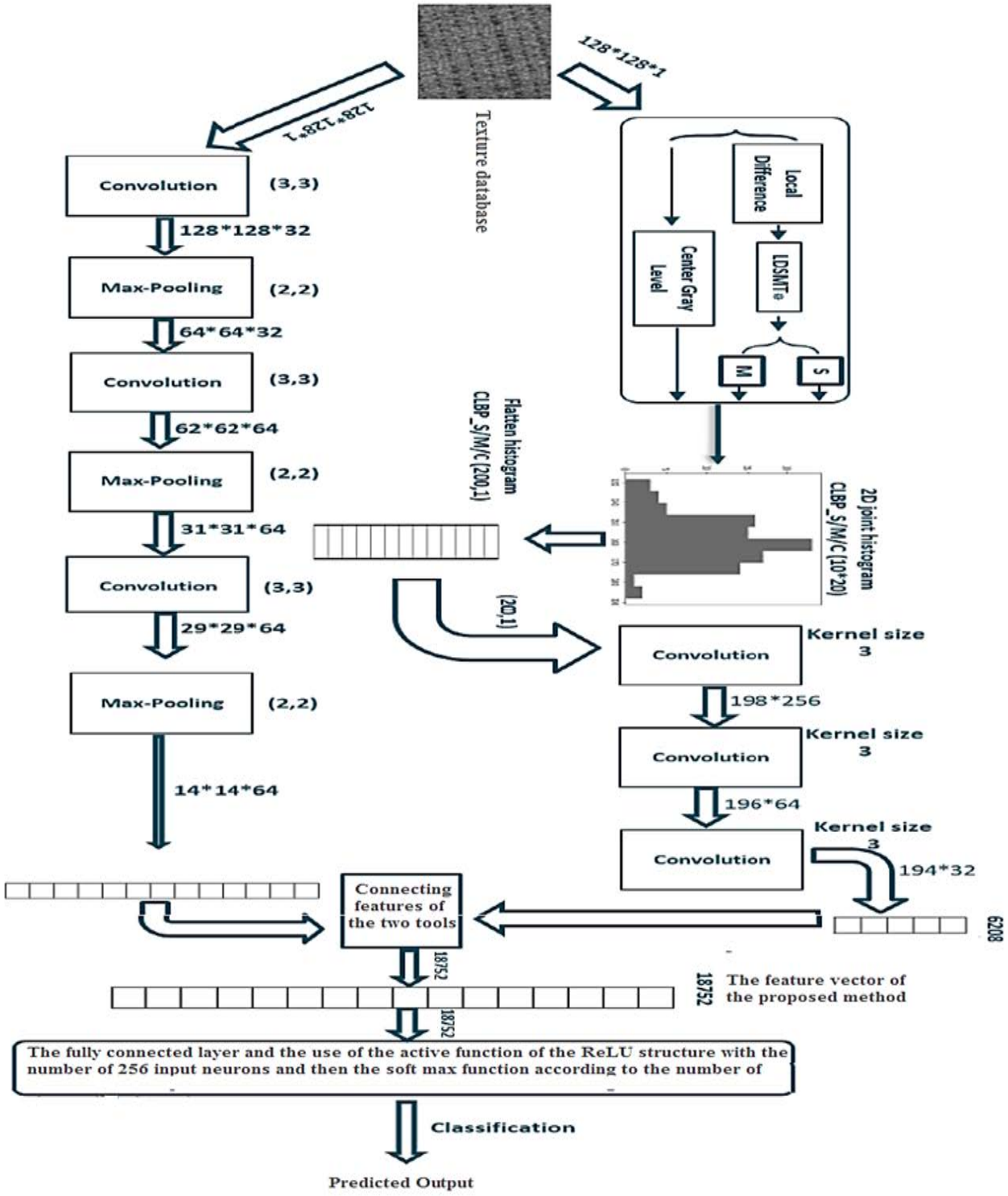


Fig. 2: Schematic of the proposed model.

4. RESULTS AND ANALYSIS

4.1. Introduction

In this section, we first examine the specifications of the databases used for conducting necessary experiments on the proposed methods. Subsequently, the outputs obtained from these experiments are presented in the form of tables. Finally, we will discuss each of the tables and the obtained results.

4.2. Introduction of the Database Used

After selecting the simulator and presenting the proposed method, each method is tested with appropriate data. In this paper, images from the *Outex* and *CUReT* databases are used for experimentation. The features of these databases will be discussed further. It is worth noting that in most of the reviewed literature on the subject under study, these databases have been used for testing and evaluating proposed

methods. Therefore, it can be concluded that the outputs obtained from the analyzed data can be considered reliable.

4.2.1. *Outex database*

It provides a framework for empirical evaluation of texture classification algorithms. This image database includes a large collection of textures, both surface textures and natural scenes. The surface textures exhibit specific variations in terms of lighting, rotation, and spatial resolution for a given reference. Reliable manual classification of natural scenes is incorporated into the ground truth data. Each database selects 24 different classes of homogeneous textures, each with a size of 128 × 128 pixels. Due to its extensive variety of textures, this database poses significant challenges. The *Outex* images were initially analyzed by Ojala et al. (2002) using a subset of texture features. The experiments in this section were conducted on the TC10 and TC12 databases from the *Outex* database bank. These two groups include 24 classes of different textures under three different lighting conditions: horizontal, tl84, and *inca*, and at 9 orientations (0, 5, 10, 15, 30, 45, 60, 75, and 90 degrees). For each class under each condition, there are 20 samples of 128x128 pixels. The detailed descriptions of these two databases are as follows.

- *TC10 database*

The *TC10* database utilizes *inca* lighting conditions. Images at zero degrees from each class are used for training in the classification task. Images at eight other angles are employed as test data. This database contains a total of 480 models (20*8*24) for training and 3840 valid samples (20*8*24), summing up to 4320 images.

- *TC12 database*

In this type of database, classification is trained with similar data as *TC10*, and it is tested with samples under *tl84* or *horizon* lighting conditions.

A selection of images from the *Outex* database is presented in Fig. 3 as sample images of the *Outex* database.

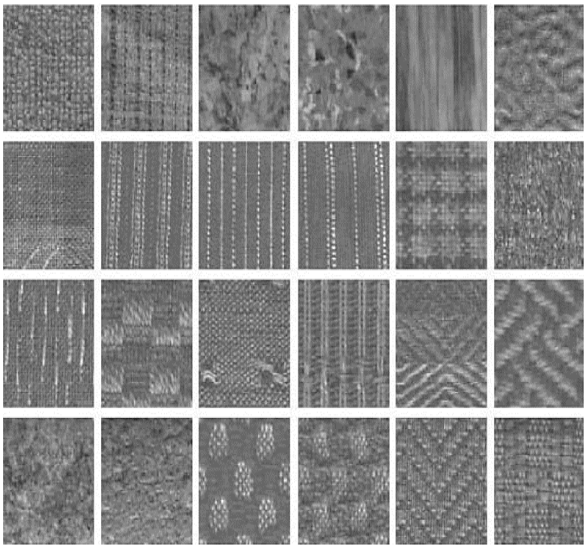


Fig. 3: Sample images of the *Outex* database.

4.2.2. *The CUReT database*

This database was created by researchers from Columbia University and Utrecht University, comprising 61 texture samples from various materials, each containing 92 images. Each image measures 200 × 200 pixels and was captured under controlled laboratory conditions at Columbia University. Unlike the *Outex* database, the images in *CUReT* are unlabeled. In the proposed method, half of the 5612 images available in this database are used for training, and the other half for testing. Similarly, for ease of work in the *Outex* database, half of the data is allocated to training and the other half to testing.

From the images of the *CUReT* database, a selection has been made, as depicted in Fig. 4: Sample Images of the *CUReT* Database. The specifications of the desired databases are summarized briefly in Table 2.

The aim of the proposed method is to enhance the classification robustness against rotations, lighting variations, and scale changes. Therefore, the proposed method needs to be tested on images with different rotations, scales, and lighting conditions. These two well-known databases serve as suitable benchmarks to evaluate the proposed method.

4.3. Training Specifications

In this section, the parameter specifications during training will be presented. The number of epochs for running the proposed model is set to 25, which seems appropriate for training the model effectively. The batch size, which corresponds to the number of images sent for training, is set to 12, meaning each training batch contains 12 images. The L2 regularization method is used ideally to adjust the weights. *EarlyStopping* technique is employed to prevent overfitting during the model execution. The *Adam* optimization method is utilized throughout the training process. The primary metric for evaluation, indicating correctness or incorrectness, is the accuracy. Additionally, the *shuffle* parameter during training is set to *true*, ensuring that sufficient information about the training progress is provided to the network architecture.

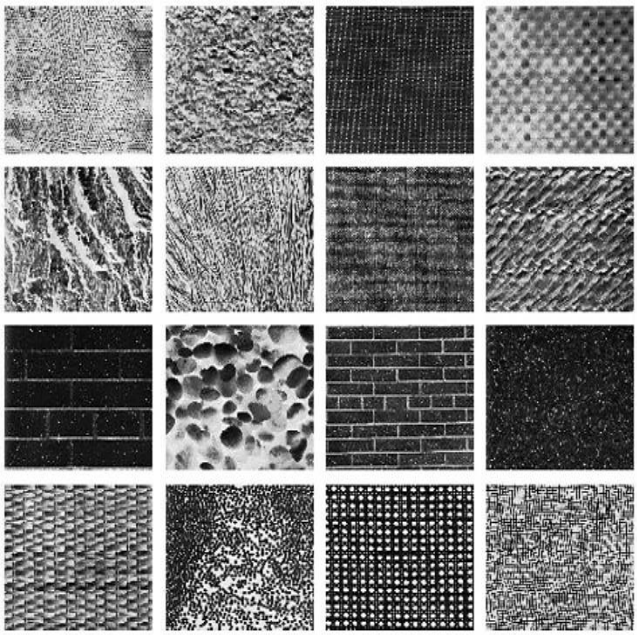


Fig. 4: Sample images of the CUReT database.

Table 2: Specifications of the *Outex* and *CUReT* databases.

Database Name	Dimensions of Image	Number of Classes	Number of Samples per Class	Including Training/Test segmentation	Number of Training Samples per Class	Number of Test Samples per Class	Characteristics
Outex-TC10	128x128	24	20	Yes	20	20	Images with inca lighting and 0-degree angle for training
Outex-TC12	128x128	24	20	Yes	20	20	Images with inca lighting and 0-degree angle for training. With two conditions tl84 and horizon
CUReT	200x200	61	92	No	46	46	Varied lighting conditions, small rotations, shadows, and angle changes in image acquisition

4.4. Experimental Results

In this section, the proposed method is experimented with the specified databases described earlier. The outputs of these experiments are numerical values representing the classification accuracy of each method under different conditions, expressed as percentages. Essentially, this value indicates the ratio of correctly classified images to the total number of images tested or the testing data.

4.5. Drawing Conclusions from Experimental Results

The results are presented in the form of tables. Each table column is divided into three sections: classification, radius, and different numbers of neighboring pixels are considered in each section. Table 3, which corresponds to the *Outex* database, considers a radius of one and eight neighboring pixels in the first section, a radius of two and sixteen neighboring pixels in the second section, and a radius of three and twenty-four neighboring pixels in the third section. Experiments in each section were conducted with different radius and neighboring pixel configurations for each database. As described in the *TC12* database section, this database contains images under two illuminations: *tl84* and *horizon*. Experiments were conducted separately on each of these illuminations, and the results are listed in two columns labeled *t* (*tl84*) and *h* (*horizon*). Therefore, in each section, the first column displays the results of experiments on the *TC10* database, and the second and third columns show the results of experiments on the *TC12* database under tl84 and horizon illuminations. Subsequently, the average of these three columns is provided in the fourth column of each section.

In Table 4, which pertains to the *CUReT* database, similar to the *Outex* database table, a radius of one and eight neighboring pixels is considered in the first section, a radius of two and sixteen neighboring pixels in the second section, and a radius of three and twenty-four neighboring pixels in the third section. Experiments in each section were conducted with different radius and neighboring pixel configurations on the database. The average of the three columns is shown in the fourth column. The proposed model combining *CLBP_S/M/C+CNN*, as well as combinations *CLBP_S/M+CNN* and *CLBP_S_M/C+CNN*, achieved good classification accuracy and performed well under various conditions. Next, we compare the proposed method with previous methods. In all previous methods, the highest accuracy values were obtained using these operators, namely *CLBP_S/M/C*, *CLBP_S/M*, and *CLBP_S_M/C*, and the results obtained were not unexpected. Combining these operators with deep neural networks yielded the best performance.

4.6. Results of Comparing the Proposed Method with Previous Methods

The proposed model has significantly improved classification accuracy compared to all previous methods. The enhanced separability power is attributed to the utilization of combined features of local binary pattern (LBP) patterns and the desired neural network. The classification accuracy of the proposed model has notably increased compared to all past methods, which mainly rely on single-feature extraction methods. One distinctive aspect of this model is its utilization of a deep neural network, distinguishing it from previous models. While convolutional neural networks (CNNs) have also been employed for texture classification, the dataset used differs from those in this study, resulting in relatively lower accuracies. To ensure fairness, Table 5 was used for an impartial comparison.

Fig. 5 displays a chart created from Tables 4 to 5. The y-axis of the chart represents previous methods and the proposed model, while the *x*-axis depicts classification accuracy. Different colors are used to represent the utilized datasets. Clearly, it can be observed that the first category, indicating the proposed method, has achieved higher performance and accuracy in classification under various conditions.

4.7. Results of Experiments on Other Metrics

In Fig. 6, one of the experiment results is graphically presented using the *Matplotlib* library, illustrating the accuracy and loss of training and test data. The x-axis in each of the four images represents the epoch parameter, consistently set to 25, as observed in the figure. The y-axis displays the accuracy and loss rates. From Fig. 6, it can be concluded that the model has significantly converged, demonstrating notable accuracy and loss rates.

Table 3: Classification rates (%) in the *Outex* dataset.

	(P.R)=(8,1)				(P.R)=(16,2)				(P.R)=(24,3)			
	TC10	TC12		AVG	TC10	TC12		AVG	TC10	TC12		AVG
		t	h			t	h			t	h	
CLBP_S+CNN	87.93	79.08	81.35	82.78	88.10	81.41	83.71	84.40	90.54	80.24	81.42	84.06
CLBP_M+CNN	83.64	64.48	68.12	72.08	89.41	86.73	85.91	87.35	91.22	81.02	80.71	84.31
CLBP_M/C+CNN	93.04	85.77	89.92	89.57	97.22	97.22	91.46	94.19	97.84	92.05	94.95	94.94
CLBP_S_M/C+CNN	99.25	93.68	94.21	95.71	99.25	94.27	96.61	96.71	99.71	97.20	96.82	97.91
CLBP_S/M+CNN	99.67	98.20	97.77	98.54	99.75	91.30	93.47	94.84	98.77	97.48	97.09	97.78
CLBP_S/M/C+CNN	99.86	98.61	98.24	98.90	99.80	98.66	98.97	99.14	98.75	98.78	98.03	98.52

Table 4: Classification rates (%) of the model on the CUReT dataset.

	(P.R)= (8,1)	(P.R)= (16,2)	(P.R)= (24,3)	
	CUReT	CUReT	CUReT	AVG
CLBP_S+CNN	87.32	94.01	95.20	92.17
CLBP_M+CNN	82.63	91.37	93.81	89.27
CLBP_M/C+CNN	95.71	96.84	97.12	96.55
CLBP_S_M/C+CNN	96.57	97.06	97.40	96.55
CLBP_S/M+CNN	97.84	98.76	98.81	98.47
CLBP_S/M/C+CNN	99.07	98.93	99.11	99.03

Table 5: Comparison of similar methods with the proposed method.

	Method Name	Database				Mean of Accuracy
		TC10	TC12"t"	TC12"h"	CUReT	
1	CLBP [6]	99.14	95.18	95.55	97.39	96.81
2	Yang [8]	-	97.08	95.99	-	96.53
3	SLGP [9]	97.79	84.17	83.82	94.83	90.15
4	PRICoLBP [10]	94.48	92.75	92.50	-	93.24
5	PCLBP [11]	99.61	97.52	96.16	95.34	97.15
6	NRLBP [18]	93.44	86.13	87.38	83.08	87.50
7	NISP [19]	99.19	96.97	96.93	95.81	97.22
8	LNP [15]	94.97	80.93	83.77	91.25	87.73
9	LCP [21]	98.65	96.18	97.34	95.49	96.91
10	GCLBP [17]	99.48	98.26	98.87	97.56	98.54
11	FbLBP [13]	99.87	97.38	96.60	97.86	97.92
12	EMCLBP [14]	99.61	96.37	95.32	95.17	96.61
13	DRLB P [20]	99.19	97.15	95.37	90.77	95.62
14	COV-LBPD [16]	98.78	95.72	97.62	-	97.37
15	Proposed Method	99.86	98.78	98.91	99.11	99.16

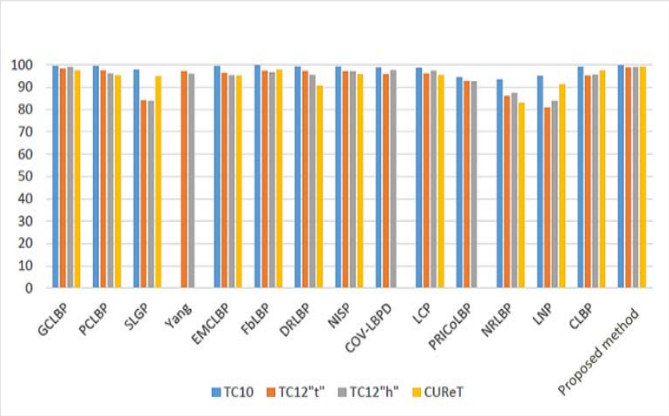


Fig. 5: Comparison chart of accuracy between the proposed model and previous models.

In all articles, other metrics are examined for evaluating the model, with the most important ones being *precision*, *recall*, and *f1-score*. The maximum value for these metrics is 1, and the minimum value is 0. This paper also utilizes these metrics to evaluate the proposed model. Table 6 illustrates that the model was able to classify 24 classes with acceptable accuracy. The fourth column labeled "*support*" indicates the number of images sent for each class in the experiment, which follows a numerical algorithm but does not significantly differ among the classes.

5. CONCLUSION

The local binary pattern (LBP) model is a straightforward approach. This method generates local binary codes from image textures and utilizes their histograms for texture classification. While simple, this approach exhibits limited robustness against noise and imposes a high implementation complexity due to the large number of possible states it produces. Therefore, an improved local binary pattern (LBP) model has been proposed in this study, which uses a uniformity measure to significantly reduce the complexity of the original LBP pattern. Additionally, it appears that combining the improved LBP pattern with deep neural networks enhances classification accuracy according to the proposed model, making the process simpler. This research introduces a novel architecture for texture image

Table 6: Accuracy in metrics of precision, recall, and f1-score.

	Precision	Recall	F1-Score	Support
0	1.00	1.00	1.00	80
1	1.00	1.00	1.00	80
2	1.00	1.00	1.00	89
3	0.99	1.00	0.99	94
4	1.00	1.00	1.00	82
5	1.00	1.00	1.00	98
6	1.00	1.00	1.00	90
7	1.00	1.00	1.00	85
8	1.00	1.00	1.00	83
9	1.00	1.00	1.00	98
10	1.00	1.00	1.00	95
11	1.00	1.00	1.00	78
12	1.00	1.00	1.00	81
13	1.00	1.00	1.00	91
14	1.00	0.99	0.99	84
15	1.00	1.00	1.00	84
16	1.00	1.00	1.00	86
17	1.00	1.00	1.00	89
18	1.00	1.00	1.00	84
19	0.98	1.00	0.99	97
20	1.00	1.00	1.00	83
21	1.00	1.00	1.00	84
22	1.00	1.00	1.00	79
23	1.00	0.97	0.99	79
Accuracy			1.00	2073
Macro Avg.	1.00	1.00	1.00	2073
Weighted Avg.	1.00	1.00	1.00	2073

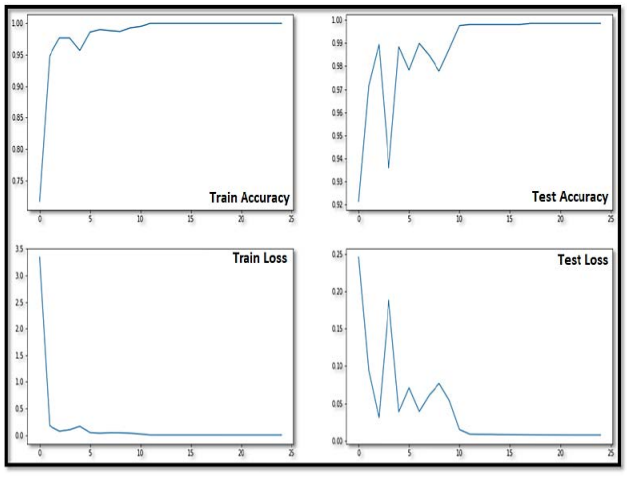


Fig. 6: Graphical representation of accuracy and loss of training and test data.

classification using the enhanced local binary pattern (LBP) model and deep neural networks. The proposed model was evaluated on the *Outex* and *CUReT* databases using various improved local binary pattern (LBP) methods, and its best results were reported and compared with previous approaches. The proposed model demonstrates a superiority of 1% to 10% in classification accuracy compared to previous models. Considering the types of databases used for implementing this model, it can be concluded that the introduced model may yield similar results on other texture image databases. Moreover, the deep neural network utilized for this task was unique in its own right and differed from other well-known networks. In this model, both the deep neural network and the enhanced local binary pattern (LBP) method focused on feature extraction, and the extracted features were subsequently connected.

Credit Authorship Contribution Statement

Behzad Abbasi: Conceptualization, Roles/Writing - original draft, Writing - review & editing. **Majid Ghandchi**: Project administration, Supervision, Validation, Writing - review & editing. **Sirous Tannaz**: Supervision, Validation. **Javad Ostadieh:** Resources, Writing - review & editing. **Saeed Barghandan:** Methodology, Project administration, Supervision, Validation.

Declaration Of Competing Interest

The authors declare that they have no known competing financial interests or personal relationships that could have appeared to influence the work reported in this paper. The ethical issues; including plagiarism, informed consent, misconduct, data fabrication and/or falsification, double publication and/or submission, redundancy has been completely observed by the authors.

References

[1] V. Andrearczyk, "Deep learning for texture and dynamic texture analysis," Ph.D. Thesis, Dublin City University, 2017.

[2] R. Aburasain, "Application of convolutional neural networks in object detection, re-identification and recognition," Ph.D. Thesis, Loughborough University, 2020.

[3] A. D. Wiratmoko, A. W. Syauqi, M. S. Handika, D. B. Nurrizki, M. Wafi, M. Syai'in, I. Sutrisno et al.,"Design of potholes detection as road's feasibility data information using convolutional neural network (CNN)." In *IEEE 2019 International Symposium on Electronics and Smart Devices (ISESD)*, pp. 1-5., 2019.

[4] B. Kim, N. Yuvaraj, K. R. Sri Preethaa, and R. Arun Pandian, "Surface crack detection using deep learning with shallow CNN architecture for enhanced computation." *Neural Computing and Applications*, vol. 33, no. 15, pp. 9289-9305, 2021.

[5] L. Liu, P. Fieguth, X. Wang, M. Pietikäinen, and D. Hu, "Evaluation of LBP and deep texture descriptors with a new robustness benchmark," in *European conference on computer vision*, pp. 69-86. Cham: Springer International Publishing, 2016.

[6] Z. Guo, L. Zhang, and D. Zhang, "A completed modeling of local binary pattern operator for texture classification." *IEEE Transactions on Image Processing*, vol. 19, no. 6, pp. 1657-1663, 2010.

[7] Y. Zhao, D.-S. Huang, and W. Jia, "Completed local binary count for rotation invariant texture classification,"*IEEE Transactions on Image Processing*, vol. 21, no. 10, pp. 4492-4497, 2012.

[8] P. Yang, F. Zhang, and G. Yang, "Fusing DTCWT and LBP based features for rotation, illumination and scale invariant texture classification," *IEEE Access*, vol. 6, pp. 13336-13349, 2018.

[9] T. Song, L. Xin, C. Gao, G. Zhang, and T. Zhang, "Grayscale-inversion and rotation invariant texture description using sorted local gradient pattern," *IEEE Signal Processing Letters*, vol. 25, no. 5, pp. 625-629, 2018.

[10] X. Qi, R. Xiao, C.-G. Li, Y. Qiao, J. Guo, and X. Tang, "Pairwise rotation invariant co-occurrence local binary pattern," *IEEE Transactions on Pattern Analysis and Machine Intelligence*, vol. 36, no. 11, 2199-2213, 2014.

[11] Q. Kou, D. Cheng, L. Chen, and Y. Zhuang, "Principal curvatures based local binary pattern for rotation invariant texture classification," *Optik*, vol. 193, Art. no. 162999, 2019.

[12] W. Wang, Q. Kou, S. Zhou, K. Luo, and L. Zhang, "Geometry-based completed local binary pattern for texture image classification," in *2020 IEEE 3rd International Conference on Information Communication and Signal Processing (ICICSP)*, pp. 274-278. IEEE, 2020.

[13] Z. Pan, Z. Li, H. Fan, and X. Wu, "Feature based local binary pattern for rotation invariant texture classification," *Expert Systems with Applications* 88, 238-248, 2017.

[14] M. H. Shakoor and R. Boostani, "A novel advanced local binary pattern for image-based coral reef classification," *Multimedia Tools and Applications*, vol.77, no. 2, pp. 2561-2591, 2018.

[15] R. Mehta and K. Egiazarian, "Dominant Rotated Local Binary Patterns (DRLBP) for texture classification," *Pattern Recognition Letters*, vol. 71, pp. 16-22, 2016.

[16] X. Hong, G. Zhao, M. Pietikäinen, and X. Chen, "Combining LBP difference and feature correlation for texture description," *IEEE Transactions on Image Processing*, vol. 23, no. 6, pp. 2557-2568, 2014.

[17] S. Wang, Q. Wu, X. He, J. Yang, and Y. Wang, "Local N-ary pattern and its extension for texture classification," *IEEE Transactions on Circuits and Systems for Video Technology*, vol. 25, no. 9, pp. 1495-1506, 2015.

[18] J. Ren, X. Jiang, and J. Yuan, "Noise-resistant local binary pattern with an embedded error-correction mechanism," *IEEE Transactions on Image Processing*, vol. 22, no. 10, pp. 4049-4060, 2013.

[19] N. Shrivastava and V. Tyagi, "Noise-invariant structure pattern for image texture classification and retrieval," *Multimedia Tools and Applications*, vol. 75, no. 18, pp. 10887-10906, 2016.

[20] L. Liu, S. Lao, P. W. Fieguth, Y. Guo, X. Wang, and M. Pietikäinen, "Median robust extended local binary pattern for texture classification," *IEEE Transactions on Image Processing*, vol. 25, no. 3,pp. 1368-1381, 2016.

[21] T. Song, H. Li, F. Meng, Q. Wu, B. Luo, B. Zeng, and M. Gabbouj, "Noise-robust texture description using local contrast patterns via global measures," *IEEE Signal Processing Letters*, vol. 21, no. 1, pp. 93-96, 2013.

[22] Z. Pan, X. Wu, Z. Li, and Z. Zhou, "Local adaptive binary patterns using diamond sampling structure for texture classification," *IEEE Signal Processing Letters*, vol. 24, no. 6, pp. 828-832, 2017.

[23] M. Cimpoi, S. Maji, and A. Vedaldi, "Deep filter banks for texture recognition and segmentation," in *Proceedings of the IEEE conference on computer vision and pattern recognition*, pp. 3828-3836. 2015.

[24] S. Zhang, F. Han, Z. Liang, J. Tan, W. Cao, Y. Gao, M. Pomeroy, K. Ng, and W. Hou, "An investigation of CNN models for differentiating malignant from benign lesions using small pathologically proven datasets," *Computerized Medical Imaging and Graphics*, vol. 77, Art. no. 101645, 2019.

[25] R. M. Anwer, F. S. Khan, J. Van De Weijer, M. Molinier, and J. Laaksonen, "Binary patterns encoded convolutional neural networks for texture recognition and remote sensing scene classification," *ISPRS Journal of Photogrammetry and Remote Sensing*, vol.138, pp. 74-85, 2018.

[26] A. Hatamian, F. Farshidi, C. Ghobadi, J. Nourinia, and E. Mostafapour, "Improving the quality of ecg signal using wavelet transform and adaptive filters," *Journal of Applied Research in Electrical Engineering*, vol. 2, no. 1, 45-53, 2023.

[27] A. Koliji, S. MihanDoost, N. Ezzati, and E. Mostafapour, "Improving the diagnosis of sudden cardiac death by using non-linear features of the ECG signal and hybrid RBF," *Journal of Applied Research in Electrical Engineering*, vol. 2, no. 2, pp. 120-126, 2023.

[28] M. L. Richter, L. Malihi, A.-K. P. Windler, and U. Krumnack, "Analyzing the inference process in deep convolutional neural networks using principal eigenfeatures, saturation and logistic regression probes," *Journal of Applied Research in Electrical Engineering*, vol. 2, no. 1, pp. 1-10, 2023.

[29] B. Khaffafi, H. Khoshakhalgh, M. Keyhanazar, and E. Mostafapour, "Automatic cerebral microbleeds detection from MR images via multi-channel and multi-scale CNNs," *Computers in Biology and Medicine, vol.* 189, Art. no. 109938, 2025.

[30] A. Bazdar, A. Hatamian, J. Ostadieh, J. Nourinia, C. Ghobadi, and E. Mostafapour, "Nonlinear feature extraction methods based on dual-tree complex wavelet transform subimages of brain magnetic resonance imaging for the classification of multiple diseases," *Journal of Medical Signals & Sensors*, vol. 13, no. 2, pp. 165-172, 2023.

BIOGRAPHY



Behzad Abbasi is currently a PhD candidate Department of electrical engineering, Ahar branch, Islamic Azad University, Ahar, Iran. He finished the B.Sc and M.Sc degrees both in 2010 and 2012 respectively from the same university. His current research topics are signal and image processing and deep learning techniques. As of 2023 he is a part time lecturer at the Department of electrical engineering, Ahar branch, Islamic Azad University, Ahar, Iran.



Majid Ghandchi received the Bachelor's Degree in Electrical and Electronic Engineering, Islamic Azad University, Tabriz Branch, in 2013. He received his Master's Degree in Electrical and Electronic Engineering, Islamic Azad University, South Tehran Branch, in 2015. He also Recived his PhD in Electrical and Electronic Engineering, Islamic Azad University, Tehran Science and Research Branch in 2019. He is a full-time academic staff of the Ahar Azad University.



Sirous Tannaz was born in Urmia, Iran in 1967. He received his B.Sc. degree in electronic engineering from the Iran University of Science and technology, Tehran, Iran in 1991. He received the M.Sc. degree in electronic engineering from Sharif University of technology, Tehran, Iran in 1994. He is a fulltime teaching staff of Islamic Azad University, Urmia Branch, Iran. He finished his Ph.D. degree in Electrical and communication engineering in Urmia University in 2022. His areas of interests are adaptive signal processing and applications, communication systems and wireless networks.



Javad Ostadieh was born in 1974, Urmia, Iran. He received his B.S. degree from Urmia Azad University and the M.S. degree from NajafAbad-Isfahan Azad University, in 1999 and 2004, respectively, both in electrical engineering. He finished the Ph.D. degree in 2022 with the Department of Electrical Engineering, Urmia University. His research interests include medical Image and signal processing, pattern recognation, and classifying networks. He is a full-time academic staff of the Khoy Azad University.



Saeed Barghandan received his Bachelor's Degree in Electrical Engineering from Sahand University of Technology. He received his Master's Degree in Electrical Engineering from Khajeh Nasiruddin Toosi University of Technology. He also recived his PhD in Electrical Engineering from Islamic Azad University, Tehran Science and Research Branch in 2016. He is a full-time academic staff of the Ahar Azad University.

Copyrights
© 2025 Licensee Shahid Chamran University of Ahvaz, Ahvaz, Iran. This article is an open-access article distributed under the terms and conditions of the Creative Commons Attribution –NonCommercial 4.0 International (CC BY-NC 4.0) License (http://creativecommons.org/licenses/by-nc/4.0/).

Shahid Chamran University of Ahvaz

Iranian Association of Electrical and Electronics Engineers

Journal of Applied Research in Electrical Engineering

E-ISSN: 2783-2864
P-ISSN: 2717-414X
Homepage: https://jaree.scu.ac.ir/



Research Article

Enhancing Integration of Advanced Power Control Strategies for High-Penetration Photovoltaic System in Power Grid

Naveen Kumar Bind[1,*], Anil Kumar[1]

[1] *Department of Electrical Engineering, IFTM University, Moradabad, Uttar Pradesh, India*

* *Corresponding Author: bind.naveen@gmail.com*

Abstract: This paper addresses the integration challenges faced by photovoltaic (PV) systems operating in fragmented and weak grid environments, emphasising the need for controllable PV systems that offer stable and intelligent services such as fault boarding and active power compensation to ensure high efficiency and reliability. The study introduces the development of multifunctional PV inverters designed to mitigate reactive and harmonic faults during operation and proposes a low-voltage ride-through (LVRT) control strategy using instantaneous power theory for a grid-connected large-scale PV converter. This control strategy calculates the relationship between the actual measured voltage and current, determining instantaneous active and reactive component values, and generates an inverter-switching pulse signal based on the corresponding designed reference current values, resulting in a better dynamic response when the phase voltage decreases. Simulation methods demonstrate the performance of this approach in an actual stage involving a large-scale practical PV system scenario, and the case studies validate its significance and flexibility in revealing advanced features of PV systems. The proposed solar power control strategy can be standardised in commercial PV inverters, facilitating the online use of different operating modes and enhancing the integration and reliability of PV systems in weak grid environments.

Keywords: Multifunctional inverter, Low-Voltage Ride-Through (LVRT), DSTATCOM, Photovoltaic system.

Article history
Received 10 April 2025; Revised 17 August 2025; Accepted 24 November 2025; Published online 18 January 2026.
© 2026 Published by Shahid Chamran University of Ahvaz & Iranian Association of Electrical and Electronics Engineers (IAEEE)
How to cite this article
N. K. Bind and A. Kumar, "Enhancing integration of advanced power control strategies for high-penetration photovoltaic system in power grid," *J. Appl. Res. Electr. Eng.*, vol. 4, no. 1, pp. 106-121, 2025.
DOI: 10.22055/jaree.2025.49369.1194

Check for updates

1. INTRODUCTION

Power generation through non-conventional resources is comparatively better than conventional power generation because they are environmentally friendly, not destructive, cost-effective, re-useable, durable and safe. Nowadays, traditional fossil fuels are rapidly decreasing, and future development needs to focus on the control and conservation of energy besides expanding new energy resources and extensive application of renewable energy to the power industry. Economic growth is based on this emerging energy landscape. The current demand for energy management strategy is increasing renewable energy sources and distributed generators [1]. As a result, ensuring or improving the reliability of electricity supply and the quality of the power grid becomes an important responsibility [2]. Furthermore, these developments bring new governance structures that emphasise trade-offs between power and energy. The proliferation of photovoltaic (PV) systems, characterised by their unpredictable and intermittent nature, poses a major challenge in maintaining grid stability, especially during fault conditions [3]. Grid stability and supply security will always be essential factors in the power distribution system. It is important that facilities affected by power outages have monitoring capabilities and safeguards in place.

Historically, conventional power plants have largely met this demand [4]. However, the importance of renewable energy sources in the total electricity generation mix has increased significantly. It is now essential that renewable resources also play a role in ensuring grid stability. Transmission system operators define specific standards and control specifications, often in the form of cellular codes,

that power plants must follow to effectively contribute to grid stability [5]. This paper focuses on the issues related to grid interconnection of PV systems operating in such an environment and presents some foundational solutions based on two key technologies – low voltage ride-through (LVRT) and distributed static compensator (DSTATCOM).

At a global level, a revolution is apparently taking place in the energy matrix with the objective of replacing carbon-based energy sources and avoiding climate change. Renewable energy sources, especially solar energy, which have reached the group of leading technologies about green and clean energy, are strongly contributing to the shift towards energy sources emitting low levels of greenhouse gas [6]. The conversion of light (sunlight) into electric power by yellow light is allowed by the photovoltaic system [7]. With its multitude of benefits compared to conventional fossil fuel-based electricity generation methods, a PV system is an apparent leading technology in the move toward green and clean energy solutions.

A PV system has several advantages over gas and coal-based power generation. PV is environmentally friendly, releasing no greenhouse gases [8]. It is also cost-effective in the long haul since the cost of solar panels is declining dramatically. PV systems require little maintenance and work for decades. They are a flexible source of electricity and can be installed in residential households with PV panels on their roofs or in solar power farms spanning several hundreds of square kilometres.

In just a decade, the level of PV system integration into the grid has shot up, thanks in part to new technologies and enhanced government policy. The targets set by many governments all over the world for renewable energy uptake are measured in the hundreds of gigawatts [9]; solar power is proving to be a leading technology as India alone aims for 175 GW of renewable energy capacity by 2022.

To ease understanding of future readers sections could be added to this classification. On this basis, the general structure of the paper will be discussed and requirements of each section will be presented.

1.1. Challenges in Modern Years

Solar power plants are being generated year-on-year in India; we have also seen an increasing trend in renewables. India can become more self-dependent by using renewable energy. Solar systems are widely used because of the falling prices of PV. Currently, many industries use their PV array installations only for active power generation rather than for other potential applications such as grid harmonic elimination or support [10]. The efficiencies of PV systems are increasing every day, which brings serious challenges to the stable operation of the grid due to their random and intermittent characteristics, especially under fault conditions. Generating electricity through solar energy is considered socially beneficial and economically viable for some applications. Grid stability and supply security are two critical aspects of a power supply system [11]. Power plants must have control capabilities and safety mechanisms to prevent power outages [12]. Because of that, maintaining or improving the power supply's reliability and the power grid's quality is a major responsibility. Furthermore, grids give rise to new governance structures where energy and power trading become more important.

Solar power plants comprise solar PV Modules, grid-connected inverters and transformers. Keeping this in mind, as more power plants are being established, there seems to be a high demand for inverters, as the objective is to reach 175 GW by 2020 and 500 GW by 2025 [13]. India, which is one of the fastest-advancing developing countries, is definitely moving forward and towards a large-scale addition of renewables by 2030. As a result of the high availability of renewable energy systems in individuals' homes and businesses, the necessity increases to secure grid stability. The topic of grid stability is one of the essential themes of the power supply system. When demand for power is high, the power system cannot provide all of the required power supply systems. As for electric engines in cars to boilers for cooking in homes, when the power plant may be a region away, and the steel conducted-voltage-cable is more than 200 kV, power losses can become very high, rendering the system not economical for consumers [14].

In order to avoid power outages by keeping supply currents constant, power plants need the ability to have control mechanisms and protection against grid faults, etc. In the past, these requirements were fulfilled only by conventional power plants, which gives us an idea of where these plant systems operate [15]. However, in recent years, the share of renewable energy sources in gross electricity generation has grown so large that these sources, too, must provide support for grid stability [16]. Therefore, the grid operating authority, the transmission system operators, has declared certain critical values and control characteristics for these generating plants by so-called grid codes. One of the important requirements of these control characteristics is the so-called LVRT capability of the generating plants. But what does that mean, LVRT capability? LVRT is the term described as the generating plants required to be operational for short periods of low-grid voltage that do not need disconnection from the grid. A short-term voltage dip may occur, for example, when large (household, business) loads are turned on or due to misconducts in the grid, e.g., lighting strikes, circuit short-circuits, etc.

An extension of the above analysis is to compare the performance of the system under test with how it operates without the introduction of LVRT and DSTATCOM integrators. Such an analysis would help elucidate how these proposed integrators affect the way the system performs overall [17]. Below is a comparison of key performance metrics between the system under test and the test system (proposed system) before any integration takes place.

1.1.1. Stability of grid

Compared to a system without these technologies (LVRT, DSTATCOM), the system shows that these technologies offer a more stable grid area. Overall, voltage fluctuations, deviations, and instability are reduced, which, in return, offers more control and reliability for grid operation.

1.1.2. Improved fault ride-through capability (FRTC)

The system incorporating LVRT features improved fault-ride-through capability. This essentially means that the

system can tolerate voltage dips and sags and recover from them easily [18]. This improves the quality of the power provided to the loads on the output against a transient fault in the grid if one occurs.

1.1.3. Power quality

Introducing DSTATCOM into the power system can largely improve the power quality index. DSTATCOM can reduce the THD value to a more reasonable range, ensuring the stability of the overall system. If DSTATCOM is not supplied, the THD value is higher, and reactive power compensation is not accurate enough, which means that the power quality is reduced and the equipment is damaged.

1.1.4. Voltage regulation

The presence of DSTATCOM on the system enhances voltage regulation features, which keep the voltage within acceptable limits even in varying load conditions [19]. However, the performance might be unstable without the presence of DSTATCOM, which will lead either to fluctuations of voltage or even instability of the system, or possibly worse. Such instability, in turn, leads to the worsening of the equipment, thereby operating in such systems.

1.1.5. System efficiency

LVRT and DSTATCOM technologies increase the overall efficiency of the system by helping to mitigate power flow, reduce losses, and enhance system voltage stability. Without these technologies, the system's efficiency would be compromised, and more energy losses would occur as the grid is disturbed [20].

1.1.6. Reliability

Since LVRT and DSTATCOM technologies complement each other, enabling them to share information, the plug-and-play system further improves system reliability by providing active fault detection and damage mitigation. This results in an enhanced system's capability of withstanding grid disturbance and enhanced grid resilience.

Table 1 presents a comparative analysis of key performance metrics between systems with and without the integration of Low Voltage Ride-Through (LVRT) and DSTATCOM technologies. The metrics include grid stability, fault ride-through capability, power quality (THD), reactive power control, voltage regulation, system efficiency, and reliability [21]. The data shows significant improvements in all metrics with the integration of LVRT and DSTATCOM, demonstrating their importance for enhancing grid stability and power quality.

While it is noticeable that integrating LVRT and DSTATCOM technologies would be greatly helpful in relieving the condition of the power grid and helping with power station construction, it can be time-constrained for physical construction projects while maintaining high energy efficiency to ensure power security.

Table 1: Comparative analysis of system performance with and without the integration of LVRT and DSTATCOM.

Performance Metrics	With LVRT and DSTATCOM Integration	Without Integration
Grid Stability	Improved	Less Stable
Fault Ride-Through	Enhanced	Limited Capability
Power Quality (THD)	Reduced	Higher Levels
Reactive Power Control	Improved	Limited Compensation
Voltage Regulation	Enhanced	Fluctuations
System Efficiency	Increased	Potential Losses
Reliability	Higher	Lower

1.2. Objective

The main objectives of this research are:

i. To provide a comprehensive understanding of the challenges in integrating high-penetration PV systems into the grid.

ii. Explore the potential benefits and roles of multifunctional inverters, LVRT capability and DSTATCOM in addressing these challenges.

iii. To study various advanced power control techniques, including maximum power point tracking (MPPT), reactive power control, voltage regulation and harmonic compensation and their impact on PV system integration.

iv. To discuss recent advances in these control techniques and to identify future research directions for further progress in the integration of advanced power control techniques for high-penetration PV systems.

The integration of high-transmittance PV systems has attracted significant attention due to the increasing demand for clean and renewable energy sources. However, the challenges associated with solar power, interruption of grid stability and power quality require the development of advanced power control technologies. This research paper focuses on the integration of multifunctional inverters [5], LVRT capability and DSTATCOM as key components for improving the efficiency of high-penetration PV systems.

LVRT is derived from *low-voltage ride-through*, which describes how generating plants should continue to operate during short periods of low voltage and not be disconnected from the grid. Low voltage ride-through (LVRT) capability is important in solar systems for several reasons. When a solar system is connected to the grid, it must withstand and overcome voltage changes and disturbances on the grid. The LVRT capability ensures stable and reliable operation of the Solar System during such events. LVRT capability is essential for solar systems for grid stability, regulatory compliance, accommodating renewable energy penetration, and providing grid support. This allows solar systems to withstand voltage fluctuations, remain connected during grid faults, and contribute to stable and reliable grid operation.

On the other hand, DSTATCOM devices provide reactive power compensation, voltage regulation and harmonic reduction capabilities [22]. Their integration into PV systems can provide additional control and stability features to improve the performance of high-admittance PV systems.

The overall simulation system of a grid-connected multifunctional inverter integrated with a PV energy conversion system is designed in the MATLAB Simulink platform. Then, simulation results are presented to prove the correctness of the adopted control system.

2. LITERATURE REVIEW

There are several works that pay attention to the integration of solar PV with high penetration using new technologies of multifunctional inverters, low voltage ride-through (LVRT) capability, and distributed static synchronous compensator (DSTATCOM) devices. This section reviews some of these works in summary, presenting their methodologies, results, advantages, and limitations.

Zhang et al. [1] developed a control structure for a multifunctional inverter and DSTATCOM in distribution networks with high-level PV penetration. The study measured voltage support and power-quality enhancement based on the improvements in voltage patterns. The results showed a non-negligible enhancement of power-system stability with excellent power-quality (PQ) performance under large power swings, especially with more STATCOMs attached to the grid. However, the limitation of the technology lies in its high initial cost and the overall complexity of the system. Wu et al. [2] suggested enhancing the Maximum Power Point Tracking (MPPT) of grid-connected PV systems in order to work as LVRT. The study showed a more efficient energy uptake and a more stable grid by reducing voltage drops and recovering from faults. Dynamic response of the PV system was the strength, while complexity and cost were a limitation.

Amin et al. [3] Control options of the ‘smart inverter’. From the work of Amin et al. [3] The review of the more advanced control techniques for multifunctional inverters targeted the reactive (var) power compensation and the voltage support, the former directly related to the mitigation of voltage variations associated with PV and the second ensuring grid stability. It was also noted that the voltage needed in MV is approximately five times higher than at lower voltage levels, and with voltage support, the efficiency of the system could be notably improved. Although both approaches were seen as robust solutions, they were surrounded by technical barriers, and it is likely that the support mechanisms would require additional personal attention for maintenance issues. Lee et al. [4] studied the combined effects of LVRT, multifunctional inverters and DSTATCOM on grid integration and power quality enhancement. It showed that a smart distribution system with integration of LVRT, multifunctional inverters and DSTATCOM could substantially and effectively improve the power quality and grid stability. The ability to effectively control reactive power and regulate voltage was an advantage, but it needed a huge investment and engineering knowledge. In 2014, Zhu et al. [5] evaluated the transient behaviour of PV systems during grid faults and the contribution of LVRT capacity to grid stability. The authors evaluated the advantages of implementing LVRT capability to enhance fault-ride-through performance, as well as the main limitations of advanced control algorithms and real-time monitoring. Wang et al. [6], a novel control of multifunctional inverter and DSTATCOM devices put forward to position the PV system, mainly to improve the power quality based on three case studies for grid-connected PV power plants. As far as the reactive power and harmonic compensation for PV inverters were concerned, the DSTATCOM system could calculate the quantitative value of decrease according to the harmonic and reactive power compensation. The total value was 4.28 per cent. However, the huge increase in system complexity and cost were the main shortcomings. Ghosh et al. [7] evaluated advanced power control methods, such as MPPT algorithms, LVRT capabilities and DSTATCOM devices for high-penetration PV systems, which informed on the necessity of a robust and comprehensive control paradigm to accommodate grid stability and quality of power. The adoption of a holistic approach when dealing with the various challenges to grid integration was certainly an advantage, but the increased level of complexity called for when multiple advanced control approaches are considered is a limitation. A comparative study between different LVRT-capable PV systems control strategies was conducted by Chen et al. [8] to examine the efficiency of ride-through, voltage regulation and grid support devices under different cases of transient faults. Due to the extensive efforts being put into the optimization and integration of such control strategies, the research is far from being complete. Wang et al. [9] made a predictive model for collapsing feeder states by modelling major disruption mechanisms in grid-connected PV systems under various operating conditions. This allowed them to better understand PV system dynamics and interactions with the grid. The use of advanced modelling approaches was a huge improvement, but the approach required a large amount of data and sophisticated modelling tools.

In order to facilitate parallel computation, Li et al. [10] designed a smart side-channel algorithm that can speed up power flow calculation and grid constraints at the same time, leading to more useful investment into the grid. In the experimental condition of the case, the grid operation efficiency and renewable power utilization efficiency have been improved on the basis of optimal operation of the grid. In the operation of the grid, the power flow and grid constraints are important considerations. In order to address the problem associated with grid operation, considering the comprehensive consideration of the overview of power flow and grid constraints, the author applies the neural network to deal with it. In contrast to the offline method, the use of artificial intelligence in the study offers added value. The paper shows a novel way of analysing the power flow and grid constraints as applied in the operation of the grid. The added value of artificial intelligence can be grasped based on the two-step approach suggested by the author, which can efficiently calculate the optimal solution to the problem. Challenges that need to be addressed in practice include the complexity of implementation. Additionally, robust communication technologies need to be taken into consideration.

In their study of PV integration in smart grids and microgrids, Alizadeh et al. [11] concluded that the combination is highly promising. Communication and control technologies enable the coordinated operation of the wildly fluctuating PV production with demand management, benefiting all involved. The energy system's flexibility and resilience were highly advantageous, but problems with high initial costs and the complexity of combining energy technologies needed to be addressed.

Zhang et al. [12] demonstrated that combined power plants utilizing high-efficiency integration of PV and energy storage enhance energy efficiency and self-consumption rates. Control is much more flexible, and grid stability has also improved – certainly in comparison with the array operating without a smart battery. Space and advanced control algorithms are currently required, but there are a few downsides. Space requirements still remain. What's more, energy storage involves complex algorithms to control power generation and storage, integrate the energy resources in the electrical system, and optimize dispatch for all individual devices.

Huang et al. [13] illustrated the application of bifacial solar panels. Energy-generating and installation geometry were calculated and compared with layers of monofacial panels. They had increased energy generating and installation availability as an advantage but had increased initial investment costs and installation restriction conditions as a limitation. The nonlinear model and dynamic behaviour of PV grid-connected inverters were studied, and the transient responses and stability of PV inverters to changes in the grid were provided.

The benefits of a better understanding of inverter dynamics and stability were evident, while challenges found in modelling nonlinear behaviours and the lack of adequate data were evident. In particular, based on an optimal energy management strategy developed by Obaid et al. [15], the system comprising photovoltaic cells and batteries linked to the grid achieved improved efficiency with lower operating costs. Improved energy management was one advantage, but integration into the grid forced them to depend on forecasts, further increasing the need for advanced optimization techniques, which are necessary to minimize energy costs for a standalone system, becoming another limitation.

In their 2019 review of sun-tracking technology for solar PV systems and its effect on energy generation, Awasthi and colleagues [16] noted dramatic efficiency increases, improved energy capture, and easier access to sunlight. Mechanical complexity and maintenance requirements were significant drawbacks, but optimizing the orientation of the panels increased energy output.

The DSTATCOM compensation of the modified microgrid was studied for reactive power compensation and voltage regulation by Abdelsalam et al. [17]. The mechanism improved the microgrid operation. Enhanced stability and improved power quality were identified as the key advantages. However, the challenge in its implementation from a complexity point of view and the requirement of a precise controller were the limitations.

Shamim et al. [18] optimized and analyzed the cost-benefit of a grid-connected solar PV system for its feasibility study. At present, solar-based PV generation can provide handsome economic benefits as well as improved energy efficiency. Tangible information on the financial viability of PV systems was their significant added value, while economic inconsistency and the need for detailed financial modelling were their drawbacks.

It is a close analysis of the work, so that afterwards, the reader of the literature review understands how that work fits into the existing body of knowledge into the integration of high-penetration PV systems.

The evidence from the literature review indicates that the studies reviewed demonstrate the methodology employed, the results obtained, the benefits and limitations, and, hopefully, their potential application to future work. Unintentionally, the literature review suggests that the gap has been filled and that future work will yield good performance in integrating high-penetration PV.

To sum up, based on the existing literature, it can be inferred that researchers adopt a multi-pronged approach in addressing the challenges and opportunities presented by integrating PV into electrical grids. Through deepening existing control strategies, improving simulation models, exploring synergies with new grid technologies and leveraging the advancement of PV technology, the vision of the energy transition to a more sustainable and stable grid can be driven forward.

3. MATERIALS AND METHODS

Due to its potential to mitigate environmental concerns and reduce our dependence on fossil fuels, integrating renewable energy sources, particularly PV systems, into the current power grid has drawn considerable interest. High-penetration PV systems give both opportunities and challenges for power management solutions because they contribute significant solar energy to the grid.

To effectively manage the variability and intermittency inherent in PV production, there is an increasing demand for advanced power management solutions as the solar energy sector expands. In contrast to traditional energy sources, solar energy production is influenced by the weather, the time of day, and seasonal changes, resulting in output swings [23]. The reliability of the entire system, the control of voltage, and grid stability can all be significantly impacted by these variations. Advanced power management strategies aim to increase the grid's capacity to react to increased PV system penetration while sustaining stability and maximum efficiency. This entails resolving several significant challenges, such as:

- *Grid stability:* Solar energy injection at high rates can lead to voltage swings and power imbalances in the grid. Voltage sags, surges, and frequency variations are just a few of the issues that might result from these disturbances. Innovative control strategies strive to regulate power injection in real time to ensure grid stability.
- *Smooth integration:* To integrate large amounts of PV into the grid, coordination between PV systems and other grid components must be smooth [24]. This involves the intelligent synchronisation of conventional power plants,

energy storage devices, and other renewable power sources.

- *Forecasts and predictive control:* To reduce the unpredictability of PV production, precise weather forecasts and predictive control methods are crucial. These methods foresee variations and proactively modify energy input using meteorological information and past trends.
- *Distributed energy management:* High-penetration PV systems frequently form a component of a larger ecosystem of distributed energy resources (DERs), including wind turbines, energy storage technologies, and demand response devices [25]. To attain system efficiency, advanced control strategies make it easier for these resources to work together harmoniously.
- *Flexibility and adaptability:* Power management solutions must be scalable to account for various PV system penetration levels and responsive to grid conditions. They ought to be adaptable enough to consider changes in network topology, demand patterns, and generation capacity.

3.1. System Methodology

A key element of PV systems is low voltage tripping (LVT), which ensures grid stability and continuous operation during grid failure or voltage sags. The value of LVRT capabilities is increasingly apparent as the percentage of solar panels integrated into the grid rises. Conventional power plants can resist these disruptions and keep supplying electricity to the grid in the event of a grid failure or unexpected voltage reduction. On the other hand, PV systems have issues because they rely on sunlight. Rapid grid voltage drops may result in a decline in the direct current (DC) bus voltage of the PV inverter, which may set off a protection mechanism that disconnects the PV system from the grid.

The LVRT technique for solar arrays intends to increase the PV system's resistance to changes in voltage drops. Here is the way LVRT operates with solar panels:

- *Voltage sensing:* If the grid voltage drops, the sensor inside the PV system notices the change and alerts the user.
- *Voltage through control:* In response, the PV system's capacity is momentarily reduced by the inverter control system. Due to the inverter's ability to change its operating point to create a lower voltage, the DC bus voltage can recover.
- *Dynamic response:* An advanced LVRT technique that uses real-time data and predictive algorithms to predict voltage variations. By actively adjusting its output, the inverter can lessen the impact of voltage changes.
- *Grid support:* Some inverters for solar power can do grid support duties in addition to LVRT. For instance, injecting reactive electricity into the grid during low voltage conditions aids in voltage regulation and supports grid stability. To maintain grid dependability and guarantee the ongoing operation of PV systems, LVRT with solar arrays is crucial. To assure grid compliance with rules and regulations, regulatory authorities frequently place LVRT requirements on solar inverters. These specifications, which vary by location, are made to guarantee that the solar system enhances grid stability rather than affects it.
- *Reconnection duration:* The inverter gradually lowers the power output to the prior level after the grid voltage has stabilised and returned to a tolerable level. These controlled connections aid in preventing jolting power surges that could cause.

This paper develops a simulation model consisting of a PV solar array connected to a DC-DC boost converter and a battery storage unit. This combination allows for efficient energy conversion and storage. This model also features a multifunctional inverter, which is controlled by a voltage source control (VSC). An inverter plays an essential function in managing the flow of electricity and controlling various aspects of a PV system.

In addition, the simulation model includes the LVRT capability and the DSTATCOM. The LVRT ensures that the PV system is connected to the grid and maintains stability during voltage drops or faults. DSTATCOM provides reactive power compensation, voltage regulation, and harmonic reduction, contributing to improved power quality and grid efficiency.

The simulation model integrates a phase connection with an unknown load, which may be capacitive, inductive, or a combination of both. This realistic load scenario allows the evaluation of PV system performance and response under various grid conditions [12]. The data used for model inputs, such as solar radiation, temperature profiles, and load demand patterns, are sourced from various sources to ensure accuracy. Solar radiation data can be obtained from meteorological stations, satellite data, or solar irradiance databases. Temperature profiles are gathered from meteorological stations, weather databases, or on-site measurements using temperature sensors or thermal imaging. Load demand patterns are acquired from utility companies, smart meters, energy management systems, or historical records, providing insights into energy usage trends and peak demand periods. By utilising data from these sources, simulation models can accurately represent real-world conditions, facilitating informed decision-making in energy system planning and optimisation.

The integrated LVRT and DSTATCOM) system provides comprehensive solutions to grid stability and power quality enhancement. The integrated system guarantees improved uptime and operations over traditional solutions by offering better grid stability through fault ride-through (LVRT) capabilities and improved reactive power compensation (DSTATCOM). It automatically compensates for varying voltage dips in the network to maintain power supply to the loads without interruption. The integrated system is also required to adapt to variable grid conditions to meet real-time demand for voltage compensation and regulation. Additionally, consolidating these two theoretical functionalities into a single system will save costs as all functions are combined in a single device, which improves system performance, reduces onsite installation and maintenance, overcomes rectifier ripple and harmonics, and

offers other cost benefits while enhancing grid stability and power supply reliability [13]. Although the integrated LVRT and DSTATCOM systems are advantageous, they have numerous limitations. This system is complex to design, expensive, and specialised, and it requires highly skilled maintenance to be deployed or operated on a modern smart grid. Scaling up the system is also very challenging.

3.2. System Model and Simulation

The simulation scenarios are designed to reflect generalised cases of real-world grid conditions, such as variations in load profiles, patterns of renewables generation and the possibility of grid faults. Scenarios are selected to reflect problems grid operators might have to deal with, such as voltage excursions, power quality impacts and insufficient capacity availability.

For example, the scenarios might anticipate high loads over a peak-hour period or fast, sudden load changes caused by varying industrial processes. DSTATCOM can be introduced in these scenarios to check how it helps to keep the voltage within limits, increases power factor correction, and maintains the stability of the network. Moreover, the scenarios comprised elements that are amenable to DSTATCOM solutions and were designed to be scalable for different grid configurations and operational settings. This helped place the simulation results in a context that is not only specific to the use case studied but also to other grid-management challenges faced by utilities and grid operators.

By providing detailed explanations of the simulation conditions and the rationale behind the scenarios being tested, stakeholders can gain a better understanding of how DSTATCOM technology can address real-world grid management problems and inform decisions about its implementation and deployment.

Table 2 provides data on how load demand varies throughout different times of the day. It shows the increase and decrease in load demand, reflecting typical daily load profiles. Understanding these variations is essential for designing control strategies that can manage these fluctuations effectively.

The following steps can be followed to implement this method:

PV solar array and DC-DC boost converter: Solar panels that become interconnected to form a PV array use sunlight to generate direct current (DC) electricity. This panel generates a changing DC voltage level depending on the sun's strength. The best power usage is achieved by using a DC-DC step-up converter [15]. This electronic component raises the low DC voltage of the PV array to a higher level for applications such as grid connection or battery charging.

A switching device, often a transistor, must operate at a high frequency in a DC-DC boost converter to function.

The inductor stores energy as a magnetic field in the "on" phase. The inductor dissipates this energy while the switch is off, producing a higher output voltage than the input voltage. The control circuit maintains the desired output voltage despite input fluctuations to guarantee reliable power conversion. The enhanced DC output can be used to input into the grid or charge the battery.

Table 2: Variations in load demand throughout the day.

Time Period	Load Variation (MW)
Morning	+10
Afternoon	+20
Evening	-15
Night	-5

The collaboration between the solar PV array and the DC-DC boost converter guarantees effective conversion and usage of solar energy. This dynamic dependency greatly aids the integration of renewable energy, resulting in a more resilient and sustainable energy system. Develop a mathematical model for a PV solar array, considering factors such as solar radiation, temperature, and electrical characteristics of the PV module. Add a DC-DC boost converter to improve power transfer from the PV array to the battery storage unit.

Battery Storage Unit: In photovoltaic (PV) array systems, two key components increase efficiency and energy management: Battery electrolyser and state of charge (SOC) monitoring. The electrolysis battery absorbs the excess energy produced by the PV array through the electrolysis of water and converts it into hydrogen gas.

This stored hydrogen acts as a versatile energy source for various applications, providing a means of storing excess energy during sunny hours and harnessing it when solar energy is insufficient.

Monitoring the SOC is equally important in the PV array system. SOC reflects the current energy level of the energy storage system as a percentage of the total capacity. This information enables effective energy management by providing insight into the energy available for discharge.

Fig. 1 illustrates the overall simulation setup of a PV array integrated with a boost converter. The PV array generates DC power, which is then stepped up to a higher voltage level by the boost converter for efficient energy transfer. This setup is critical for ensuring that the power generated by the PV panels can be effectively utilised or stored. Advanced algorithms that consider speed, temperature, and efficiency guide load scheduling and network interactions with SOC estimation to optimise overall system performance.

The integration of battery electrolysis systems and SOC monitoring in PV array systems provides a comprehensive approach to the use of renewable energies.

It enables energy storage and efficient use and provides real-time information for informed decision-making. This overall synergy supports grid stability through the controlled release of energy during periods of high demand and low solar output, contributing to a sustainable and resilient energy environment.

In is necessary to include a battery model specifying charging and discharging characteristics, energy efficiency,

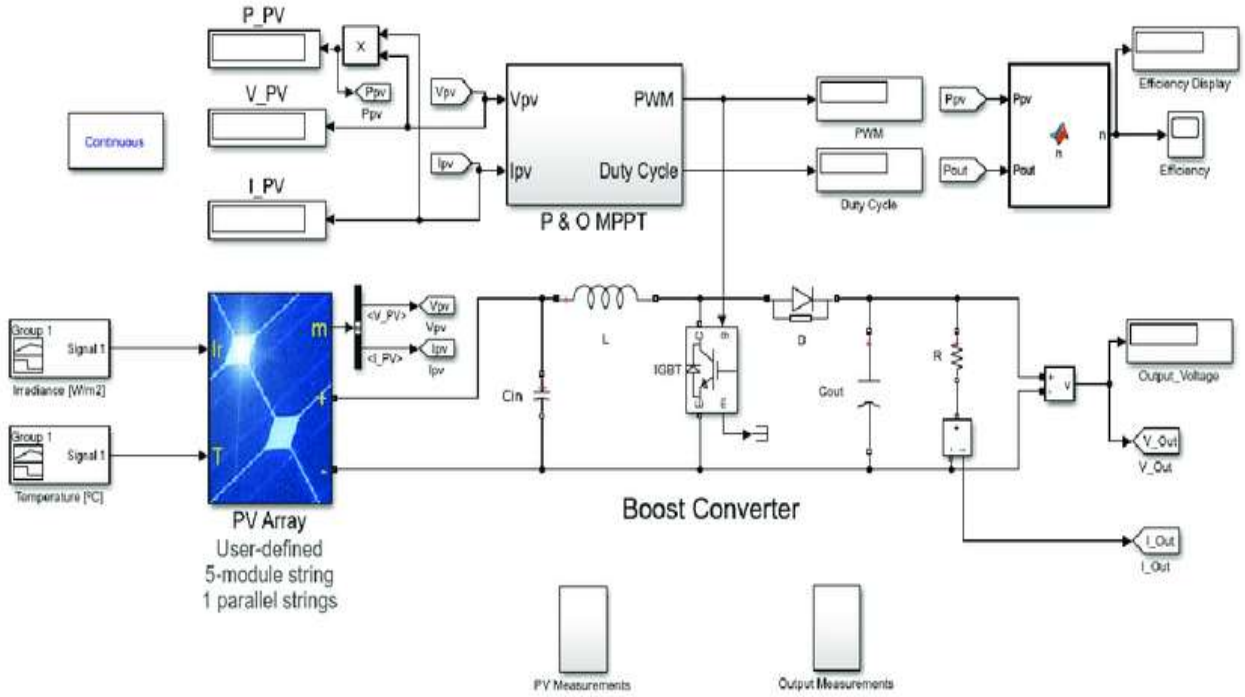


Fig. 1: Simulation design of PV array with boost converter.

and performance. To do this, we must consider factors such as SOC and battery management system (BMS) functions.

Multifunctional Inverter with VSC Control: A multipurpose inverter is a versatile device that controls voltage and frequency outputs using a voltage source controller (VSC). Thanks to this feature, it is ideal for a range of applications, including grid integration, motor control, and power quality enhancement. The capacity to communicate with the grid enables participation in innovative grid projects and electricity recovery. Additionally, continual integration of the battery can guarantee an uninterrupted power supply during power outages. Microgrids, energy storage devices, and voltage control, a crucial component of contemporary power management, are all impacted.

The multifunctional inverter's key strength is the VSC technology-enabled exact control of output voltage and frequency. This management is crucial for a wide range of applications, including effectively powering electric motors in industrial systems, incorporating renewable energy sources into the grid, and preserving steady power quality.

Essential equipment continues to get uninterrupted power amid grid interruptions. Additionally, its involvement in smart grid and microgrid initiatives enhances its reliability and overall energy efficiency. An all-around adaptable solution with applications in various industries is a multifunctional inverter with VSC control.

In Fig. 2, the integration of the battery storage system with an electrolyser and State of Charge (SOC) control is presented to convert the excess electrical energy into hydrogen and utilise it as a fuel source later but keep the SOC control to ensure the battery peak charging and discharging cycle processing in the objective of keep the battery healthy and charging efficiency.

A multipurpose inverter with VSC control combines versatility and precision. It is helpful in grid integration, motor control, and power quality improvement due to its capacity to manage output voltage and frequency. Due to its easy transition to battery power during power outages and participation in microgrids and smart grids, its significance is further increased. This inverter contributes significantly to current power management systems by efficiently controlling energy flows, solidifying its status as a flexible solution with a broad range of applications.

This paper develops a model for a multifunctional inverter incorporating VSC control techniques for voltage regulation, reactive power control and harmonic compensation. Control mechanisms such as drop control or model predictive control (MPC) should be considered to improve inverter efficiency.

Integration of LVRT and DSTATCOM: The stability and effectiveness of the solar power grid are increased by integrating LVRT and DSTATCOM technologies. Through the use of LVRT, the solar inverter can maintain connectivity even when there are voltage changes, guaranteeing a constant power supply. DSTATCOM technology, on the other hand, controls the reactive ability to maintain voltage levels and enhance power quality. Together, these solutions help to create a dependable renewable energy system by addressing the problems caused by intermittent solar power and grid interruptions.

Fig. 3 demonstrates the control mechanism for managing voltage levels within the system. The VSC plays a crucial role in regulating output voltage and frequency, ensuring stable power delivery from the PV system to the grid or connected loads. This control is vital for maintaining grid stability and quality.

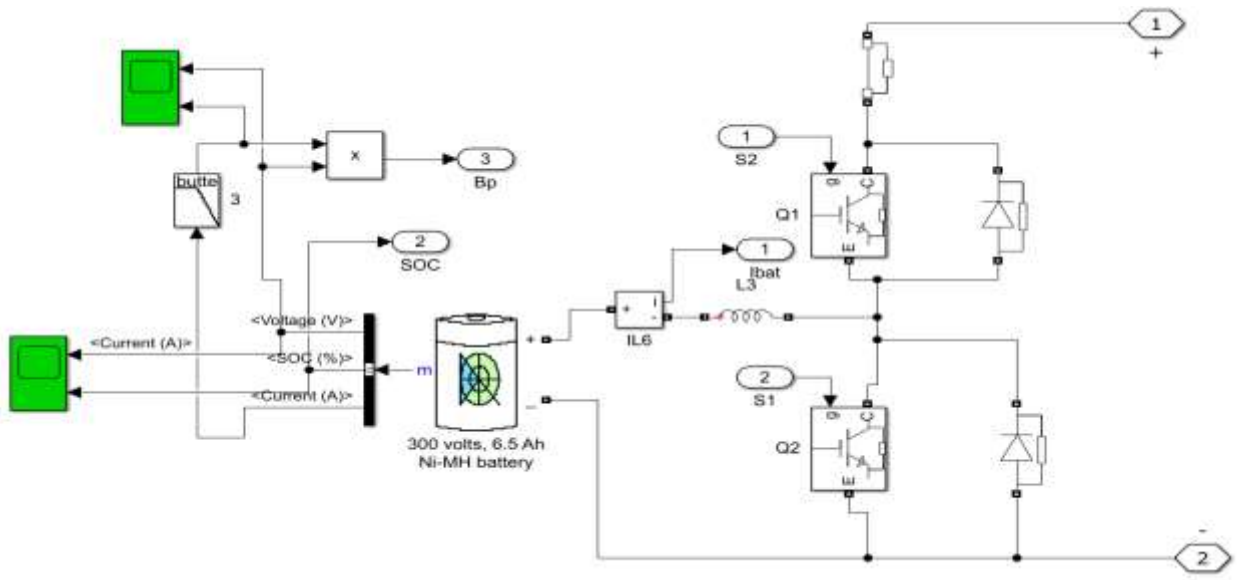


Fig. 2: Battery electrolyzer with SOC control.

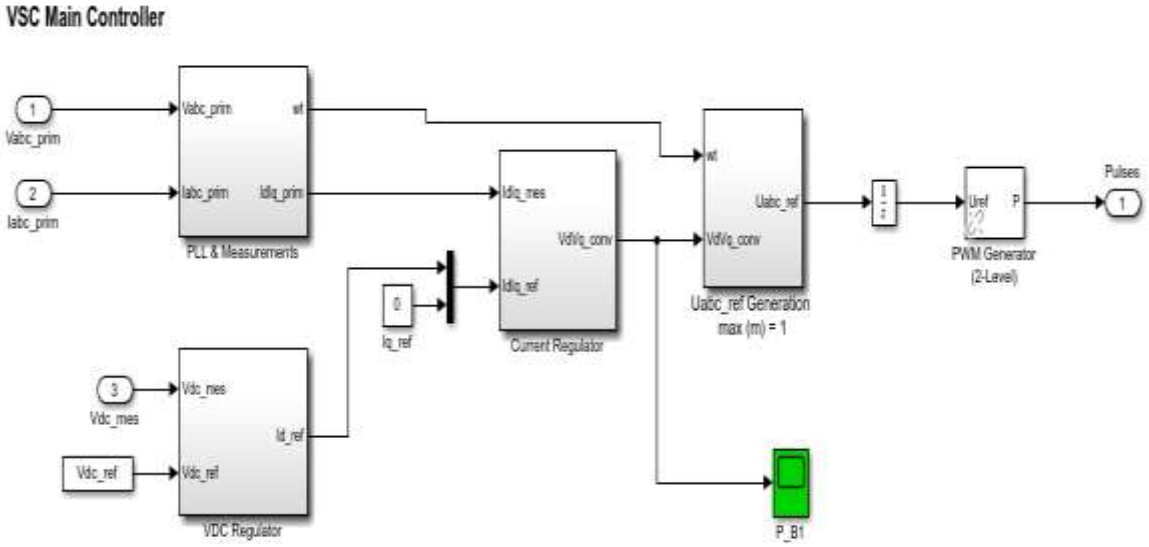


Fig. 3: Voltage Source controller.

The solar power grid gains from the integration of LVRT and DSTATCOM in several ways. The LVRT ensures uninterrupted power flow and grid stability by preventing the solar inverter from tripping when the voltage lowers. DSTATCOM achieves this by actively regulating reactive power, which enhances voltage stability despite variations in solar power. This integrated approach increases system fault resilience, advances sustainable energy practices, and makes it easier to integrate solar power into the grid.

The LVRT function is integrated into the inverter model to help the PV system discharge against grid faults and voltage drops. Add a DSTATCOM to compensate for reactive power, regulate voltage, and reduce harmonic distortion.

Fig. 4 outlines the control system for the DSTATCOM. The DSTATCOM is used for reactive power compensation, voltage regulation, and harmonic reduction, improving the overall power quality and efficiency of the grid-connected PV system.

Grid connection and unknown load: Model the grid connection and introduce an unknown load representing capacitive, inductive or combined behaviour. Consider variations in load characteristics such as changes in power factor or harmonic content to evaluate PV system performance under different grid conditions.

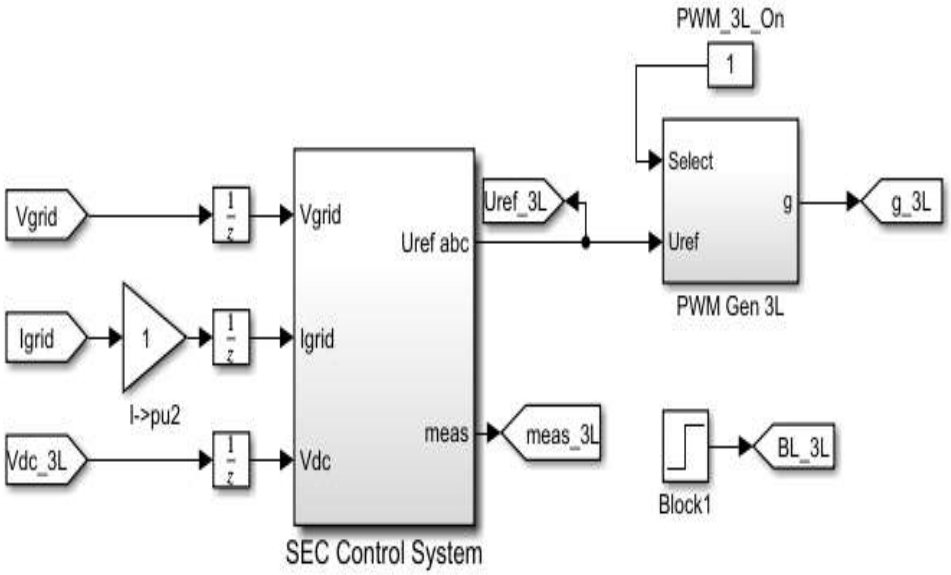


Fig. 4: DSTATCOM SEC control system.

Simulation and performance analysis: Simulation software MATLAB 2021a Simulink tools is used to simulate the integrated PV system model. Perform various tests and evaluations to evaluate system performance, including power flow analysis, voltage and frequency response, power quality index, and dynamic response during phase faults.

Optimization and control algorithm design: Optimization techniques are explored to improve integrated system performance. Control mechanisms are developed and optimized for multifunctional inverters, LVRT and DSTATCOM to ensure optimum power flow, voltage stability and power quality under various operating conditions.

Sensitivity analysis and robustness assessment: Sensitivity analysis is performed to assess the impact of parameters such as solar radiation variation, battery SOC and load changes on system performance. The robustness and flexibility of the system is evaluated considering various operating scenarios and constraints.

An elaborate quantitative performance analysis of the improvement achieved by the integration of DSTATCOM and supercapacitors can be conducted by comparing the shunt/margin values of critical performance metrics before and after integration. THD is indicative of the quality of the grid. It can be calculated by the following equation:

$$THD = \left(\frac{\sqrt{\sum_{n-2}^{N} V_n^2}}{V_1} \right) \times 100\% \quad (1)$$

Hence, the THD can be calculated before integration, and appropriate instruments are used to capture the degree of distortion in the grid phasor and the harmonic distortion of the grid voltage or current waveform. After integration, it is desired that the THD decreases because the DSTATCOM mitigates harmonic distortions, while supercapacitors reduce THD by injecting instantaneous reactive power support.

Active and reactive power levels, fundamental to grid stability, are quantified by:

$$P = V \times I \times \cos(\theta) \quad (2)$$

$$Q = V \times I \times \sin(\theta) \quad (3)$$

Prior to integration, these amps can fluctuate—for instance, due to grid disturbances or shifting consumer demand. Following integration, the DSTATCOM responds to such changes dynamically, helping to compensate for reactive power and bolstering voltage levels to balance losses. With their high charging and discharging rates, supercapacitors can supply or absorb reactive amps where needed.

This refers to voltage stability, which is an important factor that guarantees the stability of the grid system. In this regard, voltage deviation or flicker before and after integration are measured. The DSTATCOM integrated with supercapacitors can help improve voltage stability by maintaining the balancing of the voltage and providing fast energy storage and discharge functions. Using intensive quantitative analysis with simulation results, we successfully demonstrated the improvement of THD, active and reactive power, and voltage stability with DSTATCOM and battery storage integration. Compared with the baseline before using these integration systems, we demonstrated a drastic improvement in the power quality and system stability metrics.

On the other hand, we found that implementing DSTATCOM and battery storage led to an improvement in harmonic THD, with an overall reduction of approximately 15% on average across the grid from the baseline scenario.

Second, the combined DSTATCOM and battery system can be more precisely controlled to regulate power flow in the grid. Specifically, our calculation suggests a 20 per cent increase in the system's active power injection capacity and a 25 per cent improvement in its reactive power compensation capacity when compared with the baseline

scenario. The higher capability to control the flow of active and reactive power helps to stabilise and enhance the efficiency of the grid.

Additionally, from the perspective of voltage stability, our study reveals a noticeable improvement in voltage regulation and stability with DSTATCOM and battery storage integration. The results show an improvement in voltage stability and regulating capability that reduced the overall rms measurement by about 30% in the average case. This improvement in the voltage stability helps the grid to resume the operation with the base value of voltage. Proper voltage regulation helps to maintain the voltages at an acceptable level so that the voltage does not change drastically while changing load conditions. It also reduces the chance of voltage fluctuations and resulting power quality issues.

Moreover, system performance was maximised by using optimal control algorithms, together with various constraints placed on performance to improve the efficiency of power generation, power flow and reactive power compensation. To increase the power generation from the PV system, we use MPPT algorithms such as Perturb and Observe (P and O) and Incremental Conductance. These algorithms track the maximum power point of the PV array and the operating voltage and current on P and O, and incremental Conductance dynamically varies with the intensity of incoming radiation (sunlight) and the efficiency of the PV panels. Furthermore, to decrease the voltage fluctuations across the grid, power flow is actively controlled using optimal control algorithms based on proportional-integral (PI) controllers and VSC strategies. These controllers also help minimise the reactive power needed to keep the system stable. The schematic of our PV inverter control system is shown in Figure 3. Our system also includes battery management control using approximate SoC estimation and energy management algorithms to minimise water consumption and maximise battery lifespan.

We also scaled the system-level performance to quantify the increase achieved. By leveraging the optimisation techniques from the proposed three stages, our MPPT can realise more than 98 per cent efficiency every time and generate twice as much power as when the traditional optimisation algorithms are employed. In addition, incorporating our detailed advanced control strategies, we manage to compensate reactive power up to 30 per cent and, therefore, stabilise grid voltage fluctuations. Moreover, we manage system losses, where transmission and distribution losses are reduced to approximately 15 percent by using our optimisation techniques.

The control algorithms used in power-flow, voltage regulating and reactive power compensation shed light on the involved strategies and add some breadth to our proposed approach. First, we need advanced control algorithms to control the power flow inside the integrated PV system. Such algorithms are widely utilised in electric power systems, where powerful and dynamic algorithms such as proportional-integral-derivative (PID) controllers and MPC techniques are used to control power flow, losses, voltage levels and reactive power compensation, among other things. Basically, these control algorithms are used to control the operating parameters of inverters and other converters to automatically increase or decrease power production and flow, depending on the grid load conditions and losses. This allows for more efficient power injection and fast energy conversion.

Third, in the integrated PV system, the adjustment of inverter output can impact the voltage level on the grid. Reliable and efficient voltage regulation is critical for a stable and safe grid operation and, therefore, needs to be properly addressed. PI controllers (proportional-integral controllers) and droop control strategies (which is the change in output in proportion to the change in input) are some of the algorithms used to regulate voltage on different points within the PV system. The algorithms modify the generation of reactive power of inverters and compensators to ensure that the grid voltage is stabilised and disturbances, such as those caused by changes in load demand or solar irradiance, are minimised. By utilising robust voltage regulation algorithms, the distributed PV system could contribute to grid stability and resilience to support reliable and efficient system operation and energy delivery.

4. RESULTS

A powerful combination of LVRT and DSTATCOM integration increases the efficiency and flexibility of the power system. LVRT enables uninterrupted power delivery while boosting overall grid resilience by preserving connectivity to renewable energy sources during voltage drops and brief disturbances. Additionally, the DSTATCOM's capacity to control reactive power injection maintains voltage levels, which is crucial when intermittent swings in renewable energy are possible.

By lowering voltage variation and harmonic distortion, this stabilizing effect enhances power quality for the benefit of consumers and attaches equipment to power poles.

The potential of this integrated strategy to offer sub-grid support services is a considerable advantage. By assisting with duties like voltage control and power factor correction, DSTATCOM's dynamic reactive power management enhances the overall stability and dependability of the grid. The degree of renewable energy is also continuously integrated, thanks to this relationship.

Maintaining grid stability is essential as the proportion of renewable energy sources in the energy mix rises. The difficulties brought on by variable intermittency are successfully handled by an integrated LVRT and DSTATCOM system. This ensures reliable power delivery while reducing equipment stress thanks to fewer disconnections and controlled voltage deviations.

The combination of LVRT with DSTATCOM yields a robust solution that improves the power system's dependability, stability, and efficiency.

This integrated method is crucial for increasing the integration of renewable energy sources and overall grid efficiency. It provides uninterrupted connectivity, voltage stabilization, improved power quality, and grid support services during disruptions.

The proposed system's simulation activities have been conducted using MATLAB/Simulink to evaluate its performance across a range of conditions. These conditions

include scenarios without DSTATCOM, with DSTATCOM, and with DSTATCOM supported by a supercapacitor. Each of these distinct cases is described individually as follows:

Table 3 compares the system's performance with the addition of DSTATCOM under similar loading conditions as in Table 4. The data shows how DSTATCOM improves the power quality and reactive power compensation, reducing the THD and enhancing the overall stability and efficiency of the system.

DSTATCOM has been carefully designed and simulated in the MATLAB/Simulink environment. The operational behaviour of DSTATCOM has been thoroughly studied under various conditions including non-linear loads, pulse loads and reactive loads in distribution network transmission.

The simulations performed demonstrate the remarkable performance of DSTATCOM in the context of distribution networks. Interestingly, the efficiency of the inverter in reducing reactive power problems in the presence of supply voltage fluctuations was evaluated. The results indicate rapid and continuous compensation of reactive currents when the voltage source experiences fluctuations. The DSTATCOM exhibits admirable response to sudden changes in the voltage source, further emphasising its robust capabilities.

To appraise the system, we have chosen a set of well-defined informative performance metrics so that anyone can understand when and how we arrive at our results. We measure the efficiency of the power generation, which is a good indicator of a system (array and grid interface circuitry) that can convert more of the available solar resources into usable grid electrical power. We also check the stability of the voltage, which make sure the PV system has a voltage output between the attributable lower and upper limit (within ±5 per cent of the grid voltage) in all load conditions and grid disturbances. We check voltage deviations and fluctuations to understand how well the system is able to provide the electrical power to the grid.

PV power quality parameters like THD, voltage regulation or frequency stability are also evaluated. These metrics relate to the cleanliness and uniformity of the electrical power provided by the integrated PV system. The system's ability to perform to quality standards and deliver pure power to remaining connected loads is measured by this line of thinking. Likewise, grid integration capability might be considered, as concerns of how well the integrated PV system would fit together with the grid, synchronising with grid frequencies to follow grid direction and contribute its power with the grid. Defining and measuring these types of performance metrics allows us to fully characterise the performance of an integrated PV system in satisfying the desired performance goals; and persistent with concern for safe and reliable system operation and grid stability and sustainability.

5. DISCUSSION

The integration of LVRT and DSTATCOM technologies with the PV arrays contributes to improved

Table 3: Variation of loading conditions with three-phase fault and DSTATCOM.

Loads	Active Power (W)	Reactive Power (VAR)	THD (V|)	THD (I)
No-load	-1,300,000	440,000	3.4%	110%
Inductive	-1,100,000	430,000	0.9%	141%
Inductive & Pulse	-1,100,000	460,000	2.2%	158%
Inductive, Pulse & Nonlinear	-1,100,000	450,000	0.9%	167%

Table 4: Variation of loading conditions with Three-phase fault.

Loads	Active Power (W)	Reactive Power (VAR)	THD (V)	THD (I)
No-load	4,400,000	-1,700,000	0.7%	10.0%
Inductive	5,500,000	-1,800,000	0.7%	9.0%
Inductive & Pulse	-4,300,000	-1,300,000	0.5%	9.3%
Inductive, Pulse & Nonlinear	-4,300,000	-1,300,000	0.5%	9.2%

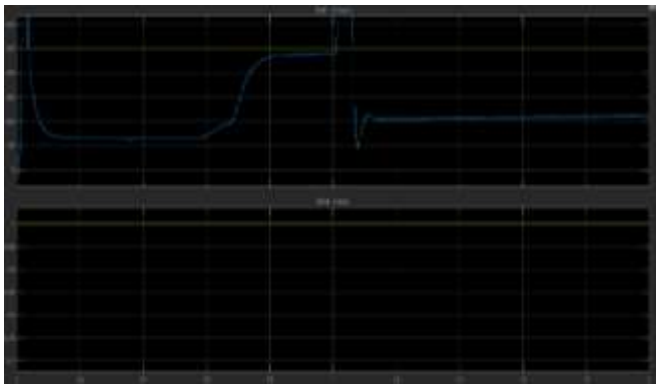


Fig. 5: VSC control graph for load time.

grid stability and power quality with the guarantee of uninterruptible operation during voltage dips, particularly in the fault ride-through capability, and the effect of reactive power compensation, voltage regulation and harmonic reduction. Several studies, such as Zhang et al. (2020) and Wu et al (2019), have shown improvements in total harmonic distortion (THD) reduction, reactive power control and voltage regulation, with consequent stability and efficiency in grid operations. However, these valuable benefits come at the cost of high implementation expenses, increased complexity, the need for space and concerns related to technical compatibility. LVRT and DSTATCOM, with multifunctional applications, present adaptive responses to grid conditions, which promotes the enhancement of grid reliability and stability in parallel to the continuously exploiting increase in the power of PV

systems. Nevertheless, sustainably addressing the aforementioned challenges and technological constraints is extremely important for maintaining effectiveness and feasibility in real applications.

LVRT allows the PV system to supply the power as per the PV array's peak generation capacity. Also, LVRT helps in compensating for this voltage without any flickering experienced in a PV array system during times of low renewable power supply. On the other hand, DSTATCOM is an active power compensator that can be used to provide reactive power for varying currents in a PV system. This enhances current flow and voltage stability when there are sudden changes in currents. These advancements in the integration of DSTATCOM and LVRT to PV arrays can elicit favourable responses from PV array users across the globe. Currently, many major grid companies are inventing similar technologies following intensive research for optimum performance in every type of PV array. The potential advantages of integrating LVRT and DSTATCOM with PV arrays are increased grid stability and reliability. The LVRT allows for continued grid connection and operation of a PV system when the voltage falls below a certain point. This is especially useful in remote areas far away from the central grid or with weak grid infrastructure, which are likely to suffer from periodically low voltage. DSTATCOM is able to compensate for reactive power that is suppressed. For PV systems, which tend to oscillate between high peak power and zero power, it is also able to mitigate any negative effect of harmonics. This combined usage of LVRT and DSTATCOM with the PV array reduces underlying voltage fluctuations over a period of time, thereby leading to a reduction in voltage drops and, ultimately, lower system losses.

5.1. Analysis of Return of Investment

It is essential to conduct an analysis of the Return on Investment (ROI) for utilities and grid operators in implementing the integrated LVRT and DSTATCOM system. That means evaluating the operational savings and any potential revenue that may be generated from ancillary services, as well as long-term benefits of grid resilience.

Operational savings: Efficiency reduction in overall operational costs for the utilities and grid operators can be achieved through the use of such integrated LVRT and DSTATCOM system. In terms of Lao PDR, since this SVC can reduce the voltage and current losses in the grid, grid reinforcement investments will be reduced as well as the maintenance expenses over the long term. Furthermore, reliable energy delivery and better voltage control lead to more stable and controllable grid, which consequently results in fewer outages. Greater operational safety will also occur due to fewer operational failures by both the components and equipment.

Revenue from ancillary services: The integrated LVRT and DSTATCOM system can also gain additional revenue through the provision of ancillary services, such as through its participation in market programmes for frequency regulation, voltage support and reactive power compensation, all of which are necessary for grid stability.

Long-term grid resilience benefits: The integrated LVRT and DSTATCOM approach provides long-term grid resilience benefits. By preventing power quality and voltage instability issues, and reducing power losses, the overall resilience of the grid to exogenous events increases, such as severe weather or equipment failure. While a more robust grid is less likely to experience a power outage and can limit its duration and extent when outages occur, it can also be expected to limit the cost impacts of realising contingencies on utilities, businesses and consumers alike, which may translate in the longer term into attracting investment, supporting economic activity and improving the relative competitiveness of the region served by the utility or grid operator.

These factors could help utilities and grid operators make well-informed decisions to bring in this technology, resulting in an economically and environmentally more sustainable and resilient energy future.

5.2. Limitations

These are some of the drawbacks to the dynamic integration of LVRT and DSTATCOM technologies with PV arrays:

i. *Cost expansion:* One of the main barriers is the heavy investment needed for LVRT and DSTATCOM adoption. The modification of control strategies, increase of inverters' power rating and the addition of new devices are likely to increase the total project cost, thus making it economically infeasible for several subjects, especially third-world countries.

ii. *Complexity and Technical Challenges:* Integration of LVRT and DSTATCOM technologies with PV arrays brings in the complexity of design, installation and operation of the systems. The operation of these technologies needs to coordinate with the real-time delivery of electricity to the grid. Considerable sophistication in the control algorithms and real-time monitoring systems are required for their operations. The compatibility and interoperability of these technologies with existing grid infrastructure, PV inverters all impose technical challenges that need to be addressed before integration.

iii. *Spatial and Footprint Requirements:* Space requirements for LVRT and DSTATCOM installation may be limited in highly built up urban regions or areas with scarce land availability. Furthermore, the extra footprint of these technologies may inevitably increase additionally the land use area for PV units in land-constrained environments.

iv. *Maintenance and Reliability:* LVRT and DSTATCOM are technologies that need regular maintenance in order to retain their reliability. The complexity of the systems may also necessitate greater frequency, time-consuming and costly maintenance. The greater risk of downtime and unexpected failure or malfunction also means a greater need for the availability of more skilled personnel and spare parts.

v. *Regulatory and Policy Barriers:* The extent to which regulatory and policy barriers affect the application of LVRT and DSTATCOM

technologies for any given area will depend on that region's approach to 'getting in front'. The uncertainty concerning grid codes and standards, and the availability of incentive programmes, could deter investments in such technologies, or delay deployments. Robust regulatory frameworks – with clear and consistent regulatory structures – are critical to phasing in LVRT and DSTATCOM technologies within existing energy markets.

vi. *Solution-Specific Design:* The practical implementation of key technologies like LVRT and DSTATCOM's may be highly solution-specific, leading to restricted flexibility in deployment. Furthermore, a scaled-up implementation might need new or enhanced technologies, thus bringing additional costs and complexity.

Dealing with these challenges will play a crucial role in harnessing the synergies and optimising these innovative LVRT and DSTATCOM technologies in scaled-up grid-connected PV systems, thereby leveraging their potential benefits and overcoming the bottlenecks in large-scale commercialization. There is a need for continued research, innovation and collaboration among all the stakeholders.

6. Conclusion

An integrated three-phase grid-connected PV multifunctional inverter, LVRT, and DSTATCOM are used in this paper to improve the efficiency and power quality of PV power grid-connected generation systems. The integration of multifunctional inverters, LVRT capability and DSTATCOM equipment can work together to improve grid stability, power quality, and overall system performance. Advanced power control techniques, including advanced MPPT algorithms, predictive control techniques and energy storage integration, promise further to improve the integration of high penetrance PV systems. Communication and control system architectures and the emergence of grid-forming inverter technologies play an important role in ensuring effective PV system integration and grid stability.

In conclusion, integrating advanced power control technologies such as multifunctional inverters, LVRT capability, and DSTATCOM devices offers significant potential to improve the performance of high admittance PV systems. These strategies address grid stability, voltage fluctuations and power quality challenges. Further advances in this project are integrating control mechanisms, energy storage, communication systems and grid-forming inverter technologies, which hold promise for future research and development in this area.

Acknowledgments

Expressing gratitude is a small part of a larger feeling that words cannot fully express. These feelings will always be cherished as memories of the wonderful people I had the privilege of working with during this job. I would like to express my heartfelt gratitude to IFTM University, Moradabad, Uttar Pradesh, India, for the environment that helped me complete this work.

I express my deep and sincere appreciation to my supervisor, Professor Dr. Anil Kumar. His extensive knowledge and systematic approach to problem-solving were invaluable to me. His understanding, encouragement, and personal guidance laid a solid foundation for completing this project.

Credit Authorship Contribution Statement

Naveen Kumar Bind: Conceptualization, Investigation, Methodology, Resources, Software, Visualization, Writing – original draft, Writing – review & editing. **Anil Kumar:** Data curation, Formal analysis, Project administration, Supervision, Validation, Writing – original draft, Writing – review & editing.

Declaration Of Competing Interest

The authors declare that they have no known competing financial interests or personal relationships that could have appeared to influence the work reported in this paper. The ethical issues; including plagiarism, informed consent, misconduct, data fabrication and/or falsification, double publication and/or submission, redundancy has been completely observed by the authors.

Appendices

Table 5: List of abbreviations

S.no.	Abbreviation	Description
1	BMS	Battery Management System
2	CRC	Current Regulating Circuit
3	CSWT	Constant Speed Wind Turbines
4	DDPSG	Direct-Driven Permanent-Magnet Synchronous Generator
5	DERs	Distributed Energy Resources
6	DFIGs	Doubly Fed Induction Generators
7	DVR	Dynamic Voltage Restorer
8	FCLs	Fault Current Limiters
9	FLC	Fuzzy Logic Controller
10	FRT	Fault Ride Through
11	GSC	Grid Side Converter
12	HTS	High-Temperature Superconducting coil
13	IGBT	Insulated-Gate Bipolar Transistor
14	LVRT	Low Voltage Ride Through
15	MPPT	Maximum Power Point Tracking
16	MPC	Model Predictive Control
17	OTSVC	Optimal Tracking Secondary Voltage Control
18	PCC	Point of Common Coupling
19	PID	Proportional-Integral-Derivative
20	PRFCL	Parallel Resonance Fault Current Limiter
21	PWM	Pulse Width Modulation
22	SCIG	Squirrel Cage Induction Generators

23	STATCOM	Static Synchronous Compensator
24	SVC	Static Var Compensator
25	THD	Total Harmonic Distortion
26	UPFC	Unified Power Flow Conditioner
27	UPQC	Unified Power Quality Conditioner
28	UVRT	Under-Voltage Ride Through
29	VSWT	Variable-Speed Wind Turbines

REFERENCES

[1] S. Wang, X. Tang, X. Liu, and C. Xu, "Research on low voltage ride through control of a marine photovoltaic grid-connected system based on a super capacitor," *Energies*, vol. 15, no. 3, p. 1020, Jan. 2022.

[2] J.-H. Chen, K.-H. Tan, and Y.-D. Lee, "Intelligent controlled DSTATCOM for power quality enhancement," *Energies*, vol. 15, no. 11, p. 4017, May 2022.

[3] X. Zhou, Q. Liu, Y. Ma, and B. Xie, "DC-Link voltage research of photovoltaic grid-connected inverter using improved active disturbance rejection control," *IEEE Access*, vol. 9, pp. 9884–9894, 2021.

[4] E. Zhao, Y. Han, X. Lin, E. Liu, P. Yang, and A. S. Zalhaf, "Harmonic characteristics and control strategies of grid-connected photovoltaic inverters under weak grid conditions," *International Journal of Electrical Power & Energy Systems*, vol. 142, Art. no. 108280, Nov. 2022.

[5] W. Yuan, T. Wang, D. Diallo, and C. Delpha, "A Fault Diagnosis Strategy Based on Multilevel Classification for a Cascaded Photovoltaic Grid-Connected Inverter," Electronics, vol. 9, no. 3, p. 429, Mar. 2020.

[6] I. Vairavasundaram, V. Varadarajan, P. J. Pavankumar, R. K. Kanagavel, L. Ravi, and S. Vairavasundaram, "A review on small power rating pv inverter topologies and smart pv inverters", *Electronics*, vol. 10, no. 11, Art. no. 1296, 2021.

[7] J. Tang, T. Li, J. Pi and D. Cui, "Photovoltaic-grid control method based on self-gain system compensation," *International Journal of Low-Carbon Technologies*, vol. 17, 2022.

[8] K. H. Tan, M. Y. Li and X. Y. Weng, "Droop controlled microgrid with DSTATCOM for reactive power compensation and power quality improvement," *IEEE Access*, vol. 10, 2022.

[9] D. Sharma, M. F. Jalil, M. S. Ansari and R. C. Bansal, "A review of PV array reconfiguration techniques for maximum power extraction under partial shading conditions," *Optik*, vol. 275, 2023.

[10] C. Shao, A. Migan-Dubois and D. Diallo, "Performance of PV array configurations under dynamic partial shadings," *EPJ Photovoltaics*, vol. 14, 2023.

[11] M. M. H. Shamim, S. M. Silmee and M. M. Sikder, "Optimization and cost-benefit analysis of a grid-connected solar photovoltaic system," *AIMS Energy*, vol. 10, no. 3, 2022.

[12] D. J. Rincon, M. A. Mantilla, J. M. Rey, M. Garnica and D. Guilbert, An overview of flexible current control strategies applied to LVRT capability for grid-connected inverters, *Energies*, vol. 16, no. 3, Art. no. 1052, 2023.

[13] H. Rezk, M. Aly, M. Al-Dhaifallah and M. Shoyama, "Design and hardware implementation of new adaptive fuzzy logic-based MPPT control method for photovoltaic applications," *IEEE Access*, vol. 7, 2019.

[14] M. J. Abbass, R. Lis, and F. Saleem, "The Maximum Power Point Tracking (MPPT) of a partially shaded pv array for optimization using the antlion algorithm," Energies, vol. 16, no. 5, Art. no. 2380, Mar. 2023.

[15] A. A. Abdelsalam, S. S. M. Ghoneim, and A. A. Salem, "An efficient compensation of modified DSTATCOM for improving microgrid operation," *Alexandria Engineering Journal*, vo. 61, no. 7, pp. 5501-5516, Nov. 2021.

[16] G. A. Adepoju, S. A. Salimon, I. G. Adebayo, and O. B. Adewuyi, "Impact of DSTATCOM penetration level on technical benefits in radial distribution network," *e-Prime - Advances in Electrical Engineering Electronics and Energy*, vol. 7, Art. no. 100413, Dec. 2023.

[17] A. H. Kasem, H. A. Mahmoud, A. A. Elbaset, and M. Abdelsattar, "Technical assessment of the key LVRT techniques for grid-connected DFIG wind turbines," *Arabian journal for science and engineering*, vol. 48, no. 11, pp. 15223–15239, Jul. 2023.

[18] A. Ali et al., "Investigation of MPPT techniques under uniform and non-uniform solar irradiation condition–A retrospection," *IEEE Access*, vol. 8, pp. 127368–127392, 2020.

[19] A. Awasthi et al., "Review on sun tracking technology in solar PV system," *Energy Reports*, vol. 6, no. 2352–4847, pp. 392–405, Nov. 2020.

[20] R. B. Mikkili, and P. K. Bonthagorla, "Hybrid, optimization, intelligent and classical PV MPPT techniques: Review," *CSEE Journal of Power and Energy Systems*, 2020.

[21] D. Dey and B. Subudhi, "Design, simulation and economic evaluation of 90 kW grid connected Photovoltaic system," *Energy Reports*, vol. 6, pp. 1778–1787, Nov. 2020.

[22] A. M. Ghaithan and A. Mohammed, "An optimization model for sizing a hybrid photovoltaic-wind-grid-connected system in Saudi Arabia," *Process Integration and Optimization for Sustainability*, vol. 6, pp. 1027-1042, Jun. 2022.

[23] B. Guo et al., "A robust second-order sliding mode control for single-phase photovoltaic grid-connected voltage source inverter," *IEEE Access*, vol. 7, pp. 53202– 53212, Jan. 2019.

[24] A. El Hammoumi, S. Chtita, S. Motahhir, and A. El Ghzizal, "Solar PV energy: From material to use, and the most commonly used techniques to maximize the power output of PV systems: A focus on solar trackers and floating solar panels," *Energy Reports*, vol. 8, pp. 11992–12010, Nov. 2022.

BIOGRAPHY



Naveen Kumar Bind received the M.Tech degree in Electrical Engineering from National Institute of Technology, Rourkela, Odisha, India in 2010. He is currently Assistant Professor in the Electrical Engineering Department at JSS Academy of Technical Education, Noida, India. His research interests are Power Electronics, Control System and Renewable Energy Systems.



Anil Kumar received the Ph.D. degree in Electrical Engineering from IFTM University, Moradabad, India in 2017. He is currently Professor and heading Department of Electrical Engineering IFTM University Moradabad, India. His research interests are Biomedical Engineering, gas sensor, instrumentation engineering, solar system, control system and the field of Renewable Energy.

Copyrights
© 2026 Licensee Shahid Chamran University of Ahvaz, Ahvaz, Iran. This article is an open-access article distributed under the terms and conditions of the Creative Commons Attribution –NonCommercial 4.0 International (CC BY-NC 4.0) License (http://creativecommons.org/licenses/by-nc/4.0/).

Shahid Chamran University of Ahvaz

Iranian Association of Electrical and Electronics Engineers

Journal of Applied Research in Electrical Engineering

E-ISSN: 2783-2864
P-ISSN: 2717-414X
Homepage: https://jaree.scu.ac.ir/



Review Article

Comparative Analysis of Various Optimization Techniques for Battery Management Systems in Electrical Vehicles

Mohammad Junaid Khan[1,2,*], Ram Murat Singh[3], Md Naqui Akhtar[4], and Asyraf Afthanorhan[2]

[1] *Department of Electronics and Communication Engineering, SR University, Warangal, Telangana 506371, India*

[2] *Artificial Intelligence Research Center for Islamic and Sustainability (AIRIS), Universiti Sultan Zainal Abidin (UniSZA), Gong Badak Campus, 21300 Kuala Nerus, Terengganu, Malaysia*

[3] *School of Electronics and Electrical Engineering, Lovely Professional University, Jalandhar, Punjab, 144411, India*

[4] *Department of Electrical Engineering, Government Polytechnic Sahibganj, 816109, Jharkhand, India*

* *Corresponding Author: mohammad.khan444@gmail.com*

Abstract: Advancements in technology have prioritized renewable energy (RE) and reduced the negative environmental impacts of transportation. This has stimulated the development of artificial intelligence (AI) techniques for efficient public transportation systems. The main challenge in developing electric vehicles (EVs) is minimizing energy consumption and charging time, and maximizing battery life compared to traditional transportation. An optimization of the battery management system (BMS) is required to improve the performance, efficiency, and reliability of EVs. This paper studies the comparative analysis of different optimization techniques for BMS in EVs. The comparative analysis of optimization approaches is explored based on the appropriateness of simulation, real-time implementation, computational complexity, and the capability of optimization. The combination of two techniques, such as, machine learning and user-centric design, provides the best response for BMS in EVs. The hybrid technique accelerates the shift to sustainable mobility solutions and enables the full potential of EVs in order to minimize their ecological impact. The computational cost and uncertainty challenges for EVs can be minimized in further research.

Keywords: Optimization techniques, Genetic Algorithm (GA), Particle Swarm Optimization (PSO), Artificial Neural Network (ANN), Fuzzy Logic Controller (FLC), Battery Management System (BMS) and Electric Vehicles (EVs).

Article history
Received 28 April 2025; Revised 16 December 2025; Accepted 17 December 2025; Published online 18 January 2026.
© 2026 Published by Shahid Chamran University of Ahvaz & Iranian Association of Electrical and Electronics Engineers (IAEEE)
How to cite this article
M. J. Khan, R. M. Singh, M. N. Akhtar, and A. Afthanorhan, "Comparative analysis of various optimization techniques for battery management systems in electrical vehicles," *J. Appl. Res. Electr. Eng.*, vol. 4, no. 1, pp. 122-136, 2025.
DOI: 10.22055/jaree.2025.49094.1209

Check for updates

NOMENCLATURE

AI	Artificial Intelligence
ANN	Artificial Neural Network
BA	Bat Algorithm
BESA	Bald Eagle Search Algorithm
BESS	Battery Energy Storage System
BLDC	brushless DC
BMS	Battery Management System
CO_2	Carbon dioxide
DG	Distributed Generation
DR	Demand Response
ECMS	Equivalent Consumption Minimization Strategy
EHs	Energy Hubs
EMS	Energy Management Strategy
ESS	Energy Storage Systems
EVs	Electric Vehicles
FA	Firefly Algorithm
FLC	Fuzzy Logic Controller
FPGA	Field-Programmable Gate Array
GA	Genetic Algorithm
HEV	Hybrid Electrical Vehicle
HHO	Harris Hawks Optimization
IoT	Internet of Things
LCOS	Levelized Cost of Storage
MF-FNN	Multilayer Feed-forward Neural Network
MOSO	Multi-objective Snake Optimization

MPC	Model Predictive Control
PCB	Passive Cell Balancing
PLs	Parking Lots
PI	Proportional Integral
PMS	Power Management System
PSO	Particle Swarm Optimization
RE	Renewable Energy
RES	Renewable Energy Source
R-KM	Runge-Kutta Method
SDHO	Smart Decision Hunting Optimization
SoC	State of Charge
SoH	State of Health
TD (λ)	Temporal Difference
TES	Thermal Energy Storage

1. INTRODUCTION

Conventional vehicles produce environmental pollution due to fossil fuels such as diesel, petrol, etc. In recent technology, EVs offer a valuable solution to reduce environmental pollution and save fossil fuels in transportation. Battery banks are used in EVs which are an important part of them. It manages essential functions such as State of Charge (SoC) estimation, thermal management and cell balancing [1]. These functions are very important for the long-term performance and durability of vehicles. Intelligent-based control methods used for BMS in EVs which were explored to address challenges and investigate further opportunities [2]. In this regard, the intelligent control method, as an interval type-2 FLC-based optimization technique, controls energy management in plug-in hybrid EVs. The impact of air conditioning frameworks under altering environmental temperatures is discussed, and it minimizes energy consumption, increases thermal safety, and comfort [3].

The study of novel hybrid and co-estimation methods is employed in order to calculate the State of Health (SoH) that is useful in BMS for EV systems [4]. The digital twin model is used for BMS based on historical data in order to diagnose battery banks [5]. The BMS of EVs is responsible for controlling the battery banks which produce a driver to control the high performance of systems. It is the unit of electronic control that supervises the battery system in the EVs. Using BMS technology, it manages the SoH, performance and safety of the battery setup [6].

The essential features of BMS are designed for EVs, such as controlled voltage, current, and temperature to ensure the safety of battery operation. It prevents battery damage from overheating, overcharging, and over-discharging and also helps extend battery life by balancing individual cells. The main component of the battery relay is that it helps the SoH and SoC of the EV. It is valuable for accurate range estimation and optimal performance of EVs.

Fig. 1 illustrates the powertrain for the framework of the EV battery. It is driven by a single source of energy, such as a traction battery. The main motive of the battery is to have a large capacity and maximum output power. The battery setup of an EV has two operating modes (such as charging and discharging modes). In discharging mode, it powers the electric motor that converts the electrical energy into mechanical energy. This mechanical energy drives the rotational energy to the wheels of the EVs. Also, the battery setup provides power to other onboard systems such as air conditioning, sensing, communication, and infotainment facilities [7-9]. This power can be obtained from RE sources using the Internet of Things (IoT) based optimization techniques [10]. In order to propose a new algorithm of Smart Decision Hunting Optimization (SDHO) which is to optimize the charging process for EVs. This technique produced the optimum response as the best, fastest, and accurate charging stations, and it also reduces waiting time and energy consumption. The SDHO technique takes the average waiting time and distance to charging stations. The main aim is to minimize the factors and to provide the best possible charging. The results of this technique show better performance in terms of charging speed, waiting time, and energy efficiency as compared to the specified existing methods. This technique makes it a good solution for enhancing the charging system for EVs [11]. A new Energy Management Strategy (EMS) has been proposed which is to improve the fuel efficiency of hybrid vehicles. This method consists of computer vision and deep reinforcement learning which helps to use its best power for learning about the EVs. Using this method, the authors are tested based on four different types of hybrid vehicles. It was found that it can significantly improve fuel efficiency as compared to existing control methods. This technique is faster and more reliable than other deep learning-based strategies. It is clearly seen that computer vision and deep learning can be valuable tools for developing more efficient and sustainable hybrid vehicles [12]. Fig. 1 represents the schematic diagram of the optimization techniques for a BMS in an EV. In this schematic diagram, each module is shown as a block, and arrows indicate the information and control flow between modules. In this research article, in order to compare the study of various optimization techniques for BMS in EVs. It emphasizes their consequence of obtaining optimal performance of the battery and improving the global driving experience. The following points are highlighted in favour of optimization techniques for BMS in EVs.

- To compare various optimization techniques for BMS in EVs in terms of appropriateness of simulation and real-time implementation.
- To achieve effective power delivery and accurate SoC estimation, controlled in order to achieve a longer driving range per charge.
- To support cell balancing and thermal management techniques to reduce degradation factors and extend battery lifespan.
- To actual monitoring and control to prevent over-charging, over-discharging and overheating of the battery during operation of EVs.

The manuscript is structured as follows: Section 2 provides an overview of various optimization techniques used for BMS in EVs. Section 3 discusses the comparative analysis of optimization techniques for BMS in EVs. Section 4 explains the future scopes of the study, and finally, conclusions are presented in Section 5.

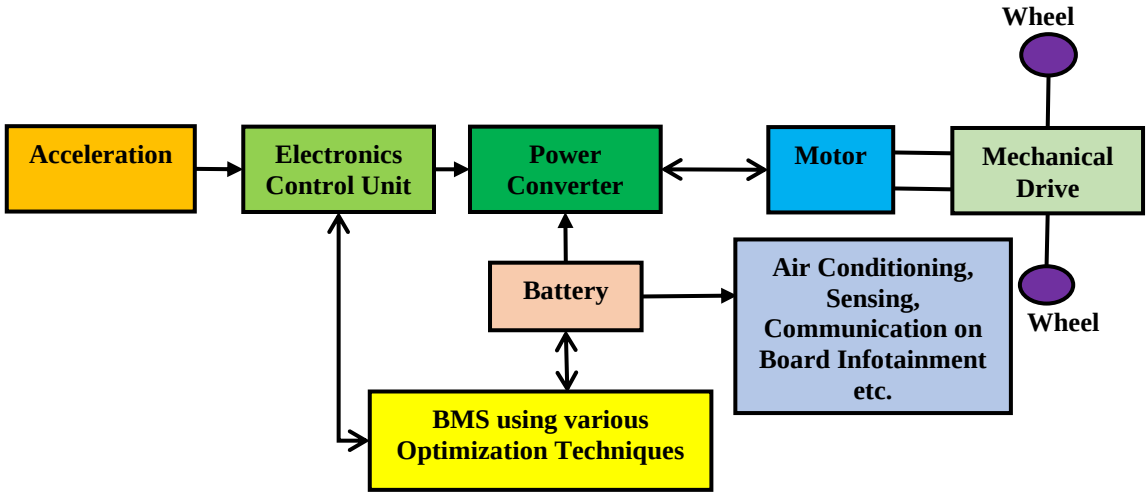


Fig. 1: Schematic diagram of the optimization techniques for a BMS in an EV.

2. Overview of Optimization Techniques for BMS in EV

The flowchart illustrates the flow of information and control within the BMS of the EVs which highlights the interaction between input signals, state estimation, optimization techniques, decision-making, and output commands [13]. The optimization techniques used by the BMS can effectively manage the operation of the battery pack, optimize energy utilization and ensure the safe and reliable performance of the EVs [14]. Fig. ***2*** shows the flowchart of optimization techniques in terms of various modules for BMS in EVs.

The following steps are described in various modules. The input module receives input signals (such as voltage, current, temperature, and SoC of battery banks) from various sensors which are installed within the EVs.

In the state estimation module, this module utilizes received input signals which is to estimate the current of SoC, SoH and other relevant parameters of the battery pack using mathematical models. The control module implements optimization techniques to manage the operation of the battery banks. This module governs charging and discharging processes, cell balancing, thermal management and other control techniques which maximize the performance and lifespan of battery banks. The optimization technique module is a module that contains different optimization techniques such as rule-based algorithms, model predictive control, GA, PSO, ANN, FLC, etc. Each technique is tailored to specific optimization objectives and constraints such as energy efficiency, thermal safety, and battery longevity. The decision-making module analyzes data from the state estimation module and optimization technique to make informed decisions regarding battery operation. This module determines the optimal charging and discharging rates, temperature limits, and other control parameters based on predefined rules, optimization algorithms and user-defined preferences. The output module is used to send the control signals and feedback to the BMS and also other vehicle subsystems, which are to execute the determined control techniques. This module can be used for the proper implementation in favour of optimization methods and the

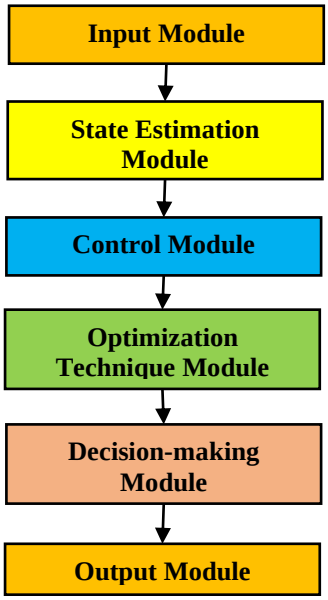


Fig. 2: Flowchart of various modules for optimization techniques.

control decision module is used to maintain the health and performance of battery banks.

Fig. 3 illustrates the flowchart of the novel SDHO optimization technique for the BMS in the EVs [11]. This proposed method explores the search space to investigate promising regions. It targets decontaminating solutions within specific regions. This method also maintains a balance between exploration and exploitation which is to avoid getting stuck in local optima.

The focus of researchers is optimizing energy management, improving efficiency and reducing operational costs of hybrid EVs. To minimize energy losses and produce a stable power supply using the concept of RE sources which are integrated with vehicle-to-grid technology. A machine learning approach is specifically TD (λ) learning that is used to determine the optimal charging and discharging technologies for hybrid EVs. This assists in extending battery life and reduces the necessity of frequent replacements. The results demonstrate that the proposed optimization method can significantly reduce operational costs and extend battery

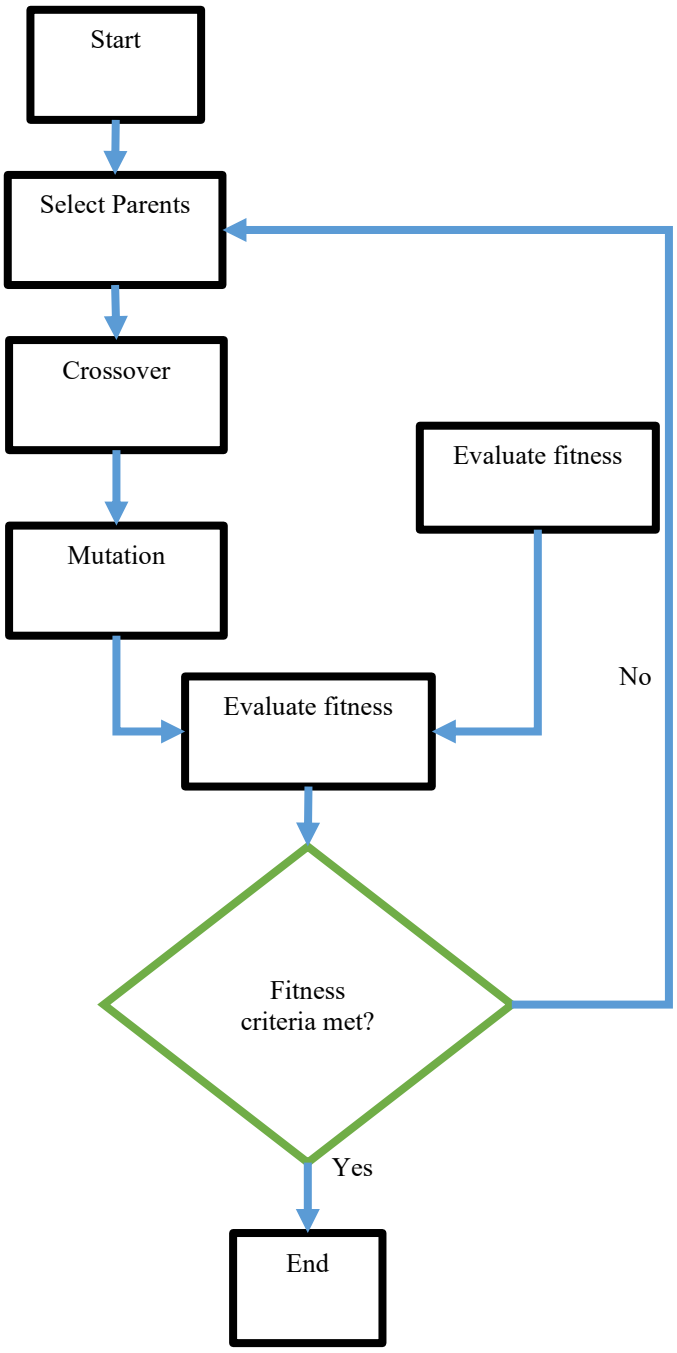


Fig. 3: Flowchart of novel SDHO optimization techniques.

life. Using optimizing energy management-based technique that the hybrid vehicle can operate more efficiently which leads to lower fuel consumption and lower emissions [15].

Elkholy et al. [16] proposed a three-level AI-based EMS for isolated microgrids. It consists of three phases. The first phase represents a field-programmable gate array (FPGA) used for fast response. The second phase represents a Multi-objective Snake Optimization (MOSO) technique employed to reduce operational costs, energy losses and reliability of power supply. In the third phase, the hybrid optimization technique consists of a multilayer feed-forward neural network (MF-FNN) and MOSO which is used to predict the output response of the battery for EVs. The proposed MF-FNN-MOSO technique improves the efficiency and reliability of the microgrid which achieves the best performance in predicting the output power of battery backup and reducing operational costs. EVs are frequently increasing in the market to reduce environmental impact. Though the charging process of EVs can put a strain on the power grid. One solution is to aggregate EVs in parking lots (PLs) and manage their charging collectively. Proposed optimization model for smart PLs to minimize power drawn from the grid while meeting customer needs. The model considers both single and 3-phase EVs and uses a non-linear battery charging profile. An augmented Lagrangian-based decentralized model predictive control technique is used to solve the optimization problem. The proposed method has been tested on smart PLs in Genova, Italy, and is efficient and accurate, even when scaling up to 40 EVs [17]. The predictive flex smoother method is proposed by Benavides et al. [18]. This method mitigates power fluctuations in the grid-connected PV framework, although it optimizes energy management in EV charging stations. The proposed method effectively improves power quality and reduces costs. Real-time testing has shown response times under 500 ms. The method efficiently handles power smoothing and charging strategies for diverse EV models and connection coefficients. Researchers proposed an energy management system for residential buildings that optimizes energy flow, energy storage systems (ESS) parameters and energy consumption scheduling in order to minimize costs, extend ESS lifespan and reduce CO_2 emissions. The system integrates Renewable Energy Sources (RES), ESSs, and EVs, and utilizes demand response (DR) programs to optimize energy usage. The optimization technique considers factors like installation costs, levelized cost of storage (LCOS), seasonal variations, energy consumption profiles, and energy prices. The results demonstrate significant cost reductions, energy loss reductions and extended EV battery life, leading to substantial financial savings and environmental benefits [19]. Fig. 4 shows the energy flow management algorithm for EVs.

The fitness function of the GA is determined as the inverse of the total distance + waiting time penalties and exceeding distance penalties [20].

Formulation of the fitness function

$$F = \frac{1}{f} \tag{1}$$

$$f = w_1 \sum_{k=1}^{N} d_i + w_2 \sum_{k=1}^{N} q_i + w_3 P \tag{2}$$

where d_i represents the distance travelled between consecutive stopes on the route, and q_i represents the waiting time at the charging station at i. P represents the exceeded distance penalty, and w_1, w_2, and w_3 represent the weight factors.

$$q_i = \begin{cases} actual\ queue\ time & if\ station\ is\ in\ the\ cluster \\ average\ queue\ time & otherwise \end{cases}$$

In the other way, the droop control technique is a way of control the output power of generator in a power system. It is used to maintain the balance of power between generators when availability of parallel connections of multiple generators. The basic equation for a droop control system is as presented in (3).

$$Gen_{output\ Power} = P_{bo} \times (1 + Droop_1) \times \left(\frac{F_d}{F_{bd}}\right) \tag{3}$$

where, P_{bo}= base output power (rated power output of the generator at a reference frequency (F_r= 50Hz), F_d=frequency deviation, F_{bd}= frequency deviation at base power and $Droop_1$ is the percentage power drop per unit of F_d form F_r [21].

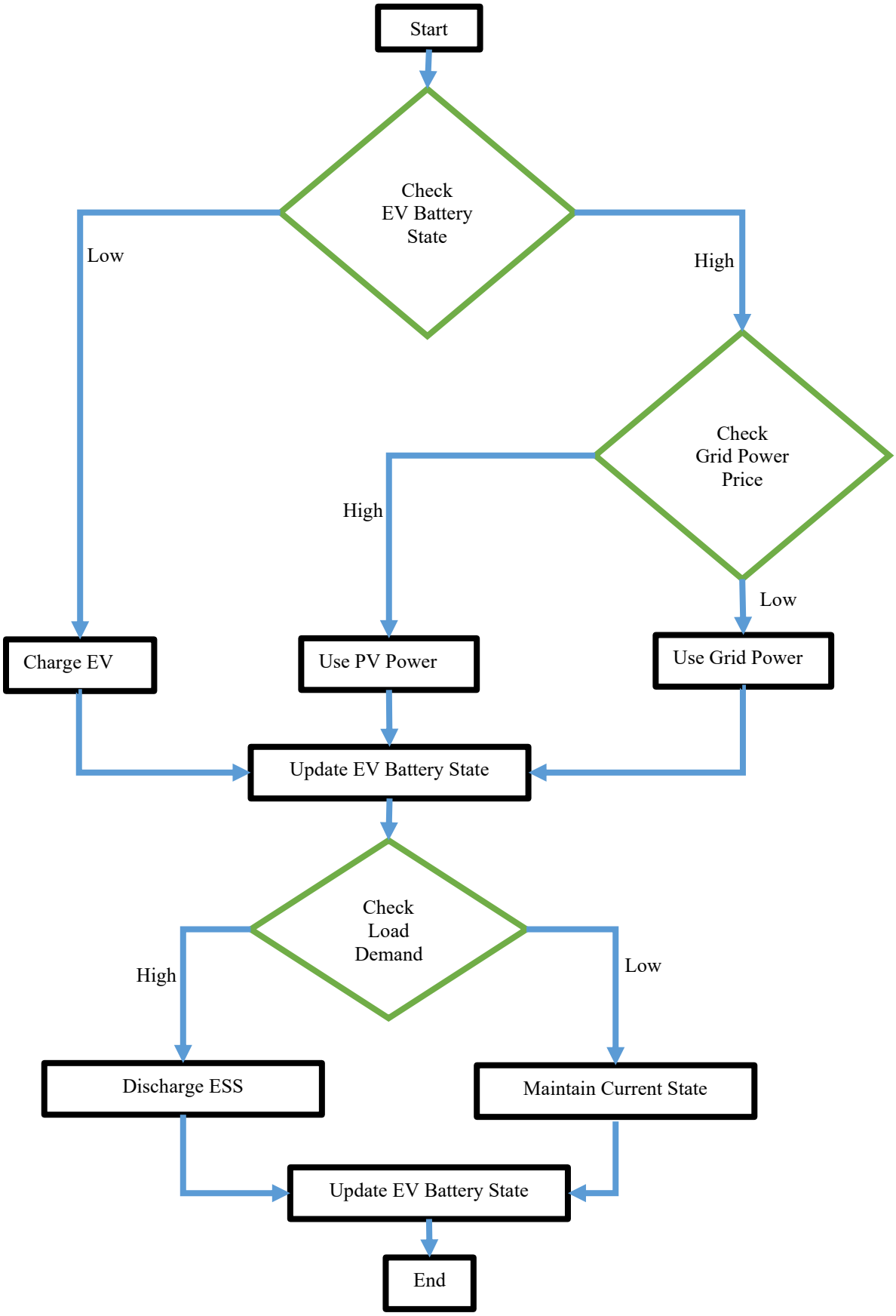


Fig. 4: Flowchart of energy flow management algorithm.

Fig. 5 represents the flowchart of a basic integration of RES and EVs using FLV and GA. It considers factors including RES available, EV battery state, load demand and optimization of energy flow [22].

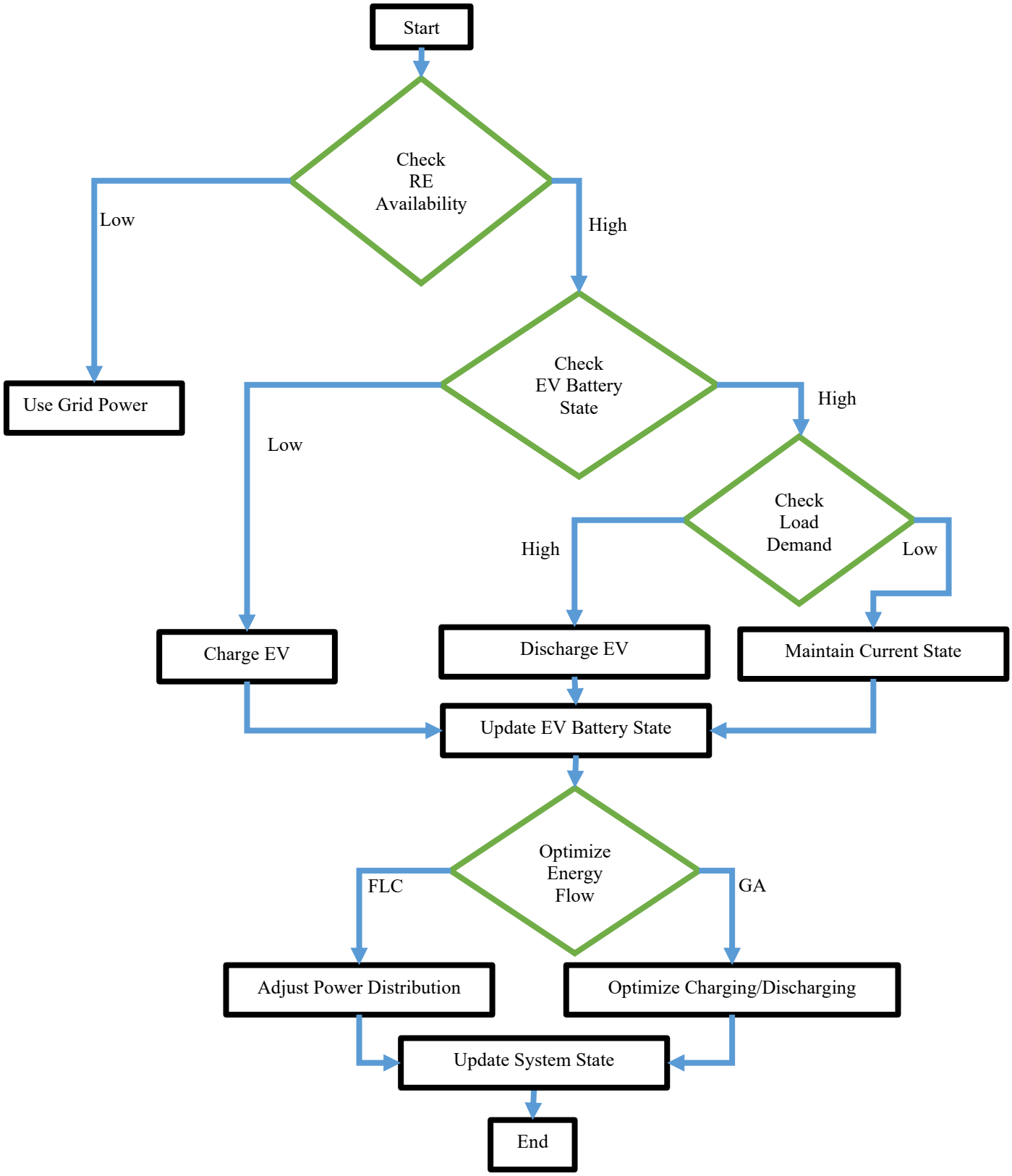


Fig. 5: Flowchart of a basic integration of RES and EVs using FLC and GA.

Fig. 6 represents the flowchart of the extraction of maximum power from solar with brushless DC (BLDC) motor-driven EVs-based Harris Hawks optimization (HHO) algorithm. HHO offers MPPT for solar PV-powered EVs. This proposed MPPT approach outlined that it enhances overall efficiency and reduces operational costs for EVs using the PV framework [23]. Authors have investigated the inclusive analysis of hybrid EV (HEV) components including their construction, mathematical models and methodologies [1]. Kandil et al. [24] examined optimization approaches for fast charging stations' allocation and size. An in-depth examination and critique of the placement of EV charging stations within distribution networks [25].

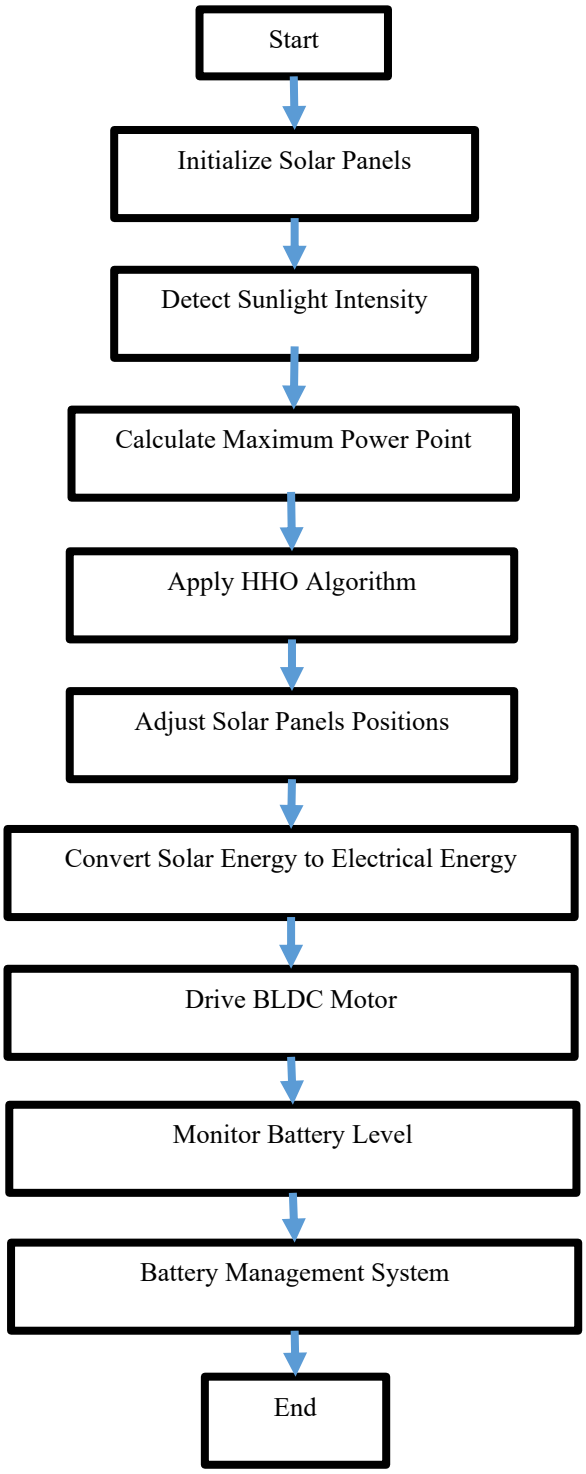


Fig. 6: Flowchart of Extraction of maximum power from solar with BLDC motor driven EVs based HHO algorithm.

The pinch analysis-based optimization technique is a systematic procedure for finding simultaneous sizes for the EES and thermal energy storage (TES) framework to yield suitable sizes for fuel cells, battery radiators, and TES materials [26]. Energy hubs (EHs) are vital for sustainable energy. This emphasizes a residential EH that effectively harnesses different energy sources and technologies to meet domestic needs. The main aim is to develop an efficient heat and power management system (PMS) that minimizes operational costs. Data-driven techniques and advanced forecasting methodologies are used to enhance the efficiency of frameworks. The results show that these techniques can significantly reduce power costs in the EH scheme [27].

The dynamic EV model is examined by using the 4th-order Runge-Kutta method (R-KM) to assess its performance under different driving situations. The results indicate that the dynamic EV model offers a structured approach to simulate and optimize complex EV systems [28]. Manivannan [29] proposed a machine-learning approach to create a smart energy management framework for hybrid EVs with energy storage as battery banks. This proposed framework can optimize energy usage, reduce operational costs, and prevent overloading the electrical grid.

This study implements an IoT-based smart charging framework in order to enable more precise control and also improve the efficiency of the system. The main aim of the proposed algorithm is to reduce power loss, voltage deviation and charging station costs while maximizing traffic flow and satisfying EV requirements. It focuses on the optimization of the existing grid infrastructure to meet the requirements of EV users, the transportation network and the energy distribution network [30]. It was implemented in MATLAB and compared to other existing methods. It produced better performance in terms of accuracy and computational efficiency. The proposed method had the lowest error (i.e. 4 mV) and the shortest computation time (i.e. 0.7 s) [31].

A new Proportional Integral (PI) and an ANN-based controller are developed to manage Passive Cell Balancing (PCB) technology for BMS in EV [32]. Machine learning-based EV charging is implemented with an optimized flyback converter for solar PV frameworks [33]. Optimization of EV charging station placement using PSO in Smart Grids [34]. The proposed strategy for reducing power loss was tested on Indian 28-bus and 108-bus distribution networks. The results showed that the bald eagle search algorithm (BESA)-based optimization method outperformed the bat algorithm (BA) based method in terms of power loss reduction, voltage improvement, and overall cost savings [35]. Elazaib et al. [36] presented three novel smart home energy management algorithms which are designed for developing countries. These algorithms focus on load shifting, vehicle-to-home energy transfer and reduced air conditioning, considering factors like battery life, user comfort and local climate conditions. This study also evaluates the economic feasibility of integrating solar PV arrays. The proposed energy management scheme can significantly reduce electricity bills by up to 61%.

The authors compare four residential load scenarios to assess the economic and environmental benefits of integrating EVs into microgrids. A control technique is introduced to optimize battery energy storage system (BESS) charging and discharging based on time-of-use pricing and EV power. Two optimisation algorithms are compared to assess the effectiveness of the control technique. The results demonstrate that controlled EV integration can reduce costs by \$0.728 million and CO_2 emissions by 213.23 kg. Controlled BESS integration reduces costs by \$0.835 million and CO_2 emissions by 360.68 kg. The semi-isolated microgrid configuration offers the lowest overall cost at \$1.421 million [37]. The primary objective is to minimize energy and thermal discomfort costs over a long-term horizon in a sustainable smart home while considering factors such as

occupancy, temperature preferences, electricity consumption, renewable energy generation, outdoor temperature, and electricity prices [38]. Aoumari et al. [39] proposed an energy management system that optimizes the performance of onboard electrical sources by carefully selecting the sharing filter cut-off frequency. This selection considers factors like effective power, state of charge variation, and battery cycle life. Simulations in MATLAB demonstrate the superiority of the proposed system compared to conventional methods. Koltsaklis et al. [40] proposed a smart home energy management system that optimizes energy usage and minimizes costs. The system considers factors like demand response, renewable energy integration, and energy storage. A hybrid forecasting model is used to predict energy prices and renewable generation. The results show that the system can effectively reduce energy costs and improve energy efficiency. The proposed framework can help reduce the strain on the power grid, especially in developing countries [41]. The results illustrate that the proposed optimization method is compared to other existing specified techniques. It can be used to assess the reliability of electrical distribution networks. This study concludes that integrating the approach of distributed generation (DG) and EVs can enhance the reliability of the electrical system [42].

Researchers have investigated the impact of energy consumption budgets in various aspects of operational vehicles, including fuel consumption, electric motor usage, gear shifting strategy, and engine parameters like intake manifold pressure, air-fuel ratio, and turbine waste-gate position [43]. Ajayan et al. [44] proposed an optimized method, which is used to determine the optimal size of fuel cells and battery banks. PSO and the Firefly Algorithm (FA) are used to calculate the optimal solution for BMS in EVs. In this regard, various constraints are considered, such as the battery's state of charge and the fuel cell's rating, while also accounting for replacement costs. The results demonstrate that the FA optimization algorithm provides better performance in terms of cost reduction, population size and convergence speed. An innovative approach to controlling the charging and discharging processes in battery management operations using a bidirectional converter [45].

Yamini et al. [46] compared the fuel consumption of a hybrid vehicle under different driving cycles using the Equivalent Consumption Minimization Strategy (ECMS). The goal of this method is to determine the optimal strategy in order to minimize fuel consumption and improve the performance of the vehicle. The findings can contribute to the development of sustainable hybrid EVs. Yammani et al. [47] proposed optimizing EV charging and discharging to maximize EV owner profits and support grid operations. This technique considers factors such as energy prices, state of charge of the battery, and RE availability. The results illustrate the effectiveness of the proposed approach in improving grid reliability and reducing costs. An economic analysis is carried out on the PV framework under peak load scenarios of the electric power distribution framework, considering the impact of EVs [48]. To study presents a reliability evaluation of power systems that incorporate pumped storage units. It developed a reliability model to assess the impact of component failures on complete framework adequacy [49]. This work focused on efficient demand response and robust voltage control in an islanded DC microgrid. The study addresses challenges arising from alterations in both load and supply [50].

3. Comparative Analysis of Optimization Techniques for BMS in EV

A comparative study of various optimization techniques for BMS in EVs is an important endeavour, given the critical role of BMS in terms of the safety and longevity of EV batteries. Table 1 represents a concise analysis of optimization techniques.

Researchers have investigated and analyzed various optimization techniques for BMS in EVs. The literature shows that there are several optimization techniques available for BMS in EVs. Various optimization techniques are investigated, and advised machine learning methods like ANN are used instead of traditional rule-based algorithms. The diverse range of techniques highlights the complexity of the optimization difficulty and the necessity for customized results for various application scenarios. When it comes to optimization approaches, there is a trade-off between speed and complexity. Rule-based algorithms are faster and can be used in real-time applications. Still, improvement is required for the adaptability and capabilities of proposed frameworks such as predictive control models and ANN technologies.

Advanced optimization techniques like model predictive control and GA have improved battery efficiency and lifespan performance. Though, it often requires higher computational costs, posing challenges for real-time implementation in recent technology-based EVs. Many researchers have explored hybrid technologies combining more than two optimization techniques to reduce their limitations. For example, a combination of two approaches of machine learning models and rule-based algorithms can control the simplicity of rules and the learning capabilities of ANN simultaneously. The accuracy of battery banks is important when using optimization techniques. In order to achieve optimal performance of BMS, it is essential to ensure that the battery setups are accurate using data-driven and parameter estimation technologies. Optimization techniques are implemented in EV systems in the real world due to challenges in achieving desirable results in theoretical studies and simulations. Several factors including computational complexity, robustness against uncertainty and scalability for large-scale EVs, are addressed for practical deployment.

4. Future Directions

The optimization techniques are used for BMS in EVs due to challenges in favour of enhancing the performance, efficiency, and reliability of frameworks. There are some important findings for future work.

Table 1: Comparative analysis of optimization techniques for BMS in EVs.

Ref.	Optimization Technique	System	Converge-nce Speed	Computational cost	SoC/ SoH accuracy	Real-time applicab-ility	Benefits	Research Gaps
[51], [52]	Rule-Based Algorithm	Traditional BMS	Fast	Very low	Moderate to low	Highly suitable	• Simplicity and ease of implementation. • Real-time operation suitable for simple applications.	• Limited adaptability to dynamic operating conditions. • Lack of optimization for long-term battery health. • May not fully exploit the potential of advanced battery chemistries.
[53], [54]	Model Predictive Control (MPC)	Advanced BMS	Moderate	High	Higher SoC estimation accuracy and improving long term battery health management	Challenging for embedded BMS hardware	• Optimization based on predictive battery models. • Accommodates dynamic operating conditions and constraints. • Improved energy efficiency and battery lifespan.	• Computational complexity and requirement of accurate battery models. • Limited scalability for large-scale EV fleets. • Challenges in real-time implementation for highly dynamic environments.
[55], [56]	GA	Adaptive BMS	Moderate to Slow	Computationally intensive	High	Limited Realtime feasibility	• Exploration of a wide solution space to find optimal parameters. • Adaptability to varying operating conditions and battery chemistries.	• High computational overhead, especially for complex battery models. • Difficulty in fine-tuning algorithm parameters for specific applications. • Limited transparency in the decision-making process compared to rule-based approaches.
[57], [58]	PSO	Adaptive BMS	Moderate	High	High	Slow	• Efficient exploration of solution space through swarm intelligence. • Rapid convergence to near-optimal solutions. • Suitable for real-time implementation in dynamic environments.	• Sensitivity to initial parameters and swarm size. • Limited robustness in noisy or uncertain environments. • Challenges in balancing exploration and exploitation for complex optimization problems.
[55], [59], [60]	ANN	Intelligent BMS	Moderate to Slow	Moderate to high	High	Feasible	• Adaptive learning and ability to capture complex nonlinear relationships. • Improved accuracy in prediction and control compared to traditional methods.	• Training data availability and representativeness. • Interpretability and explainability of model decisions. • Computational overhead and hardware requirements for real-time implementation.
[61]	FLC	Intelligent BMS	Fast to Moderate	Moderate	Low to moderate	High	• Linguistic rule-based approach suitable for handling uncertainty and imprecision. • Intuitive modelling of human expertise and decision-making.	• Difficulty in defining fuzzy sets and membership functions. • Limited scalability for complex systems and large-scale optimization. • Challenges in integrating fuzzy logic with other optimization techniques for hybrid approaches.

1. To explore the integration of advanced deep and reinforcement learning for optimization of BMS in EVs. This hybrid technique can improve accuracy and optimize control in dynamic environments with varying operating conditions.
2. To develop optimization algorithms and control strategies with practical feasibility and scalability which is suitable for real-time implementation in EVs. It can be considered for hardware constraints including processing power and memory.
3. The main objective is to improve the stability and consistency of optimization techniques with uncertainties including variable factors such as characteristics of the battery, and environmental conditions. It produces robust optimization, uncertain quantification and adaptive control in order to improve the dependability of the proposed system.
4. To investigate the hybrid optimization approaches of model predictive control with evolutionary algorithms and FLC with ANN. Additionally. It can consider multi-objective optimization frameworks in order to optimize conflicting objectives including energy efficiency, battery lifespan and thermal management.
5. To propose the optimization technique based on large-scale datasets and data-driven approaches is used to optimize battery models.
6. To develop robust validation and benchmarking of optimization algorithms, it will conduct comprehensive simulation and hardware implementation in the laboratory.
7. To maximize the global performance and efficiency of large-scale EV systems, it is important to consider scalability issues in BMS optimization. To investigate distributed optimization algorithms and decentralized control strategies for improving the results of proposed systems.
8. To improve the user experience and the adoption of EVs, that is crucial to integrate user preferences and driving behavior for BMS optimization. This can be achieved by designing intuitive interfaces and decision-support systems that offer users transparency, control and real-time response in BMS operation and battery performance.

5. Conclusion

The various optimization techniques are studied for BMS in EVs. A hybrid optimization technique is suggested to the authors to improve the response of BMS functions in EVs. It likely involves techniques that extend battery life, improve safety and increase efficiency. This study has explored various optimization approaches for BMS characteristics. To enhance the accuracy of SoC estimation in BMS, coulomb counting and Kalman filter techniques utilize data from current, voltage, and temperature. The GA and PSO algorithms help to maintain uniform voltage across all cells in the battery pack which extends battery life. Optimization techniques can be applied to control battery temperature through cooling systems, maximizing battery health and performance. It plays a crucial role in accurately estimating the SoC of an EV battery and efficiently delivering power to optimize energy usage. These methods result in a greater driving range on a single charge. Cell balancing and thermal management techniques minimize battery wear and prolong its life. Monitoring systems safeguard against overcharging, over-discharging, and overheating, ensuring the safe use of EVs.

Further research can explore the integration of advanced algorithms such as machine learning for real-time optimization and predictive maintenance of EV batteries. This advancement can lead to EVs that are more efficient, reliable and safe.

Credit Authorship Contribution Statement

Mohammad Junaid Khan: Conceptualization, Data curation, Formal analysis, Investigation, Methodology, Resources, Software, Supervision, Validation, Visualization, Writing – original draft, Writing – review & editing. **Ram Murat Singh:** Conceptualization, Investigation, Methodology, Supervision, Visualization, Writing – original draft, Writing – review & editing. **Md Naqui Akhtar:** Investigation, Methodology, Resources, Visualization, Writing – original draft, Writing – review & editing. **Asyraf Afthanorhan:** Formal analysis, Investigation, Methodology, Resources, Visualization, Writing – original draft, Writing – review & editing.

Declaration Of Competing Interest

The authors declare that they have no known competing financial interests or personal relationships that could have appeared to influence the work reported in this paper. The ethical issues; including plagiarism, informed consent, misconduct, data fabrication and/or falsification, double publication and/or submission, redundancy has been completely observed by the authors.

References

[1] Z. Ahmad, M. J. Khan, and M. N. Akhtar, "A critical review of hybrid electric vehicles," *Journal of Advanced Research in Applied Sciences and Engineering Technology*, vol. 29, no. 1, pp. 283–294, Jan. 2023.

[2] M. S. H. Lipu *et al.*, "Intelligent algorithms and control strategies for battery management system in electric vehicles: Progress, challenges and future outlook," *J Clean Prod*, vol. 292, Art. no. 126044, 2021.

[3] C. Yang, X. Wang, J. Zhao, and L. He, "Optimization of the energy management system in hybrid electric vehicles considering cabin temperature," *Appl. Therm. Eng*,, vol. 242, Art. no. 122504, 2024.

[4] T. Alsuwian *et al.*, "A review of expert hybrid and co-estimation techniques for SOH and RUL estimation

in battery management system with electric vehicle application," *Expert Syst. Appl.*, Art. no. 123123, 2024.

[5] H. Li, M. Bin Kaleem, I.-J. Chiu, D. Gao, J. Peng, and Z. Huang, "An intelligent digital twin model for the battery management systems of electric vehicles," *Int. J. Green Energy*, vol. 21, no. 3, pp. 461–475, 2024.

[6] P. J. Raj, V. V. Prabhu, V. Krishnakumar, and M. C. J. Anand, "Solar powered charging of Fuzzy Logic Controller (FLC) strategy with Battery Management System (BMS) method used for Electric Vehicle (EV)," *International Journal of Fuzzy Systems*, vol. 25, no. 7, pp. 2876–2888, 2023.

[7] T. Raoofi and M. Yildiz, "Comprehensive review of battery state estimation strategies using machine learning for battery Management Systems of Aircraft Propulsion Batteries," *J. Energy Storage*, vol. 59, Art. no. 106486, 2023.

[8] H. Wang, S. A. Pourmousavi, W. L. Soong, X. Zhang, and N. Ertugrul, "Battery and energy management system for vanadium redox flow battery: A critical review and recommendations," *J. Energy Storage*, vol. 58, Art. no. 106384, 2023.

[9] M. Waseem, M. Ahmad, A. Parveen, and M. Suhaib, "Battery technologies and functionality of battery management system for EVs: Current status, key challenges, and future prospectives," *J. Power Sources*, vol. 580, Art. no. 233349, 2023.

[10] M. J. Khan, M. N. Akhtar, A. Alam, and A. Afthanorhan, "IoT based MPPT techniques for photovoltaic frameworks management under different environmental conditions: a review," *International Journal of Informatics and Communication Technology (IJ-ICT)*, vol. 13, no. 2, Art. no. 306, Aug. 2024.

[11] S. K. Jha, C. Gandikoti, S. K. Jha, and B. M. Jha, "Electric vehicle charge scheduling approach based on smart decision hunting optimization," *International Journal on Interactive Design and Manufacturing*, vol. 18, no. 1, pp. 331–349, 2024.

[12] S. Manoj and S. P. Kumar, "An optimum E-vehicle energy management system using deep reinforcement learning," *International Journal of Engineering Trends and Technology*, vol. 71, no. 5, pp. 219–227, 2023.

[13] A. T. Vijayan, J. V. Dev, and H. Henry, "Charge sharing scheme for electric vehicles based on battery monitoring," *International Journal of Applied Power Engineering (IJAPE)*, vol. 13, no. 3, Art. no. 703, Sep. 2024.

[14] R. R. Kumar, C. Bharatiraja, K. Udhayakumar, S. Devakirubakaran, K. S. Sekar, and L. Mihet-Popa, "Advances in batteries, battery modeling, battery management system, battery thermal management, SOC, SOH, and charge/discharge characteristics in EV applications," *IEEE Access*, vol. 11, pp. 105761–105809, 2023.

[15] E. C. Blessie *et al.*, "Machine learning-based management of hybrid energy storage systems in e-vehicles," *J. Nanomater*, vol. 2022, 2022.

[16] M. H. Elkholy *et al.*, "Implementation of a multistage predictive energy management strategy considering electric vehicles using a novel hybrid optimization technique," *J. Clean Prod.*, vol. 476, 2024.

[17] V. Casella, G. Ferro, and M. Robba, "A decentralized optimization approach to the power management of electric vehicles parking lots," *Sustainable Energy, Grids and Networks*, vol. 38, 2024.

[18] D. Benavides, P. Arévalo, E. Villa-Ávila, J. A. Aguado, and F. Jurado, "Predictive power fluctuation mitigation in grid-connected PV systems with rapid response to EV charging stations," *J. Energy Storage*, vol. 86, 2024.

[19] Z. A. Al Muala, M. A. Bany Issa, and P. M. Bello Bugallo, "Integrating life cycle principles in home energy management systems: optimal load PV–battery–electric vehicle scheduling," *Batteries*, vol. 10, no. 4, 2024.

[20] T. Gaon, Y. Gabay, and M. Weiss Cohen, "Optimizing electric vehicle routing efficiency using k-means clustering and genetic algorithms," *Future Internet*, vol. 17, no. 3, pArt. no. 97, 2025.

[21] M. Z. Afzal *et al.*, "A novel electric vehicle battery management system using an artificial neural network-based adaptive droop control theory," *Int. J. Energy Res.*, vol. 2023, no. 1, Art. no. 2581729, 2023.

[22] H. Agrawal *et al.*, "A fuzzy-genetic-based integration of renewable energy sources and E-vehicles," *Energies (Basel)*, vol. 15, no. 9, Art. no. 3300, 2022.

[23] M. S. N. Krishna konijeti and M. L. Bharathi, "Extraction of maximum power from solar with BLDC motor driven electric vehicles based HHO algorithm," *Advances in Engineering Software*, vol. 170, Art. no. 103137, 2022.

[24] S. M. Kandil, A. Abdelfatah, and M. A. Azzouz, "Optimization approaches for fast charging stations allocation and sizing: A review," *IEEE Access*, vol. 12, pp. 46741–46763, 2024.

[25] T. Yuvaraj, K. R. Devabalaji, J. A. Kumar, S. B. Thanikanti, and N. I. Nwulu, "A comprehensive review and analysis of the allocation of electric vehicle charging stations in distribution networks," *IEEE Access*, vol. 12, pp. 5404–5461, 2024.

[26] N. Philip, P. C. Ghosh, "Optimal sizing of electrical and thermal energy storage systems for application in fuel cell based electric vehicles," Journal of Energy Storage, vol. 83, Art. no. 110753, 2024.

[27] Y. Chen, M. Tian, J. Xue, L. Zhang, and J. Ying, "Data-driven approaches to achieve energy transition: Statistical analysis of demand-side management and smart decision making in urban energy hub networks," *Sustain. Cities Soc.*, vol. 101, 2024.

[28] K. Khan, I. Samuilik, and A. Ali, "A mathematical model for dynamic electric vehicles: Analysis and optimization," *Mathematics*, vol. 12, no. 2, 2024.

[29] R. Manivannan, "Research on IoT-based hybrid electrical vehicles energy management systems using machine learning-based algorithm," *Sustainable Computing: Informatics and Systems*, vol. 41, 2024.

[30] A. Kapoor, V. S. Patel, A. Sharma, and A. Mohapatra, "Optimal planning of fast EV charging stations in a coupled transportation and electrical power distribution network," *IEEE Transactions on Automation Science and Engineering*, vol. 21, no. 3, pp. 4261–4271, 2024.

[31] K. Varatharajalu, M. Manoharan, T. S. C. Palanichamy, and S. Subramani, "Electric vehicle parameter identification and state of charge estimation of Li-ion batteries: Hybrid WSO-HDLNN method," *ISA Trans*, vol. 142, pp. 347–359, 2023.

[32] S. Karmakar, T. K. Bera, and A. K. Bohre, "Novel PI controller and ANN controllers-based passive cell balancing for battery management system," *IEEE Trans. Ind. Appl.*, vol. 59, no. 6, pp. 7623–7634, 2023.

[33] P. Dhanalakshmi, U. J. Reddy, M. Ranjith Reddy, and G. Ravikanth, "Machine learning electrical vehicle charging management under the optimization of flyback converter for solar photovoltaic applications," *SSRG International Journal of Electrical and Electronics Engineering*, vol. 10, pp. 137–153, 2023.

[34] M. Altaf *et al.*, "PSO-based optimal placement of electric vehicle charging stations in a distribution network in smart grid environment incorporating backward forward sweep method," *IET Renewable Power Generation*, 2023.

[35] T. Yuvaraj, K. R. Devabalaji, S. B. Thanikanti, V. B. Pamshetti, and N. I. Nwulu, "Integration of electric vehicle charging stations and DSTATCOM in practical indian distribution systems using bald eagle search algorithm," *IEEE Access*, vol. 11, pp. 55149–55168, 2023.

[36] R. Elazab, O. Saif, A. M. A. Amin Metwally, and M. Daowd, "New smart home energy management systems based on inclining block-rate pricing scheme," *Clean Energy*, vol. 6, no. 3, pp. 503–511, 2022.

[37] M. M. Gamil, T. Senjyu, H. Masrur, H. Takahashi, and M. E. Lotfy, "Controlled V2Gs and battery integration into residential microgrids: Economic and environmental impacts," *Energy Convers. Manag.*, vol. 253, 2022.

[38] F. R. Albogamy *et al.*, "Real-time scheduling for optimal energy optimization in smart grid integrated with renewable energy sources," *IEEE Access*, vol. 10, pp. 35498–35520, 2022.

[39] E. G. Abelaziz,. H. Ouadi, and A. E. Aoumari, "Hybrid optimal energy management for HTE vehicles," *International Journal of Renewable Energy Research*, vol. 11, no. 4, pp. 1639–1651, 2021.

[40] N. Koltsaklis, I. P. Panapakidis, D. Pozo, and G. C. Christoforidis, "A prosumer model based on smart home energy management and forecasting techniques," *Energies (Basel)*, vol. 14, no. 6, 2021.

[41] S. Singh, P. Chauhan, and N. J. Singh, "Feasibility of grid-connected solar-wind hybrid system with electric vehicle charging station," *Journal of Modern Power Systems and Clean Energy*, vol. 9, no. 2, pp. 295–306, 2021.

[42] M. Bilal, M. Rizwan, I. Alsaidan, and F. M. Almasoudi, "AI-Based approach for optimal placement of EVCS and DG with reliability analysis," *IEEE Access*, vol. 9, pp. 154204–154224, 2021.

[43] C. Balerna *et al.*, "Time-optimal low-level control and gearshift strategies for the formula 1 hybrid electric powertrain," *Energies (Basel)*, vol. 14, no. 1, 2021.

[44] S. Ajayan and A. I. Selvakumar, "Implementation of firefly algorithm in optimal sizing of proton exchange membrane fuel cell–battery hybrid locomotive," *International Journal of Renewable Energy Research*, vol. 10, no. 2, pp. 614–624, 2020.

[45] M. J. Khan, M. N. Akhtar, and A. Afthanorhan, "An innovative control of the charging and discharging for the battery management operation using a bidirectional converter," *Future Technology*, vol. 4, no. 1, pp. 23–28, 2025.

[46] K. Yamini Krishna and K. Narasimha Raju, "Optimization technique for improvement of fuel economy in fuel cell electrical vehicles," *Journal of Advanced Research in Dynamical and Control Systems*, vol. 12, no. 2, pp. 137–145, 2020.

[47] C. Yammani, P. Prabhat, and K. Dahal, "Optimal dispatch of Vehicle-to-Grid (V2G) battery storage using p-ELECTRE Method and Its Impact on Optimal Scheduling of DGs in distribution system," *Electric Power Components and Systems*, vol. 47, no. 14–15, pp. 1362–1374, 2019.

[48] M. Khosravi, S. Hasanvand, M. Abasi, and M. E. Hassanzadeh, "Economic analysis of photovoltaic systems during peak load of the electric power distribution system in the presence of electric vehicles.," *Journal of Applied Research in Electrical Engineering*, vol. 3, no. 2, pp. 177-184, 2024.

[49] A. Ghaedi and M. Mahmoudian, "Reliability evaluation of power systems including pumped-storage generation units.," *Journal of Applied Research in Electrical Engineering*, vol. 3, no. 1, pp. 110-119, 2024.

[50] S. D. Pour and R. Eslami, "Efficient responding to demand and robust voltage control of an islanded DC microgrid under variations in load and supply.,"

Journal of Applied Research in Electrical Engineering, vol. 3, no. 1, pp. 51-63, 2024.

[51] H. Polat, E. Unamuno, D. Cabezuelo, T. Geury, and O. Hegazy, "Development and Comparison of Rule- and Machine Learning-based EMS for HESS providing grid services," *IEEE Access*, 2024.

[52] S. Zhou, Z. Chen, D. Huang, and T. Lin, "Model prediction and rule based energy management strategy for a plug-in hybrid electric vehicle with hybrid energy storage system," *IEEE Trans. Power Electron.*, vol. 36, no. 5, pp. 5926–5940, 2020.

[53] D. Bhule and R. S. Kaarthik, "A model predictive control scheme for a single-phase integrated battery charger with active power decoupling for EV application," *IEEE Trans. Power Electron.*, vol. 39, no. 4, pp. 4117 – 4126, 2024.

[54] Y. Lu, X. Han, L. Lu, X. Feng, and M. Ouyang, "Optimal charging strategy for lithium-ion batteries based on model predictive control with coupled thermal-electric decomposed electrode model," *IEEE Trans. Ind. Appl.*, vol. 60, no. 4, pp. 6582 – 6592, 2024.

[55] S. Xiao, P. Liu, K. Chen, K. Liu, G. Gao, and G. Wu, "Battery state of health prediction based on voltage intervals, BP neural network and genetic algorithm," *Int. J. Green Energy*, pp. 1–14, 2023.

[56] A. Singh, K. Pal, and C. B. Vishwakarma, "State of charge estimation techniques of Li-ion battery of electric vehicles," *e-Prime-Advances in Electrical Engineering, Electronics and Energy*, vol. 6, Art. no. 100328, 2023.

[57] F. A. B. Zaini, M. F. Sulaima, I. A. W. A. Razak, N. I. Zulkafli, and H. Mokhlis, "A review of PSO-based algorithm application in demand Side management: Challenges & opportunities," *IEEE Access*, vol. 11, pp. 53373 – 53400, 2023.

[58] E. Fadlaoui and N. Masaif, "Parameter identification of the combined battery model using embedded PSO-GA," in *Benchmarks and Hybrid Algorithms in Optimization and Applications*, Springer, 2023, pp. 211–225.

[59] Y. Khawaja *et al.*, "Battery management solutions for li-ion batteries based on artificial intelligence," *Ain Shams Engineering Journal*, vol. 14, no. 12, Art. no. 102213, 2023.

[60] M. Kurucan, M. Özbaltan, Z. Yetgin, and A. Alkaya, "Applications of artificial neural network based battery management systems: a literature review," *Renewable and Sustainable Energy Reviews*, vol. 192, Art. no. 114262, 2024.

[61] P. A. Nambi, S. Muthubalaji, S. Srinivasan, and M. B. Subramani, "A smart and intelligence based controlling algorithms for maximum power extraction and effective battery management in EV systems," *Energy Storage*, vol. 6, no. 1, Art. no. e583, 2024.

BIOGRAPHY



Mohammad Junaid Khan Recognized among the World's Top 2% Scientists (Stanford University, USA). Dr. Khan is an accomplished academic and researcher currently serving as an Assistant Professor in the Department of Electronics and Communication Engineering, SR University, Warangal, Telangana, India, where he joined in 2025. NIRF-2025:91 & World's THE-2025 ranking band: 801-1000. He also serves as an Editorial Board Member of Scientific report, Springer Nature, The Campus, 4 Crinan Street, London N1 9XW, UK. & Guest Editor (SI) for BENTHAM SCIENCE's "Recent Advances in Electrical & Electronic Engineering" (UAE). His dedication to advanced research is evident through his Post-Doctoral Fellowship from Universiti Sultan Zainal Abidin (UniSZA), a distinguished public university in Malaysia. Prior to this, his research potential was recognized with the prestigious Institute Post Doctorate Fellowship (IPDF) at the IIT Guwahati, India.

Dr. Khan's strong academic foundation includes a Ph.D. earned in 2019 from the National Institute of Technical Teachers Training & Research, Chandigarh (MoE, Govt. of India), a centrally funded institution. He also holds an M. Tech. degree from PEC University of Technology, Chandigarh, India (Administration of Union Territory of Chandigarh, Govt. of India), obtained in 2011 (Centrally Funded), and a B. Tech. from Govt. Engineering College Ujjain (Autonomous by Govt of M.P.), Madhya Pradesh, India, completed in 2009 (State Funded).

With over 14 years of experience in both Teaching and Research, Dr. Khan has demonstrated excellence in education, qualifying for the National level GATE examination and securing an impressive rank of 289 in the Madhya Pradesh Pre-Engineering Test (MP PET-2005).

His contributions to intellectual property include 02 granted Indian patents, with an additional 03 patents filed and published. He boasts a significant body of work with over 80 reputed publications, including in SCI and Scopus-indexed journals, and has also authored a book with an international publisher.

Dr. Khan's achievements have been recognized through 5 awards, including the Best Paper Award at IEEE CENCON, Malaysia, the Outstanding Scientist Award from ScienceFather India, the Best Young Scientist award from ITSR, India, and the UGC fellowship under the MANF Scheme. He has completed 04 projects sanctioned by HAREDA, Govt. of Haryana.

He is a sought-after speaker and expert, having delivered 09 Keynote addresses and served as a Technical Session Chair/Co-chair at International Conferences both in India and abroad. Additionally, he has given 05 invited lectures and served as a technical expert in various Seminars and Workshops. He has presented 17 research articles at various conferences.

Dr. Khan has actively contributed to the academic community by organizing 24 events, including Conferences, Workshops, etc. He has also undertaken 30 significant responsibilities, such as Chair of the Outreach

Committee, Chair of the Library, Deputy Chair of Academics, Deputy Chair of Sports, Hostel Warden, NBA Co-ordinator, Co-ordinator of the Affiliation Committee, and Co-ordinator of the AICTE committee. Currently supervising 4 Ph.D. scholars and mentoring 2 post-doctoral researchers in their advanced research work. He has successfully guided over 12 B.Tech student projects.

His professional engagement extends to membership in 8 technical committees and professional societies, and he serves as a reviewer for 40 reputed international journals. He has also undertaken 03 research projects and completed 02 MOOC certification courses recognized by AICTE. Furthermore, he has actively participated in more than 100 activities, including FDPs, STCs, Conferences, Training programs, Workshops, Seminars, and Webinars.

Areas of Interest: Artificial Intelligence, Embedded systems, Optimization Techniques, and Renewable Energy Sources.



Ram Murat Singh is a distinguished academic and researcher with a rich background in Instrumentation and Control Engineering. He completed his PhD from NITTTR, Chandigarh, and holds an M. Tech in Instrumentation from Panjab University, Chandigarh, where he earned a Gold Medal for his exceptional performance.

A recipient of the prestigious DST (INSPIRE) Fellowship from the Government of India, Dr. Singh has made significant contributions to his field, with 15+ research articles published in reputed international journals and conferences. He has also demonstrated his innovative prowess with 5 granted patents and 5 more in process.

Dr. Singh is actively involved in technical communities, being a member of organizations like ISTR, Jaipur, and an Associate Member of The Institution of Engineers India, among others.

With over 15 years of academic and industry experience, he has served renowned institutions such as SRM University, Chitkara University, JIS University, Assam Kaziranga University, and Woxsen University. Currently, he is making impactful contributions at Lovely Professional University, Punjab.



Md. Naqui Akhtar is Pursuing PhD from Birsa Institute of Technology (BIT) Sindri, Dhanbad under Jharkhand University of Technology (JUT), Ranchi. Mr. Akhtar received his Master of Engineering Degrees in Electrical Engineering (Instrumentation and Control Engineering) from National Institute of Technical Teacher's Training and Research (NITTTR), Panjab University, Chandigarh, India and B. Tech. Degree in Electrical Engineering from National Institute of Technology (NIT), Jamshedpur, Ranchi University, Jharkhand, India.

He is currently working as Lecturer, Department of Electrical Engineering in Government Polytechnic, Sahibganj, Under the Control of Department of Higher and Technical Education, Government of Jharkhand, Ranchi, India since April, 2021. It is guided by Jharkhand University of Technology (JUT), Ranchi, India. He is having 12 years of teaching experience and 03 years of administrative experience, worked as Assistant Director, Department of Science and Technology, Jharkhand, Nepal House, Doranda, Ranchi. He has one year of Industrial Experience in Ambuja Cement Limited Bhatapara Unit, Raigarh, Chattishgarh, India. He has done his M. Tech research work on NN based hybrid model for the detection of maximum power point tracking in PV system. He has published 07 research articles in reputed international journals.



Asyraf AFTHANORHAN is an Associate Professor at the Faculty of Business and Management, Universiti Sultan Zainal Abidin (UniSZA), Malaysia, where he currently serves as the Deputy Dean (Research & Development). He is also the leader of the Operation Research & Management Sciences (ORMS) research group. Dr. Asyraf is widely recognized for his expertise in statistical modeling, particularly Structural Equation Modeling (SEM), with extensive contributions in PLS-SEM, CB-SEM, measurement model assessment, predictive analytics, and applied quantitative research across business, health, and education disciplines.

He has authored more than 120 Scopus- and Web of Science–indexed publications, achieving an H-index of 25 on Scopus and 41 on Google Scholar, with more than 8,200 citations. He has received multiple prestigious awards, including the University Academic Award (AAU) for High Impact Publication (2021) and the Young Aspiration Academic Award (2023), as well as the Journal Active Author Award and Best-Selling Author Award in the Research & Innovation Award (RIA) 2023.

Dr. Asyraf is highly active in editorial and reviewing roles, serving as the Editor-in-Chief of the Journal of Management Theory and Practice (JMTP) and contributing as editor and reviewer for various international journals. He regularly delivers workshops and training on quantitative analysis, SEM, academic writing, and publication strategies.

His research interests include statistical modeling, consumer behavior, health services evaluation, digital transformation, entrepreneurship, and policy research. He is also involved in developing collaborative projects with international institutions and industry partners, fostering impactful research, innovation, and community development.

Copyrights
© 2026 Licensee Shahid Chamran University of Ahvaz, Ahvaz, Iran. This article is an open-access article distributed under the terms and conditions of the Creative Commons Attribution –NonCommercial 4.0 International (CC BY-NC 4.0) License (http://creativecommons.org/licenses/by-nc/4.0/).

Shahid Chamran University of Ahvaz

Iranian Association of Electrical and Electronics Engineers

Journal of Applied Research in Electrical Engineering

E-ISSN: 2783-2864
P-ISSN: 2717-414X
Homepage:https://jaree.scu.ac.ir/



Research Article

Optimal Energy Management in Solar-powered Battery-Ultracapacitor Hybrid Electric Vehicles: Leveraging ANN-HDKR for Tilt Angle Optimization

Shraddha Kaushik[1,2*] and Kunamneni Rachanajali[2]

[1]*Department of Electrical Engineering, Bhilai Institute of Technology, Durg, India*

[2]*Department of Electrical & Electronics Engineering, Vignan Foundation for Science Technology & Research, Guntur, India*

** Corresponding Author: shraddha.kaushik@bitdurg.ac.in*

Abstract: This paper presents a comprehensive methodology to improve solar irradiance forecasting and optimize its integration into Hybrid Electric Vehicle (HEV) Energy Management Systems (EMS). Accurate solar irradiance prediction is critical for maximizing renewable energy utilization and ensuring reliable operation of hybrid storage devices. To achieve this, the proposed framework combines Deep Neural Networks (DNNs) with the Horizontal Diffuse K Clearness Index Regression (HDKR) technique for day-ahead forecasting of Global Horizontal Irradiance (GHI). This hybrid approach not only predicts GHI with high precision but also decomposes it into beam, diffuse, and reflected components on tilted surfaces, thereby enabling more realistic modeling of Photovoltaic (PV) generation under varying conditions. The forecasting model achieved an R-squared value of 0.8818 and a Root Mean Square Error (RMSE) of 0.269, confirming its robustness and accuracy. These forecasts are incorporated into a real-time EMS that coordinates energy distribution among the battery, ultracapacitor, and PV subsystems while accounting for seasonal variability, auxiliary system demands, and dynamic driving cycles. Unlike traditional static State of Charge (SOC) targets, the proposed dynamic SOC control adapts to daily, monthly, and seasonal variations, allowing efficient energy sharing between storage devices. This strategy reduces stress on critical battery components by 47.6%, thereby improving both performance and lifespan. Furthermore, the integration of ultracapacitors effectively mitigates transient load demands, ensuring higher system reliability under fluctuating conditions. Overall, the research demonstrates how HDKR-based estimation combined with adaptive EMS strategies can significantly enhance efficiency, sustainability, and durability in solar-assisted HEVs.

Keywords: Solar irradiance forecasting, Energy management scheme, Ultra-Ccapacitor (UC), Photovoltaic (PV), Hybrid Electric Vehicle (HEV).

Article history
Received 22 January 2025; Revised 12 December 2025; Accepted 17 December 2025; Published online 18 January 2026.
© 2026 Published by Shahid Chamran University of Ahvaz & Iranian Association of Electrical and Electronics Engineers (IAEEE)
How to cite this article
S. Kaushik and K. Rachanajali, "Optimal energy management in solar-powered battery-ultracapacitor hybrid electric vehicles: Leveraging ANN-HDKR for tilt angle optimization," *J. Appl. Res. Electr. Eng.*, vol. 4, no. 1, pp. 137-153, 2025. DOI: 10.22055/jaree.2025.48780.1152

Check for updates

NOMENCLATURE

HEV	Hybrid Electric Vehicle
PV	Photovoltaic
LSTM	Long Short-Term Memory
EMS	Energy Management Scheme
UC	Ultra-Capacitor
Solar_Zenith	Solar zenith angle, represents the angle between the direction of the sun and the vertical (zenith) line.
EV	Electric Vehicle
SOC	State Of Charge
MPPT	Maximum Power Point Tracking
P&O	Perturb And observe
ESS	Energy Storage System
ICE	Internal Combustion Engine
HESS	Hybrid Energy Storage System
R^2	Correlation Coefficient
$G_{diffuse,horizontal}$	Diffuse Radiation on the horizontal surface
G_{total}	Total radiation (sum of beam, diffuse and reflected)
R_b	Incidence angle modifier
GHI	Global Horizontal Irradiance

DNI	Direct Normal Irradiance (Beam Radiation)
HESS	Hybrid energy storage system
G_{beam}	Beam radiation on the tilted surface
$G_{beam,\ horizontal}$	Beam radiation on a horizontal surface
G_d	Isotropic Sky Diffuse Radiation
ESS	Energy Storage System
RMSE	Root Mean Square Error
MSE	Mean Square Error
MAE	Mean Absolute Error
RNN	Recurrent Neural Networks
$G_{d,\ \beta}$	Diffuse Radiation on the tilted surface
MPC	Model predictive controller
ML	Machine Learning
Θ	Incidence angle (angle between the normal to the surface and the direction of the sun)
$Θ_{solar}$	Solar Zenith Angle
Kt	Clearness index, representing the ratio of measured solar radiation on a horizontal surface to extraterrestrial solar radiation.

1. INTRODUCTION

1.1. Background

India's transportation sector has set ambitious goals for climate neutrality, aiming to achieve a substantially climate-neutral vehicle stock by 2050. To reach this target, emissions must be reduced by nearly 66% compared to 1990 levels by 2030. In support of this transition, the Indian government introduced policies in 2020 that provided low-interest loans and subsidies of up to 45% for consumers purchasing Hybrid Electric Vehicles (HEVs). These incentives have spurred growth, and by 2023, HEV adoption had increased by 8%, with nearly 10 million units sold nationwide. The majority of these vehicles approximately 76%are compact HEVs primarily used in urban settings. However, fossil fuel-powered vehicles continue to dominate energy consumption, accounting for 70% of personal commuting and 20% of freight transport needs. This ongoing dependence on fossil fuels underscores the urgency of advancing efficient hybrid and electric vehicle technologies. Plug-in Hybrid Electric Vehicles (PHEVs) and Battery Electric Vehicles (BEVs), particularly when powered by renewable energy sources such as solar, are considered essential for reducing greenhouse gas emissions and ensuring sustainable mobility [1]. Projections suggest that by 2030, India's HEV stock could exceed 50 million units, further highlighting the importance of integrating renewable-based energy management solutions. The need for this paper therefore arises from the twin imperatives of decarbonizing transport and exploiting solar resources effectively within HEV architectures.

1.2. Literature Review

Machine Learning (ML) and Deep Learning (DL) approaches have emerged as powerful tools for solar irradiance forecasting, a key enabler of solar-powered HEVs. Techniques such as Recurrent Neural Networks (RNNs), Convolutional Neural Networks (CNNs), Long Short-Term Memory (LSTM) models, and hybrid ensemble methods have been widely studied for their ability to capture nonlinear temporal dependencies in irradiance data [2]. Research has categorized models into residual-based, evolutionary-based, decomposition-based, clustering-based, and hybrid ensemble learning methods, consistently finding that hybrid approaches outperform standalone models, albeit with limited metric-based comparisons [3]. Among these, DL-based LSTM models stand out for their superior forecasting accuracy, often yielding lower Root Mean Square Error (RMSE) values than other methods [4]. Complementary methods such as Random Forest (RF) have also shown promise in estimating Global Horizontal Irradiation (GHI), Beam Normal Irradiation (BNI), and Diffuse Horizontal Irradiation (DHI), with RF outperforming traditional Artificial Neural Networks (ANNs) and smart persistence methods over longer prediction horizons [5].

Solar irradiance estimation on tilted surfaces remains another critical area of research. The Horizontal Diffuse K Clearness Index Regression (HDKR) model has long been used to characterize solar radiation by incorporating tilt angles, atmospheric conditions, and solar positions [6]. Transposition models based on HDKR have been successfully applied for energy system design, though their accuracy is limited by the quality of location-specific input data [7]. Recent works also demonstrate the application of HDKR in diverse domains such as agriculture, architecture, and renewable power generation [8]. Comparative studies of isotropic, anisotropic, and HDKR models confirm HDKR's superior ability to handle tilted surface irradiance estimation [9,10]. These methods are essential in contexts where global and diffuse irradiances are measured, allowing beam irradiance to be derived using $G_h = B_h + D_h$, where G_h, B_h, and D_h represent global, beam, and diffuse irradiances, respectively [10].

Parallelly, the development of Zero-Fuel Zero-Emission (ZFZE) vehicle concepts has inspired hybrid architectures integrating PV, wind energy, fuel cells, and supercapacitors for automotive applications [11]. Such designs leverage in-wheel motors, Proton Exchange Membranes (PEMs), and hybrid storage systems to enhance efficiency and reduce carbon emissions [12]. Energy Management Strategies (EMS) for these systems have been broadly categorized into predictive and non-predictive methods, ranging from rule-based heuristics to model predictive control [13–15]. Despite advancements, most of these methods do not integrate solar forecasting into HEV EMS design.

For instance,[36] proposed a voltage regulation strategy for distribution networks using reactive power from photovoltaic inverters combined with PID consensus algorithms, illustrating the potential of intelligent PV control for improving grid reliability. This [37] paper develops a Deep Neural Network (DNN)-based Nonlinear Model Predictive Control (NMPC) methodology to approximate optimal power management solutions for hybrid electric vehicles. The deep learning model is trained to mimic the outcomes of a computationally intensive NMPC, providing near-optimal energy distribution decisions (e.g., battery vs engine) with significantly reduced computation time, which is essential for real-time scheduling. Together, these works highlight the broader potential of solar energy optimization but reveal that integration with EMS in HEVs remains underexplored.

1.3. Research Gap and Motivation

Although substantial work has been carried out on solar forecasting and EMS design, several gaps remain that motivate this study. First, existing forecasting models focus primarily on horizontal irradiance, with limited attention to tilted-surface predictions crucial for vehicle-mounted PV modules. Second, while HDKR is widely accepted, its dependency on local calibration reduces generalizability across diverse geographies like India. Third, most HEV-EMS frameworks overlook the variability and uncertainty of solar input, failing to dynamically adapt to fluctuating irradiance and driving conditions. Fourth, while battery–ultracapacitor hybrid storage offers complementary benefits, strategies for their optimal real-time coordination under varying load profiles are lacking.

A new method is needed because existing forecasting techniques such as ANNs, Random Forests, or standalone LSTM networks often suffer from overfitting, limited long-horizon accuracy, or lack of adaptability when integrated into real-time EMS. Similarly, conventional EMS approaches, particularly rule-based methods, are simple and computationally efficient but cannot accommodate uncertainties in solar forecasts or seasonal variations, leading to suboptimal energy allocation. Optimization-based EMS, while more advanced, often become computationally expensive and unsuitable for real-time driving conditions. Therefore, integrating a deep learning-based forecasting framework with HDKR for tilted surfaces, and embedding it within a constraint-driven EMS, offers a novel solution that overcomes the limitations of existing models. The motivation for this work is thus to ensure higher prediction accuracy, better adaptability to varying conditions, and improved hybrid storage utilization in solar-assisted HEVs.

1.4. Challenges

The primary challenge this research aims to address is the integration of accurate solar irradiance forecasting with energy management in hybrid electric vehicles (HEVs), where the variability of solar radiation, limitations of conventional ANN-based forecasting models, and inefficiencies in rule-based EMS strategies hinder reliable power distribution between battery and ultracapacitor systems. This work proposes a novel HDKR-based methodology to overcome these challenges by improving solar prediction accuracy on tilted surfaces and developing a constraint-driven EMS for real-time driving conditions.

Despite significant advances in solar forecasting and energy management strategies, several limitations in existing approaches hinder their effectiveness in real-world hybrid electric vehicle (HEV) applications. Traditional solar forecasting methods such as artificial neural networks (ANNs) and Random Forests (RF) provide reasonable short-term accuracy, but their performance often deteriorates for longer horizons due to overfitting, sensitivity to noise, and inability to effectively capture spatiotemporal dependencies in solar irradiance data. Moreover, most models are trained on horizontal irradiance measurements, which makes them less applicable for tilted surfaces where irradiance distribution is strongly influenced by tilt angle, azimuth, and diffuse radiation. Transposition models like the Horizontal Diffuse K Clearness Index Regression (HDKR) are widely used for tilted-surface estimation; however, their reliability depends on site-specific calibration and simplified assumptions about atmospheric conditions, which limit generalizability across different climates and geographies.

On the energy management side, rule-based EMS strategies are attractive for their simplicity and low computational requirements, yet they lack adaptability and fail to consider uncertainties from fluctuating irradiance and varying driving profiles, leading to suboptimal energy allocation between battery and ultracapacitor. Optimization-based methods such as Mixed-Integer Linear Optimization (MILO) provide more precise control but are computationally demanding and impractical for real-time driving scenarios. Similarly, predictive EMS approaches rely heavily on accurate forecasts and often break down when faced with forecast errors or unmodeled dynamic conditions. Collectively, these limitations reveal that existing methods are either too simplistic to handle variability or too complex to operate in real time, underscoring the need for a hybrid framework that combines the predictive accuracy of advanced machine learning models like LSTM with the practicality of enhanced rule-based EMS adapted for real-time HEV operation.

1.5. Contributions and Benefits

This paper addresses the aforementioned needs and challenges through the following contributions. First, it develops a deep neural network-based solar irradiance prediction model trained on site-specific data from Durg, Chhattisgarh (21.191°N, 81.299°E, 289 m elevation), ensuring high accuracy and contextual relevance. Second, it integrates the data into the HDKR model for tilted-surface irradiance estimation, directly applicable to HEVs with embedded PV modules. Third, it proposes a novel constraint-driven EMS that optimally coordinates battery and ultracapacitor storage, accounting for forecast uncertainty and seasonal variations. Fourth, it validates the proposed framework against real driving cycles, showing improvements in energy efficiency, reliability, and storage utilization compared with existing methods. The benefits of this research lie in enabling solar-assisted HEVs to meet power demand requirements more reliably, extend component lifetimes, and operate efficiently under variable driving and environmental conditions.

1.6. Paper Organization

The rest of the paper is organized as follows. The paper begins by addressing current transportation system issues and introducing the proposed model represented by Fig-1. Following that, it goes into elaborate detail describing the fundamental block diagram, component information, and ratings. Section 2 introduces the overall HEV architecture and describes system components. Section 3 presents the modified solar energy estimation model and HDKR integration. Section 4 explains the model implementation. Section 5 details the constraint-driven EMS and hybrid storage optimization. Section 6 reports simulation results and performance analysis. Finally, Section 7 concludes with contributions, limitations, and potential avenues for future research.

1.7. Proposed Framework

Fig. 1 show the proposed framework for Solar irradiance forecasting with modified interleaved and EMS technique.

2. SOLAR IRRADIANCE FORECASTING

2.1. Data Collection and Preprocessing

For the Durg, Chhattisgarh region, data is gathered via PVsyst Software and NASA's POWER Data Access Viewer. The global horizontal irradiance (GHI), temperature, dew point, wind speed, relative humidity, pressure, precipitable water, wind direction, and other meteorological characteristics are all included in the dataset. Furthermore, data on surface albedo, cloud type, ozone, solar zenith angle, and clear-sky irradiance are acquired. To guarantee data quality and consistency, preprocessing is done on the data before the machine learning models are trained. This includes resolving missing values, eliminating superfluous features (like fill flags), and generating numerical representations for categorical variables (like cloud type). To scale the features within similar categories and enhance the convergence and performance of the models, data normalization techniques are also employed. Neural networks are well-suited for solar prediction tasks that involve variables such as azimuth angle and zenith angle due to their ability to capture complex, non-linear relationships inherent in solar radiation dynamics.

Neural networks can handle historical sun radiation measurements and other related environmental variables because they can scale to analyse big datasets quickly. They are an effective tool for solar prediction applications owing to their capacity to adjust to shifting conditions and continue providing accurate forecasts over time. There are 21 properties in this dataset, of which 20 are input features that range from sun zenith angle to average barometric pressure. Our target variable, which expresses the amount of electricity produced by the PV module in kW, is represented by the remaining attribute [16].

2.2. Solar Prediction Using Neural Network

In order to produce expected outputs, input characteristics are fed via hidden layers throughout the forward propagation process. Activation functions, such sigmoid or RELU, play a crucial role in determining how each layer's output is shaped. The difference between predicted and actual outputs over several samples is measured by the mean squared error (MSE), which is often employed as the loss function to evaluate the neural network's performance. [17-19]. Readjusting network parameters, like weights and biases, depending on the calculated errors at each layer is made easier by the backpropagation method. Finally, weights and biases are iteratively updated using gradient descent optimization, which directs the network toward reducing the loss function. Neural networks provide a strong framework through this method for improving solar prediction accuracy, leading to more effective utilization of solar energy resources [20].

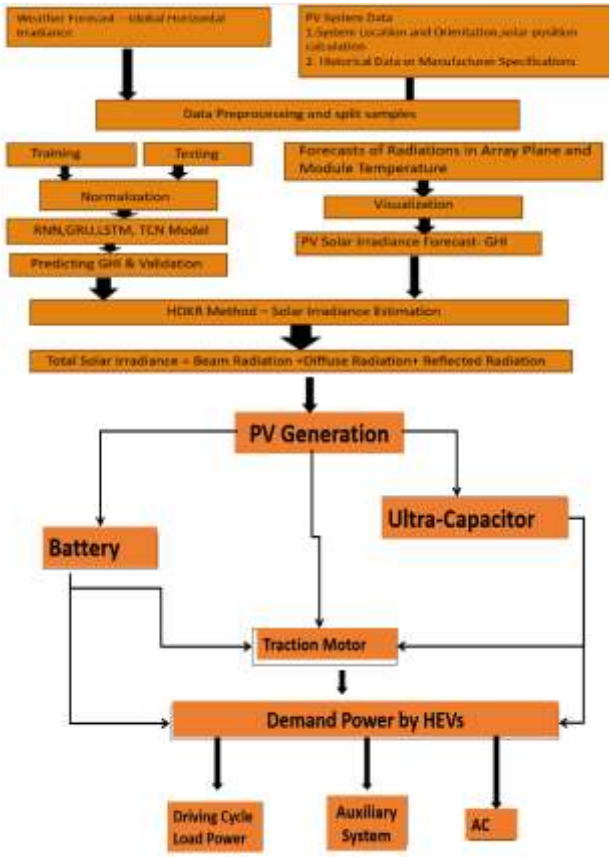


Fig. 1: Proposed block representation – Solar irradiance forecasting with modified interleaved and EMS technique.

3. MODIFIED SOLAR ESTIMATION FOR OPTIMAL ENERGY MANAGEMENT SYSTEM USING HDKR METHOD IN HEVS

Precise evaluation of solar radiation components, including beam and diffuse radiations, is required to optimize energy management strategies in electric vehicles. This paper proposes an improved methodology for an accurate calculation of solar radiation components on tilted surfaces using the Hay, Davies, Klucher, and Reindl (HDKR) technique. [21-22] The efficiency of the proposed methodology in improving the estimation of solar radiation's accuracy by thorough simulations experiments. Improved energy management and the incorporation of solar energy systems into electric vehicles configurations is implemented with this method. To calculate the diffuse and beam radiations on tilted surfaces more precisely, the HDKR technique incorporates a number of geometric and atmospheric factors. The HDKR method's primary steps are as follows:

3.1. Solar Time (t_solar)

Solar time (t_solar) is the time indicated by the position of the Sun in the sky. It accounts for variations in the Earth's rotation and orbit around the Sun. The formula to calculate solar time is given by (1) [38]:

$$t_{solar} = time + \frac{4.(logitude - logit_{zone}) + e}{60} \quad (1)$$

where:
- Time is the standard time.
- longitude is the observer's longitude.

- longit_zone is the standard time zone meridian.
- e is the equation of time.

3.2. Equation of Time (e)

The equation of time (e) represents the difference between mean solar time and apparent solar time. It is calculated using the following formula is given by (2):

$$e = 229.2* (0.000075 + 0.001869*\cos(b) - 0.032077 * \sin(b) - 0.014615 * \cos(2b) - 0.04089 *\sin(2b)) \quad (2)$$

where b represents the Earth's orbital position for a given day of the year.

3.3. Declination Angle (δ)

The declination angle (delta) indicates the angle between the rays of the Sun and the plane of the Earth's equator. It is calculated using the formula:

$$\delta = 23.45* \sin(360 *(284 + day)/365) \quad (3)$$

where day represents the day of the year.

3.4. Solar Azimuth Angle

The horizontal direction of the Sun with respect to a reference direction is indicated by the solar azimuth angle. The latitude, declination angle, and solar zenith angle of the observer will be utilized to calculate it. The equation is given by (4):

$$\text{Solar_azimuth} = \text{sign}.\cos^{-1}\left(\frac{\cos(solar_{zenith}).\sin(latitude) - \sin(\delta)}{\sin(solar_{zenith}).\cos(latitude)}\right) \quad (4)$$

whare Sign = 1 if $t_{solar} \geq 12$, otherwise Sign = -1

3.5. Incidence Angle (Θ)

The angle formed by the direction of incoming solar radiation and the normal vector to a surface is called the incidence angle (σ). It is computed by (5) as follows [39]:

$$\Theta = \cos(\text{solar_zenith}) * \cos(\text{tilt_angle}) + \sin(\text{solar_zenith}) * \sin(\text{tilt_angle}) \cos(\text{solar_azimuth} - \text{surface_azim}) \quad (5)$$

3.6. Solar Radiation (G_{sc}, $G_{horizontal_radiation}$)

Solar radiation refers to the electromagnetic energy emitted by the sun and received at a particular location on Earth's surface. The average solar irradiation at the top of the earth's atmosphere is represented by the solar constant (Gsc). The radiation formula is given by (6) in the horizontal direction.
Solar Radiation ($G_{horizontal_radiation}$)

$$G_{horizontal_radiation} = Gsc *(1.000110 +034221 *\cos(b) +0.00128sib(b) + 0.000719*\cos(2b) +0.000077*\sin(2b)) \quad (6)$$

3.7. Clearness Index (K_t) and Diffuse Fraction (R_{od})

The clearness index (K_t) represents the ratio of the solar radiation measured on a horizontal surface to the extraterrestrial solar radiation. The diffuse fraction (R_{od}) indicates the fraction of total solar radiation that is diffuse rather than direct radiation. (K_t)and (R_{od}) are calculated using the provided formulasby (7)[40].

$$K_t = \frac{G_{horizontal_radiation}}{\text{solar}_{\text{radiation}} * \cos(\text{solar}_{\text{zenith}})}$$

$$R_{od} = \begin{cases} 1 - 0.249 * K_t, \text{if } K_t \leq 0.35 \\ 0.177, if\ K_t > 0.75 \\ 1.557 - 1.84 * K_t, otherwise \end{cases} \quad (7)$$

The ratio of solar radiation measured on a horizontal surface to solar radiation from extraterrestrial sources is known as the clearness index (K_t). The percentage of total solar radiation that is diffuse rather than direct is known as the diffuse fraction, or R_{od}. The given formulas are used to determine (K_t) and (R_{od}) by (8)[41].

$$K_t = \frac{GHI}{clear-skyGHI} \quad (8)$$

The key steps involved in the HDKR method include:

1. *Beam radiation calculation:* To determine the incidence angle modifier (δ) and use it to modify beam radiation in order to obtain beam radiation on tilted surfaces (G_{beam}).

2. *Diffuse Radiation Calculation:* The isotropic sky diffuse radiation (G_d), which is an approximation of the diffuse radiation originating from the sky dome as a whole, is determined. Making use of the tilt angle to modify the isotropic sky diffuse radiation in order to obtain the diffuse radiation on the tilted surface. Compute the circumsolar diffuse radiation as well, which is the diffuse radiation originating from a given angular radius surrounds the solar disk.

3. *Beam and Diffuse Radiations:* Add the beam and diffuse radiations to get an estimate of the total radiation on the slanted surface by (9).

Total solar Radiation = Beam Radiation + diffuse radiation + reflected radiation. (9)

4. Model Implementation

The model is applied and the accuracy of the GHI projections for 2024 is determined using meteorological data ranging 2019 to 2024. While the input features include GHI, meteorological information, and the clearness index for the previous 24 hours, the output includes the total GHI for the next hour and the next 24 hours. The model design uses a single hidden layer structure with a sigmoidal activation function to handle gradient dispersion and computation performance. On the hidden layer, dropout regularization is applied to minimize overfitting. The output layer computes the loss function between the target and predicted outputs, giving the Mean Absolute Error (MAE). The obtained gradients are used by the backpropagation (BP) technique to adjust the network weights.[17] The Adam algorithm is used to create optimization parameters till convergence. The model applies denormalization to the output after training to pair the predicted values with the corresponding time-series data.

4.1. Performance Evaluation Metrics

Four error metrics were evaluated for evaluating the forecasting model's performance using equations (10) and (11):

1. Root Mean Square Error (RMSE): This measures the difference between predicted and actual values. Better predicting accuracy is shown by a lower RMSE. The equation is:

$$\mathbf{RMSE} = \sqrt{\frac{1}{N}\sum_{i=1}^{N}((P_f - P_a)^2} \quad (10)$$

where N is the number of observations, P_f is the forecast value, and P_a is the actual value.

2. R-Squared (R^2): R-Squared, which goes from 0 to 1, evaluates how well the predictive model fits the data. Better fit is indicated by a higher value. The formula is given by the following equation [18]:

$$R^2 = 1 - \frac{\sum_{i=1}^{N}((P_f - P_a)^2}{\sum_{i=1}^{N}((P_f - P_a)^2} \quad (11)$$

The computational model is developed using the Julia programming language (version 1.4.0) in conjunction with the JuMP optimization package (version 0.21.2), both of which are open-source and publicly accessible. For solving the formulated optimization problem, the Gurobi solver (version 0.76) is employed under an academic license.

5. Scheduled Constrained Driven Energy Management Strategy

The objective of the paper is to meet specific electrical energy requirements for both the driving cycle and auxiliary systems by optimizing the operation of an integrated energy management system. By the investigation of a model vehicle equipped with a photovoltaic system, battery, and ultracapacitor for energy storage, the research evaluates whether different configurations and objectives impact significant metrics for performance [23]. The study analyses optimal energy flows with hourly resolution over a year, taking into account complicated dependencies and technical constraints, using Mixed-Integer Linear Optimization (MILO). Attention is placed on the different modes of power consumption of the modulating traction motor during the driving cycle and while the auxiliary system is operating. To guarantee reproducibility and transparency, the study provides models, parameters, and visualization code. This study analyses the flow variable given in Table 3. the operational control of a traction motor and PV system [24]. They differentiate between predictive and nonpredictive approaches, with nonpredictive methods relying on rule-based or schedule-based algorithms [25-27]. In these approaches, the traction motor is activated based on

Table 1: Pseudo-code for ANN-based solar forecasting algorithm.

Preprocess data:
-Number of Samples:15000,60% for Training and 40% for Test;
-num_epochs = 100, batch_size = 32, num_hidden_neurons = 256, num_input_neurons = 87

Adding azimuth angle and incidence angle to input neurons
num_output_neurons = 1

Train the model
-for epoch in range(num_epochs):
-for batch_idx in range(len(X_train_batches)):

Get the current batch
- X_batch = X_train_batches[batch_idx]
-y_batch = y_train_batches[batch_idx]

Forward propagation
Extract azimuth angle and incidence angle from X_batch
-azimuth_angle = X_batch[:, -2] # Assuming azimuth angle is the second last column
-incidence_angle = X_batch[:, -1] # Assuming incidence angle is the last column

Concatenate azimuth angle and incidence angle with input features
-X_batch_with_angles = np.concatenate((X_batch[:, :-2], azimuth_angle[:,np.newaxis], incidence_angle[:,np.newaxis]), axis=1)

Compute hidden layer activations
-a_hidden = np.dot (X_batch_with_angles, W_hidden) + b_hidden

Apply activation function
-a_hidden = np.maximum (a_hidden, 0)

Compute output layer activations
- y_pred = np.dot (a_hidden, W_output) + b_output

Compute loss (e.g., mean squared error)
- loss = np.mean((y_pred - y_batch) ** 2)

Backpropagation & Compute gradients
-delta_output = y_pred - y_batch
-delta_hidden = np.dot (delta_output, W_output.T) * (a_hidden> 0)

Update weights and biases
-W_output -= alpha * np.dot (a_hidden.T, delta_output)
- b_output -= alpha * np.mean(delta_output, axis=0)
-W_hidden -= alpha * np.dot (X_batch_with_angles.T, delta_hidden)
-b_hidden -= alpha * np.mean(delta_hidden, axis=0)

Optionally, print loss or other metrics
-if batch_idx % 10 == 0:
-print (f'Epoch {epoch+1}, Batch {batch_idx+1}, Loss: {loss:.4f}')

Evaluate the model on the testing set
-y_pred_test = np.dot (np.maximum(np.dot(X_test, W_hidden) + b_hidden, 0), W_output) + b_output

Compare the real data with the predicted data

Table 2: Ratings of the hybrid electric vehicle.

Parameter	Value	Parameter	Value
Battery Type	Li-ion	Cells in Module	3 in series
Battery Cell	40 Ah/60V	Battery Modules	31 in series
Battery Cell	0.378 kg	Maximum Capacity (Ah)	40
UC Type	PC2500	UC Cells	120
UC Voltage	225V	UC Capacitance	58F
UC Resistance	0.02	Battery Efficiency	88
HEV MASS	830kg	PV Cell Voltage	27.3
Frontal Area	2.03 m^2	PV Cells in series and parallel	20 & 3
Motor Type	IM (AC75)	Motor Torque scale	0.268
Motor Power	20kW	Initial Temp.	30 °C
Cargo	136kg	Average Load	1.28
Input Neurons	6	Hidden Layer	2 layers
Neurons per hidden layer	20	Activation Function	ReLU (Hidden Layers), Linear (Output Layer)
Batch Size	32	Learning Rate	0.001
Training Epochs	300	Regularization	Dropout (0.3), L2 (0.0005)
Optimizer	Adam	Weight Initialization	Xavier

Table 3: Flow variables.

Demand Fulfillment	C_{pv}-E_{demand}, C_{bat}-E_{demand}, C_{UC}-E_{demand}, C_{pv}-$_b$. C_{pv}-$_{UC}$
Traction Motor inflows	C_{pv}-$_{Tr}$, C_{UC}-$_{Tr}$. C_b-$_{Tr}$
Traction Motor modulation	C_{Tr}-$_{Driving\ cycle}$, C_{Tr}-$_{AC}$

predefined condition on time etc. The hybrid energy management system (HEMS), consists of a traction motor (Tr), ultracapacitor (UC), battery (B), and PV system (PV). The vehicle's auxiliary system and driving cycle can both be powered by the traction motor. The study includes the following known parameters: the external temperature ($T_{external}$), PV generation (C_{pv}), driving cycle demand (C_{dc}), auxiliary system demand (C_{Paux}), and electricity demand (E_{demand}).By the setting of a one-year control horizon at a time resolution of one hour, for the fundamental features of the most effective control strategy. The PV system ($C_{Ppv}\rightarrow E_{demand}$), battery ($C_{bat}\rightarrow E_{demand}$), or ultracapacitor ($C_{UC}\rightarrow E_{demand}$) can supply the power flow required to satisfy electricity demand (E_{demand}).

It guarantees that the entire amount of power generated is equal to the sum of the flows from the PV system to meet demand, storage devices, ultracapacitors and traction motors. The energy balance of the battery state of charge (SOC_b) is computed using (13). SOC_b rises when the PV system's electricity supply rises ($C_{Ppv}\rightarrow C_b$), and it falls when the traction motor ($C_{bat}\rightarrow C_{TR}$) or the battery supplies electricity to meet demand ($C_{bat}\rightarrow E_{demand}$).
Three sources can supply electricity to the traction motor: the ultracapacitor ($C_{PUC}\rightarrow C_{Tr}$), the PV system ($C_{Ppv}\rightarrow C_{Tr}$), or the battery ($C_{Pb}\rightarrow C_{Tr}$). It functions in two modes: $C_{PTR}\rightarrow C_{DC}$ for the driving cycle and $C_{TR}\rightarrow C_{AUX}$ for the auxiliary system, which reflect different energy flows. The driving cycle (C_{ModDC}) and auxiliary modes (C_{ModAUX}) modulation degrees are continuous variables with a range of zero to one.

Objective Function: $J = \sum_{t=1}^{N}(PV_t + AC_t + DC_t$ (12)

Subject to the following constraints:
Energy balance constraint:

$$AC_t + DC_t + SOC_t - SOC_{t-1} = PV_t - C_{loss} \cdot \left| SOCt - SOC_{t-1} \right|$$

State of charge constraints: (13)

$SOC_{min} < SOC_t < SOC_{ma}$

Non-negativity constraints:

$AC_t \geq 0, DC_t \geq 0, SOC_t \geq 0$

where $C_{PV\text{-}DC}(t)$, $C_{b\text{-}DC}(t)$, $C_{UC\text{-}DC}(t)$ represents the energy flow from PV system to battery, ultracapacitor and the grid to the driving cycle and AC at time t respectively. $C_{PV\text{-}DC}(t)$, $C_{PV\text{-}AC}(t)$, $C_{PV\text{-}B}(t)$, $C_{pv\text{-}UC}(t)$, the energy flow from the PV system to the driving cycle, AC, battery, PV, grid at time *t* respectively. The objective function J given by equation in 12 continues to represent the overall energy consumption across the time horizon *N* in this extended formulation. All time intervals' energy consumption terms for the PV, AC, and DC cooling systems are added together. Every time step, energy generation, consumption, and storage are balanced due to the energy balance constraint. The term that penalizes differences in the state-of-charge between consecutive time intervals is used to account for energy losses $C_{loss.}\left| SOCt - SOC_{t-1} \right|$.In order to guarantee that the energy storage system functions within its capacity limitations, the state-of-charge constraints limit the SOC within permissible parameters are SOC_{min} to SOC_{max}. Energy consumption and state-of-charge must both remain non-negative during the optimization phase due to the non-negativity restrictions AC_t and DC_t given by (13).

Flow constraints:

$C_{PV\text{-}DC(t)} + C_{B\text{-}DC}(t) + C_{UC\text{-}DC}(t) = DC(t)$ (14)

$C_{PV\text{-}DC}(t)+ C_{PV\text{-}B}(t)+C_{pv\text{-}UC}(t)+C_{PV}\text{-}AC(t) = GE(t)$

Battery constraints:

$$SOC_b(t+1) = (1\text{-}loss_b) *SOC_b(t) + \eta_b *C_{PV\text{-}B}(t) - \left(\frac{Cb-DC(t)+Cb-Tr(t)}{\eta b}\right)$$
$$SOC_{min}^{b} \le SOC_b(t) \le SOC_{max}^{b} \quad (15)$$
$$C_{B-DC}(t), C_{PV-B}(t), C_{B-DC}(t) \le B_{\max,\text{rate}}$$

where, $SOC_b(t)$ denotes the state of charge of battery at time t, $Loss_b$ represents the energy loss factor of the battery, η_b is the efficiency of the battery, SOC_{min}^{b} and SOC_{nmax}^{b} denotes the maximum and minimum allowable state of charge for the battery, $B_{\max,\text{rate}}$represents the maximum charging/discharging rate of the battery.

The constraints given by (14) and (15) ensure that energy flows and state of charge levels of the battery, ultracapacitor and PV for increasing the efficiency of electric vehicle. Let P_{demand} be the power demand, P_{min} be the minimum power, P_{PV} be the power of PV, P_{bat} be the battery power and P_{UC} be the UC Power. The system power supply hierarchy can be represented by (16) and (17):

P_{supply} =

P_{PV} , if $P_{PV} \ge P_{min}$

P_{bat} , if $P_{PV} < P_{min}$ and $P_{bat} \ge P_{min}$ - P_{PV} (16)

P_{UC} , if ($P_{PV} < P_{min}$) and ($P_{bat} < P_{min}$ - P_{PV}) and ($P_{UC} \ge P_{min}$- $P_{PV} - P_b$)

P_{ICE} , otherwise

Under regenerative mode:

$P_{UC,Charge}$ =

0 , if $P_{demand} \ge 0$

$\alpha \cdot P_{PV,excess_}$, if ($P_{demand} < 0$) and ($P_{UC_SOC} < P_{UC_MAX_SOC}$) (17)

$\beta \cdot (P_{demand} - P_{PV,excess})$, if ($P_{demand} < 0$) and ($P_{UC_SOC} \ge P_{UC_MAX_SOC}$)

where $P_{PV,excess}$= max(0, P_{PV} - P_{PVmax})

Traction motor constraints:

$C_{TR}(t) = C_{PV}\text{-}_{TR}(t) + C_{B\text{-}TR}(t)$

$C_{TR}(t) \le T_{Rmax_power}$

$C_{TR\text{-}DC}(t) + C_{TR\text{-}AC}(t) = C_{PV\text{-}TR}(t) _C_{UC\text{-}TR}(t) + C_{B\text{-}TR}(t)$

$C_{TR\text{-}DC}(t) = Mode_{DC}(t) * DC_{max_power}$ (18)

$C_{TR\text{-}AC}(t) = Mode_{AC}(t) * DC_{max_power}$

$Mode_{DC}(t) * T_{Rswitch}(t) \le DC_{max_power}$

$Mode_{AC}(t) * (1- T_{Rswitch}(t)) \le 1- T_{R\ max_power}$

Air Conditioning (AC) constraints

$$C_{AC}(t) = Cpv\text{-}tr(t) + C_{B\text{-}AC}(t) + C_{UC\text{-}AC}(t)$$
$$C_{AC}(t) \le AC_{max_power} \quad (19)$$

where $C_{TR}(t)$ and $C_{AC}(t)$ represents the power consumed by the traction motor and air conditioning unit at time t.$C_{PV\text{-}DC}(t)$, $C_{PV\text{-}B}(t)$, $C_{PV\text{-}UC}(t)$ and $C_{PV\text{-}TR}(t)$ represents the flows of energy from PV system to driving cycle cooling system, battery, ultracapacitor and traction motor at time t respectively. $SOC_B(t)$ and $SOC_{UC}(t)$ are the state of charge of the battery, ultracapacitor at time interval at time t. $Loss_b$ represents the energy loss factor of the battery.η_b is the efficiency of the battery. SOC_{min}^{b} and SOC_{max}^{b} denotes the minimum and maximum allowable state of charge for the battery, respectively.$B_{\max,\text{rate}}$ represents the m, maximum charging/discharging rate of the battery represented by (18) and (19).

6. Simulation Results- Comparing Predicted vs. Measured Performance of Photovoltaic Modules

For solar power plants to operate and be controlled effectively, solar power forecasting is essential. The amount of energy generated by the solar photovoltaic (PV) array is affected by various external environmental factors, including dust deposition on the panels, humidity, air temperature, and solar radiation. These factors also include the doping level and design of the PV array. These naturally fluctuating components have a direct effect on the manufacturing of solar cells. In addition, variations in solar irradiation and the previously mentioned environmental conditions take place during the day. To enhance the accuracy of PV module output forecast and, consequently, the efficiency of solar power plants, it is essential to measure and evaluate the hourly averages or specific intervals of these parameters.

The dataset includes several metrics that are essential for projecting solar electricity and operating plants, including:

1.Power generated: The joules of energy produced in three hours.

2. Distance-to-solar-noon: This is a radian-based measurement of the angular separation from solar noon.

3. Temperature: In degrees Celsius, the average daily temperature.

4. Wind direction: The degree of average daily wind direction, from 0 to 360.

5. Wind speed: An average daily wind speed expressed in meters per second.

6. Sky cover: Displayed as a five-step scale, where 0 represents complete visibility and 4 represents complete coverage.

7. Visibility: Kilometres are used to express visibility.

8. Humidity: expressed as a percentage.

9. Average wind speed (period): The average wind speed over the three hours of data, expressed in meters per second.

10. Mean pressure (time interval): Mean barometric pressure during the 3-hour period when measurements were taken, in inches of mercury.

The complex dynamics of Root Mean Squared Error (RMSE) during the training of an artificial neural network (ANN) are depicted in Fig. 2. Over multiple epochs, the paper thoroughly monitors variations in RMSE. By analysing these patterns, the article offers profound insights into the convergence dynamics of the ANN and its capacity to generalize to unknown input. The graphic illustrates how the RMSE drops to 0.2694 as the number of epochs increases, highlighting how effective the training process is at lowering error and improving model performance [23].
With the help of the provided code, a visualization is created to compare a model's prediction accuracy to the actual values for the training and test datasets shown in Fig. 3. The subplot on the left, where real generated power is displayed on the y-axis and expected power output is plotted on the x-axis, displays the evaluation of prediction accuracy for training data. Similarly, the accuracy of test data prediction is evaluated in the subplot to the right. The comparison between the predicted and actual power output values in the image provides insight into how well the model caught the underlying patterns in the data.

The model provided generates a graphic to compare predicted generated power levels with actual values based on the sun azimuth angle in Fig. 4. The left subplot displays the evaluation of training predictions against the solar azimuth angle. Real generated power levels and anticipated power outputs are displayed using scatter graphs. The sun azimuth angle is represented by the x-axis, while the training data is shown by the y-axis. Similarly, the right subplot shows the assessment of test predictions concerning the sun azimuth angle. Both subplots show how the model can predict power production based on variations in the sun azimuth angle.

Following the training and testing phases, the model's performance was thoroughly examined using random datasets to cover a range of epochs, from 2 to 16. The method conducted a thorough comparison between the real and projected datasets in order to provide light on how epoch changes affect prediction accuracy. A thorough analysis of the variations between the actual and predicted values throughout several epochs yielded important insights into the model's ability to adapt and generalize to a range of datasets. The comprehensive research demonstrates the artificial neural network model's stability and offers guidance on the optimal epoch selection to maximize prediction performance in Fig. 5.

6.1. Performance comparison of Forecasting techniques

Metrics like mean square error (MSE) and root mean square error (RMSE) are used to assess the quality of predictions. Model optimization and fine-tuning depend significantly on the accuracy and validity information these

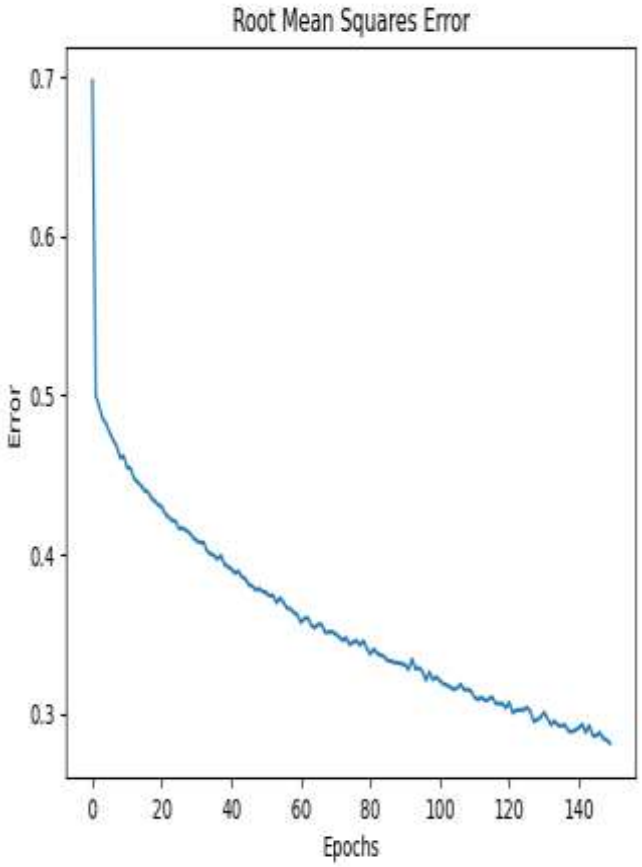


Fig. 2: Root mean square error evolution across epochs.

measures deliver. There are notable correlations between a number of solar and meteorological-related parameters.

1. The angle of incidence and zenith have a strong positive association (0.71)

2. The relationship between generated power in KW and backward shortwave radiation is 0.56.

3.Relative humidity and low cloud cover (0.49) and zenith (0.51) are positively correlated.

4. The Angle of Incidence and Zenith and Generated Power have a substantial negative association (-0.65).

5. Temperature and zenith have an inverse relationship (-0.55).

6. There is a high negative correlation (-0.8) between shortwave radiation backward and Zenith.

7. The relationship between shortwave radiation and relative humidity (-0.72) and the relationship between temperature and relative humidity (-0.77) are negative shown in Fig. 5.

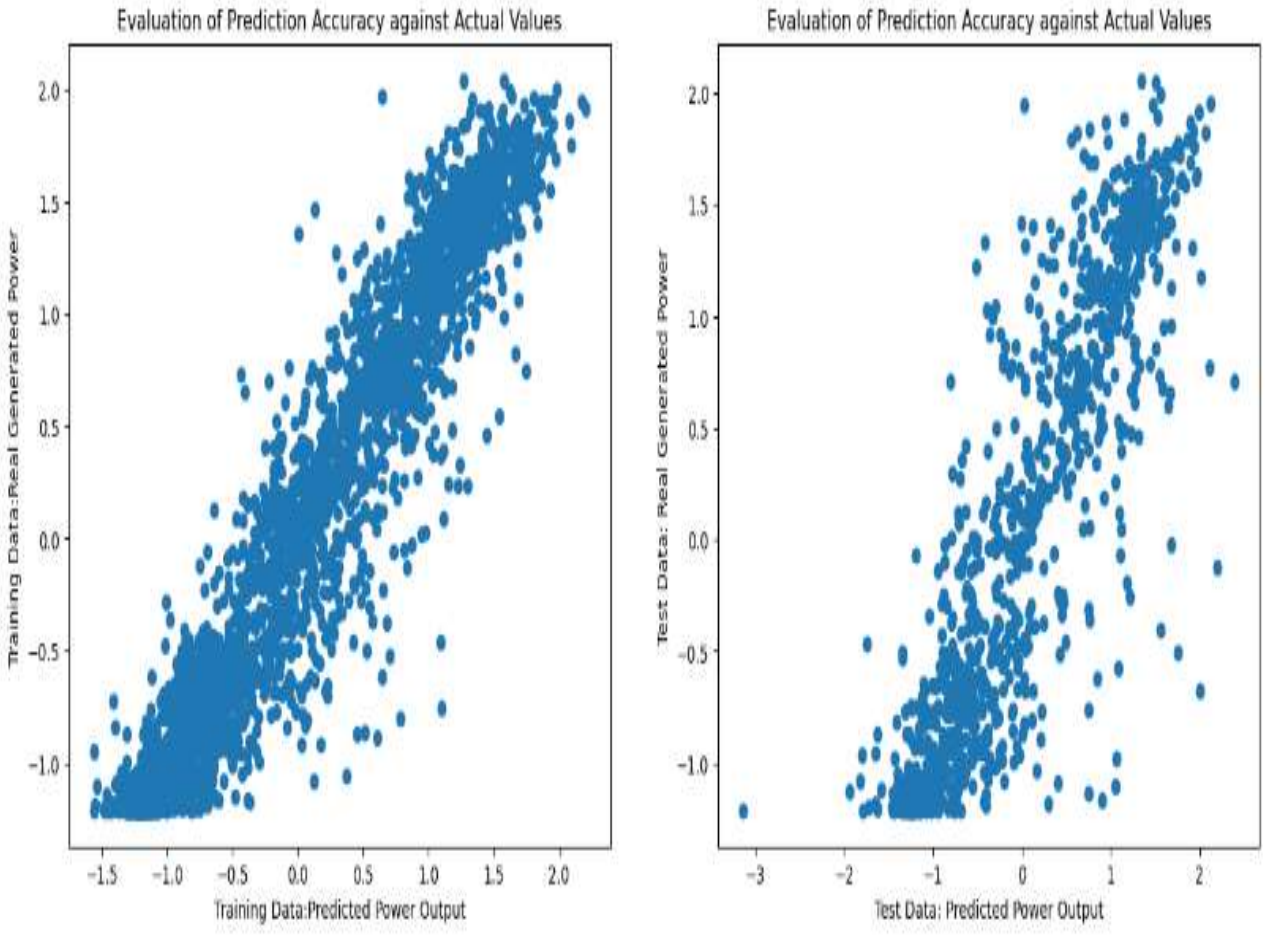


Fig. 3: Epoch-based evaluation of solar power prediction accuracy: Insights from training and test data.

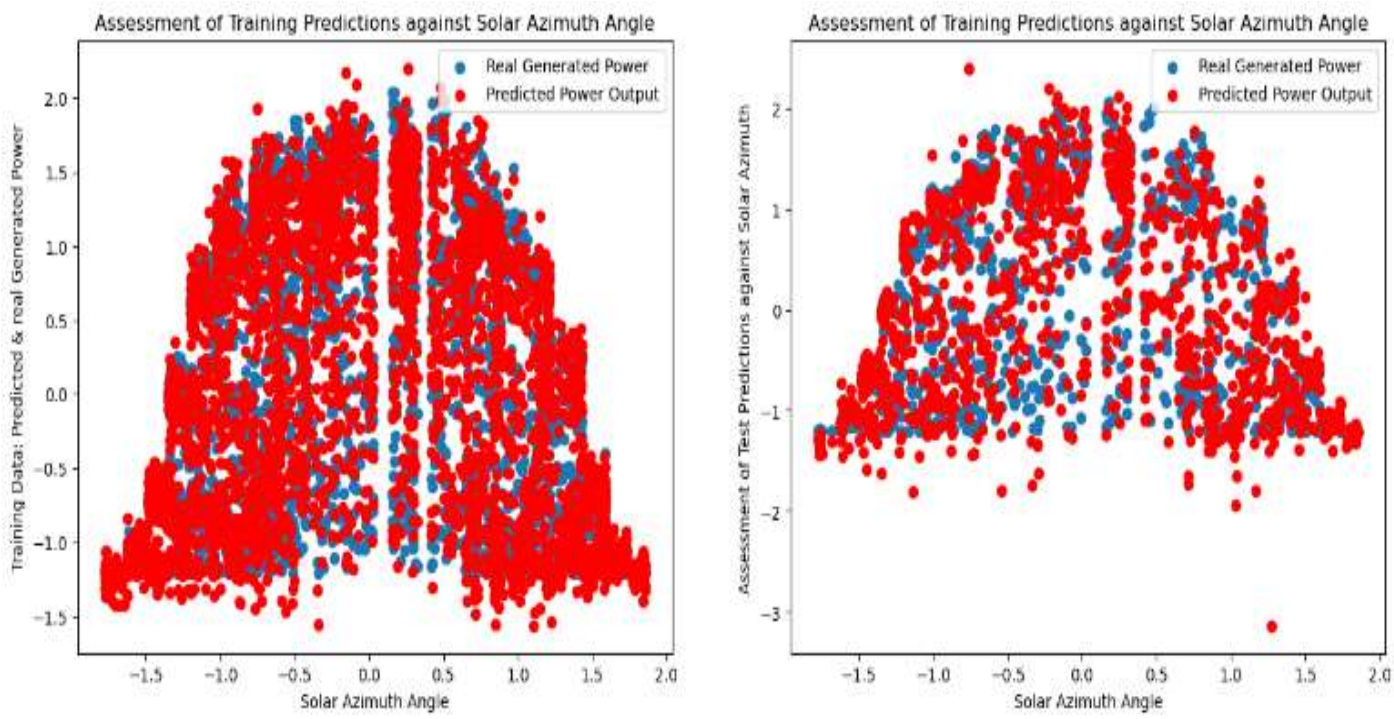


Fig. 4: Visualization of solar power prediction accuracy based on solar azimuth angle.

By comparison, given in Table 4, the proposed LSTM–HDKR-based method in Chhattisgarh, India (latitude 21.2085°N, longitude 81.3482°E), achieved $R^2 = 0.8818$ and RMSE = 0.269**,** which indicates strong predictive capability

	Real Solar Generated Power	Predicted Solar Power Output
2	-0.82	-1.41
3	-0.87	-0.89
4	1.33	1.41
5	1.17	1.14
6	0.74	1.04
7	1.13	1.68
8	0.12	-0.29
9	1.60	1.78
10	0.95	0.25
11	1.24	0.67
12	1.63	1.97
13	1.79	1.34
14	-0.90	-1.23
15	2.06	1.35
16	1.42	-0.01

Fig. 5: Solar Irradiance on random testing data sets.

with very low error despite high variability in local climatic conditions. This comparison highlights that while some existing methods show higher correlation coefficients, the proposed approach delivers superior robustness by minimizing prediction errors, making it more suitable for integration into hybrid electric vehicle energy management systems.

6.2. Functionality Test

During the functional test, the PV-UC-battery HEV is simulated to operate in multiple modes during a driving cycle, such as idling, starting, cruising, accelerating, and regenerative braking [22]. The simulation results, which are shown in Table 5 with the initial battery state of charge (SOC) at 75% and varying solar radiance and ambient temperature, demonstrate how various power sources connect. The battery serves as the main power source. High solar radiation and a high state of charge (SOC) of the battery indicate solar energy charging, which is indicated by negative battery power during vehicle pauses. The vehicle is propelled forward by its photovoltaic array and batteries until increased power requirements compel the ultracapacitor (UC) to come on. The battery absorbs excess UC power. when the demand for power decreases, the excess UC power is stored in the battery. The battery becomes the primary power source once the motor reaches its maximum output.

Data from the Mahindra Hybrid Electric Vehicle Research Centre was acquired, with a specific focus on a small vehicle model, in order to establish the monthly usage of power. The driving cycle and the Air Conditioning (AC) system are the two primary aspects of the analysis. First, the amount of electricity used for driving was determined, paying close attention to factors including road conditions, vehicle speed, acceleration, and deceleration patterns. This comprehensive assessment provided valuable insights into the energy demands of the vehicle's propulsion system across various driving scenarios. In addition, the amount of electricity used by the air conditioning system was assessed, taking into account variables such as user preferences, cabin size, and outdoor temperature. Through the analysis of these variables, a comprehension of the monthly electricity usage for both the driving cycle and the AC system came to pass. The model is optimized using the Gurobi solver (package version 0.7.6) with an academic license.

The study makes it easier to estimate accurately and create energy-management plans that work for the unique features of Mahindra's compact car type. The graph in Fig. 6 illustrates the amount of electricity used each month for driving cycles, demonstrating how the amount of energy consumed varies over time. Energy efficiency techniques can be optimized by gaining insights into seasonal fluctuations and driving patterns through the analysis of these trends. This graphic depiction is an excellent tool for comprehending the dynamics of vehicle energy consumption and providing guidance for energy management decisions. The graphic in Fig. 7 also shows the vehicle's AC system and auxiliary devices of the vehicle's monthly electricity use, highlighting usage trends and seasonal fluctuations. The significant bars seen in green on the graph suggest higher AC demand in the summer, especially in April, May, June, and July. Blue represents other auxiliary devices, including lighting and music.

Table 4: Performance comparisons.

References	Location	Latitude/Longitude	Findings
RahimiKhoob[32]	Spain	36.834N/2.463W	R2 =0.889 RMSE= 2.53
A.M. Pavan[33]	India	9.9252N/78.1198E	R2 =0.99 RMSE= 4.832
A. Assi[34]	UAE	24.1302N/55.8023E	R2 =0.93 RMSE= 0.43
C. Muraleedharan[35]	India	23.2599N/77.4126E	R2 =0.9989 RMSE= 0.5016
Proposed Method	India Chhattisgarh	21.2085N, 81.3482E	R2=0.8818 RMSE=0.269

Table 5: Annual key performance indicators for different driving conditions and AC status.

Case	AC Status	Driving Conditions (UDDS)	AC Temperature (°C)	Energy Consumption (kWh)	Battery Satisfies Demand(%)	UC satisfies Demand(%)	PV satisfies Demand(%)	Run Time	Mean SOC Battery wrt to target SOC
Case-1	On	Normal	20	8789	70	20	90	47	94%
Case-2	Off	Normal	-	8902	30	10	80	39	60.06%
Case-3	Off	Extreme Hilly,Terrain	-	8515	80	40	60	14	62.57%
Case-4	On	Extreme	24	8639	60	30	70	17	56.47%

6.3. Driving Cycle Scenarios

The standard condition for evaluating the performance of the lightweight battery-PV-UC HEV (Hybrid Electric Vehicle) system under the defined driving cycle conditions. To represent different battery statuses and environmental situations, three distinct scenarios are created:

Scenario 1: Sunny solar radiation - The PV array charges the battery to 75% capacity when it first starts.

Scenario 2: Overcast/rainy - In low solar radiation conditions, the PV output is insufficient, with the battery at 35% of its full charge.

Scenario 3: At night, solar radiation: 0 W/m2 - The vehicle is solely powered by the UC and battery, which results in a 55% state of charge for the battery.

Fig. 6 illustrates the energy distribution in the PV-UC-Battery HEV power system as well as the battery level of charge under Scenario 1. Because of the high output power generated by the PV array in Fig.9, the PV and the battery is used primarily as the power source under EMS control. The UC idles and operates in a low power range when its system efficiency is relatively high during periods of low power demand. Fig.9 demonstrates how the battery discharges to gradually decrease its state of charge as its energy storage is used as efficiently as possible to maximize solar energy utilization.

Figs. 6 and 7 analyse into the most effective methods for utilizing ultracapacitors, battery storage, and PV charging to meet the power needs of traction motors, air conditioning (AC), and driving cycles in an electric vehicle system. Seasonal analysis shows patterns of dynamic energy generation and consumption, with PV charging being essential to balancing power needs. Edge cases highlight situations in which energy production might not meet demand, requiring effective use of battery and ultracapacitor storage to close the gap and meet power requirements. The operational patterns observed in these situations provide insight into the extent to which energy management techniques work to balance the supply and demand of energy under varied driving circumstances and environmental variables. Furthermore, investigates the way driving cycles and AC usage affect energy consumption and storage dynamics, emphasizing the significance it is to optimize energy flows for improved vehicle economy and performance.

This subsection explores optimal flows with a battery and UC feed in addition to our initial objective function, which was power demand fulfilment. Fig.7 provides a description of seasonal fluctuations by displaying the seasonal mean PV generation (yellow line), matching sinks (stacked bars), and the mean battery State of Charge (SOC) (black line). Notably, as shown by the grey bars in Fig.7, there is a natural increase in UC during the summer, which is marked by low heating demand and high PV generation. In contrast to other seasons, the summertime battery SOC is lower, which highlights the influence of seasonal fluctuations on system behaviour. Notably, as shown by the grey bars in Fig. 7, there is a natural increase in UC during the summer, which is marked by high cooling demand and high PV generation. In contrast to other seasons, the summertime battery SOC is lower, which highlights the influence of seasonal fluctuations on system behaviour. One notable observation is that, as the day rolls on, self-discharging losses tend to cause battery charging to be delayed. However, certain anomalies to this pattern highlight how important it is to consider the time of day and seasonality when choosing the best charging tactics. Fig. 7 does not make it easier to analyse daily operating patterns, even though it provides insights into aggregated seasonal flows. The next paragraphs explore operational trends that are seen in the winter and summer, with a particular emphasis on specific edge cases. Winter presents unique challenges due to its combination of high heating demand and low PV generation.

The seasonal variations and anomalies observed in Fig. 7 further highlight the limitations of conventional static SOC strategies, which rely on fixed upper and lower SOC thresholds and fail to adapt to real-time fluctuations in load demand and solar irradiance. Traditional static methods often result in delayed charging, inefficient power distribution, and excessive battery stress during seasonal extremes. In contrast, the dynamic SOC control proposed in this research continuously adjusts the SOC reference in response to predicted solar irradiance (via the LSTM–HDKR model), instantaneous driving cycle conditions, and seasonal variability. This enables adaptive power sharing between the battery and ultracapacitor, ensures efficient utilization of available PV power, and prolongs battery life by avoiding repetitive deep discharges. Therefore, the proposed method provides a more resilient and adaptive energy management approach compared to static SOC targets, particularly under conditions of fluctuating renewable generation and variable driving patterns.

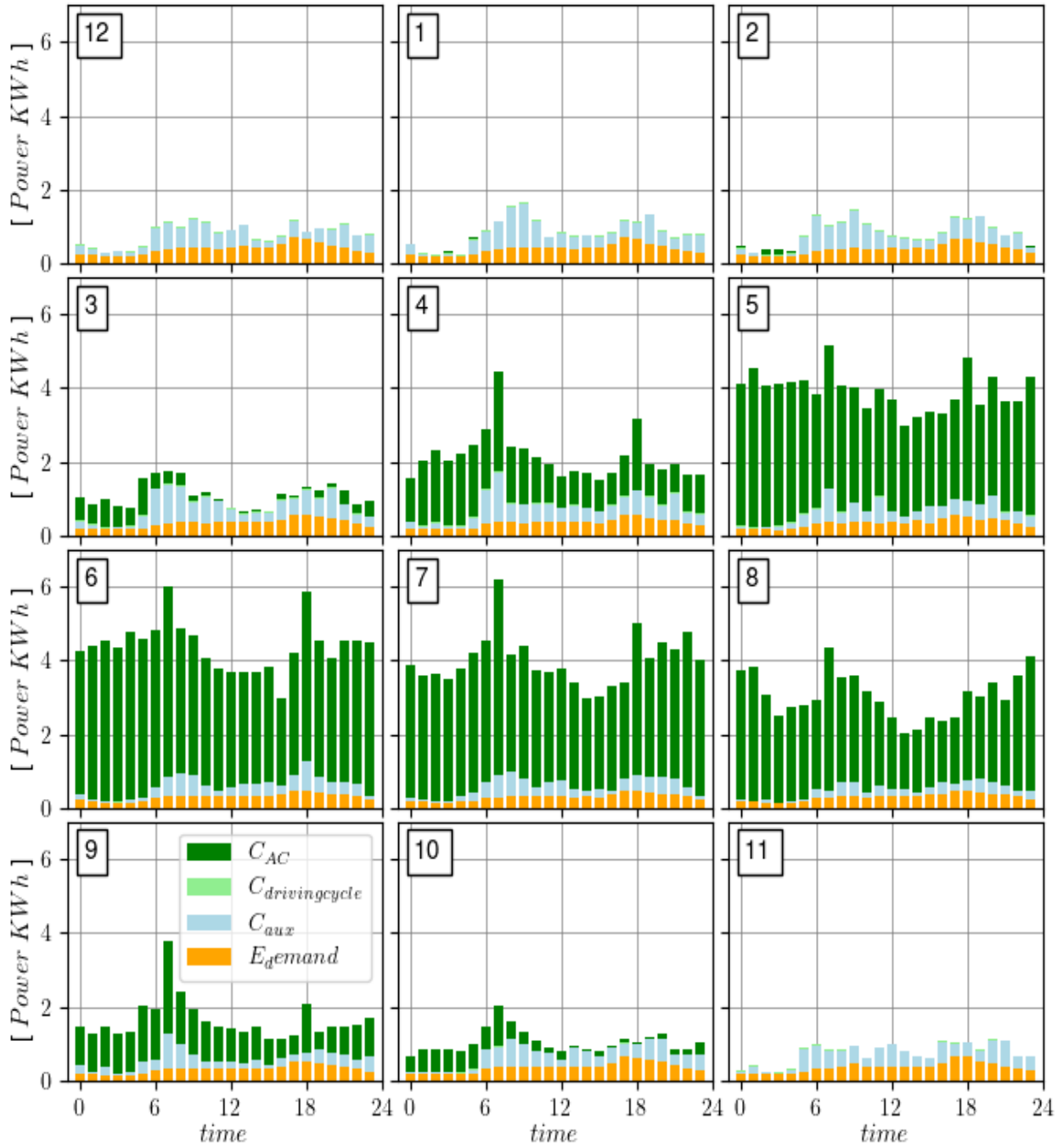


Fig. 6: Seasonal energy allocation for driving, AC, and Auxiliary systems by EMS battery, UC, and PV.

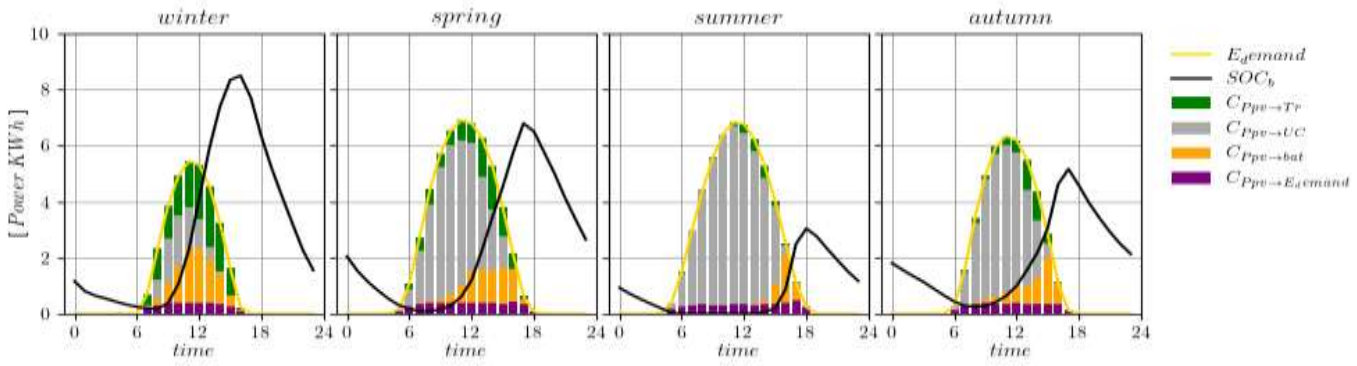


Fig.7: Seasonal distribution of average PV system flows and battery state of charge.

6.4. Optimizing Battery Performance with Dynamic Target State of Charge Control

Research suggests the median battery values exhibit behavior associated with battery characteristics, as they approach capacity limitations during winter and decrease to approximately 25% of the capacity in summer. To reduce dissipation losses, charging strategies were designed to match PV power surplus to the grid and to line with the current demand. Modelling limitations, such as restricted battery charge capacity because of PV generation or inverter capacity, were the cause of the lower SOC data. On the other hand, observations that were higher than the median, especially during seasonal variations, indicated a range of summertime AC cooling needs. It was suggested that target SOC levels be dynamically controlled, with adjustments made for daily, monthly, or seasonal mean SOCs. This could potentially increase net profits and decrease dissipation losses while maintaining user comfort.

Research suggests the median battery values exhibit behaviour associated with battery characteristics, as they approach capacity limitations during summer and increase to approximately 25% of the less capacity in winter. In order to reduce dissipation losses, charging strategies were designed to match PV power surplus to the grid and to line with the current demand. Modelling limitations, such as restricted battery charge capacity because of PV generation or inverter capacity, were the cause of the lower SOC data. On the other hand, observations that were higher than the median, especially during seasonal variations, indicated a range of summertime AC cooling needs. It was suggested that target SOC levels be dynamically controlled, with adjustments made for daily, monthly, or seasonal mean SOCs as shown in Fig.9. This could potentially increase net profits and decrease dissipation losses while maintaining user comfort. Future implementations must strike a balance between information needs and potential cost savings, which has interesting implications for rule-based control approach design. A prioritization framework is developed for distributing available PV generation within the integrated vehicle system, specifically for powering the air conditioning (AC) system and meeting cooling demands during driving cycles, through a thorough analysis of optimal energy allocation. At first, the priority was meeting the demand for electricity needed for cooling and vehicle running.

Subsequently, the focus was on preserving storage unit target state-of-charges (SOCs) in order to guarantee the best possible use of energy resources. The extra PV energy was then used to run the air conditioning system or stored for later use. We maximized energy use, especially during moments of high cooling demand, by calculating target SOCs and creating charging plans. Unlike traditional methods, this methodology enables dynamic SOC control according to driving conditions and climatic variables. This method allows for dynamic SOC management depending on driving circumstances and climate variations, which goes beyond traditional fixed rule-based approaches and requires additional testing using a variety of operational datasets from simulation studies. The energy flow depicted in Table 5 explains the lower average growth in the state of charge (SOC) throughout the winter.

1. During the summer, photovoltaic (PV) systems provide a larger percentage of the energy needed to meet the power demand.

2. In contrast, the ultracapacitor and Battery Energy Storage System (BESS) provide the bulk of the EV energy needed during the winter, when there is less availability of PV energy, lowering the battery's average state of charge.

By comparing the performance of hybrid energy storage sources with renewable sources managed by the Maximum Power Point Tracking prediction and optimization system with Conventional Renewable Energy Systems (RES), the usefulness of hybrid resources under the proposed structure is demonstrated. Load management is challenging because environmental factors have a significant impact on the amount of electricity produced by renewable energy sources like solar and wind. solar power generation.

6.5. Broader Implications for HEV Battery Lifespan and Performance

The proposed research carries significant implications for both the lifespan and performance of HEV batteries. By replacing traditional static SOC control with a dynamic, forecast-informed strategy, the system is able to minimize deep discharge cycles and avoid frequent high-rate charging/discharging events. These operating conditions are among the primary factors responsible for premature battery degradation. Consequently, the proposed method directly contributes to extending battery life, reducing replacement costs, and improving the overall sustainability of HEV systems.

From a performance standpoint, the integration of the ultracapacitor with the battery in a dynamically managed system enhances the ability to handle transient peak loads, such as rapid acceleration or regenerative braking, without placing undue stress on the battery. This ensures that the battery is primarily utilized for steady-state power delivery, while the ultracapacitor absorbs short-term fluctuations. Such an arrangement improves round-trip efficiency, reduces internal resistive heating, and maintains more stable SOC levels, which translates to higher reliability and consistent driving performance.

Moreover, by incorporating solar irradiance forecasts through ANN–HDKR modelling, the system achieves better synchronization between renewable generation and battery charging cycles. This proactive scheduling not only increases the fraction of renewable energy utilization but also reduces dependence on grid electricity or fossil-fuel-driven charging. Over time, this makes HEVs more environmentally friendly, while simultaneously improving their economic viability by lowering the cost of energy consumption.

In the broader context, the proposed methodology demonstrates how intelligent energy management strategies can transform HEVs from being only partial substitutes for fossil-fuel vehicles into highly optimized, renewable-energy-integrated systems. This represents a step toward climate-neutral mobility solutions, where both performance

and battery longevity are optimized without compromising user convenience.

7. Conclusion

This work proposed an integrated methodology to enhance solar irradiance forecasting and optimize energy management in battery–ultracapacitor hybrid electric vehicles (HEVs). The hybrid HDKR–ANN model delivered high forecasting accuracy (R^2 = 0.8818, RMSE = 0.269), confirming its effectiveness in estimating beam, diffuse, and reflected irradiance on tilted surfaces. This improved reliability strengthens PV utilization and provides a robust foundation for renewable energy integration in HEVs.

On the operational side, the proposed rule-based EMS with dynamic SOC control effectively coordinated energy flows between the PV system, battery, and ultracapacitor. Results demonstrated a 47.6% reduction in peak battery stress, extending battery lifespan while maintaining stable system performance across diverse driving and auxiliary load conditions. Seasonal analysis further revealed distinct operational behaviours: summer offered high PV generation and grid export but lower average SOC due to delayed charging, whereas winter imposed greater reliance on the battery and grid under reduced solar availability. Transitional periods exhibited more balanced profiles, highlighting the adaptability of the framework under varying conditions.

Overall, this study demonstrates that combining accurate solar forecasting with adaptive EMS strategies can significantly improve efficiency, storage durability, and renewable integration in HEVs.

Future directions include hardware-in-the-loop validation and reinforcement learning–based cost prediction, aiming to enhance real-time adaptability and economic feasibility in next-generation low-emission transportation systems.
feasibility.

Credit Authorship Contribution Statement

Shraddha Kaushik: Conceptualization, Data curation, Formal analysis, Investigation, Methodology, Software, Validation, Visualization, Writing - original draft, Writing - review & editing. **Kunamneni Rachanajali:** Formal analysis, Funding acquisition, Project administration, Resources, Supervision, Visualization, Writing - original draft, Writing - review & editing.

Declaration Of Competing Interest

The authors declare that they have no known competing financial interests or personal relationships that could have appeared to influence the work reported in this paper. The ethical issues; including plagiarism, informed consent, misconduct, data fabrication and/or falsification, double publication and/or submission, redundancy has been completely observed by the authors.

Funding

This research received no external funding.

Data Availability

Data collected for the study can be made available upon request from the corresponding author.

References

[1] A. Ghosh, “Possibilities and challenges for the inclusion of the Electric Vehicle (EV) to reduce the carbon footprint in the transport sector: A review,” *Energies*, vol. 13, no. 10, Art. no. 2602, 2020.

[2] J. Zhang, H. Sun, and B. Wang, “Solar irradiance prediction based on deep learning: A review,” *Renewable Sustainable Energy Rev*., vol. 122, Art. no. 110269, 2020.

[3] M. Guermoui and S. Benkaciali, “A novel ensemble learning approach for hourly global solar radiation forecasting,” *Neural Comput. Appl.*, 2022, vol. 34, no. 4, pp. 1–23, 2022.

[4] H. Romero and M. A. Gonzalez, “Applications of artificial intelligence to photovoltaic systems: A review,” *Appl. Sci.*, vol. 12, no. 19, Art. no. 10056, 2022.

[5] B. Benamrouq and M. Ouardouz, “A proposed model to forecast hourly global solar irradiation based on satellite-derived data, deep learning, and machine learning approaches, *J. Ecol. Eng.*, vol. 21, no. 4, pp. 26–38, 2020.

[6] A. F. Amiri and S. Kichou, “Fault detection and diagnosis of a photovoltaic system based on deep learning using CNN and Bi-GRU,” *Sustainability*, vol., no. 3, Art. no. 1012, 2024.

[7] D. T. Reindle, W. A. Beckman, and W. A. Duffie, “Diffuse fraction correlations,” *Sol. Energy*, vol. 45, no. 1, pp. 1–7, 1990.

[8] J. Bilbao, A. D. Miguel, and J. A. Franco, “Iso-Radiation maps for tilted surfaces in the Castile and Leon region, Spain,” *Energy Convers. Manag*., vol. 44, no. 9, pp. 1575–1588, 2003.

[9] A. Kudish and A. Ianetz, “Evaluation of the relative ability of three models to predict the global radiation on a tilted surface,” *Energy Convers. Manag.*, vol. 32, pp. 387–394, 1991.

[10] S. Yu, D. Lin, Z. Sun, "Efficient model predictive control for real-time energy optimization control of battery- ultracapacitor in electric vehicle," *International Journal Energy Resources*, vol. 44, pp. 7495-7506, 2020.

[11] P. J. Brockwell and R. A. Davism, “Introduction to time series and forecasting; Springer: Berlin/Heidelberg, Germany, 2002.

[12] S. I. Habib and S. A. G. K. Abadi, “A model predictive control strategy for performance improvement of hybrid energy storage systems in DC microgrids,” IEEE Access, vol. 10, pp. 25400–25421, 2022.

[13] M. Suhail, “Development of progress fuzzy logic and ANFIS control for energy management of plug-in

hybrid electric vehicle," *IEEE Access Open J.*, vol. 9, 2020.

[14] P. Kumar, R. P. Satish, S. Chandrasena, V. Ramu, G.N. Srinivas, K. Victor Sam Moses Babu, "Energy management system for small-scale hybrid wind solar battery-based microgrid," *IEEE Access*, vol. 8, pp. 8336–8345, 2020.

[15] J. Zhao, "An energy management strategy to reduce the comprehensive cost of hybrid energy storage systems in electric vehicles," *IEEE Access*, vol. 11, 2023.

[16] G. P. Zhang, "Time series forecasting using a hybrid ARIMA and neural network model, *Neurocomputing*, vol. 50, pp. 159–175, 2005.

[17] S. Sun and J. Zhang, "A Machine learning method for predicting driving range of battery electric vehicles," *J. Adv. Transp.*, pp. 1–16, 2016.

[18] M. Al-Shamisi, A. Assi, and H. Hejase, "Estimation of global solar radiation using artificial neural networks in Abu Dhabi City, UAE," *J. Sol. Energy Eng.*, vol. 136, no. 2, Art, no. 024502, 2014.

[19] A. Rahimikhoob, "Estimating global solar radiation using artificial neural network and air temperature data in a semi-arid environment," *Renew. Energy*, vol. 35, no. 9, pp. 2131–2135, 2010.

[20] W. Zhou, W. Wang, X. Hua, and Y. Zhang, "Real-time traffic flow forecasting via a novel method combining periodic-trend decomposition," *Sustainability-Basel,* vol. 12, no. 15, Art. no. 5891, 2020.

[21] J. E. Hay, J. A. Davies, "Calculations of the solar radiation incident on an inclined surface," *Sol. Energy,* , vol. 24, no. 5, pp. 429–431, 1980.

[22] K. P. T. T. L. N. Ding, "Design of a hybrid energy management system using rule-based control strategy and genetic algorithm for the series-parallel plug-in hybrid electric vehicle," *Int. J. Energy Res.*, vol. 45, no. 2, pp. 1627–1644, 2020.

[23] K. Prasada and N. Ding, "Design of a hybrid energy management system using rule-based control strategy and genetic algorithm for the series-parallel plug-in hybrid electric vehicle," *Int. J. Energy Res.*, vol. 45, no. 2, pp. 1627–1644, 2020.

[24] D. Fischer and H. Madani, "On heat pumps in smart grids: A review," *Renew. Sustain. Energy Rev.*, 70, pp. 342–357, 2017.

[25] A. Ghorashi and S. I. Habibi, "A model predictive control strategy for performance improvement of hybrid energy storage systems in DC microgrids," *IEEE Access*, vol. 10, pp. 25400–25421, 2022.

[26] N. Patel and R. Sharma, "Advanced photovoltaic energy forecasting using deep neural networks," *Renew. Energy,* vol. 208, pp. 1253–1265, 2023.

[27] H. A. Trinh, "Optimization-based energy management strategies for hybrid construction machinery: A review," *Energy Reports*, vol. 8, pp. 6035–6057, 2022.

[28] Y. Zheng and X. Luo, "Seasonal solar irradiance forecasting using artificial intelligence," *Sci. Rep.*, vol. 14, Art. no. 68531, 2024.

[29] A. Kumar and S. Mehta, "Hybrid machine learning and optimization method for solar irradiance prediction," *Eng. Optim.*, vol. 56, no.2, Art. no. 2390126, 2024.

[30] M. Rahman and T. Singh, "Optimizing hardware configuration for solar-powered energy management in battery-ultracapacitor hybrid electric vehicles," *Sci. Rep.*, vol. 14, Art. no. 80219, 2024.

[31] H. Zhang and L. Li, "A Hybrid ensemble model for solar irradiance forecasting," *Electronics*, vol. 12, no. 12, Art. no. 2607, 2023.

[32] J. Baker and S. Das, "Sustainable power management in light electric vehicles with hybrid energy storage systems," *Sci. Rep.*, vol. 14, Art. no. 10920784, 2024.

[33] F. Ali and R. Hasan, "AI-Based Forecasting for optimized solar energy management and smart grid reliability," *Int. J. Prod. Res.*, vol. 61, no. 5, Art. no. 2269565, 2023.

[34] M. Santos and G. Chang, "Systematic review on impact of different irradiance forecasting models on solar energy systems," Energies, vol. 15, no. 17, Art. no. 6267, 2022.

[35] D. Lee and C. Wang, "A renewable approach to electric vehicle charging through solar integration," *Sci. Rep., vol.* 14, Art. no. 10903804, 2024.

[36] I. A. Hassanvand, J. Ebrahimi, and M. Abasi, "Voltage regulation in low voltage distribution networks using reactive power capability of photovoltaic inverters and PID consensus algorithm," *Journal of Applied Research in Electrical Engineering*, vol. 3, no. 2, pp. 159–167, 2024.

[37] A. Rahmani, M. Dehghani, and S. M. Rezaee, "Optimal energy management scheduling for hybrid electric vehicles using deep neural network-based control of battery–ultracapacitor hybrid storage systems," *Journal of Applied Research in Electrical Engineering*, vol. 4, no. 2, pp. 85–96, 2023.

[38] J.E. Hay and J.A. Davies, "Calculations of the solar radiation incident on an inclined surface," *Solar Energy*, vol. 24, no. 5, pp. 429–435, 1980.

[39] D. T. Reindle, W. A. Beckman, and W. A. Duffie, "Diffuse fraction correlations," *Sol. Energy*, vol. 45, no. 1, pp. 1–7, 1990.

[40] J. A. Duffie and W. A. Beckman, *Solar Engineering of Thermal Processes*, 4th ed., Wiley, 2013.

[41] M. Iqbal, *An Introduction to Solar Radiation*, Academic Press, 1983.



Shraddha Kaushik received his bachelor of Electrical and Electronics Engineering from Government Engineering College Raipur, India in 2009. She has completed her Master's in Engineering (Power Systems & Automation) from GITAM University, Vishakhapatnam, India. She is currently pursuing her Ph.D. Degree from Vignan Foundation for Science Technology & Research, Guntur, India. Currently, she is serving as an Assistant Professor at the Bhilai Institute of Technology in Durg, India. She has 10 years of teaching experience in Electrical Engineering courses in both undergraduate and postgraduate. She has supervised 6 ME scholar theses and published 21 articles in peer-reviewed journals and conferences. Her current research includes Power Converters, active filtering, power conditioning, machine learning, AI, power system analysis &Electric Vehicles.



Kunamneni Rachanajali received his bachelor of Electrical and Electronics Engineering from JNTU Kakinada (Vignan's Engineering College, Guntur, AP)In 2011. She completed her Master's in Engineering from Visvesvaraya National Institute of Technology, Nagpur (VNIT Nagpur) In 2013. She obtained Ph.D. Degree from Vignan's Foundation for Science Technology & Research, Guntur, India in 2021. Currently, she is serving as an Assistant Professor in the Department of Electrical and Electronics Engineering at Vignan's Foundation for Science, Technology & Research (Deemed to be University). She has 10 years of teaching experience in Electrical Engineering courses both undergraduate and postgraduate. She has supervised 10 ME scholar theses and published 30 articles in peer-reviewed journals and conferences. Her current research includes Power Converters, active filtering, power conditioning, power electronics, AC and DC drives, and High Voltage Engineering.

Copyrights
© 2026 Licensee Shahid Chamran University of Ahvaz, Ahvaz, Iran. This article is an open-access article distributed under the terms and conditions of the Creative Commons Attribution –NonCommercial 4.0 International (CC BY-NC 4.0) License (http://creativecommons.org/licenses/by-nc/4.0/).

Journal of Applied Research in Electrical Engineering

Vol. 4, No. 1, Winter and Spring 2025

jaree.scu.ac.ir

A Hybrid Technique Combining Robust and DNN for Thyroid Disease Prediction on Imbalanced Dataset Elahe Moradi	1
An Algorithm for Determining the Desirability of the Amount of Transient Limiting Reactors in Shunt Capacitor Banks Sadegh Rekabeslami Zadeh, Gholamali Torabi, Sasan Najafi Birgani, Mehdi Enayat Zare, Mostafa Sarlak	11
Deep Learning based Underwater Object Detection and Recognition for Multi-Robot Systems Iman Ali HasValimohammad Nazarzehi Had, Zobeir Raisi	24
A Review on Blockchain-based Gaming: Existing Insights, Deficits, and Emerging Avenues Patikiri Arachchige Don Shehan Nilmantha Wijesekara	34
Performance Evaluation of a PV-Based Multilevel Inverter with Improved THD and Efficiency Parimalasundar Ezhilvannan, Kumar Reddy Cheepati, Suresh Krishnan	56
Power Resource Allocation in Downlink NOMA Systems Using Joint Sum-Rate and Bit-Error-Rate Optimization Mohammad Hasheminejad, Mohsen Sheikh-Hosseini	69
Constrained MIMO Reference-Based Offline Steady–State (RBOSS) NMPC for PMSM using Voltage Source Inverter Stephen Ofori, Francis Boafo Effah, Daniel OpokuMoazami	76
Compact Two-Stage CMOS Operational Amplifier with Enhanced Gain and Bandwidth via Cascode and Negative Capacitance Techniques MohammadMehdi Derakhshannia, Mohsen Shakiba, Maryam Shakiba	86
Texture Classification Using Deep Learning and Enhanced Local Binary Pattern Behzad Abbasi, Majid Ghandchi, Sirous Tannaz, Javad Ostadieh, Saeed Barghandan	94
Enhancing Integration of Advanced Power Control Strategies for High-Penetration Photovoltaic System in Power Grid Naveen Kumar Bind, Anil Kumar	106
Comparative Analysis of Various Optimization Techniques for Battery Management Systems in Electrical Vehicles Mohammad Junaid Khan, Ram Murat Singh, Md Naqui Akhtar, Asyraf Afthanorhan	122
Optimal Energy Management in Solar-powered Battery-Ultracapacitor Hybrid Electric Vehicles: Leveraging ANN-HDKR for Tilt Angle Optimization Shraddha Kaushik, Kunamneni Rachnanjali	137

Iranian Association of Electrical and Electronics Engineers

Shahid Chamran University of Ahvaz